

Interactions and Dynamics of Cryoprotectants, Energy Materials and Other Complex Mixtures

Thesis Submitted for the degree of

Doctor of Philosophy (Science)

of

Jadavpur University

By

Kajal Kumbhakar



Department of Chemical, Biological and Macromolecular Sciences

S. N. Bose National Centre for Basic Sciences

Block – JD, Sector – III, Salt Lake

Kolkata - 700106, India

October 2020



सत्येन्द्र नाथ बसु राष्ट्रीय मौलिक विज्ञान केन्द्र
SATYENDRA NATH BOSE NATIONAL
CENTRE FOR BASIC SCIENCES
সত্যেন্দ্র নাথ বসু জাতীয় মৌল বিজ্ঞান কেন্দ্র

CERTIFICATE FROM THE SUPERVISOR

This is to certify that the thesis entitled “Interactions and Dynamics of Cryoprotectants, Energy Materials and Other Complex Mixtures” submitted by Smt Kajal Kumbhakar (Index No: 141/16/Chem./25), who got her name registered on 12/08/2016 for the award of Ph.D. (Science) degree of Jadavpur University, is absolutely based upon her own work under the supervision of Professor Ranjit Biswas and that neither this thesis nor any part of it has been submitted for either any degree/diploma or any other academic award anywhere before.

Ranjit Biswas
09/10/2020
Dr. Ranjit Biswas

Senior Professor,

Department of Chemical, Biological and Macromolecular Sciences

S. N. Bose National Centre for Basic Sciences

DR. RANJIT BISWAS
Senior Professor
Dept. of Chemical, Biological & Macromolecular Sciences
S. N. Bose National Centre for Basic Sciences
Block - JD, Sector-III, Salt Lake, Kolkata - 700 106, India

Block-JD, Sector-III, Salt Lake,

Kolkata-700106, West Bengal, India

ब्लॉक – जे.डी., सेक्टर –III, सॉल्ट लेक, कोलकाता– 700 106 / Block - JD, Sector - III, Salt Lake, Kolkata - 700 106

दूरभाष / Phones : (00) 91 - (0) 33 - 2335 5706-8, 2335 3057 / 61, 2335 0312 / 1313

टेलीफैक्स / TELEFAX : +91 -33-2335 3477 / 2335 1364 / 2335 9176

वेबसाइट / Website: <http://www.bose.res.in>

भारत सरकार के विज्ञान एवं प्रौद्योगिकी विभाग के अंतर्गत एक स्वायत्त संस्थान

AN AUTONOMOUS INSTITUTE UNDER DEPARTMENT OF SCIENCE & TECHNOLOGY, GOVERNMENT OF INDIA

Dedicated to

My Parents, Uncle, Grandmother and Sister

Acknowledgement

I got the privilege to be a research scholar in the department of Chemical, Biological and Macromolecular Sciences in Satyendra Nath Bose National Centre for Basic Sciences (SNBNCBS) since last five years. In the edge of present course I wish to express my cordial thanks to them who have helped me a lot in their own way.

First of all, I wish to express my heartfelt thanks and sincere gratitude to my supervisor, Prof. Ranjit Biswas for his continuous and effortless guidance. He always encouraged me to explore the research field quite independently. He gave me a very comfortable working platform. I got his generous support irrespective of my academic and non-academic issues. I am very fortunate for being trained under the guidance of a person like him.

I am very much grateful to Council of Scientific and Industrial Research, India for fellowship throughout my Ph. D. tenure.

I am thankful to Prof. Priyadarsi De, IISER Kolkata for his extremely positive collaboration. Thanks to Prof. Prasun Kumar Mandal, IISER Kolkata for his collaboration for an interesting measurement. I am grateful to Prof. Mark Maroncelli, Pennsylvania State University, USA for kindly allowing me to access his spectra analysis software. I thank Prof. S. K. Ray, Director of SNBNCBS.

I thank all the members of my thesis committee, for their generous help and critical comments. My special thanks to Prof. Asoke Prasun Chattopadhyay, Kalyani University, the external expert of my Thesis committee.

I would like to thanks to the all faculty members, Academic and non-Academic personals of the Centre.

I am very much grateful to Department of Chemistry, Jadavpur University for allowing me to register for Ph. D. degree.

I must thank to my senior past lab members, Dr. Sandipa Indra, Dr. Suman Das, Dr. Kallol Mukherjee, Dr. Sirshendu Dinda and Dr. Ejaj Tarif for their guidance and support. Specially I have

been very much benefited in all aspects of research from Dr. Kallol Mukherjee and Dr. Ejaj Tarif throughout these five years. Dr. Sirshendu Dinda helped me to learn the basic understanding of various experimental techniques and data analyses. Thanks to Dr. Harun Al Rasid Gazi, Dr. Biswajit Guchhait, Dr. Snehasis Daschakraborty, Dr. Tamisra Pal, Dr. Anuradha Das for their care and guidance for me. I also thank Koushik Chanda, past lab member. I am thankful to my junior past lab members, Arnab and Indrajit and Soumita. Thanks to all of my present lab members, Juriti Rajbangshi, Atanu Baksi, Jayanta, Dhruvajyoti, Narayan, Amrita. I spent wonderful five years in my lab with such understandable and affectionate lab members. I received a lot of care and help from them. They always provide me a healthy and homely atmosphere.

My sincere regards to Dr. Parijat Das for her caring and affectionate manners to me whenever we meet. The sweet moments spent with our adorable Rwitoban and Arshaman will be a memory of my life.

I want to thank all the staffs of SNB Mess and Bhagirathi Guest House Canteen for their untiring efforts to provide healthy and delicious foods.

I am very fortunate to have enormous support and encouragements from many respectable persons including my school teachers and kind well-wishers of my village throughout my academic career. I am grateful to them.

I received a lot of help from many great persons to carry out my higher studies. I am grateful to all of them. Among them, no word will be sufficient for my uncle, Surja Kumar Jana. Without his support it was nearly impossible for me to reach where I am.

I will be always grateful to my paternal grandfather late Dhananjay Kumbhakar, my paternal grandmother Malati Kumbhakar and my loving sister Manasi.

Finally, I want to express my gratitude from the bottom of my heart to two best persons of my life my parents, Pushpa Kumbhakar and Haradhan Kumbhakar for their loves, blessings and lessons.

Abstract

In this Thesis we have investigated molecular level interactions and dynamics of various complex systems that have potential applications in different fields, such as, cryopreservation, energy storage and tapping, pharmaceuticals etc. The complex systems considered in this Thesis are cryoprotectants, electrolyte solutions (used in energy storage devices), aqueous solutions of various stimuli-responsive smart polymers etc. Steady state and time resolved fluorescence (TRF) spectroscopy have been extensively employed to understand different kinds of possible interactions and dynamics in the medium doped with foreign fluorophore solutes at micro-molar concentration. Dielectric relaxation spectroscopy (DRS) in kHz-GHz frequency regime has been utilized to study the reorientation dynamics of dipolar species in some of these media. Temperature and glucose concentration dependent reorientation relaxation dynamics and its decoupling with medium viscosity in biodegradable glucose/glycerol cryoprotectant solutions have been studied via DRS measurements. Significant fractional viscosity dependence of dielectric relaxation observed in this glucose/glycerol solutions is the manifestation of medium dynamic (temporal) heterogeneity. Signature of strong spatio-temporal heterogeneity in the same glucose/glycerol cryoprotectant solutions has been registered via steady state and TRF spectroscopy measurements of the dissolved fluorophore solutes, coumarin 153 (C153) and coumarin 343 (C343). Furthermore, steady state and TRF emission studies employing reactive (trans-2-[4-[(dimethylamino)styryl]benzothiazole (DMASBT)) and non-reactive (C153) fluorophores indicate significant impact of gradual increase of higher dielectric constant cosolvent, ethylene carbonate (EC) in the interaction and relaxation dynamics of Li-ion battery electrolyte solution consist of lithium perchlorate (LiClO_4), EC and propylene carbonate (PC). Fractional viscosity dependence of solute (C153) rotation and translation diffusion time as well as solution dynamics, the signature of dynamic heterogeneity in medium, have been registered in the polymer gel electrolyte (PGE) systems, consist of lithium perchlorate (LiClO_4), propylene carbonate (PC) and polypropylene glycol (PPG425) using TRF and fluorescence correlation spectroscopy (FCS) techniques. Cloud point driven interaction and relaxation dynamics of aqueous solutions of amphiphilic thermoresponsive copolymers have been explored via steady state and TRF measurements employing hydrophilic (C343) and hydrophobic (C153) solute probes of comparable sizes. Probe centric interaction and dynamics in aqueous polymer solutions are mainly

dictated by a balance between the hydrophobic/hydrophilic segments in the studied thermoresponsive polymer molecules. TRF and DRS measurements in aqueous solution of pH responsive copolymers contain structure, interaction and relaxation dynamics.

Chapter 1 of this Thesis presents an introduction to the work and the relevant literature. In chapter 2, a concise description of the used experimental techniques and data analysis protocols are provided. Chapter 3 presents reorientation relaxation dynamics and viscosity coupling of biodegradable glucose/glycerol cryoprotectant solutions via DRS measurements. The spatio-temporal heterogeneity in the glucose/glycerol solutions studied via steady state and TRF emission spectroscopy are elaborated in chapter 4. Chapter 5 reveals impact of gradual increase of higher dielectric constant cosolvent in the interaction and relaxation dynamics of Li-ion battery electrolyte solution. Translation-rotation decoupling at well above (~ 100 K) the glass transition temperature of the polymer gel electrolyte solution has been discussed in chapter 6. In chapter 7, cloud point driven relaxation dynamics in aqueous solution of thermoresponsive copolymers are compared with criticality driven relaxation dynamics. Chapter 8 contains structure, interaction and relaxation dynamics of aqueous solution of pH responsive copolymers. The Thesis ends with concluding remarks and some important future problems in chapter 9.

List of Publications

1. “Solvent dependent relaxation dynamics in lithium ion battery electrolytes: Coupling to medium friction” by **Kajal Kumbhakar**, Ejaj Tarif, Kallol Mukherjee and Ranjit Biswas *J. Mol. Liq.* **290**, 111225 (2019).
2. “Cloud point driven dynamics in aqueous solutions of thermoresponsive copolymers: Are they akin to criticality driven solution dynamics?” by **Kajal Kumbhakar**, Biswajit Saha, Priyadarsi De and Ranjit Biswas *J. Phys. Chem. B* **123**, 11042 (2019).
3. * “Dynamics at the non-ionic micelle/water interface: Impact of linkage substitution” by Ejaj Tarif, Kallol Mukherjee, **Kajal Kumbhakar**, Anjan Barman and Ranjit Biswas *J. Chem. Phys.* **151**, 154902 (2019).
4. “Dynamics in glucose/glycerol cryoprotectant system: Temperature and composition dependent kHz-GHz dielectric relaxation spectroscopic studies” by **Kajal Kumbhakar**, Narayan Chandra Maity, Ejaj Tarif and Ranjit Biswas *J. Phys. Chem. B* (Submitted).
5. “Spatio-temporal heterogeneity in glucose/glycerol cryoprotectant system: Probe dependent fluorescence spectroscopic study” by **Kajal Kumbhakar**, Narayan Chandra Maity and Ranjit Biswas *J. Chem. Phys.* (Submitted).
6. “Use of translational-rotational decoupling for development of new energy materials: A representative study with polymer gel electrolytes” by **Kajal Kumbhakar**, Saptarshi Mandal, Prasun Kumar Mandal and Ranjit Biswas *J. Phys. Chem. B* (Submitted).
7. “Interactions and dynamics in aqueous solutions of pH-responsive polymers: A combined fluorescence and dielectric relaxation studies” by **Kajal Kumbhakar**, Ashmita Dey, Amrita Mondal, Priyadarsi De and Ranjit Biswas (To be Submitted).
8. * “Frictional coupling of relaxation in a polymer gel electrolyte system: Combined fluorescence and dielectric relaxation spectroscopic studies” by **Kajal Kumbhakar**, Kallol Mukherjee and Ranjit Biswas *Phys. Chem. Chem. Phys.* (Submitted).

9. **“Exploring interaction and dynamics in ethanol/water binary mixtures at near azeotrope region: Time-resolved fluorescence and dielectric relaxation spectroscopic studies”* by **Kajal Kumbhakar**, Narayan Chandra Maity and Ranjit Biswas (**Manuscript in Preparation**).

10. **“Anomalous dynamics in aqueous hyaluronic acid gel: A probe dependent fluorescence study”* by **Kajal Kumbhakar**, Ejaj Tarif, Kallol Mukherjee and Ranjit Biswas (**Manuscript in Preparation**).

11. **“Solute and solvent dynamics in neat and wet-octanol: Steady state and time-resolved fluorescence measurements”* by Narayan Chandra Maity, **Kajal Kumbhakar** and Ranjit Biswas (**To be Submitted**).

12. **“Azeotrope temperature and composition driven interaction and dynamics in ternary solvent mixtures”* by Amrita Mondal, **Kajal Kumbhakar** and Ranjit Biswas (**Manuscript in Preparation**).

*not included in this Thesis

Contents

Chapter 1: Introduction.....	1
Chapter 2: Main Experimental Techniques and Data Analysis Protocols....	15
2.1 Steady State UV-Vis Absorption Spectroscopy.....	15
2.2 Steady State Fluorescence Spectroscopy	16
2.3 Time-Resolved Fluorescence Measurement: Technique, Data Collection and Analysis.....	17
2.3.1 TCSPC Technique.....	17
2.3.2 Data Analysis.....	18
2.3.2.1 Solvation Dynamics.....	18
2.3.2.2 Rotational Dynamics.....	20
2.4 Dielectric Relaxation Spectroscopy (DRS).....	21
2.4.1 General Discussion about DRS.....	22
2.4.2 Measurements of Dielectric Properties.....	23
2.4.2.1 Instruments.....	23
2.4.2.2 Different Mathematical Models and Data Analysis.....	24
2.4.2.2.1 Debye Model.....	24
2.4.2.2.2 Non-Debye Model.....	25
2.4.2.2.3 Combination of Models.....	25
2.4.2.2.4 Data Processing	26

2.4.2.2.5 Conductivity Corrections	26
------------------------------------------	----

Chapter 3: Dynamics in Glucose/Glycerol Cryoprotectant System: Temperature and Composition Dependent kHz-GHz Dielectric Relaxation Spectroscopic Studies**29**

3.1 Introduction.....	29
-----------------------	----

3.2 Experimental Details.....	31
-------------------------------	----

3.2.1 Materials and Sample Preparation.....	31
---------------------------------------------	----

3.2.2 Density and Viscosity Coefficient Measurements.....	32
-----------------------------------------------------------	----

3.2.3 Refractive Index Measurements.....	33
------------------------------------------	----

3.2.4 Data Collection and Analysis for Dielectric Relaxation Spectroscopy.....	33
--------------------------------------------------------------------------------	----

3.3 Results and Discussion.....	33
---------------------------------	----

3.3.1 Dielectric Relaxation in Neat Gly.....	34
----------------------------------------------	----

3.3.1.1 Origin of DR Time Constants in Neat Gly.....	35
------------------------------------------------------	----

3.3.1.2 Partial Viscosity Coupling of Dielectric Relaxation Dynamics in Neat Gly.....	37
---------------------------------------------------------------------------------------	----

3.3.2 Impact of Glu Concentration (in wt%) on DR in Glu/Gly Solution.....	37
---------------------------------------------------------------------------	----

3.3.2.1 Glu Concentration Dependence.....	37
-------------------------------------------	----

3.3.2.2 Temperature Dependence	40
--------------------------------------	----

3.4 Conclusion.....	47
---------------------	----

Chapter 4: Spatio-Temporal Heterogeneity in Glucose/Glycerol Cryoprotectant System: Probe Dependent Fluorescence Spectroscopic Study.....**52**

4.1 Introduction.....	52
-----------------------	----

4.2 Experimental Details.....	54
4.2.1 Materials and Sample Preparation.....	54
4.2.2 Density and Viscosity Coefficient Measurements.....	54
4.2.3 Data Collection and Analysis for Steady State UV-Vis Absorption and Fluorescence Emission Measurements.....	56
4.2.4 Data Collection and Analysis for Time-Resolved Fluorescence Emission Spectra.....	56
4.3 Results and Discussion.....	56
4.3.1. Steady State UV-Vis Absorption and Fluorescence Studies.....	56
4.3.1.1 Impact of Temperature.....	56
4.3.1.2 Glu Concentration Dependence.....	59
4.3.1.3 Spatial Heterogeneity in Glu/Gly Solutions.....	61
4.3.2 Time-Resolved Fluorescence Measurements.....	64
4.3.2.1 Stokes Shift Dynamics.....	64
4.3.2.2 Time-Resolved Fluorescence Anisotropy Studies.....	72
4.4 Conclusion.....	78
Chapter 5: Solvent Dependent Relaxation Dynamics in Lithium Ion Battery Electrolytes: Coupling to Medium Friction.....	83
5.1 Introduction.....	83
5.2 Experimental Details.....	85
5.2.1 Materials.....	85
5.2.2 Sample Preparation.....	86

5.2.3 Measurements of Density and Viscosity Coefficients.....	86
5.2.4 Conductivity Measurements.....	86
5.2.5 Data Collection and Analysis for Steady State Optical Measurements.....	87
5.2.6 Data Collection and Analysis for Time-Resolved Fluorescence Emission Spectra.....	87
5.3 Results and Discussion.....	88
5.3.1 Steady State Spectral Characteristics	88
5.3.2 Time-Resolved Measurements: Lifetime and Dynamic Stokes Shift.....	94
5.3.3 Time-Resolved Anisotropy ($r(t)$) Measurements: Solute Rotation and Viscosity Coupling.....	101
5.4 Conclusion.....	106

Chapter 6: Use of Translational-Rotational Decoupling for Development of New Energy Materials: A Representative Study with Polymer Gel Electrolytes

.....	110
6.1 Introduction.....	110
6.2 Experimental Details.....	112
6.2.1 Materials and Sample Preparation.....	112
6.2.2 Density and Viscosity Coefficients Measurements.....	113
6.2.3 Conductivity Measurements.....	113
6.2.4 Differential Scanning Calorimetry (DSC) Measurements.....	114
6.2.5 Steady State Measurements and Spectral Analysis.....	114

6.2.6 Time-Resolved Fluorescence Measurements and Data Analysis.....	115
6.2.7 Fluorescence Correlation Spectroscopy (FCS) Measurements and Data Analysis.....	115
6.2.7.1 FCS Theory.....	115
6.2.7.2 FCS Measurements.....	115
6.3 Results and Discussion.....	116
6.3.1 Steady State Fluorescence Measurements.....	116
6.3.2 Time-Resolved Fluorescence Measurements.....	122
6.3.2.1 Stokes Shift Dynamics.....	122
6.3.2.2. Time-Resolved Fluorescence Anisotropy: Rotational Diffusion of Solute.....	126
6.3.3 Fluorescence Correlation Spectroscopy: Translational Diffusion of Solute.....	133
6.3.4 Translation-Rotation Decoupling.....	139
6.4 Conclusion.....	139
Chapter 7: Cloud Point Driven Dynamics in Aqueous Solutions of Thermoresponsive Copolymers: Are They Akin to Criticality Driven Solution Dynamics?.....	143
7.1 Introduction.....	143
7.2 Experimental Details.....	145
7.2.1 Materials Sample Preparation for Fluorescence Measurements.....	145
7.2.2 Dynamic Light Scattering (DLS).....	146
7.2.3 Density and Viscosity Coefficient Measurements.....	146
7.2.4 Data Collection and Analysis for Steady State Optical Measurements.....	146

7.2.5 Data Collection and Analysis for Time-Resolved Fluorescence Emission Spectra.....	146
7.3 Results and Discussion.....	147
7.3.1 Determination of Critical Aggregation Concentration (CAC) of the Copolymers	147
7.3.2 Cloud Point Temperature (T_{cp}).....	149
7.3.3 Density and Viscosity Coefficient Measurements.....	152
7.3.4 Steady State UV-Vis Absorption and Fluorescence Emission Studies.....	152
7.3.5 Time-Resolved Fluorescence Spectroscopy Measurements.....	157
7.3.5.1 Fluorescence Lifetime Measurements.....	157
7.3.5.2 Time-Resolved Fluorescence Anisotropy Decay Measurements.....	159
7.4 Conclusion.....	168
Chapter 8: Interactions and Dynamics in Aqueous Solutions of pH- Responsive Polymers: A Combined Fluorescence and Dielectric Relaxation Studies	172
8.1 Introduction.....	172
8.2 Experimental Details.....	174
8.2.1 Materials and Sample Preparation for Measurements.....	174
8.2.2 pH- Measurements.....	175
8.2.3 Dynamic Light Scattering (DLS) Measurements.....	175
8.2.4 Density and Viscosity Coefficient Measurements.....	175
8.2.5 Refractive Index Measurements.....	175

8.2.6 Data Collection and Analysis for Steady State UV-Vis Absorption and Fluorescence Emission Studies.....	175
8.2.7 Data Collection and Analysis for Time-Resolved Fluorescence Emission Studies.....	176
8.2.8 Data Collection and Analysis for Dielectric Relaxation Spectroscopy Studies	176
8.3 Results and Discussion.....	177
8.3.1 Determination of Phase Transition pH.....	177
8.3.2 Density, Viscosity Coefficients and Refractive Indices: pH Dependence.....	180
8.3.3 Steady State UV-Vis Absorption and Fluorescence Emission Studies.....	180
8.3.4 Time-Resolved Fluorescence Spectroscopy Measurements.....	188
8.3.4.1 Fluorescence Lifetime Measurements.....	188
8.3.4.2 Time-Resolved Fluorescence Anisotropy Decay Measurements.....	188
8.3.5 Dielectric Relaxation Spectroscopic Study.....	192
8.4 Conclusion.....	195
Chapter 9: Concluding Remarks and Future Problems.....	200
9.1 Concluding Remarks	200
9.2 Future Problems	201
9.2.1 Heterogeneity in Biocompatible Cryoprotectant Mixtures: Temperature and Composition Dependent Time-Resolved Fluorescence (TRF) and Dielectric Relaxation Spectroscopic (DRS) Studies	201
9.2.2 Exploring Medium Static and Dynamic Properties in Highly Potential Polymeric Cryoprotectant Mixtures	201
9.2.3 Impact of Water on Interactions and Dynamics of Cryoprotectants Mixtures	202

9.2.4 Dielectric Relaxation of Lithium-Ion Battery Electrolytes	202
9.2.5 Polymer Chain Length Induced Interaction and Dynamics of Polymer Gel Electrolytes: TRF and DRS Measurements	202
Appendix A.a.....	205
Appendix A.b.....	208
Appendix A.c.....	215
Appendix A.d.....	227
Appendix A.e.....	232
Appendix A.f.....	238

Chapter 1

Introduction

Tremendous development in science and technology in the last few decades demands new materials and appropriate reaction media through liquid solvent engineering for synthesizing exotic materials via large scale synthesis. The properties (even states) of the matter depend on the interaction of their constituent components (atoms, molecules, ions etc.). Out of the three states of matter, the liquid state is ubiquitous and extensively utilized medium for a variety of purposes such as reaction media,¹⁻⁷ preserving formulations,⁸⁻¹⁶ delivery agents,¹⁷⁻¹⁹ electrolyte solution in electrochemical devices²⁰⁻²⁶ etc. Often the property of a given medium can be modified to change the interaction and associated dynamics within it; this could be done either by changing the identity of the neat liquid or using a multi-component mixture. Biodegradability, recyclability, cost effectiveness etc. are some of the fundamental aspects that need prior consideration irrespective of their projected applications.^{25,27-31} Apart from this, a subtle balance between medium polarity (dielectric constant, ϵ_s) and viscosity (η) is a dictating factor for carrying out any reaction in a liquid medium.^{25,26,32,33} On the other hand, high glass transition temperature (T_g), good hydrogen bond (H-bond) forming ability, non-toxicity etc. are relevant for solvent engineering focussing on preservation formulations.^{11,34-37} The above mentioned parameters are largely controlled by microscopic interactions and dynamics. The inter-relationship between interactions and dynamics in neat and multi-component mixtures tremendously influence technological and industrial applications of liquid solvents. Therefore, understanding interactions and dynamics is critical for engineering designer reaction media for tailoring reactions leading to desired products. Several experimental³⁸⁻⁵³ and computational tools⁵⁴⁻⁶⁴ are now available to investigate microscopic structure, interactions and dynamics of complex chemical systems.

In this Thesis several potential complex systems, having prominent significance in both fundamental aspects as well as technology sector, have been carefully selected for thorough and systematic investigation. For low temperature preservation of biological important materials such as cells, tissues, organs, proteins etc., several osmolytes, for example, dimethyl sulfoxide (DMSO), ethylene glycol (EG), propylene glycol (PG), glycerol, trehalose, sucrose, glucose, polyethylene glycol (PEG) etc. are used as preserving formulations.⁸ Such osmolytes

also termed as cryoprotectants increase the cell viability in cryopreservation by minimizing ice-crystal formation. Biocompatibility, high glass transition temperature,^{34,35,65-67} strong H-bond forming ability^{36,37} of a cryoprotectant formulation have been found to increase the stability of preserved bio-molecules. Crystallization process of preserved substances is dictated by interaction and dynamics of host cryoprotectant systems. Being glassy in nature, inherent heterogeneity of cryoprotectant formulation might have potential role in their preserving action and ability. Thus exploring interaction, dynamics and heterogeneity aspects of cryoprotectant formulations are of utmost importance for development of cryopreservation technology. The focus of our research interest has been further extended to interaction and dynamics of electrolyte material, used in various electrochemical devices such as Li-ion battery, dye sensitized solar cells, super capacitors, sensors etc.⁶⁸⁻⁷³ Concentration of electrolyte salt, viscosity and polarity of solvent and ion transport are fundamental factors that regulate function and efficiency of an electrolyte material.^{25,49,74-77} We are also interested in biodegradable and biocompatible synthetic smart polymers, that exhibit sharp reversible changes in properties in response to external stimuli such as pH,^{78,79} temperature,⁸⁰⁻⁸² ionic strength,^{83,84} chemical agent,⁸¹ light,^{85,86} redox potential,^{87,88} electric⁸⁹ and magnetic field⁹⁰. These smart materials have potential application in drug delivery,^{17,18} gene carrier,^{17,19} tissue engineering,⁹¹ chemo/bio-sensors,^{92,93} environmental remediation etc. Understanding the microscopic interaction and relaxation dynamics in aqueous solutions of different stimuli-responsive polymers is necessary for optimization and development of these materials for various applications.

Steady state UV-Vis absorption, fluorescence emission and time-resolved fluorescence emission spectroscopy^{49,94-96} have been employed extensively to study interaction and dynamics of these complex systems. Reactive and non-reactive external fluorophore solutes (also termed as 'dye' and 'probe' in this Thesis) dissolved in systems under investigation play the role of a local reporter in the UV-Vis absorption and fluorescence spectroscopic measurements. Non-reactive coumarin 153 (C153), coumarin 343 (C343) are the most used dyes in the experiments described in this Thesis. Coumarin dyes are standard fluorophores and the fluorescence as well as UV-Vis absorption features of these molecules are sensitive to local environment.^{97,98} Hydrophobic probe C153 and hydrophilic C343, owing to their different chemical nature, report qualitatively different local environments.^{95,99-101} The reactive probe trans-dimethyl amino styryl benzothiazole (trans-DMASBT or simply DMASBT) having much shorter fluorescence lifetime ($\langle \tau_{life} \rangle$) of DMASBT \sim 200-500 ps^{49,102} while for

C153/C343 are $\sim 2\text{-}5\text{ ns}$ ^{95,97,101}) than C153/C343 is also occasionally employed in order to detect the relatively faster density fluctuations that are not captured by coumarin dyes in experimental systems.^{48,49,53} Dielectric relaxation spectroscopy (DRS), on the other hand, is employed in some of the works presented in the Thesis to investigate inherent relaxation dynamics (i.e. without any foreign solute such as fluorophore) of dipolar systems.

Steady state fluorescence emission spectroscopy has been extensively applied to investigate the solution phase structure exploiting the fluorophore solute-medium interaction. Generally, fluorescence emission of a photo-excited fluorophore occurs from lowest vibrational level of completely energy-relaxed first electronic excited state (i.e. singlet, S₁) irrespective of the excitation wavelength (λ_{exc}) (according to Kasha's rule).^{103,104} However, in several complex systems, fluorescence emission of dissolved fluorophore has been found to shift towards red edge upon changing λ_{exc} to longer wavelength values.^{48,55,105-108} Such λ_{exc} dependent red shifted fluorescence emission spectra arises when fluorophores surrounded by different microscopic solvation shell (also termed as micro-domain) and the inter-conversion timescale of these different solvation shell is larger or comparable to $\langle \tau_{life} \rangle$ of the fluorophore. This λ_{exc} dependent fluorescence emission reflects heterogeneous solvation environment around the probe molecules.

Time-resolved fluorescence (TRF) technique has been employed for comprehensive understanding of medium relaxation dynamics in two ways: Stokes shift dynamics and time-resolved fluorescence anisotropy. In dynamic Stokes shift measurements, the underlying principle is that upon photo-excitation, dipolar fluorophore surrounded by an equilibrated solvent configuration (i.e. in ground electronic state, S₀) undergo ultrafast (in femtosecond) electronic transition to first excited electronic state (S₁) followed by charge redistribution. Due to this charge redistribution, the solvent configuration surrounding excited fluorophore experience a non-equilibrium situation. In this scenario solvent dipoles rearrange themselves to achieve an equilibrated solvent configuration surrounding excited fluorophore, and energy of S₁-state of the excited fluorophore gradually gets minimized. The time evolution of this energy minimization process is captured in time-resolved emission spectra (TRES) of the fluorophore. Therefore, dynamic Stokes shift obtained from such TRES carry information about fluorophore-centric medium dynamics.^{49,53,97,98} On the other hand, time-resolved fluorescence anisotropy is an important method where rotational diffusion of photo-excited

fluorophore is monitored. Fluorescence anisotropy of a fluorophore decays with time from a maximum value (~ 0.4) just after photo-excitation to zero at time much longer than the characteristic rotation correlation time of the fluorophore.¹⁰⁶ The anisotropy decay ($r(t)$) and obtained rotational correlation time ($\langle \tau_{rot} \rangle$) provide information about friction exerted by the medium on a rotating fluorophore solute dissolved in that medium. According to hydrodynamic rotational diffusion model (i.e. the Stokes Einstein Debye, SED model), rotational correlation time is linearly proportional to temperature reduced medium viscosity $\left(\frac{\eta}{T}\right)$.¹⁰⁹ In several complex medium, fractional $\frac{\eta}{T}$ dependence of $\langle \tau_{rot} \rangle$, following the equation: $\langle \tau_{rot} \rangle = A \left(\frac{\eta}{T}\right)^p$, has been observed.^{55,99,101} Such fractional viscosity dependence of diffusion timescale is well observed phenomena in various heterogeneous systems such as glass, super cooled liquids etc.¹¹⁰⁻¹¹⁵

Furthermore, dielectric relaxation spectroscopy (DRS), an important experimental technique to probe the orientation relaxation dynamics of dipolar species, has been employed in some systems described in this Thesis to enrich the discussion of results obtained via fluorescence spectroscopy. Unlike the dynamic Stokes shift measurements where foreign fluorophore molecule is utilized as a reporter to investigate medium dynamics, inherent relaxation dynamics of medium can be directly probed via DRS measurements.

Research works described in this Thesis includes dielectric relaxation (DR) dynamics of cryoprotectant solutions and aqueous solution of stimuli-responsive polymers. Steady state and time-resolved fluorescence spectroscopic measurements are performed in cryoprotectant solutions, battery electrolyte materials and aqueous solution of stimuli responsive polymers. Dielectric measurements actually strongly help to clarify the relevant Stokes shift dynamics. In addition, some other relevant experiments such as medium viscosity, refractive index, dynamic light scattering (DLS), fluorescence correlation spectroscopy (FCS), differential scanning calorimetry (DSC) etc. have been carried out as and when required.

The present Thesis consists of nine chapters with the first chapter being the introduction. Chapter 2 is devoted to the discussion of experimental techniques, data recording and methods of data analyses employed while investigating the interaction and dynamics of the complex systems considered in the present Thesis. In chapter 3, DRS measurements of glucose (Glu)/glycerol (Gly) cryoprotectant mixtures are described where temperature ($T= 300-333$ K)

and Glu concentration (0, 5, 15 and 25 wt% Glu) dependent DRS features are investigated. DRS measurements have been performed with two different instruments covering frequency window 20 kHz to 10 MHz (impedance analyzer) and 200 MHz to 50 GHz (network analyzer), respectively. Complex dielectric spectra in neat Gly (i.e. 0 wt% Glu) are adequately described by 3-Debye model with a dominant ($\sim 80\%$) ~ 1200 ps time component along with ~ 200 ps and ~ 50 ps time components at 300 K. These relaxation time components become faster with gradual increase of solution temperature and concomitantly decrease of medium viscosity. Temperature dependent dielectric relaxation times ($\langle \tau_{DR} \rangle$) and medium viscosity are well described by Arrhenius equation although activation energy required for dielectric relaxation ($E_a^{DR} = 42 \text{ kJmol}^{-1}$) is smaller than activation energy associated with medium viscosity ($E_a^\eta = 56 \text{ kJmol}^{-1}$). Departure of E_a^{DR} from E_a^η has also been manifested in the fractional temperature-reduced viscosity $\left(\frac{\eta}{T}\right)$ coupling of $\langle \tau_{DR} \rangle$ according to $\langle \tau_{DR} \rangle = A \left(\frac{\eta}{T}\right)^p$ with $p \sim 0.7$. Upon increasing Glu concentration beyond 5 wt%, a long time component ($\sim 25\text{-}30$ ns) emerges and its magnitude increases with increasing Glu wt% in the Glu/Gly solution. Apart from this slow component, other three Debye time components observed in most of the temperatures and Glu concentrations reflect the solution viscosity effect. Like neat Gly, temperature dependent average DR relaxation times ($\langle \tau_{DR} \rangle$) and η in Glu/Gly solutions also exhibit Arrhenius temperature dependence. In Glu/Gly solutions, viscosity decoupling of $\langle \tau_{DR} \rangle$ results fractional p value ~ 0.6 . Such partial viscosity decoupling of dielectric relaxation time is signature of dynamic heterogeneous systems.^{110-114,116}

Temperature ($T = 283\text{-}343$ K) and concentration (0, 5, 15 and 25 wt% Glu) dependent steady state and time-resolved fluorescence emission spectroscopic studies in Glu/Gly cryoprotectant solutions are discussed in chapter 4. Two dipolar fluorophore, hydrophilic C343 and hydrophobic C153, are employed as local reporters in the fluorescence measurements. With increase of solution temperature, steady state fluorescence emission spectra of C153/C343 show red shift. With increase of Glu concentration, steady state absorption and fluorescence emission of C153 gradually shifts to blue end while for C343, prominent red shift after 15 wt% Glu has been found. The maximum λ_{exc} dependent steady state fluorescence emission peak shift which is a signature of medium spatial heterogeneity has been detected in Glu/Gly solutions with highest Glu wt% (here 25 wt%) for both C153 and C343. Rotational diffusion

profile of C153/C343 measured via time-resolved fluorescence anisotropy decay show two widely different time-components: ~100 ps and a dominating several nanoseconds time component. Strong viscosity decoupling of solute rotation ($\langle \tau_{rot} \rangle = A \left(\frac{\eta}{T} \right)^p$) is observed in these Glu/Gly cryoprotectant solutions and extent of decoupling increases with Glu wt% in the solutions. For C153 ($p \sim 0.5$) fractional power p is slightly greater than C343 rotation ($p \sim 0.4$). Temperature dependent rotation of C153/C343 can be described by Arrhenius equation. Activation energy required for solute (C153/C343) rotation ($\sim 30 \text{ kJmol}^{-1}$) is much smaller than the activation energy associated with medium viscosity ($\sim 60 \text{ kJmol}^{-1}$). In high viscosity regime, rotational motions of both fluorophore solutes (C153/C343) exhibit sub-slip diffusion (non-hydrodynamic movement such as jump dynamics¹¹⁷). Pronounced viscosity decoupling of solute rotation and fractional power ($p \sim 0.4-0.5$) much lower than unity indicate temporally heterogeneous dynamics in the present Glu/Gly cryoprotectant solutions. On the other hand, dynamic Stokes shift has been detected for both C343 and C153 dissolved in Glu/Gly solutions. Solvation response function of C153 shows bi-exponential decay characteristics while it is tri-exponential for C343. Temperature dependent average solvation times ($\langle \tau_s \rangle$) of C343 in the present Glu/Gly solutions show Arrhenius dependence with activation energy $\sim 15-30 \text{ kJmol}^{-1}$. C343 reports increase of fractional viscosity dependence of solvation time ($p \sim 0.5$ in neat Gly to 0.1 in 25w% Glu) with Glu wt% in the present cryoprotectant solutions. Study of strong spatio-temporal heterogeneity in these Glu/Gly cryoprotectant solutions probed via steady state and time-resolved fluorescence techniques are systematically discussed in chapter 4.

In chapter 5, the heterogeneity aspect and solute-centred dynamics in lithium ion battery electrolytes have been explored by using two fluorescent probes, C153 and DMASBT. The electrolytes consist of ethylene carbonate (EC), propylene carbonate (PC) and lithium perchlorate (LiClO_4). Concentration of the electrolyte solutions are $\sim 1 \text{ M}$ having composition, $[9.795(x\text{EC}+(1-x)\text{PC})+0.869\text{LiClO}_4]$, where 9.795 is the total mole number of (EC+PC) binary mixtures and 0.869 denotes mole number of LiClO_4 while 'x' is the mole fraction. Significant λ_{exc} dependent steady state fluorescence emission of DMASBT in electrolyte solutions, which is absent for C153, indicates for solution spatial heterogeneity with relatively faster domain inter-conversion times. The magnitude of λ_{exc} induced total shift of emission frequency of DMASBT remain constant ($\sim 750 \text{ cm}^{-1}$) for the studied temperature range $T = 293-318 \text{ K}$. Dynamic Stokes shift measurements using C153 report $\sim 700-900 \text{ cm}^{-1}$ dynamic shifts in this

electrolyte systems with an estimated missing portion¹¹⁸ of ~ 40-50%. Dynamic Stokes shift and rotation dynamics in these electrolyte solutions measured using C153 are biphasic in nature. Temperature dependent rotation times for C153 suggests hydrodynamic viscosity coupling while those for DMASBT reflect strong fractional viscosity dependence.

In chapter 6, frictional coupling of solute (C153) rotation and translation motion as well as medium relaxation dynamics in a polymer gel electrolyte (PGE) system using TRF and FCS technique are discussed. C153 and DMASBT are used in the fluorescence measurements. The polymer gel electrolyte system consists of LiClO₄ as electrolyte salt, PC as organic solvent with high dielectric constant ($\epsilon_s = 65$ at 298 K) and PPG425 (also termed as PPG) as polymeric substance. Impact of increasing polymer content on interaction and dynamics in the polymer gel electrolytes are also explored. We varied the PPG concentration from 0 wt% to 60 wt% in PGE with composition [(PC+LiClO₄)+wt% PPG]. In these PGE solutions, signature of spatial heterogeneity, probed via λ_{exc} dependent steady state fluorescence emission, has been reported by short lifetime (~ 200 ps) probe DMASBT and not by multi-ns lifetime fluorophore (here C153). Rotational diffusion of 153 dissolved in these polymer gel electrolytes are biphasic while monomodal character has been observed for translational diffusion of C153. Fractional power (p) dependence of solute (C153) rotation and translation diffusion times with viscosity is found although rotation reports comparatively greater p (~ 0.7) than translation diffusion time (p ~ 0.6). This result suggests that a mild translation rotation decoupling¹¹⁹⁻¹²⁴ is present in the present PGE at temperature regime T = 293-318 K, much higher than their glass transition temperature ($T_g \sim 170-200$ K). Solvation time, obtained from dynamic Stokes shift measurements, becomes ~ 2 times faster with increasing polymer concentration from 0 to 100 wt% in the solutions although medium viscosity increases ~ 10 times. A negative viscosity coupling (p ~ -0.5) of the average solvation time of C153 along with fractional viscosity decoupling of C153 rotation and translation motion emphasizes the presence of temporal heterogeneity in the medium.

In chapter 7, cloud point driven interaction and relaxation dynamics of aqueous solutions of a series of amphiphilic thermoresponsive copolymers (P1, P2 and P3) comprised of methyl methacrylate (MMA) as hydrophobic segment and polyethylene glycol monomethyl ether methacrylate (PEGMA) as hydrophilic segment are explored through picosecond resolved and steady state fluorescence measurements employing hydrophilic (coumarin 343, C343) and hydrophobic (coumarin 153, C153) solute probes of comparable sizes. These thermoresponsive

random copolymers, with tunable cloud point temperatures (T_{cp} 's) between 298 and 323 K, are rationally designed, synthesized and characterized by a polymer research group at the IISER, Kolkata⁹⁵. The polymers have hydrophobic/hydrophilic segment ratio in the order P1<P2<P3. The T_{cp} of P1, P2 and P3, determined via transmittance measurements of aqueous polymer solutions, are 323 K, 316 K and 301 K, respectively. Below individual T_{cp} , the aqueous polymer solutions are transparent which turn cloudy (milky white) on or above T_{cp} . DLS measurements also reflect phase separation near T_{cp} : below T_{cp} , polymers form small size particle (> 10 nm) while above T_{cp} , large size particle (~ 500 nm). A balance between the hydrophilic (PEGMA) and the hydrophobic (MMA) content dictates the critical aggregation concentration (CAC), with CAC ~ 2 –14 mg/L for these copolymers in aqueous media. No abrupt changes in the steady state spectral features of both C153 and C343 in the aqueous solutions of these polymers near but below the cloud point temperatures have been observed. Interestingly, steady state spectral properties of C153 in these solutions show the impact of hydrophobic/ hydrophilic interaction balance but not by those of C343. More specifically, C153 reports a blue shift (relative to that in neat water) and heterogeneity in its local environment. This suggests different locations for the hydrophilic (C343) and the hydrophobic (C153) probes. In addition, the fluorescence lifetime, ($\langle \tau_{life} \rangle$), of C153 increases with increase of hydrophobic (MMA) content in the copolymers and $\langle \tau_{life} \rangle$ of C153 in polymer solutions are higher than neat water. However, C343 reports no such variations, although fluorescence anisotropy decays for both solutes are significantly slowed down in these aqueous solutions compared to neat water. Anisotropy decays indicates bimodal time-dependent friction for these solutes in aqueous solutions of these copolymers but monomodal in neat water. A linear dependence of the average rotational relaxation rates ($\langle k_{rot} \rangle = \langle \tau_{rot} \rangle^{-1}$) of the type $\langle k_{rot} \rangle \propto (|T - T_{cp}|/T_{cp})^\gamma$ with negative values for the exponent γ has been observed for both solutes. No slowing down of the solute rotation with temperature approaching the T_{cp} has been detected; rather, rotation becomes faster upon increasing the solution temperature, suggesting domination of the local friction.

In chapter 8, steady state, time-resolved fluorescence (TRF) of C153 and MHz-GHz dielectric relaxation spectroscopic (DRS) studies in aqueous copolymer solutions are described. A series of pH-responsive random copolymers (DPL, DP20, DP40 and DP60) comprising of pH-responsive moiety 2-((leucinyloxy)ethyl methacrylate (L-Leu-HEMA) and a hydrophobic methyl methacrylate (MMA) are synthesized and characterized by a polymer research group at

Chapter 1

the IISER, Kolkata.¹²⁵ A balance between the pH-responsive (L-Leu-HEMA) and the hydrophobic (MMA) content dictates the phase transition pH which is found ~ 5-7 for these aqueous copolymer solutions (1 mg/mL). DLS measurements in aqueous solutions of these polymers reflect small size particle (> 10 nm) at solution pH below their individual transition pH while large size particle (~ 200 nm) forms beyond their phase transition pH. No signature of phase transition pH driven abrupt change in static and dynamic properties of aqueous polymer solutions have been registered from pH dependent dielectric relaxation as well as solute (C153) -centric fluorescence measurements. Significant impact of varying L-Leu-HEMA/ MMA segment ratio on steady state fluorescence emission and rotational anisotropy decay of the fluorophore solute (C153) has been observed. Bulk water like dielectric features are reflected from MHz-GHz dielectric relaxation spectroscopy in aqueous solutions of these pH-responsive polymers.

The thesis ends with chapter 9 that contains a brief concluding remark and few relevant future problems.

References

1. W. Wei, C. C. K. Keh, C. J. Li and R. S. Varma, *Clean Technol. Environ. Policy* **7**, 62 (2004).
2. E. Pines, B. Z. Magnes, M. J. Lang and G. R. Fleming, *Chem. Phys. Lett.* **281**, 413 (1997).
3. W. H. Thompson and J. T. Hynes, *J. Phys. Chem. A* **105**, 2582 (2001).
4. K. Dahl, R. Biswas, N. Ito and M. Maroncelli, *J. Phys. Chem. B* **109**, 1563 (2005).
5. B. Bagchi, *Annu. Rev. Phys. Chem.* **40**, 115 (1989).
6. A. G. Zawadzki and J. T. Hynes, *J. Phys. Chem.* **93**, 7031 (1989).
7. M. Maroncelli, J. MacInnis and G. R. Fleming, *Science* **243**, 1674 (1989).
8. S. Barun, *The Beats Nat. Sci.* **2**, 1 (2015).
9. F. Franks, *J. Solution Chem.* **24**, 1093 (1995).
10. L. Slade, H. Levine and J. E. Kinsella, *Kinsella, J. Ed* (1995).
11. C. A. Angell, R. D. Bressel, J. L. Green, H. Kanno, M. Oguni and E. J. Sare, *Water in Foods*, 115 (1994).
12. M. T. Cicerone and C. L. Soles, *Biophys. J.* **86**, 3836 (2004).
13. A. S. Rudolph and J. H. Crowe, *Cryobiology* **22**, 367 (1985).
14. M. De los Reyes, L. Saenz, L. Lapierre, J. Crosby and C. Barros, *Vet. Rec.* **151**, 477 (2002).
15. F. Guo and J. M. Friedman, *J. Phys. Chem. B* **113**, 16632 (2009).
16. L. M. Sasnoor, V. P. Kale and L. S. Limaye, *Transplantation* **80**, 1251 (2005).
17. M. A. Ward and T. K. Georgiou, *Polymers* **3**, 1215 (2011).
18. P. C. Bessa, R. Machado, S. Nürnberger, D. Dopler, A. Banerjee, A. M. Cunha, J. C. Rodríguez-Cabello, H. Redl, M. van Griensven and R. L. Reis, *J. Control. Release* **142**, 312 (2010).
19. S.-o. Han, R. I. Mahato, Y. K. Sung and S. W. Kim, *Mol. Ther.* **2**, 302 (2000).
20. M. Armand and J. M. Tarascon, *Nature* **451**, 652 (2008).
21. J. M. Tarascon and M. Armand, *Nature* **414**, 359 (2001).
22. Y. C. Lu, Z. Xu, H. A. Gasteiger, S. Chen, K. Hamad-Schifferli and Y. Shao-Horn, *J. Am. Chem. Soc.* **132**, 12170 (2010).
23. P. Simon and Y. Gogotsi, *Nat. Mater.* **7**, 845 (2008).
24. T. Ogasawara, A. Débart, M. Holzapfel, P. Novák and P. G. Bruce, *J. Am. Chem. Soc.* **128**, 1390 (2006).
25. K. Xu, *Chem. Rev.* **104**, 4303 (2004).

26. F. Croce, G. B. Appetecchi, L. Persi and B. Scrosati, *Nature* **394**, 456 (1998).
27. A. Paiva, R. Craveiro, I. Aroso, M. Martins, R. L. Reis and A. R. C. Duarte, *ACS Sustainable Chem. Eng.* **2**, 1063 (2014).
28. E. L. Smith, A. P. Abbott and K. S. Ryder, *Chem. Rev.* **114**, 11060 (2014).
29. M. Francisco, A. van den Bruinhorst and M. C. Kroon, *Angew. Chem. Int. Ed.* **52**, 3074 (2013).
30. H. Tian, Z. Tang, X. Zhuang, X. Chen and X. Jing, *Prog. Polym. Sci.* **37**, 237 (2012).
31. D. Aurbach, M. L. Daroux, P. W. Faguy and E. Yeager, *J. Electrochem. Soc.* **134**, 1611 (1987).
32. Y. Dai, J. van Spronsen, G.-J. Witkamp, R. Verpoorte and Y. H. Choi, *Anal. Chim. Acta* **766**, 61 (2013).
33. M. Espino, M. de los Ángeles Fernández, F. J. Gomez and M. F. Silva, *Trends. Anal. Chem* **76**, 126 (2016).
34. L. N. Bell, M. J. Hageman and L. M. Muraoka, *J. Pharm. Sci.* **84**, 707 (1995).
35. W. Wang, *Int. J. Pharm.* **203**, 1 (2000).
36. L. M. Crowe, D. S. Reid and J. H. Crowe, *Biophys. J.* **71**, 2087 (1996).
37. J. H. Crowe, J. F. Carpenter and L. M. Crowe, *Annu. Rev. Physiol.* **60**, 73 (1998).
38. M. Flämig, L. Gabrielyan, R. Minikejew, S. Markarian and E. A. Rössler, *Phys. Chem. Chem. Phys.* **22**, 9014 (2020).
39. B. Klassen, R. Aroca, M. Nazri and G. A. Nazri, *J. Phys. Chem. B* **102**, 4795 (1998).
40. L. Yang, A. Xiao and B. L. Lucht, *J. Mol. Liq.* **154**, 131 (2010).
41. E. Cazzanelli, P. Mustarelli, F. Benevelli, G. B. Appetecchi and F. Croce, *Solid State Ion.* **86**, 379 (1996).
42. H. L. Yeager and H. Reid, *J. Phys. Chem.* **80**, 850 (1976).
43. M. Takeuchi, Y. Kameda, Y. Umebayashi, S. Ogawa, T. Sonoda, S.-i. Ishiguro, M. Fujita and M. Sano, *J. Mol. Liq.* **148**, 99 (2009).
44. L. Aguilera, S. Xiong, J. Scheers and A. Matic, *J. Mol. Liq.* **210**, 238 (2015).
45. T. Yamaguchi, T. Yonezawa, K. Yoshida, T. Yamaguchi, M. Nagao, A. Faraone and S. Seki, *J. Phys. Chem. B* **119**, 15675 (2015).
46. T. Yamaguchi, K. Yoshida, T. Yamaguchi, Y. Kameda, K. Ikeda and T. Otomo, *J. Phys. Chem. B* **121**, 5355 (2017).
47. S. Indra and R. Biswas, *J. Chem. Phys.* **142**, 204501 (2015).
48. A. Das and R. Biswas, *J. Phys. Chem. B* **119**, 10102 (2015).
49. K. Kumbhakar, E. Tarif, K. Mukherjee and R. Biswas, *J. Mol. Liq.* **290**, 111225 (2019).

50. K. Mukherjee, A. Barman and R. Biswas, *J. Mol. Liq.* **222**, 495 (2016).
51. K. Mukherjee, A. Das, S. Choudhury, A. Barman and R. Biswas, *J. Phys. Chem. B* **119**, 8063 (2015).
52. B. Guchhait, S. Das, S. Daschakraborty and R. Biswas, *J. Chem. Phys.* **140**, 104514 (2014).
53. B. Guchhait, S. Daschakraborty and R. Biswas, *J. Chem. Phys.* **136**, 174503 (2012).
54. S. Indra, B. Guchhait and R. Biswas, *J. Chem. Phys.* **144**, 124506 (2016).
55. S. Indra and R. Biswas, *J. Phys. Chem. B* **120**, 11214 (2016).
56. H. K. Kashyap and R. Biswas, *J. Chem. Sci.* **119**, 391 (2007).
57. H. K. Kashyap and R. Biswas, *J. Chem. Phys.* **127**, 184502 (2007).
58. T. Pal and R. Biswas, *J. Chem. Phys.* **141**, 104501 (2014).
59. S. Daschakraborty, T. Pal and R. Biswas, *J. Chem. Phys.* **139**, 164503 (2013).
60. T. Pal and R. Biswas, *Theor. Chem. Acc.* **132**, 1348 (2013).
61. S. Das, R. Biswas and B. Mukherjee, *J. Chem. Phys.* **145**, 084504 (2016).
62. K. Mukherjee, S. Das, E. Tarif, A. Barman and R. Biswas, *J. Chem. Phys.* **149**, 124501 (2018).
63. K. Shimizu, A. A. Freitas, R. Atkin, G. G. Warr, P. A. FitzGerald, H. Doi, S. Saito, K. Ueno, Y. Umebayashi and M. Watanabe, *Phys. Chem. Chem. Phys.* **17**, 22321 (2015).
64. S. Kaur, A. Gupta and H. K. Kashyap, *J. Phys. Chem. B* **120**, 6712 (2016).
65. J. L. Green, J. Fan and C. A. Angell, *J. Phys. Chem.* **98**, 13780 (1994).
66. R. H. M. Hatley, *Pharm. Dev. Technol.* **2**, 257 (1997).
67. S. L. Shamblin, X. Tang, L. Chang, B. C. Hancock and M. J. Pikal, *J. Phys. Chem. B* **103**, 4113 (1999).
68. A. M. Stephan, *Eur. Polym. J.* **42**, 21 (2006).
69. J. Y. Song, Y. Y. Wang and C. C. Wan, *J. Power Sources* **77**, 183 (1999).
70. X. Cheng, J. Pan, Y. Zhao, M. Liao and H. Peng, *Adv. Energy Mater.* **8**, 1702184 (2018).
71. O. A. Ileperuma, *Mater. Technol.* **28**, 65 (2013).
72. J. Wu, Z. Lan, J. Lin, M. Huang, Y. Huang, L. Fan and G. Luo, *Chem. Rev.* **115**, 2136 (2015).
73. H. Yu, J. Wu, L. Fan, Y. Lin, K. Xu, Z. Tang, C. Cheng, S. Tang, J. Lin and M. Huang, *J. Power Sources* **198**, 402 (2012).
74. D. Battisti, G. A. Nazri, B. Klassen and R. Aroca, *J. Phys. Chem.* **97**, 5826 (1993).
75. K. Kondo, M. Sano, A. Hiwara, T. Omi, M. Fujita, A. Kuwae, M. Iida, K. Mogi and H. Yokoyama, *J. Phys. Chem. B* **104**, 5040 (2000).
76. R. S. McMillan and M. W. Juzkow, *J. Electrochem. Soc.* **138**, 1566 (1991).

77. S. Tobishima, M. Arakawa, T. Hirai and J. Yamaki, *J. Power Sources* **26**, 449 (1989).
78. K. Bauri, S. G. Roy, S. Pant and P. De, *Langmuir* **29**, 2764 (2013).
79. G. Kocak, C. Tuncer and V. Bütün, *Polym. Chem.* **8**, 144 (2017).
80. A. Bordat, T. Boissenot, J. Nicolas and N. Tsapis, *Adv. Drug Deliv. Rev.* **138**, 167 (2019).
81. J. Zhuang, M. R. Gordon, J. Ventura, L. Li and S. Thayumanavan, *Chem. Soc. Rev.* **42**, 7421 (2013).
82. D. Roy, W. L. Brooks and B. S. Sumerlin, *Chem. Soc. Rev.* **42**, 7214 (2013).
83. G. Ma, W. Lin, Z. Yuan, J. Wu, H. Qian, L. Xu and S. Chen, *J. Mater. Chem. B* **5**, 935 (2017).
84. M. C. García, in *Stimuli responsive polymeric nanocarriers for drug delivery applications* (Elsevier, 2019), pp. 393.
85. Q. Yan, D. Han and Y. Zhao, *Polym. Chem.* **4**, 5026 (2013).
86. D. Roy and B. S. Sumerlin, *Macromol. Rapid. Commun.* **35**, 174 (2014).
87. X. Zhang, L. Han, M. Liu, K. Wang, L. Tao, Q. Wan and Y. Wei, *Mater. Chem. Front.* **1**, 807 (2017).
88. B. Saha, U. Haldar and P. De, *Macromol. Rapid. Commun.* **37**, 1015 (2016).
89. J. Ge, E. Neofytou, T. J. Cahill III, R. E. Beygui and R. N. Zare, *ACS Nano* **6**, 227 (2012).
90. T. Manouras and M. Vamvakaki, *Polym. Chem.* **8**, 74 (2017).
91. S. E. Stabenfeldt, A. J. García and M. C. LaPlaca, *Journal of Biomedical Materials Research Part A* **77**, 718 (2006).
92. M. A. C. Stuart, W. T. S. Huck, J. Genzer, M. Müller, C. Ober, M. Stamm, G. B. Sukhorukov, I. Szleifer, V. V. Tsukruk and M. Urban, *Nat. Mater.* **9**, 101 (2010).
93. J. Hu and S. Liu, *Macromolecules* **43**, 8315 (2010).
94. E. Tarif, K. Mukherjee, K. Kumbhakar, A. Barman and R. Biswas, *J. Chem. Phys.* **151**, 154902 (2019).
95. K. Kumbhakar, B. Saha, P. De and R. Biswas, *J. Phys. Chem. B* **123**, 11042 (2019).
96. T. Pradhan, P. Ghoshal and R. Biswas, *J. Chem. Sci.* **120**, 275 (2008).
97. M. L. Horng, J. A. Gardecki, A. Papazyan and M. Maroncelli, *J. Phys. Chem.* **99**, 17311 (1995).
98. M. Maroncelli and G. R. Fleming, *J. Chem. Phys.* **86**, 6221 (1987).
99. E. Tarif, J. Mondal and R. Biswas, *J. Mol. Liq.* **303**, 112451 (2020).
100. E. Tarif, B. Saha, K. Mukherjee, P. De and R. Biswas, *J. Phys. Chem. B* **123**, 5892 (2019).
101. E. Tarif, J. Mondal and R. Biswas, *J. Phys. Chem. B* **123**, 9378 (2019).
102. M. Kondo, X. Li and M. Maroncelli, *J. Phys. Chem. B* **117**, 12224 (2013).

Chapter 1

103. J. B. Birks, *Aromatic Molecules* (Wiley, New York, 1970).
104. M. Kasha, *Discuss. Faraday Soc.* **9**, 14 (1950).
105. A. Samanta, *J. Phys. Chem. B* **110**, 13704 (2006).
106. J. R. Lakowicz, *Principles of Fluorescence Spectroscopy* (Springer Science & Business Media, 2013).
107. K.-i. Itoh and T. Azumi, *J. Chem. Phys.* **62**, 3431 (1975).
108. A. P. Demchenko, *Luminescence: the journal of biological and chemical luminescence* **17**, 19 (2002).
109. M. L. Horng, J. A. Gardecki and M. Maroncelli, *J. Phys. Chem. A* **101**, 1030 (1997).
110. H. Sillescu, *J. Non-Cryst. Solids* **243**, 81 (1999).
111. D. Chakrabarti and B. Bagchi, *Phys. Rev. Lett.* **96**, 187801 (2006).
112. C. Angell, *J. Chem. Phys.* **46**, 4673 (1967).
113. C. T. Moynihan, *J. Phys. Chem.* **70**, 3399 (1966).
114. I. Chang, F. Fujara, B. Geil, G. Heuberger, T. Mangel and H. Sillescu, *J. Non-Cryst. Solids* **172**, 248 (1994).
115. M. D. Ediger, C. A. Angell and S. R. Nagel, *J. Phys. Chem.* **100**, 13200 (1996).
116. B. Guchhait, H. Al Rasid Gazi, H. K. Kashyap and R. Biswas, *J. Phys. Chem. B* **114**, 5066 (2010).
117. M. F. Shlesinger, G. M. Zaslavsky and J. Klafter, *Nature* **363**, 31 (1993).
118. R. S. Fee and M. Maroncelli, *Chem. Phys.* **183**, 235 (1994).
119. M. D. Ediger, *Annu. Rev. Phys. Chem.* **51**, 99 (2000).
120. K. L. Ngai, *Relaxation and Diffusion in Complex Systems* (Springer Science & Business Media, 2011).
121. K. V. Edmond, M. T. Elsesser, G. L. Hunter, D. J. Pine and E. R. Weeks, *Proc. Natl. Acad. Sci.* **109**, 17891 (2012).
122. P. J. Griffin, A. L. Agapov and A. P. Sokolov, *Phys. Rev. E* **86**, 021508 (2012).
123. C. A. Angell, K. L. Ngai, G. B. McKenna, P. F. McMillan and S. W. Martin, *J. Appl. Phys.* **88**, 3113 (2000).
124. J. C. Dyre, *Rev. Mod. Phys.* **78**, 953 (2006).
125. K. Kumbhakar, A. Dey, A. Mondal, P. De and R. Biswas, *Interactions and Dynamics in Aqueous Solutions of pH-Responsive Polymers: A Combined Fluorescence and Dielectric Relaxation Studies* (Ready for Submission)

Chapter 2

Main Experimental Techniques and Data Analysis Protocols

The main experimental techniques used to investigate various complex systems discussed in this Thesis are steady state UV-Vis absorption, fluorescence, time-resolved fluorescence based on time-correlated single photon counting (TCSPC) principle, and dielectric relaxation spectroscopy. This chapter mainly contains a brief description of these experimental techniques and data analysis protocols. Nearly all the complex systems reported in the Thesis are intrinsically non-fluorescent. Thus the two external fluorophores, coumarin 153 (C153)¹⁻⁴ and coumarin 343 (C343)⁵⁻⁷ have been used extensively to characterize the complex systems investigated.

2.1 Steady State UV-Vis Absorption Spectroscopy

Steady state UV-Vis absorption spectra presented in this Thesis have been recorded using UV-2600 (SHIMADZU) spectrophotometer. A schematic description of an UV-Vis absorption spectrophotometer is provided in Figure 2.1. Two light sources, tungsten and deuterium lamp are used to cover the visible and ultraviolet wavelength region, respectively. The ray coming from lamp is directed by a mirror to pass through filter and fall on monochromator. Monochromator splits beam of polychromatic light into various monochromatic rays. The light of specific wavelength is split into two parts: one is directed to reference and the other one passes through sample. The transmitted light from both reference and sample reaches the photodiode detectors. After few sequential data processing steps like signal enhancement, analog to digital conversion, the final absorption spectra is recorded.

The underlying principle of the UV-Vis absorption spectroscopy is based on the well-known Beer-Lambert Law: Absorbance (A) is proportional to the path length (l) and concentration (c) of the sample, $A = \log_{10} \frac{I_0}{I} = \epsilon cl$. Here I_0 and I are the intensity of incident and transmitted light, respectively. ϵ is the proportionality constant, known as molar extinction coefficient or molar absorptivity. All the absorption measurements discussed in this Thesis have been carried out by taking $l = 1$ cm and $c \leq 10^{-5}$ M.

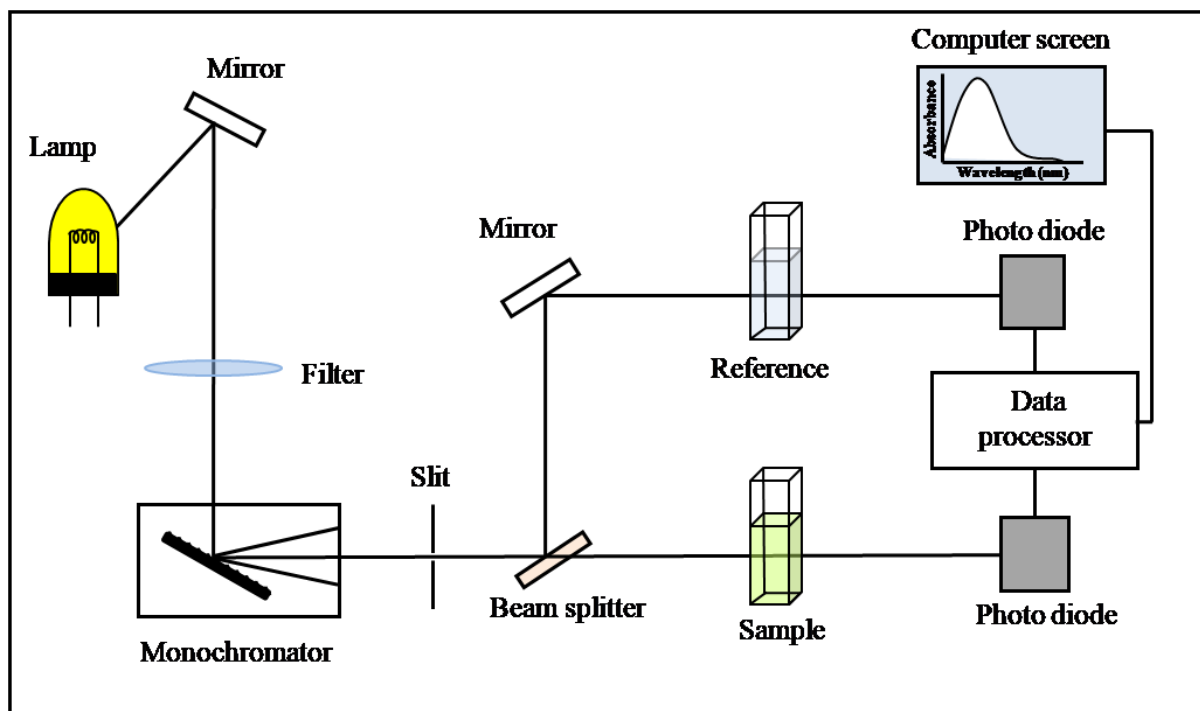


Figure 2.1: Schematic representation of an UV-Vis absorption spectrophotometer.

2.2 Steady State Fluorescence Spectroscopy

Steady state fluorescence emission measurements mentioned in the Thesis are collected in fluorimeter (Fluorolog, Jobin-Yvon, Horiba). Figure 2.2 is the schematic diagram of a fluorescence spectrophotometer. Continuous xenon (Xe) lamp is used as excitation light source. The light from Xe lamp is passed through excitation monochromator where light is split into monochromatic one and blocked the undesired wavelengths (stray light). The equipped motor in monochromators allows auto selecting and scanning wavelengths. The monochromatic light of required wavelength is used to excite the sample under investigation. The emitted light reaches to an emission monochromator placed at perpendicular direction with respect to path of excitation light. Then the fluorescence emission detected by photomultiplier tube (PMT) is projected in the computer screen after amplification and appropriate electronic conversion.

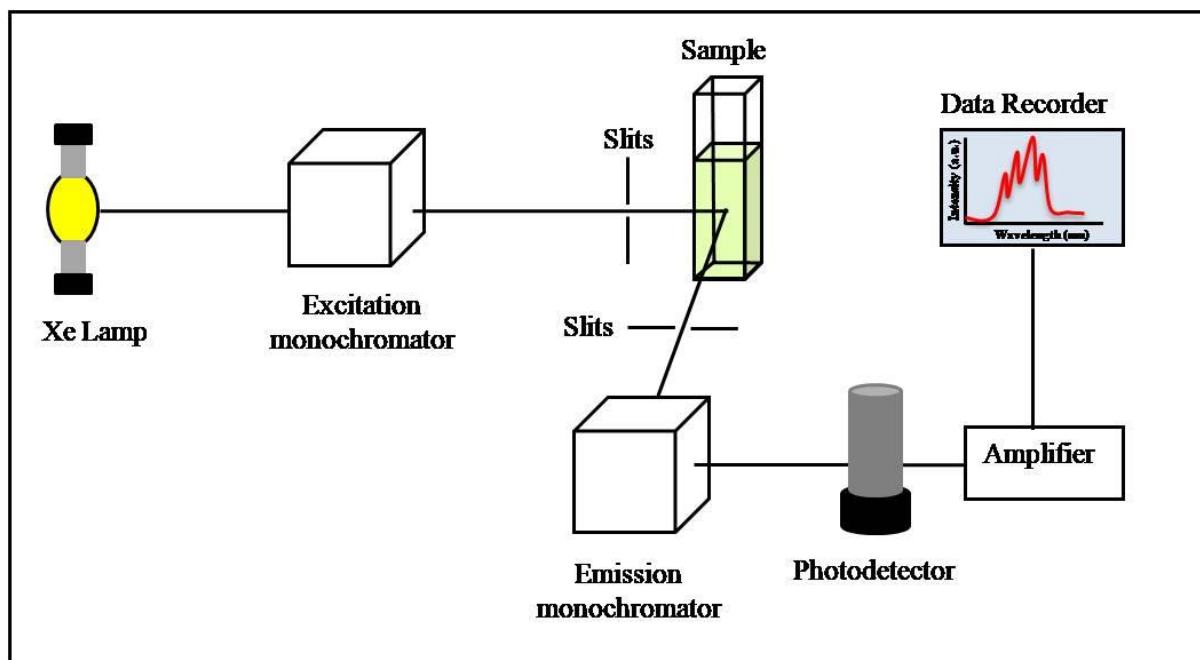


Figure 2.2: Schematic diagram of a fluorescence spectrophotometer.

2.3 Time-Resolved Fluorescence Measurement: Technique, Data Collection and Analysis

Time-resolved fluorescence studies reported in the Thesis are mainly based on time-correlated single photon counting (TCSPC) technique.⁸⁻¹⁰ We have used 409 nm and 375 nm pulsed diode lasers in the time-resolved fluorescence measurements.

2.3.1 TCSPC Technique

The LifeSpec-ps from Edinburgh Instruments (Livingston, U.K.) is used for TCSPC measurements. We have recorded time-resolved fluorescence emission data from the TCSPC setup working in reverse mode. The schematic description of a typical TCSPC set-up in reverse mode is provided in Figure 2.3. Pulsed diode laser is used to excite the sample. The first excitation pulse (vertically polarized) from the laser excites the fluorophore molecules dissolved in sample kept in a quartz cuvette. Simultaneously, a signal is generated and passed through a constant fraction discriminator (CFD). The signal due to first photon emitted by excited fluorophores passes through CFD to record its arrival time and subsequently, the signal is passed to time-to-amplitude converter (TAC) where voltage ramp is triggered. The voltage in TAC will start to increase with time until the stop signal is detected. In reverse mode of

TCSPC, the simultaneous signal is generated, when the second excitation pulse from laser excites the sample, and is passed through CFD and subsequently to TAC to stop the voltage ramp. Then, the output pulse from the TAC which is proportional to the delay time (Δt) between the start and stop signal, processes through ADC and passes to a multichannel analyzer (MCA) for the numerical value generation. The multi-times repetition of the above described process generates a histogram of the decay containing photon count and time channel in MCA.

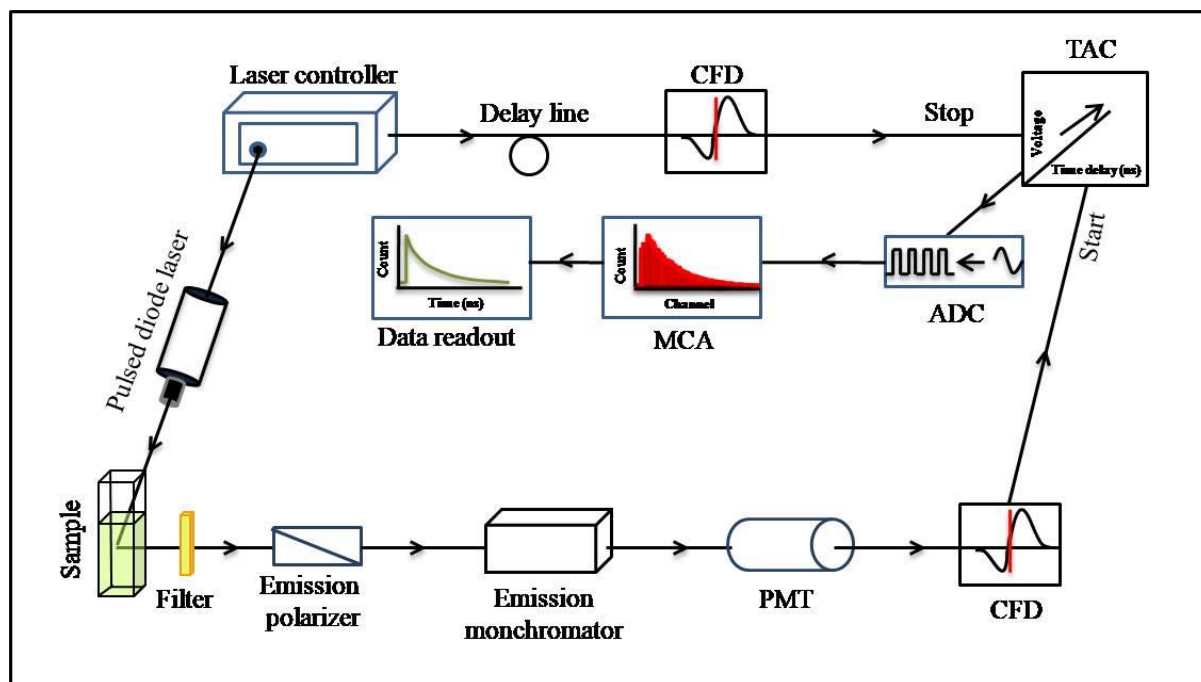


Figure 2.3: Schematic presentation of a TCSPC set-up in reverse mode.

2.3.2 Data Analysis

Before collecting the emission decay of fluorophore dissolved in the systems, instrument response function is checked with a scattering medium. For example, magic angle (54.7°) intensity decay at 409 nm of a scattering medium (water) after excitation by 409 nm laser produced the FWHM of the instrument response function (IRF) ~ 85 ps.

2.3.2.1 Solvation Dynamics

For solvation dynamics (also called Stokes shift dynamics) studies, typically 14-16 magic angle (54.7°) decays at equally spaced wavelengths across the steady state emission spectrum of fluorophore dissolved in the sample were recorded. Only decay at the blue end and rise

followed by decay at the red end wavelength with respect to peak of steady state emission spectrum is the hallmark of dynamic Stokes shift. The fluorescence decay ($N(t)$) recorded in TCSPC is a convolution of IRF ($R(t)$) and sample response ($I(t)$). Iterative reconvolution method¹¹ using a nonlinear least square analysis was used to extract $I(t)$ from $N(t)$ and $R(t)$ data.

A sum of multi-exponential function, $I(t) = \sum_{i=1}^N \alpha_i \exp(-t/\tau_i)$ where α_i and τ_i are the pre-exponential factors and characteristic lifetimes, respectively was used to fit experimental $I(t)$. Time-resolved emission spectra (TRES) were then reconstructed from the collected intensity decays for each of the systems by following the standard protocol.^{1,8,11} As discussed above, the fluorescence decays collected at various wavelengths (λ_j) were fitted with multi-exponential function,

$$I(\lambda_j, t) = \sum_{i=1}^N \alpha_i(\lambda_j) \exp(-t/\tau_i(\lambda_j)), \quad (2.1)$$

where $\alpha_i(\lambda_j)$ denotes the pre-exponential factor, with $\sum_i \alpha_i(\lambda_j) = 1$. Subsequently, a new sets of normalized intensity decays were generated so that the time integrated intensity at each wavelength was equal to the steady state intensity at that wavelength ($F(\lambda_j)$). The normalization factor is

$$H(\lambda_j) = \frac{F(\lambda_j)}{\int_0^{\infty} I(\lambda_j, t) dt} = \frac{F(\lambda_j)}{\sum_i \alpha_i(\lambda_j) \tau_i(\lambda_j)} \quad (2.2)$$

The normalization factor ($H(\lambda_j)$) was multiplied with $I(\lambda_j, t)$ to obtain the appropriate normalized function

$$I'(\lambda_j, t) = H(\lambda_j) I(\lambda_j, t) = \sum_{i=1}^N \alpha'_i(\lambda_j) \exp(-t/\tau_i(\lambda_j)), \quad (2.3)$$

where $\alpha'_i(\lambda_j) = H(\lambda_j) \alpha_i(\lambda_j)$. TRES at any wavelength and time can be calculated from $\Gamma(\lambda_j, t)$. For further analyses, the TRES were converted to frequency representation after properly weighting the intensity with λ^2 . Each of the TRES was fitted with log-normal shape function to get the continuous representation of the spectrum. The peak frequencies obtained from fitted spectra were used to construct the solvation response function $S(t)$,¹

$$S(t) = \frac{\nu(t) - \nu(\infty)}{\nu(0) - \nu(\infty)}, \quad (2.4)$$

where, $\nu(0)$, $\nu(t)$ and $\nu(\infty)$ represent the frequency (usually peak) for the reconstructed time-resolved emission spectrum at $t = 0$ (immediately after excitation), at any given instant (t), and at a sufficiently long time ($t = \infty$) enough for complete solvent relaxation, respectively. Note $S(t)$ is a normalized response function that decays from unity at $t = 0$ to zero at $t = \infty$ as the environment relaxes with time in response of instantaneous alteration of charge distribution of solute (fluorophore) due to photo-excitation. For a particular system, it is expected that $\nu(\infty)$ will be equal to the steady state emission peak frequency. However, in several cases steady state emission spectrum is slightly blue shifted compared to time-resolved emission spectrum at $t = \infty$, that is, when excited fluorophore is surrounded by completely solvent-relaxed environment. Steady state emission from excited solute with incompletely relaxed solvent environment is responsible for the observed blue shift. Subsequently, the average solvation time, $\langle \tau_s \rangle$, was obtained via time-integrating the measured $S(t)$ decays as follows:

$$\langle \tau_s \rangle = \int_0^{\infty} dt S(t) = \int_0^{\infty} dt \sum_{i=1}^n a_i \exp[-t / \tau_i] = \sum_{i=1}^n a_i \tau_i, \quad (2.5)$$

with $\sum_{i=1}^n a_i = 1$. a_i and τ_i respectively denote the amplitude and time constants related to the i -th component of $S(t)$ decay.

2.3.2.2 Rotational Dynamics

TCSPC technique is also used to study reorientational dynamics of fluorophore dissolved in the medium and time-dependent frictional profile of the medium.^{8,11,12} The underlying principle of reorientational dynamics measurements is: the photoselective excitation of those fluorophores which have absorption transition dipole parallel to the electrical vector of polarized excitation light. The emission intensity decays collected through parallel ($I_{para}(t)$) and perpendicular ($I_{perp}(t)$) emission polarizations depend on the reorientation of the excited fluorophore and vary with time. The difference between $I_{para}(t)$ and $I_{perp}(t)$ gradually decreases with time. The loss of anisotropy is utilized to extract information about reorientational dynamics provided that the lifetime of fluorophore, dissolved in a given medium, should be comparable or larger than its reorientational time. Fluorescence anisotropy measurements were performed at the peak wavelength of the steady state emission spectrum by collecting the vertically ($I_{para}(t)$), and horizontally ($I_{perp}(t)$) polarized emissions (with respect to the vertically

polarized excitation). The dynamic fluorescence anisotropy, $r(t)$, was then generated as follows⁸

$$r(t) = \frac{I_{para}(t) - I_{perp}(t)}{I_{para}(t) + 2I_{perp}(t)}. \quad (2.6)$$

The polarization characteristics of the optical set-up have important influence to the measured anisotropy. Thus, a correction is required to minimize the error originating from the instrumental preference for a specific polarization. This correction factor, G , is usually known as geometric-factor and is defined as the ratio between the transmission efficiency for vertically polarized and that of horizontally polarized light ($G = \frac{I_{para}(t)}{I_{perp}(t)}$). The geometric factor (G) is

obtained by the tail matching of vertically (parallel) and horizontally (perpendicular) polarized fluorescence emission intensity decays. Now the corrected time-resolved fluorescence anisotropy, $r(t)$, is represented as

$$r(t) = \frac{I_{para}(t) - GI_{perp}(t)}{I_{para}(t) + 2GI_{perp}(t)}. \quad (2.7)$$

The $r(t)$ so obtained was then fitted with single and multi-exponential function as

$$r(t) = r(0) \sum_i \alpha_i \exp(-t/\tau_i), \text{ with } \sum_i \alpha_i = 1, \quad (2.8)$$

where $r(0)$ is the initial anisotropy. α_i and τ_i are the amplitude and time constant of the i -th decay component. In this Thesis, we have fixed $r(0)$ at 0.376 for C153¹², 0.35 for C343⁵ and 0.38 for trans-2-[4-(dimethylamino)styryl]-benzothiazole (trans-DMASBT)¹³ while fitting the $r(t)$.

The average rotational correlation time was then estimated as follows:

$$\langle \tau_{rot} \rangle = \int_0^{\infty} dt [r(t)/r(0)] = \sum_i \alpha_i \tau_i \text{ with } \sum_i \alpha_i = 1. \quad (2.9)$$

2.4 Dielectric Relaxation Spectroscopy (DRS)

Dielectric relaxation spectroscopy (DRS) is used to explore the relaxation of macroscopic electric polarization, which is the ensemble average of dipole-dipole correlation, of a liquid in presence of frequency dependent external electric field. As orientation motion of molecular

dipoles contributes significantly to the macroscopic electric polarization, DRS becomes an important tool to get the information of collective orientational motion of dipolar liquids.¹⁴

2.4.1 General Discussion about DRS

In room temperature liquid, to reach a certain polarization, microscopic particles like molecules, ions, atoms, electrons etc. require a characteristic time $\sim 1 \mu\text{s}$ or less. If the electric field strength varies at a time period comparable with the characteristic time for particles motion, the macroscopic polarization cannot reach its equilibrium value. As a result the actual polarization value will lag behind the changing electric field. When the electric field varies slowly compared to the particle motion, the system gets enough time to reach its equilibrium polarization value.¹⁵

Maxwell's equations¹⁶ describe the interaction of electromagnetic field with matter as follows

$$\text{rot } E = -\frac{\partial}{\partial t} B \quad (2.10)$$

$$\text{rot } H = j + \frac{\partial}{\partial t} D \quad (2.11)$$

$$\text{div} D = \rho_e \quad (2.12)$$

and

$$\text{div} B = 0 \quad (2.13)$$

In the equations 2.10 to 2.13, E and H respectively represent the electric and magnetic field, D the dielectric displacement, B denotes the magnetic induction, j is the current density and density of charges is defined by ρ_e . For homogeneous, non-dispersive, isotropic material and weak electric field strength, D can be expressed by

$$D = \varepsilon^* \varepsilon_0 E, \quad (2.14)$$

where ε_0 ($8.854 \times 10^{-12} \text{ Fm}^{-1}$) is the dielectric permittivity of the free space and ε^* represents the complex dielectric function. According to Maxwell's equation, ε^* is time (or frequency) dependent when time dependent phenomena takes place within the sample. For a periodic electric field $E(t) = E_0 \exp(-i\omega t)$, where ω is the angular frequency and $i = \sqrt{-1}$, the ε^* is expressed as

$$\varepsilon^*(\omega) = \varepsilon'(\omega) - i\varepsilon''(\omega), \quad (2.15)$$

where ε' and ε'' are the real (dielectric constant) and imaginary (dielectric loss) part of the complex dielectric function, respectively.

2.4.2 Measurements of Dielectric Properties

2.4.2.1 Instruments

The dielectric measurements presented in this Thesis were measured using two instrumental set-ups. The E4990A impedance analyzer with liquid test fixture (16452A) covers frequency range from 20 Hz to 10 MHz. A schematic representation of the instrument is shown in the Figure 2.4. The 16452A and E4990A impedance analyzer use the ‘‘Capacitive Method’’ to obtain relative permittivity by measuring the capacitance of a material that is sandwiched between two parallel electrodes. Short compensation, measurement of air capacitance and subsequently capacitance of liquid sample measurements were carried out to get the complex dielectric spectra of the sample.

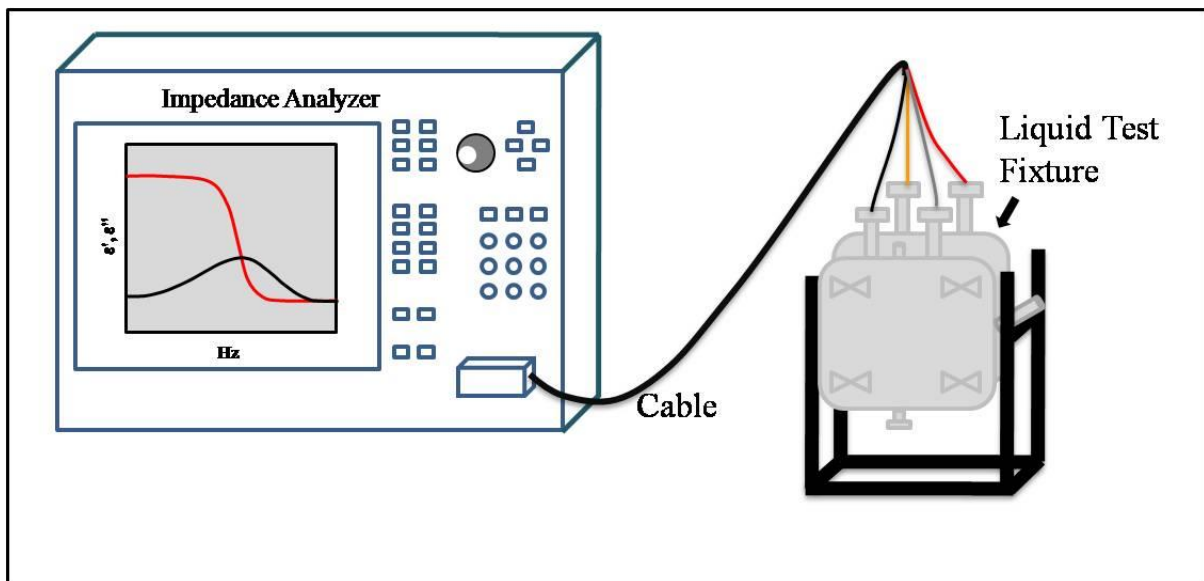


Figure 2.4: Schematic diagram of DR measurement (impedance analyzer) set-up.

PNA-L network analyzer (N5235B) combined with an open-ended coaxial probe kit (N1501A), shown in Figure 2.5, was used to perform the dielectric measurements of the sample in the frequency range of $0.2 \leq \nu / GHz \leq 50$. Calibration of the instrument has been done prior

to each set of measurement using air, shorting block and water as open, short and load respectively.

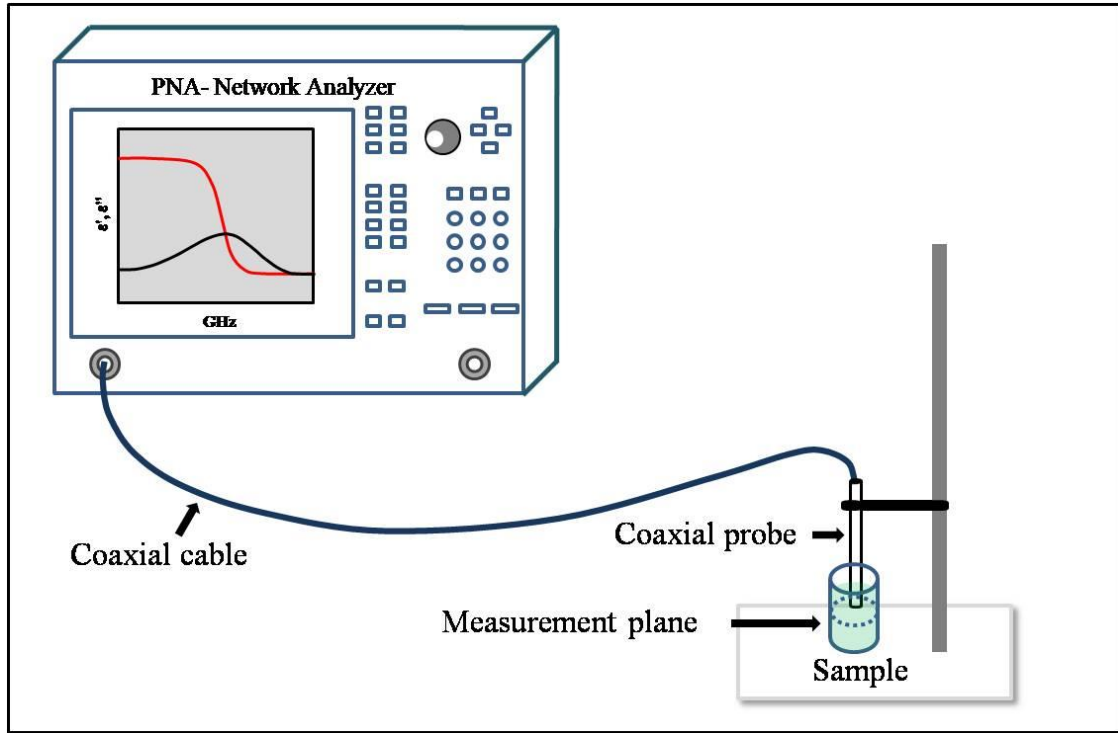


Figure 2.5: Schematic diagram of DR measurement (network analyzer) set-up.

2.4.2.2 Different Mathematical Models and Data Analysis

In order to have a comprehensive understanding about orientation polarization in the complex systems discussed in the Thesis, a number of mathematical models have been employed to define the collected DR data adequately. These models are discussed below.

2.4.2.2.1 Debye Model

Debye model is the simplest one to describe the complex dielectric response (ϵ^*) of many systems. Debye Model¹⁷ is expressed as

$$\epsilon^* = \epsilon_\infty + \frac{\Delta\epsilon}{1 + i\omega\tau_D}, \quad (2.16)$$

where dielectric strength $\Delta\epsilon$ is the difference between static dielectric constant (ϵ_s) ($\epsilon_s = \epsilon'(\omega \rightarrow 0)$) and limiting infinity frequency dielectric constant ($\epsilon_\infty = \epsilon'(\omega \rightarrow \infty)$),

$\Delta\varepsilon = \varepsilon_s - \varepsilon_\infty$. ω is the angular frequency and it is related to linear frequency ν by $\omega = 2\pi\nu$ and τ_D is the characteristic Debye relaxation time.

2.4.2.2.2 Non-Debye Model

The symmetric broadening of the dielectric function is usually described by Cole-Cole model¹⁸ which is expressed as

$$\varepsilon^* = \varepsilon_\infty + \frac{\Delta\varepsilon}{1 + (i\omega\tau_{cc})^{1-\alpha}}, \quad (2.17)$$

where the parameter α denotes a symmetric broadening of the dielectric function. α can have the any values within the range, $0 \leq \alpha < 1$ and τ_{CC} is the characteristic Cole-Cole relaxation time.

On the other hand, asymmetric broadening of the dielectric function is defined by Cole-Davidson model.^{19,20} The mathematical description of Cole-Davidson model is as below

$$\varepsilon^* = \varepsilon_\infty + \frac{\Delta\varepsilon}{(1 + i\omega\tau_{CD})^\beta}, \quad (2.18)$$

where the parameter β denotes asymmetric broadening of the dielectric function. β can have the any values within the range, $0 < \beta \leq 1$ and τ_{CD} is the characteristic Cole-Davidson relaxation time.

Havriliak-Negami (HN) function²¹ is more general model used to characterize complex dielectric response with the expression

$$\varepsilon^* = \varepsilon_\infty + \frac{\Delta\varepsilon}{(1 + (i\omega\tau_{HN})^{1-\alpha})^\beta}, \quad (2.19)$$

where α ($0 \leq \alpha < 1$) and β ($0 < \beta \leq 1$) are the parameters to define symmetric and asymmetric broadening, respectively. τ_{HN} is the characteristic relaxation time.

2.4.2.2.3 Combination of Models

The dielectric response of many real systems may be described by superposition of multi relaxation modes. In this regards, the general expression of Havriliak-Negami (HN) model is as follow

$$\varepsilon^* = \varepsilon_\infty + \sum_j \frac{\Delta\varepsilon_j}{(1 + (i\omega\tau_j)^{1-\alpha_j})^{\beta_j}}. \quad (2.20)$$

2.4.2.2.4 Data Processing

To extract physically significant information from complex dielectric response, choice of suitable mathematical models is very crucial. The quality of the fit was determined by checking both the ‘goodness-of-fit’ parameter (χ^2) and residual. χ^2 is defined as²²

$$\chi^2 = \frac{1}{2m - \ell} \sum_{i=1}^m \left[\left(\frac{\partial\varepsilon_i'}{\sigma(\varepsilon_i')} \right)^2 + \left(\frac{\partial\varepsilon_i''}{\sigma(\varepsilon_i'')} \right)^2 \right], \quad (2.21)$$

where m is the number of data triples $((\nu, \varepsilon', \varepsilon''))$, ℓ denotes the number of adjustable parameters, $\partial\varepsilon_i$ and $\sigma(\varepsilon_i)$ are the residuals and standard deviations of the individual data points, respectively.

2.4.2.2.5 Conductivity Corrections

DC conductivity of medium contributes significantly to the imaginary component of complex dielectric response. Thus conductivity correction in the complex dielectric response for a conducting sample is expressed as^{15,23}

$$\varepsilon^*(\nu) = \varepsilon'(\nu) - \left[i\varepsilon''(\nu) + \frac{i\kappa}{2\pi\varepsilon_p\nu} \right], \quad (2.22)$$

Where ν ($\nu = \frac{\omega}{2\pi}$) is the linear frequency, κ is the DC conductivity of the sample and ε_p is the permittivity of the free space.

This above mentioned conductivity correction has been employed in all the dielectric data fitting presented in the Thesis.

References

1. M. L. Horng, J. A. Gardecki, A. Papazyan and M. Maroncelli, *J. Phys. Chem.* **99**, 17311 (1995).
2. K. Kumbhakar, E. Tarif, K. Mukherjee and R. Biswas, *J. Mol. Liq.* **290**, 111225 (2019).
3. B. Guchhait, H. Al Rasid Gazi, H. K. Kashyap and R. Biswas, *J. Phys. Chem. B* **114**, 5066 (2010).
4. E. Tarif, J. Mondal and R. Biswas, *J. Phys. Chem. B* **123**, 9378 (2019).
5. S. Koley, H. Kaur and S. Ghosh, *Phys. Chem. Chem. Phys.* **16**, 22352 (2014).
6. K. Kumbhakar, B. Saha, P. De and R. Biswas, *J. Phys. Chem. B* **123**, 11042 (2019).
7. E. Tarif, B. Saha, K. Mukherjee, P. De and R. Biswas, *J. Phys. Chem. B* **123**, 5892 (2019).
8. J. R. Lakowicz, *Principles of Fluorescence Spectroscopy* (Springer Science & Business Media, 2013).
9. D. V. O'Connor and D. Phillips, in *Time Correlated Single Photon Counting* (Academic Press London, 1984).
10. M. C. Chang, S. H. Courtney, A. J. Cross, R. J. Gulotty, J. W. Petrich and G. R. Fleming, *Analytical Instrument* **14**, 433 (1985).
11. D. J. S. Birch and R. E. Imhof, *Topics in Fluorescence Spectroscopy, Vol. 1: Techniques*. (Plenum Press, New York, 1991).
12. M. L. Horng, J. A. Gardecki and M. Maroncelli, *J. Phys. Chem. A* **101**, 1030 (1997).
13. S. K. Saha, P. Purkayastha, A. B. Das and S. Dhara, *Journal of Photochemistry and Photobiology A: Chemistry* **199**, 179 (2008).
14. B. Bagchi, *Molecular Relaxation in Liquids* (Oxford University Press. New York, 2012).
15. C. J. F. Böttcher and P. Bordewijk, *Theory of Electric Polarization* (Elsevier: Amsterdam, The Netherlands, 1978).
16. J. C. Maxwell, *A Treatise on Electricity and Magnetism* (Clarendon press, 1881).
17. P. J. W. Debye, *Polar Molecules* (Chemical Catalog Company, Incorporated, 1929).
18. K. S. Cole and R. H. Cole, *J. Chem. Phys.* **9**, 341 (1941).
19. D. W. Davidson and R. H. Cole, *J. Chem. Phys.* **18**, 1417 (1950).
20. D. W. Davidson and R. H. Cole, *J. Chem. Phys.* **19**, 1484 (1951).
21. S. Havriliak and S. Negami, *Polymer* **8**, 161 (1967).

Chapter 2

22. P. R. Bevington and D. K. Robinson, *Data Reduction and Error Analysis* (McGraw-Hill, New York, 2003).

23. R. Buchner and J. Barthel, *Annu. Rep. Prog. Chem. Sect. C: Phys. Chem.* **91**, 71 (1994).

Chapter 3

Dynamics in Glucose/Glycerol Cryoprotectant System: Temperature and Composition Dependent kHz-GHz Dielectric Relaxation Spectroscopic Studies

3.1 Introduction

Various inhabitant of low temperature environment (like sea ice) including bacteria, fungi, algae, protozoa, metazoan etc.,¹ plants inhabiting harsh environments,² polar marine fish,³ some other lower vertebrates,⁴ terrestrial arthropods etc. adopt peculiar strategies to survive at extreme environment in their native habitat.⁵ Among them, some organisms are known to synthesize various metabolites including sugars, sugar alcohols for example glucose,⁴ trehalose,⁶ glycerol,⁷ fructose etc. in high level to prevent formation of ice crystals in intra and intercellular fluid during extreme cold. Such natural mechanism to cope with extreme environmental stresses are exploited in food preservation technology as well as low temperature preservation (also called cryopreservation⁸) of living cells, proteins, tissues, organs in the field of biotechnology, pharmaceuticals etc.⁹⁻¹⁵ The chemical substances used in low temperature preservation are basically known as cryoprotectants.¹⁶ Among the common cryoprotectants, glycerol, a trihydroxy alcohol, is the most utilized one by a number of organisms¹⁷⁻²⁰ as well as in cryopreservation technology.^{16,21} Glycerol is a very effective cryoprotectant agent due to its low inherent toxicity to cells²¹ and ability to maintain the structure of biological macromolecules.^{22,23} Glucose, a biocompatible and biodegradable monosaccharide, is also utilized in cryopreservation technology.²⁴ It was evident that cryopreservation efficiency improved when multi-component cryoprotectants such as trehalose/proline,²⁵ glucose/glycerol,²⁶ trehalose/glycerol¹³ were utilized instead of single component alone.^{27,28}

In low temperature preservation of live cells, tissues, organs etc., dehydration arising from intracellular ice formation causes cell death. Optimum exposure of cyoprotectants play the vital role by minimizing ice formation and reduce cell injury.⁵ Vitrification, that is, rapid cooling in order to avoid ice crystal formation by achieving a supercooled glassy state in presence of cryoprotectants at high concentrations had been proven to have more preservative efficiency

as compared to conventional cryopreservation.²⁹ Good glass forming properties of glycerol (Glass transition temperature, $T_g \sim 190$ K³⁰⁻³²) make this substance attractive in preservation technology. Due to high T_g of carbohydrates (T_g of Glucose ~ 300 K³³), they are considered as promising cryoprotectant candidates for preservation of foods, proteins and peptides.³⁴⁻³⁶ The substances with high T_g are known to have strong hydrogen bonding (H-bonding) propensity.³⁷ Henceforth, irrespective of preservation techniques (conventional cryopreservation and vitrification), H-bonding interactions of cryoprotectant agents with water and biological moieties play a vital role.³⁸⁻⁴¹ Cryoprotectant action is the result of relative preference of H-bonding interactions among cryoprotectant-cryoprotectant, cryoprotectant-water and water-water interactions.⁴⁰ A number of computer simulations have reported that cryoprotectants disrupt tetrahedral arrangement of proximal water molecules due to its steric constraints and form stable H-bonds with the proximal water molecules. While doing so, cryoprotectants decreases H-bond propensity among water molecules.⁴²⁻⁴⁵ A comprehensive knowledge about the underlying working principle of cryopreservation is therefore essential for gaining control over the cryopreservation process and improve the efficiency. A proper and system-specific choice of suitable cryoprotectants and tuning their relative proportions in solutions for achieving optimized condition is critical for solvent engineering in this domain.

Investigation of H-bond interaction of cryoprotectants with water was performed in the last few decades via various experimental and simulation techniques.^{38-40,46-50} Despite several attempts, a comprehensive insight about the impact of cryoprotectants on water H-bond network is yet to be elucidated. This lack of information demands a thorough understanding of structure, interactions, dynamics of cryoprotectants itself to generate the desired database. Dielectric and NMR relaxation studies on glycerol/DMSO mixtures,⁵¹ NMR measurements with propanol/glycerol mixtures,⁵² sugar alcohols,⁵³ and neutron scattering studies on glycerol/trehalose mixtures⁵⁴ were attempted. Time-resolved fluorescence spectroscopic measurements in combination with molecular dynamics (MD) simulations of trehalose/glycerol cryoprotectant solutions³⁰ reported solution dynamic heterogeneity (DH) at temperatures, $T=298-353$ K. It was proposed in that study that an interconnection between dynamic heterogeneity and cryopreservation properties of such systems might exist. Although DH is well studied phenomenon for supercooled system such as glycerol,⁵⁵ very less is explored about DH at around room temperature and its impact on cryopreservation. The present study is prompted by this lacunae where solution heterogeneity has been explored via broadband dielectric relaxation spectroscopy (DRS) in the frequency regime 20 Hz to 10 MHz and 200

MHz to 50 GHz. We have considered glycerol (Gly) and glucose (Glu)/glycerol (Gly) solution for this purpose.

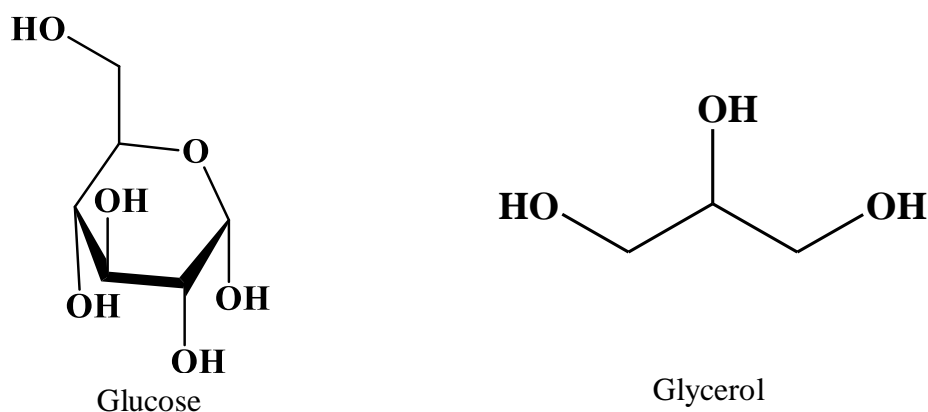
Both Glucose and glycerol have poly hydroxyl ($(-OH)_n$) groups that exhibit high propensity to form H-bonds with water and other neighbouring molecules. In this way, they can obstruct water crystallization through a disruption of the tetrahedral hydrogen bond (H-bond) network structure. This bears a strong biological relevance and possesses application potential. Gly and Glu/Gly possess extensive inter and intra species H-bonding. Since dielectric relaxation spectroscopy probes the reorientation polarization of dipolar species present in the medium in presence of frequency dependent external electric field, it is anticipated that the impact of H-bond network dynamics in Glu/Gly will be reflected in the DR response of solution. DR dynamics in Glu/Gly solutions and decoupling of relaxation from the medium viscosity is the main focus of the present study where solution DH has been explored through the analysis of the viscosity dependent average relaxation times.

Four different compositions have been chosen: 0, 5, 15 and 25 wt% of Glu in Glu/Gly solutions in the temperature range $T = 293\text{-}343$ K. Notice here that the maximum amount of Glu that is completely soluble in Gly is 25wt%.

3.2 Experimental Details

3.2.1 Materials and Sample Preparation

D-(+)-Glucose ($\geq 99.5\%$), glycerol ($\geq 99\%$) were purchased from Sigma Aldrich and used without further purification. The chemical structures of these molecules are shown in Scheme 3.1. The cryoprotectant solutions of glucose (Glu) and glycerol (Gly) were prepared via dissolving at high temperature with continuous stirring for 3-4 hrs. The detailed strategies to prepare the three experimental Glu/Gly solutions (5, 15 and 25 wt% Glu in glycerol) were as follows: for 5 wt% Glu, required amount of Glu and Gly were weighed in an airtight glass vial and heated on a hot plate (fitted with magnetic stirrer) at ~ 333 K for 3 hrs at 400 rpm in a tightly humidity-controlled environment. This produced a transparent colourless solution. Similarly, 15 and 25 wt% Glu solution have been prepared by heating at 343 K for 3 hrs and at 353 K for 4 hrs, respectively. The prepared solutions were then allowed to attain room temperature gradually before recording any experimental data.



Scheme 3.1: Chemical structures of glucose (Glu) and glycerol (Gly).

3.2.2 Density and Viscosity Coefficient Measurements

Temperature dependent densities (ρ) and viscosity coefficients (η) of Glu/Gly solutions were recorded by using an automated temperature-controlled density and sound velocity analyzer (Anton Paar, model DSA 5000) and automated micro viscometer (AMVn, Anton Paar), respectively.^{30,56} Measured η values are summarized in Table 3.1 while the ρ values are provided in Table A.a.1 (Appendix).

Table 3.1: Temperature dependent viscosity coefficients (η /cP) values of Glu/Gly solutions at various Glu concentrations.^a

T/K	Viscosity coefficients (η /cP) of Glu/Gly solutions			
	0 wt%	5 wt% Glu	15 wt% Glu	25 wt% Glu
293	1507	2143		
303	634	876	1586	
313	298	399	685	1446
318	211	280	467	954
323	153	201	327	647
328	114	148	236	448
333	87	111	172	317
338	67	84	129	230
343	53	66	98	170

^aViscosity coefficient values can be reproduced within $\pm 10\%$ of the reported values (based on limited set of measurements).

3.2.3 Refractive Index Measurements

Refractive indices of the samples were measured using an automated temperature-controlled refractometer (RUDOLPH, J357).⁵⁷ The measured refractive indices (n) are summarized in Table 3.2.

3.2.4 Data Collection and Analysis for Dielectric Relaxation Spectroscopy

Dielectric relaxation spectra of the liquid samples were recorded using two different dielectric set-ups, covering different frequency window. The E4990A impedance analyzer with liquid test fixture (16452A) covers frequency range from 20 Hz to 10 MHz. PNA-L network analyzer (N5235B) combined with an open-ended coaxial probe kit (N1501A) was used to perform the dielectric measurements of the sample in the frequency range of $0.2 \leq \nu / \text{GHz} \leq 50$. Details of measurements techniques and data analyses are the same as discussed in chapter 2 and references.⁵⁷⁻⁶² Temperature dependent DRS measurements were performed in high frequency set-up ($0.2 \leq \nu / \text{GHz} \leq 50$) only. DRS measurements in the frequency window, $\nu = 20 \text{ Hz} - 10 \text{ MHz}$, were recorded at room temperature ($\sim 300 \text{ K}$) because of inaccessibility to an appropriate temperature controller.

3.3 Results and Discussion

Temperature dependent real (ϵ') and imaginary component (ϵ'') of complex dielectric spectra in Glu/Gly solutions are represented in Figure 3.1. Multi-Debye fits required to describe the experimental DR spectra are shown (lines through the ϵ' and ϵ'' data points) in the same figure. Combination of Debye, Cole-Cole, Cole-Davidson descriptions were attempted but multi-Debye model has been found to provide the best simultaneous description for the real ($\epsilon'(\nu)$) and the imaginary ($\epsilon''(\nu)$) components of the recorded complex dielectric spectra for Glu/Gly solutions. Corresponding residuals are presented in Figure A.a.2. Note the main relaxation peaks of imaginary (the loss part) component around room temperature fall in lower frequency than 0.2 GHz which shifts gradually to the higher frequency and appears in the frequency window: $0.2 \leq \nu / \text{GHz} \leq 50$ with rise of solution temperature. A representative dielectric spectrum of Glu/Gly solutions at $\sim 300 \text{ K}$ in the broadband (kHz to GHz) frequency window is shown in Figure 3.2. Though a full experimental spectra is lacking due to non-availability of DR data in the 10-200 MHz region, a qualitative description of the full dielectric spectra covering the 1 kHz to 50 GHz range could be constructed from fit. Interestingly, dielectric studies of Glycerol in 50 MHz - 500 GHz range reported peak of imaginary component centred at $\sim 145 \text{ MHz}$ at 298 K ⁶³ which corroborates well with the relaxation peak $\sim 147 \text{ MHz}$ estimated

from fit of our experimental data points ($T \sim 298$ K) in this work. Multi-Debye fit parameters are summarized in Table 3.2 and Table 3.3. Before discussing about the impact of Glu concentration on DR dynamics of Glu/Gly solutions, relaxation dynamics of neat Gly needs to be measured first.

3.3.1 Dielectric Relaxation in Neat Gly

3-Debye fit parameters, summarized in Table 3.2 and Table 3.3 for neat Gly in the temperature range, $T = 300$ to 333 K, indicate three steps relaxation process characterizes the collected DR spectra. The main relaxation process at 300 K corresponds to a relaxation time, $\tau_1 \sim 1200$ ps. With the rise of medium temperature, the magnitude of τ_1 decreases with the relaxation amplitude remaining nearly unchanged. Similar observation has also been observed for the other two components (τ_2 and τ_3). DR response mainly probes the reorientational polarization relaxation and is therefore linked to rotational diffusion of medium dipolar molecules. Rotational diffusion time for a Gly molecule calculated via the Stokes-Einstein-Debye (SED) relation, $\tau_{rot} = \frac{3V\eta}{k_B T}$, with V being the van der Waals volume of Gly ($=86.82 \text{ \AA}^3$)⁶⁴ and η the medium viscosity (for η values, see Table 3.1), results $\tau_{DR} \sim 100$ ns at 300 K. Such a long diffusion time is approximately two orders of magnitude slower than the experimentally observed slowest time (τ_1) at this temperature. Therefore, full molecular rotation of Gly cannot account for this experimentally detected ~ 1 ns relaxation time. The question is then what could be the possible sources of multiple relaxations times that feature the recorded dielectric spectra of neat Gly?

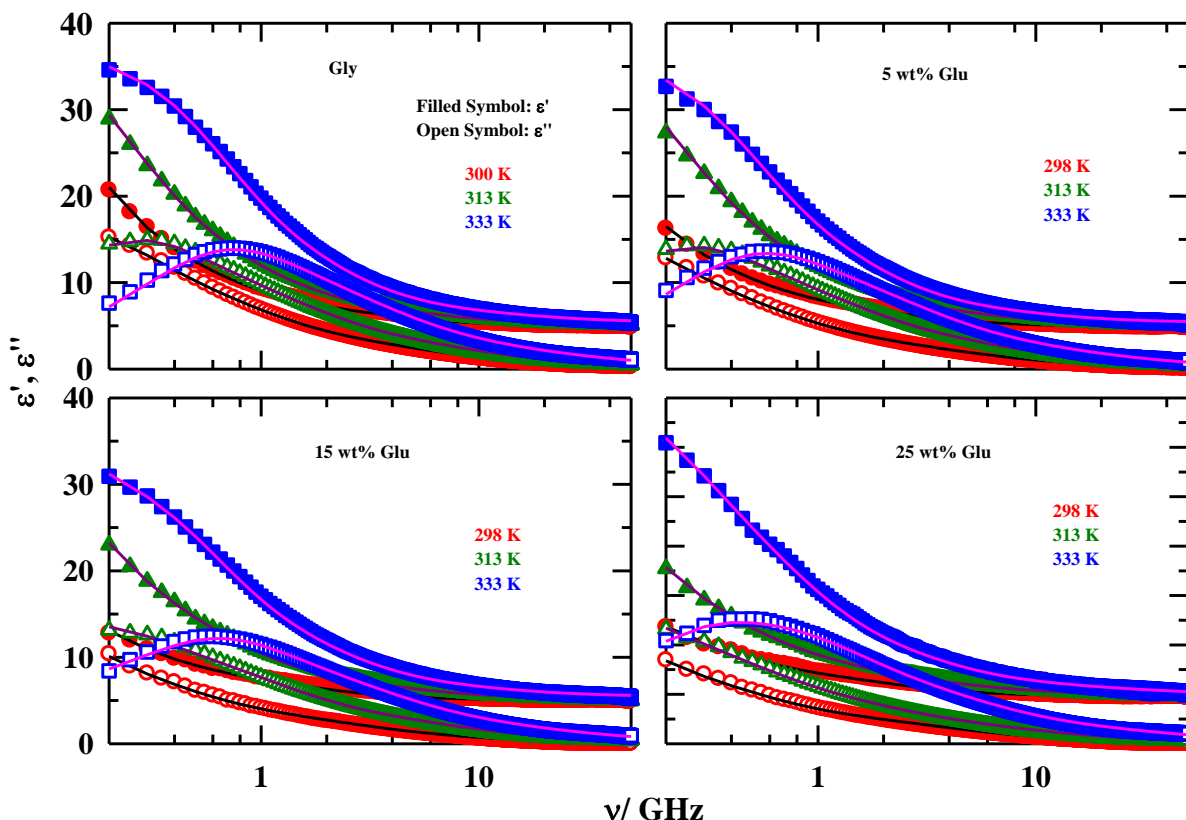


Figure 3.1: Temperature dependent real (ϵ') and imaginary (ϵ'') components of the complex dielectric spectra recorded for Glu/Gly solution at different Glu concentrations. Experimental data points are shown as symbols while lines passing through them represent multi-Debye fits. All representations are colour-coded.

3.3.1.1 Origin of DR Time Constants in Neat Gly

Fit parameters summarized in Table 3.2 suggest that the dominating DR component at 333 K is characterized by a time constant, $\tau_1 = 235$ ps. This corroborates well with the time corresponding to the peak frequency of ϵ'' spectrum ($\nu_{peak} \sim 800$ MHz), $\tau_{peak} = \frac{1}{2\pi\nu_{peak}} \sim 200$

ps, suggesting a describing of data by the corresponding fit. Highly viscous liquid glycerol possesses extensive hydrogen bond network, and it is expected that the signature of H-bond dynamics will be registered on the DR data. Temperature dependent individual DR time constants as well as the average relaxation times in glycerol exhibit Arrhenius-type temperature

dependence, $\frac{1}{\tau} = A \exp\left(-\frac{E_a}{RT}\right)$, shown in Figure 3.5 and Figure 3.6. This is generally

associated with β -relaxation process.^{63,65} Molecular dynamics simulation study⁶⁶ reported three characteristic relaxation times of H-bond network dynamics in glycerol. Among those, the time component ~ 20 ps at temperature $T=320$ K was attributed to the exchange of neighbours forming the cage structure of a molecule. Similar relaxation time constant has been observed in our DRS measurements (τ_3). A previous work⁶⁶ has suggested that glycerol molecules exhibit conformation jump dynamics with ~ 100 ps/ jump at $T\sim 320$ K. Interestingly, the DR time τ_2 obtained in the present measurements match quite well with this reported conformational jump dynamics.⁶⁶ Thus, the dielectric relaxation times, τ_2 and τ_3 obtained in our measurements are attributed to conformational jump dynamics and exchange of neighbours forming the cage structure, respectively.

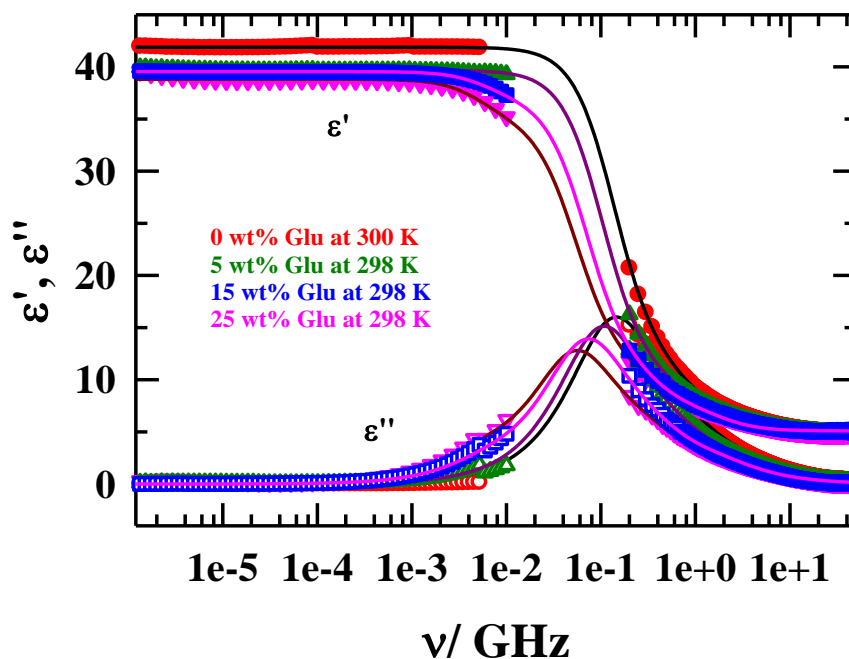


Figure 3.2: Glu concentration dependent real (ϵ') and imaginary (ϵ'') components of complex dielectric spectra in Glu/Gly solutions at ~ 298 K. Experimental data points are shown as symbols while lines going through the data points depict multi-Debye fits. All representations are colour-coded.

Now what are the possible origins of slowest DR time (τ_1) in glycerol. The slowest DR time reported for molten urea⁶⁷ was ~ 100 ps, which is close to the estimated centre-of-mass diffusion (translational motion ~ 150 ps) and the longest time component of the simulated

structural H-bond relaxation (130 ps). It was pointed out in that work that the translational diffusion through the cooperative H-bond fluctuations dynamics is coupled to the slowest DR time. MD simulation studies performed earlier⁶⁶ for neat glycerol showed a good correlation between the translational diffusion coefficient and the slowest time component (~ 500 ps at 320 K) of the hydrogen bond network dynamics. But translation diffusion time calculated for Gly molecule using the Stokes-Einstein formula, shown in Table 3.4, is much higher than the slowest DR time component in present study. Thus, the idea of DR response exclusively controlled by the centre-of-mass diffusion may not be valid. If we look at the DR study in (Acetamide+Urea+PEG) deep eutectic solvent (DES),⁶² a system that possesses an extensive H-bond network, provides the following: the second slowest relaxation time component τ_2 , arising from the reorientation coupled to H-bond dynamics, was 164 ps at 313 K. Note the medium viscosity ratio between (Acetamide+Urea+PEG) DES⁶² and glycerol (our study) at 313 K, $\frac{\eta^{Glycerol}}{\eta^{DES}} \sim 5$, while the ratio $\frac{\tau_1^{Glycerol}}{\tau_2^{DES}}$ is ~ 4 . This suggests that the most probable origin of τ_1 for neat glycerol is reorientational motion coupled to H-bond fluctuation dynamics.

3.3.1.2 Partial Viscosity Coupling of Dielectric Relaxation Dynamics in Neat Gly

With increase of temperature, the average dielectric relaxation times decrease. This is because rise in temperature decreases medium viscosity. The partial decoupling of relaxation dynamics with medium viscosity has been investigate using the power dependence relation: $\tau \propto \left(\frac{\eta}{T}\right)^p$ which results a fractional 'p' value ~ 0.7 (<1). This is shown in Figure 3.4. Interestingly, fractional viscosity dependence of relaxation times is well-known for dynamically heterogeneous systems, such as, super-cooled liquids, ionic liquids, and deep eutectic solvents.⁶⁷⁻⁷²

3.3.2 Impact of Glu Concentration (in wt%) on DR in Glu/Gly Solution

3.3.2.1 Glu Concentration Dependence

With increasing Glu concentration in Glu/Gly solutions, DR dynamics becomes slower. Figure 3.3 presents the imaginary and real components of complex dielectric spectra of Glu/Gly solutions at four different concentrations of Glu at a representative temperature (313 K). Corresponding residuals are shown in Figure A.a.3 (Appendix). Note in none of the Glu concentrations, ϵ' reaches a plateau in the low frequency limit. The relaxation peak of ϵ''

shifts toward lower frequency with increase of Glu concentration and the main relaxation peak moves further to the lower frequency regime beyond 0.2 GHz at Glu concentration 15 wt% or higher. Glu concentration dependent change of dielectric spectra at room temperature can be well understood from the kHz-GHz DR measurements, shown in Figure 3.2. The corresponding fit parameters, summarized in Table 3.3, suggest the estimated value of the static dielectric constant ϵ_s , ($\epsilon(\nu \rightarrow 0)$) decreases gradually as Glu concentration in the solution increases and the main relaxation peak shifts toward lower frequency value. Note at lower Glu concentration (5 wt%) the 3-Debye model, similar to neat Gly, adequately describes the experimental DR spectra. Further increase of Glu concentration imparts a new slow component with a time constant ~ 25 -30 ns; amplitude of this component increases with the increase of Glu concentration in solution. The other three time constants also slow down with the increase of Glu concentration as the increase of latter in solution increases the medium viscosity.

Dipolar species (Gly) reorientation coupled with structural H-bond relaxation, as observed for neat Gly, contributes to the component with a time constant of a few nanoseconds. This is the main relaxation mode in the Glu/Gly solutions. The inter-species H-bonding interaction between Gly and Glu and subsequently increased solution viscosity is manifested in lengthening of this timescale with increase of Glu concentration. Note that the amplitude of this component decreases as the wt% of Glu in Glu/Gly solution increases which not only eliminates the participation of Glu reorientation-coupled structural H-bond dynamics, but suggests also Glu-induced reduction of the corresponding dispersion amplitude. No significant impact of increasing Glu wt% on the individual amplitudes of the other two relatively faster components (τ_2 and τ_3 for neat Gly) are observed; a slowing down of these time constants is registered. MD simulations are required to fully understand the origin of these timescales in terms of H-bond fluctuation dynamics and collective single particle reorientational relaxation.

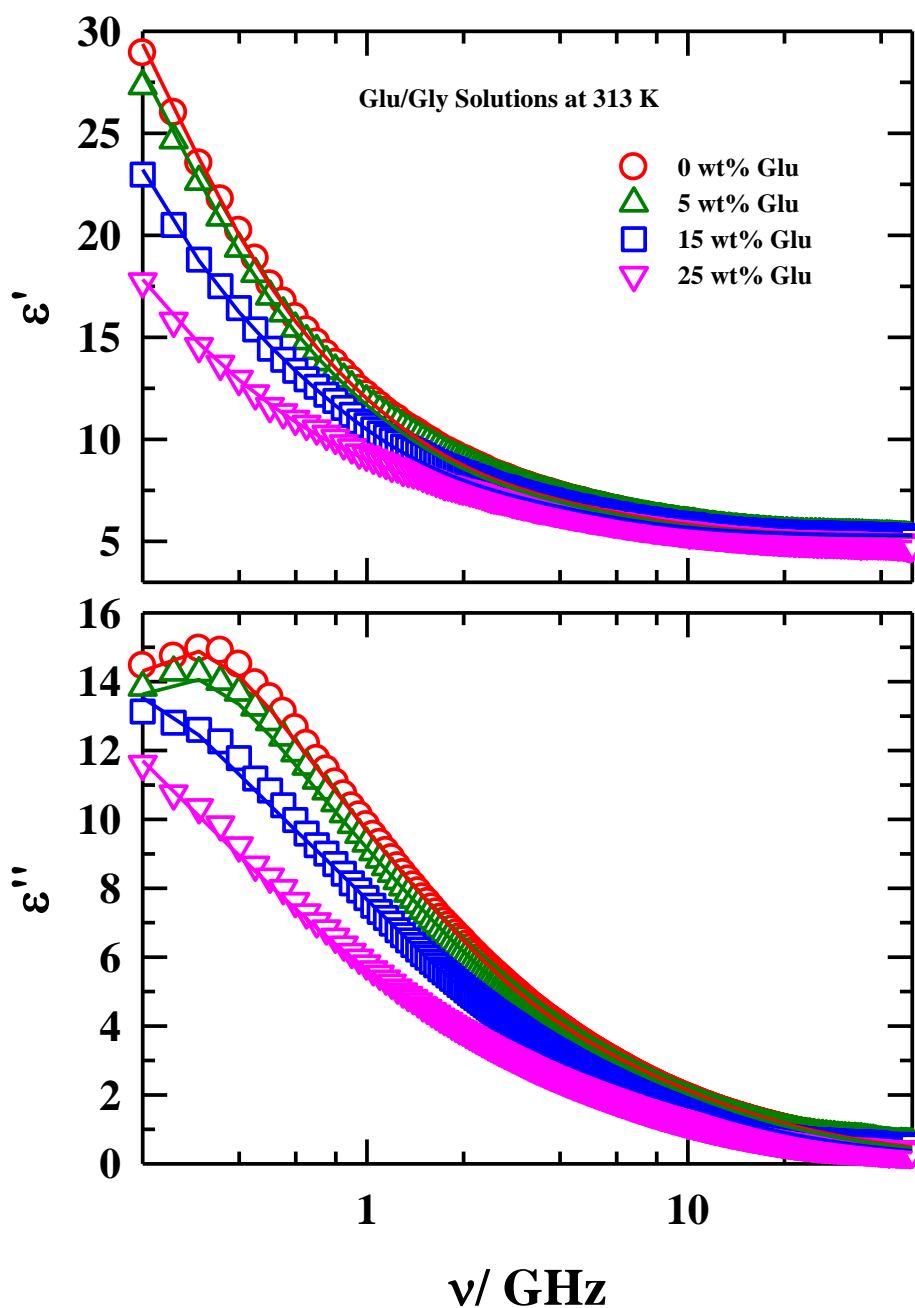


Figure 3.3: Real (ϵ') (upper panel) and imaginary (ϵ'') (lower panel) components of complex dielectric spectra for various Glu concentrations in Glu/Gly solutions at a representative temperature 313 K. Experimental data points are shown as symbols while lines going through the data points depict multi-Debye fits. All representations are colour-coded.

Now, what could be the likely origin of the slowest time constant which is a few tens of nanoseconds ($\sim 20\text{-}30$ ns)? From the concomitant increase of amplitude and magnitude of this time component as Glu wt% varies from 15 to 25, we may ascribe this component to the

restricted dynamics of Glu. To have a comprehensive understanding about the origin of this ~ 20-30 ns time component, further investigation employing NMR measurements and MD simulation are required. The emergence of such a slow relaxation mode and its Glu concentration dependence suggests that Glu/Gly system can be an efficient candidate for cryopreservation application where ‘plasticity’ of the system can be tuned rather easily.

3.3.2.2 Temperature Dependence

Impact of temperature on DR has been explored in the frequency window $0.2 \leq \nu / \text{GHz} \leq 50$ only. With rise of solution temperature, the peak frequency of $\epsilon''(\nu)$ gradually shifts towards higher value. This is shown in Figure 3.1 and can be explained in terms temperature-induced decrease of medium viscosity. The estimated values of the static dielectric constant, summarized in Table 3.2, show a decrease by ~ 10% with an increase of solution temperature by ~35 K. In the lower Glu concentration regime (~5wt%), experimental DR spectra are well described by 3-Debye model throughout the temperature range, T=298-333 K. All the three DR time constants become faster with the increase of solution temperature. Emergence of new relaxation modes in higher Glu concentrations (15 and 25 wt%), particularly at higher temperatures, demand 4-Debye fit to adequately describe the DR spectra. From the fit data summarized in Table 3.3, it can be anticipated that a slow component with a time constant longer than ~30 ns may exist in the Glu/Gly binary mixture even at lower temperature; this could not be detected simply because the relevant relaxation peak remained at a frequency lower than the low frequency accessed in the frequency window, $0.2 \leq \nu / \text{GHz} \leq 50$. With the rise of temperature solution dynamics becomes faster because of decrease in medium viscosity, allowing the slower component of the DR entering into the frequency window accessed in the present measurements. Hence it is expected that Glu concentration induced emergence of slow time component (provided in Table 3.1) will be manifested in the temperature dependent DR of this binary mixture. Similar observation of a slow relaxation mode at higher temperature (> 310 K), which was absent at a comparatively lower temperature (298 K), was also reported in highly viscous trehalose/glycerol cryoprotectant system via the fluorescence Stokes shift dynamics measurements.³⁰

Table 3.2: Multi-Debye (3-Debye/4-Debye) fit parameters of temperature dependent experimentally measured DR spectra (frequency regime: $0.2 \leq \nu/\text{GHz} \leq 50$) for various Glu concentrations in Glu/Gly solutions.^a

T/K	ϵ_s	$\Delta\epsilon_1$	τ_1 /ps	$\Delta\epsilon_2$	τ_2 /ps	$\Delta\epsilon_3$	τ_3 /ps	$\Delta\epsilon_4$	τ_4 /ps	ϵ_∞	n^2	$\langle\tau_{DR}\rangle$ /ps
Glycerol (0 wt% Glu)												
300	41.95	29.78 (81) ^b	1185	5.27 (14)	225	1.87 (5)	40	-	-	5.03		990
303	40.97	28.70 (80)	1103	5.50 (15)	215	1.83 (5)	37	-	-	4.95	2.17 0	913
308	40.91	28.07 (78)	843	5.99 (17)	174	1.77 (5)	30	-	-	5.08		691
313	40.20	26.98 (77)	642	6.30 (18)	140	1.66 (5)	25	-	-	5.26	2.16 7	522
318	39.17	26.23 (78)	492	6.18 (18)	110	1.48 (4)	20	-	-	5.27	2.16 7	402
323	37.95	25.79 (79)	380	5.69 (17)	84	1.25 (4)	14	-	-	5.22	2.16 6	315
328	38.01	25.13 (77)	306	6.11 (19)	75	1.25 (4)	13	-	-	5.52	2.16 6	251
333	37.02	24.90 (79)	235	5.58 (18)	57	1.11 (3)	8	-	-	5.43	2.16 5	196
5 wt% Glu												
298	39.96	28.24 (81)	1640	4.73 (14)	305	2.02 (6)	56	-	-	4.97		1368
303	39.5	26.87 (78)	979	5.52 (16)	201	1.93 (6)	39	-	-	5.18	2.17 7	801
308	39	26.22 (77)	828	5.87 (17)	173	1.81 (5)	32	-	-	5.10		672
313	38.56	25.33 (76)	662	6.26 (19)	147	1.74 (5)	28	-	-	5.23	2.17 5	532
318	38.02	24.24 (74)	518	6.85 (21)	123	1.62 (5)	22	-	-	5.31	2.17 5	411
323	37.66	23.89 (74)	464	6.82 (21)	113	1.56 (5)	20	-	-	5.39	2.17 5	368
328	37.29	23.81 (75)	388	6.65 (21)	94	1.38 (4)	17	-	-	5.45	2.17 4	311
333	36.62	23.60 (76)	312	6.38 (20)	75	1.23 (4)	13	-	-	5.41	2.17 4	252
15 wt% Glu												
298	39.5	28.05 (82)	2493	4.06 (12)	443	2.3 (7)	86	-	-	5.09		2090
303	39.2	25.82 (76)	1736	6.18 (18)	318	2.1 (6)	54	-	-	5.10	2.19 3	1375
308	39	24.76 (73)	1243	6.95 (21)	246	2.01 (6)	42	-	-	5.28		966
313	38.7	24.09 (72)	1025	7.54 (23)	201	1.8 (5)	32	-	-	5.27	2.19 2	786

Chapter 3

318	38.4	16.21 (49)	1138	13.17 (40)	318	3.29 (10)	58	0.49 (1)	10	5.24	2.19 2	689
323	38	15.79 (48)	918	13.01 (40)	276	3.32 (10)	54	0.52 (2)	9	5.36	2.19 1	560
328	37.5	10.62 (33)	942	16.33 (51)	291	4.09 (13)	66	0.89 (3)	15	5.57	2.19 0	471
333	37	5.66 (18)	1226	20.01 (63)	250	4.87 (15)	56	0.98 (3)	10	5.48	2.19 0	388
25 wt% Glu												
298	38.80	27.47 (81)	3250	-	-	4.47 (13)	432	2.01 (6)	69	4.86		2693
303	38.50	26.44 (79)	2634	-	-	5.24 (15)	365	1.97 (6)	53	4.85	2.21 1	2139
308	38.25	23.86 (71)	2217	6.02 (18)	493	2.37 (7)	119	1.17 (4)	30	4.83		1672
313	38.00	23.12 (70)	1693	6.37 (19)	382	2.49 (8)	94	1.06 (3)	24	4.97	2.21 0	1266
318	37.80	21.53 (66)	1387	7.72 (24)	314	2.69 (8)	67	0.77 (2)	16	5.09	2.21 0	996
323	37.65	16.67 (51)	1180	11.12 (34)	337	3.49 (11)	79	1.20 (4)	19	5.17	2.20 9	726
328	37.26	15.05 (47)	984	12.08 (38)	283	3.73 (12)	65	1.08 (3)	15	5.32	2.20 9	578
333	37.07	16.59 (52)	570	11.42 (36)	172	3.17 (10)	38	0.82 (2)	6	5.07	2.20 8	362

^aIndividual amplitudes and time constants can be reproduced within $\pm 5\%$ of the reported values.

^bNumber in parenthesis indicates dispersion amplitude of a given dispersion step in percentage.

Table 3.3: Multi-Debye (3-Debye/4-Debye) fit parameters of experimentally observed dielectric data (kHz-GHz frequency) for various Glu concentrations in Glu/Gly solutions at ~ 298 K.

wt% of Glu	T/K	ϵ_s	$\Delta\epsilon_1$	τ_1 /ps	$\Delta\epsilon_2$	τ_2 /ps	$\Delta\epsilon_3$	τ_3 /ps	$\Delta\epsilon_4$	τ_4 /ps	ϵ_∞	$\langle\tau_{DR}\rangle$ /ps
0	300	41.88	-	-	30.08 (82)	1160	4.97 (13)	211	1.80 (5)	39	5.02	981
5	300	39.65	-	-	28.75 (83)	1541	4.04 (12)	262	1.89 (5)	54	4.97	1313
15	298	39.54	2.56 (7)	25510	25.72 (75)	2256	3.85 (11)	442	2.32 (7)	86	5.09	3532
25	298	38.82	3.90 (12)	29201	23.24 (68)	2926	4.75 (14)	470	2.07 (6)	70	4.86	5564

If we closely follow Table 3.1 and Table 3.2, the prominent anomaly between temperature induced variations of viscosity and the average DR time can be observed which is well summarized in Table A.a.4 (Appendix). Extent of such decoupling can be immediately quantified from the temperature-reduced viscosity ($\frac{\eta}{T}$) dependence of DR time according to

$\tau \propto \left(\frac{\eta}{T}\right)^p$ relation where a departure of ‘ p ’ from unity (according to the hydrodynamic prediction $p=1$) is considered as a signature of decoupling. Figure 3.4 illustrates the decoupling

of $\langle\tau_{DR}\rangle$ with $\frac{\eta}{T}$ in double logarithmic fashion along with linear fits throughout the measured

data. Note that in these Glu/Gly solutions, the value of p ranges between ~ 0.5 and ~ 0.8 depending upon Glu wt% in the solutions. A global fit taking all the measured data points (which includes data at all Glu concentrations and temperatures considered) produces a value for the fraction power $p \sim 0.6$. Fractional viscosity dependence of DR time was reported in (Acetamide+Urea)⁶⁷ and (Acetamide+Urea+PEG) DES⁶² and interpreted in terms of temporal heterogeneity of the medium. Solvation times, explored via fluorescence Stokes shift dynamics in various media including DESs,^{56,73} molten mixtures,⁷¹ cryoprotectant solutions³⁰ etc. registered such a partial viscosity decoupling near room temperature. Note that in deeply supercooled liquids fractional viscosity dependence of diffusive time scales is a common observation and is explained in terms of temporal heterogeneity.^{68-72,74-77} Following this, fraction power ($p \sim 0.6$) obtained in the present DR measurements is attributed to the presence of substantial dynamic heterogeneity in Glu/Gly cryoprotectant solutions.

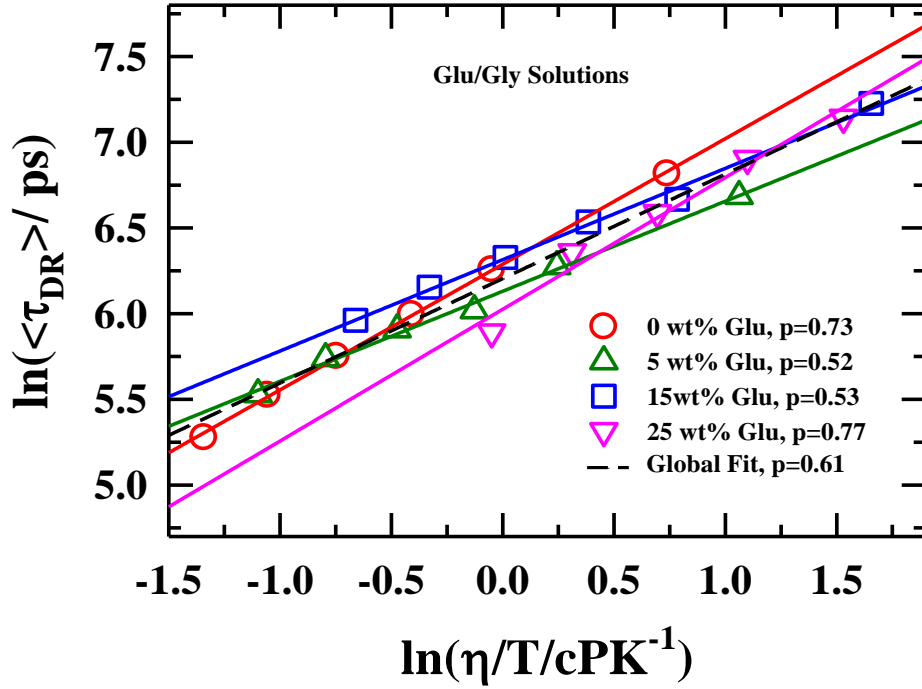


Figure 3.4: Temperature-reduced viscosity $\left(\frac{\eta}{T}\right)$ dependence of the average DR time, $\langle \tau_{DR} \rangle$ at various wt% of Glu in Glu/Gly solutions. Solid lines passing through the data points represent fits. Different colours have been used to denote different wt% of Glu in this binary mixture.

As discussed before, the DR time constants in neat Gly follow Arrhenius-type temperature dependence in the range $T = 300\text{--}333$ K. Consequently, attempts have been made to estimate the activation energies (E_a) associated with DR times in Glu/Gly solutions from the respective temperature-dependent DR measurements. Arrhenius-type dependencies have been found for both $\langle \tau_{DR} \rangle$ and η . This is presented in Figure 3.6. Note that the activation energies associated with medium viscosity, ($E_a^\eta \sim 60$ kJmol⁻¹) is ~ 1.5 times larger than those associated with $\langle \tau_{DR} \rangle$ ($E_a^{DR} \sim 40$ kJmol⁻¹). Interestingly, E_a^η obtained from Arrhenius temperature dependencies of experimentally measured macroscopic viscosity η corroborates well with the estimated activation energy, $(E_a^\eta)^{est}$ ($(E_a^\eta)^{est} \sim 65$ kJmol⁻¹) according to $(E_a^\eta)^{est} = \frac{E_a^{DR}}{p^{DR}}$ ⁷². Here E_a^{DR} and p^{DR} are DR activation energy and fractional power obtained in Figure 3.4, respectively). This confirms that the relaxation dynamics probed via DR measurements in these Glu/Gly

cryoprotectant solutions is partially decoupled from the frictional resistance arising from the medium viscosity. This provides further support to the view of temporal heretogeneity of these Glu/Gly solutions.

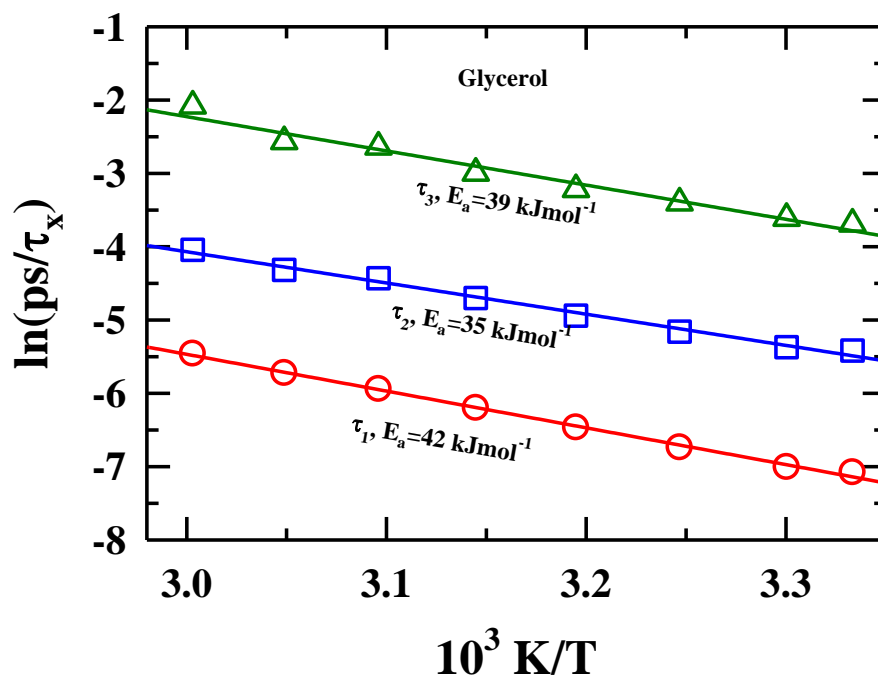


Figure 3.5: Arrhenius-type temperature dependence of individual DR times (τ_x) measured for glycerol. Solid lines passing through the data points represent the linear fits. Different colours have been used for individual time constants. Estimated activation energies have been mentioned.

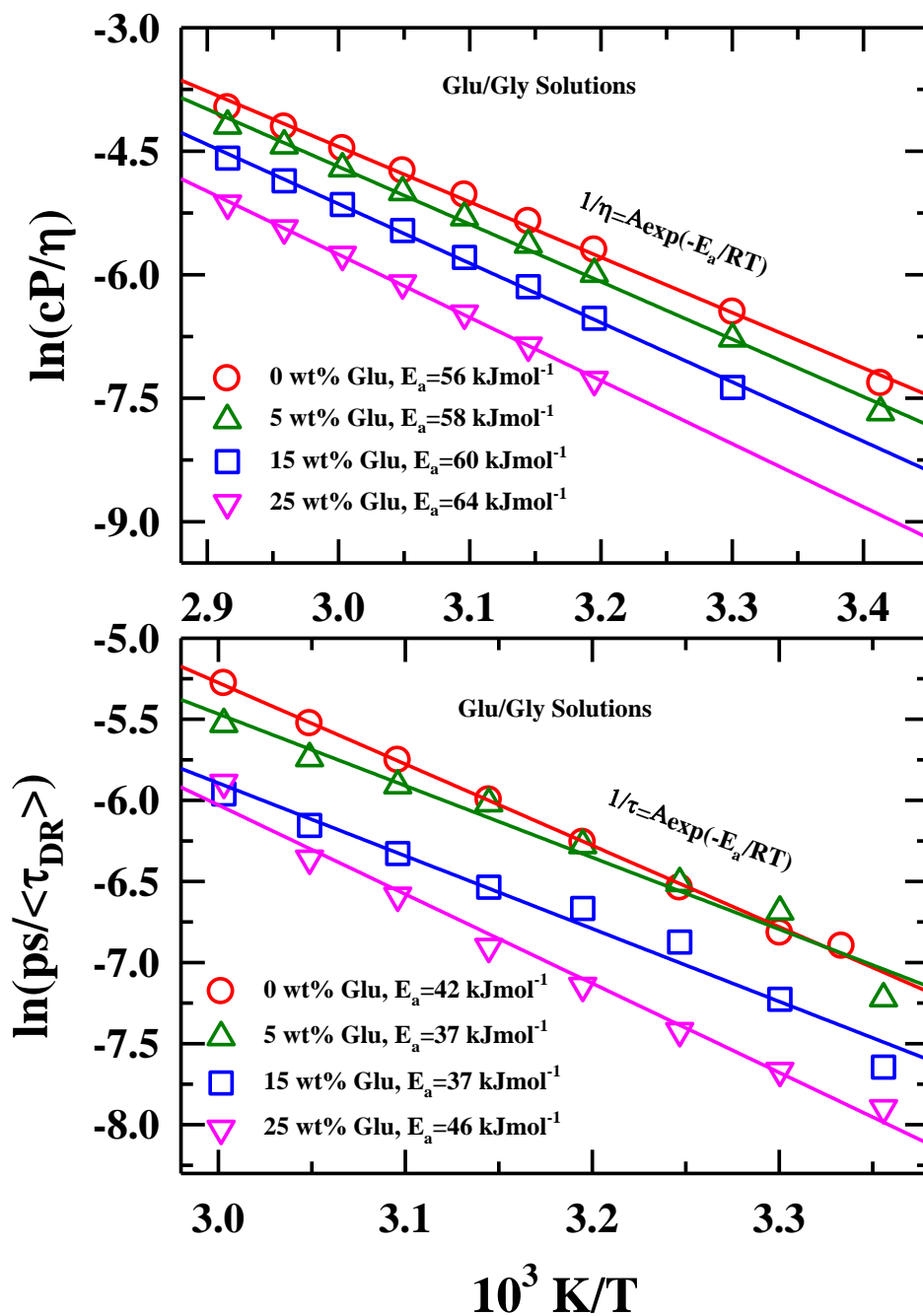


Figure 3.6: Arrhenius-type temperature dependence of medium viscosity (upper panel) and average DR time ($\langle\tau_{DR}\rangle$) (lower panel) for Glu/Gly solutions. Estimated activation energies at various wt% of Glu in Glu/Gly solutions are shown. Solid lines passing through the data points represent linear fits. Different colours have been used for various wt% of Glu.

Table 3.4: Estimated hydrodynamic molecular rotation time ($\tau_{rot} = \frac{3V\eta}{k_B T}$) of Gly at 313 K using Stokes-Einstein-Debye (SED) relation for dielectric relaxation and translation time ($\tau_{trans} = \frac{\sigma^2}{D_{trans}}$, where σ denotes the diameter of diffusing species with diffusion constant $D_{trans} = \frac{k_B T}{6\pi\eta R}$ and $R = \frac{\sigma}{2}$) according to Stokes-Einstein (SE) relation. The viscosity (η) at T=313 K is 298 cP (Table 3.1) and van der Waals volume (V) of Gly, estimated from Reference 42 is 86.82 Å³.

Species	τ_{rot} / ns	τ_{trans} / ns
Glycerol	17.97	107.82

3.4 Conclusion

To summarize, the present DR spectroscopic measurements have revealed pronounced temporal heterogeneity in the Glu/Gly cryoprotectant mixtures in the temperature range T = 300-333 K. A significant slowing down of DR time with increasing Glu concentration in Glu/Gly solutions has been detected along with the emergence of a much slower component (with time constant ~ 20-30 ns) in the higher Glu concentration region (> 5 wt% Glu in Glu/Gly solutions). Due to emergence of such a slow dynamics for higher Glu wt% (~ 15 wt% and more) in the current solutions, Glu/Gly systems may be useful in designing more efficient cryoprotectant media. Temperature and composition dependent DR measurements covering KHz-THz frequency window are required for further exploration of a possible interconnection between dynamic heterogeneity and cryopreservation efficiency of these and other cryoprotectant systems. Strong spatio-temporal heterogeneity reported already for trehalose/glycerol cryoprotectant solutions³⁰ motivates such a study for these systems employing steady state and time-resolved fluorescence emission spectroscopic measurements.

References

1. C. Krembs, H. Eicken, K. Junge and J. Deming, *Deep Sea Res. Part I Oceanogr. Res. Pap.* **49**, 2163 (2002).
2. U. Bechtold, *Front. Plant Sci.* **9**, 543 (2018).
3. C. Verde, D. Giordano and G. di Prisco, *IUBMB life* **60**, 29 (2008).
4. J. P. Costanzo, R. E. Lee and P. H. Lortz, *J. Exp. Biol.* **181**, 245 (1993).
5. B. J. Fuller, *CryoLetters* **25**, 375 (2004).
6. O. Kandror, A. DeLeon and A. L. Goldberg, *Proc. Natl. Acad. Sci.* **99**, 9727 (2002).
7. M. R. Michaud and D. L. Denlinger, *J. Comp. Physiol. B* **177**, 753 (2007).
8. D. E. Pegg, *Semin. Reprod. Med.* **20**, 005 (2002).
9. C. Paiva and A. D. Panek, *Biotechnol Annu Rev* **2**, 293 (1996).
10. J. H. Auh, H. G. Lee, J. W. Kim, J. C. Kim, H. S. Yoon and K. H. Park, *J. Food Sci.* **64**, 418 (1999).
11. J. Kapla, B. Stevansson and A. Maliniak, *J. Phys. Chem. B* **120**, 9621 (2016).
12. C. Olsson, H. n. Jansson and J. Swenson, *J. Phys. Chem. B* **120**, 4723 (2016).
13. M. T. Cicerone and C. L. Soles, *Biophys. J.* **86**, 3836 (2004).
14. T. Eto, R. Takahashi, T. Kamisako, K. Hioki and Y. Sotomaru, *Cryobiology* **68**, 147 (2014).
15. Z. A. Muchlisin, W. N. Nadiah, N. Nadiya, N. Fadli, A. Hendri, M. Khalil and M. N. Siti-Azizah, *Czech J. Anim. Sci.* **60**, 10 (2015).
16. S. Bhattacharya, in *Cryopreservation Biotechnology in Biomedical and Biological Sciences* 2018.
17. J. R. Layne Jr, *J. Exp. Zool.* **283**, 221 (1999).
18. S. Izawa, M. Sato, K. Yokoigawa and Y. Inoue, *Appl. Microbiol. Biotechnol.* **66**, 108 (2004).
19. J. M. Lewis, K. V. Ewart and W. R. Driedzic, *Physiol. Biochem. Zool.* **77**, 415 (2004).
20. Y. Izumi, S. Sonoda, H. Yoshida, H. V. Danks and H. Tsumuki, *J. Insect Physiol.* **52**, 215 (2006).
21. G. D. Elliot, S. Wang and B. J. Fuller, *Cryobiology* **76**, 74 (2017).
22. P. R. Davis-Searles, A. J. Saunders, D. A. Erie, D. J. Winzor and G. J. Pielak, *Annu. Rev. Biophys. Biomol. Struct.* **30**, 271 (2001).
23. R. Sousa, *Acta Crystallogr. Sect. D: Biol. Crystallogr.* **51**, 271 (1995).

24. Y. A. Lee, Y. H. Kim, S. J. Ha, B. J. Kim, K. J. Kim, M. S. Jung, B. G. Kim and B. Y. Ryu, *Fertil. Steril.* **101**, 1165 (2014).
25. A. S. Rudolph and J. H. Crowe, *Cryobiology* **22**, 367 (1985).
26. M. De los Reyes, L. Saenz, L. Lapierre, J. Crosby and C. Barros, *Vet. Rec.* **151**, 477 (2002).
27. F. Guo and J. M. Friedman, *J. Phys. Chem. B* **113**, 16632 (2009).
28. L. M. Sasnoor, V. P. Kale and L. S. Limaye, *Transplantation* **80**, 1251 (2005).
29. W. F. Rall and G. M. Fahy, *Nature* **313**, 573 (1985).
30. S. Indra and R. Biswas, *J. Phys. Chem. B* **120**, 11214 (2016).
31. W. Zheng and S. L. Simon, *J. Chem. Phys.* **127**, 194501 (2007).
32. C. T. Moynihan, S. N. Crichton and S. M. Opalka, *J. Non-Cryst. Solids* **131**, 420 (1991).
33. A. Simperler, A. Kornherr, R. Chopra, P. A. Bonnet, W. Jones, W. D. S. Motherwell and G. Zifferer, *J. Phys. Chem. B* **110**, 19678 (2006).
34. L. Slade, H. Levine and J. E. Kinsella, *Kinsella, J. Ed* (1995).
35. F. Franks, *J. Solution Chem.* **24**, 1093 (1995).
36. C. A. Angell, R. D. Bressel, J. L. Green, H. Kanno, M. Oguni and E. J. Sare, *Water in Foods*, 115 (1994).
37. C. A. Angell, *Chem. Rev.* **102**, 2627 (2002).
38. J. L. Dashnau, N. V. Nucci, K. A. Sharp and J. M. Vanderkooi, *J. Phys. Chem. B* **110**, 13670 (2006).
39. T. Nash, *Cryobiology* **46**, 179 (1966).
40. R. J. Fort and W. R. Moore, *Trans. Faraday. Soc.* **61**, 2102 (1965).
41. L. Weng, S. L. Stott and M. Toner, *Annu. Rev. Biomed. Eng.* **21**, 1 (2019).
42. S. L. Lee, P. G. Debenedetti and J. R. Errington, *J. Chem. Phys.* **122**, 204511 (2005).
43. P. B. Conrad and J. J. de Pablo, *J. Phys. Chem. A* **103**, 4049 (1999).
44. G. Bonanno, R. Noto and S. L. Fornili, *J. Chem. Soc., Faraday Trans.* **94**, 2755 (1998).
45. C. Chen, W. Z. Li, Y. C. Song and J. Yang, *J. Mol. Liq.* **146**, 23 (2009).
46. S. E. McLain, A. K. Soper and A. Luzar, *J. Chem. Phys.* **124**, 074502 (2006).
47. L. Dougan, S. P. Bates, R. Hargreaves, J. P. Fox, J. Crain, J. L. Finney, V. Reat and A. K. Soper, *J. Chem. Phys.* **121**, 6456 (2004).
48. S. E. McLain, A. K. Soper, A. E. Terry and A. Watts, *J. Phys. Chem. B* **111**, 4568 (2007).
49. S. G. Chou, A. K. Soper, S. Khodadadi, J. E. Curtis, S. Krueger, M. T. Cicerone, A. N. Fitch and E. Y. Shalaev, *J. Phys. Chem. B* **116**, 4439 (2012).
50. S. E. Pagnotta, S. E. McLain, A. K. Soper, F. Bruni and M. A. Ricci, *J. Phys. Chem. B* **114**, 4904 (2010).

51. M. Flämig, L. Gabrielyan, R. Minikejew, S. Markarian and E. A. Rössler, *Phys. Chem. Chem. Phys.* **22**, 9014 (2020).
52. M. Pöschl and H. G. Hertz, *J. Phys. Chem.* **98**, 8195 (1994).
53. A. Döß, M. Paluch, H. Sillescu and G. Hinze, *Phys. Rev. Lett.* **88**, 095701 (2002).
54. R. Busselez, R. Lefort, M. Guendouz, B. Frick, O. Merdrignac-Conanec and D. Morineau, *J. Chem. Phys.* **130**, 214502 (2009).
55. S. A. Mackowiak, T. K. Herman and L. J. Kaufman, *J. Chem. Phys.* **131**, 244513 (2009).
56. E. Tarif, J. Mondal and R. Biswas, *J. Phys. Chem. B* **123**, 9378 (2019).
57. K. Mukherjee, A. Das, S. Choudhury, A. Barman and R. Biswas, *J. Phys. Chem. B* **119**, 8063 (2015).
58. C. J. F. Böttcher and P. Bordewijk, *Theory of Electric Polarization* (Elsevier: Amsterdam, The Netherlands, 1978).
59. F. Kremer and A. Schönhal, *Broadband dielectric spectroscopy* (Springer Science & Business Media, 2002).
60. P. R. Bevington and D. K. Robinson, *Data Reduction and Error Analysis* (McGraw-Hill, New York, 2003).
61. K. Mukherjee, A. Barman and R. Biswas, *J. Mol. Liq.* **222**, 495 (2016).
62. K. Mukherjee, E. Tarif, A. Barman and R. Biswas, *Fluid. Phase. Equilib.* **448**, 22 (2017).
63. A. Charkhesht, D. Lou, B. Sindle, C. Wen, S. Cheng and N. Q. Vinh, *J. Phys. Chem. B* **123**, 8791 (2019).
64. Y. H. Zhao, M. H. Abraham and A. M. Zissimos, *J. Org. Chem.* **68**, 7368 (2003).
65. A. Anopchenko, T. Psurek, D. VanderHart, J. F. Douglas and J. Obrzut, *Phys. Rev. E* **74**, 031501 (2006).
66. R. Chelli, P. Procacci, G. Cardini and S. Califano, *Phys. Chem. Chem. Phys.* **1**, 879 (1999).
67. K. Mukherjee, S. Das, E. Tarif, A. Barman and R. Biswas, *J. Chem. Phys.* **149**, 124501 (2018).
68. M. D. Ediger, C. A. Angell and S. R. Nagel, *J. Phys. Chem.* **100**, 13200 (1996).
69. C. A. Angell, *J. Chem. Phys.* **46**, 4673 (1967).
70. M. D. Ediger, *Annu. Rev. Phys. Chem.* **51**, 99 (2000).
71. B. Guchhait, H. Al Rasid Gazi, H. K. Kashyap and R. Biswas, *J. Phys. Chem. B* **114**, 5066 (2010).
72. B. Guchhait, S. Daschakraborty and R. Biswas, *J. Chem. Phys.* **136**, 174503 (2012).
73. E. Tarif, J. Mondal and R. Biswas, *J. Mol. Liq.* **303**, 112451 (2020).
74. H. Sillescu, *J. Non-Cryst. Solids* **243**, 81 (1999).

Chapter 3

75. I. Chang, F. Fujara, B. Geil, G. Heuberger, T. Mangel and H. Sillescu, *J. Non-Cryst. Solids* **172**, 248 (1994).
76. C. T. Moynihan, *J. Phys. Chem.* **70**, 3399 (1966).
77. D. Chakrabarti and B. Bagchi, *Phys. Rev. Lett.* **96**, 187801 (2006).

Chapter 4

Spatio-Temporal Heterogeneity in Glucose/Glycerol Cryoprotectant System: Probe Dependent Fluorescence Spectroscopic Study

4.1 Introduction

Cryoprotectants have now become indispensable for low-temperature preservation of living cells, tissues, organs, proteins etc.¹ Cryoprotectants are the substances added to living cells, tissues etc. prior to low-temperature preservation (cryopreservation) to achieve higher post-thaw survival rate.² Importance of cryoprotectants in preservation technology has been inspired by natural mechanism adopted by living systems. For example, synthesis of different osmolytes, such as, sugars, polyalcohols, antifreeze proteins etc. in high concentration have been found to be carried by living bodies in order to survive in harsh environments, ranging from extreme cold, high salinity to sharp and large temperature change and drought-like situations.³⁻¹¹ Such natural mechanism to cope with extreme environmental stress are exploited in food preservation as well as low temperature preservation (cryopreservation¹²) of living cells, proteins, tissues, organs in the field of biotechnology, pharmaceuticals etc.¹³⁻¹⁹ Glycerol was first used in cryopreservation in 1949.²⁰ Cryoprotectants increase the viability of preserved substances mainly via decreasing free water (accessible to form ice crystal) in intracellular or extracellular fluid depending on individual physicochemical properties of cryoprotectants.^{21,22} Generally, low molecular weight substances, such as, glycerol, ethylene glycol, propylene glycol, methanol etc. act as intracellular cryoprotectant agents (CPA) while high molecular weight glucose, sucrose, trehalose etc. function as extracellular agents.²³

Vitrification, that is, rapid cooling to avoid ice crystal formation by achieving a glassy state in presence of high concentrated cryoprotectant formulation had been proven to have more preservative efficiency as compared to conventional cryopreservation.²⁴ Glass formation can effectively slow down large-scale molecular transport which in turn enhances the preservation time.^{25,26} Thus the substances possessing high glass transition temperature (T_g), for example, carbohydrates (T_g of Glucose ~ 300 K²⁷) are considered as promising cryoprotectant candidates for preservation of foods, proteins and peptides.²⁸⁻³⁰ Several groups suggested that high T_g of carbohydrates play the primary role for their protein preservation efficiency.³¹⁻³⁵ Though an

alternative perspective on mechanism of protein preservation that includes importance of strong H-bond interaction of carbohydrates with protein has also been claimed.^{36,37} A strong glass-forming liquid has been found to enhance protein stability.³⁸ One can therefore expect that glucose (carbohydrate with high $T_g \sim 300$ K), in combination with glycerol (good glass forming liquid, $T_g \sim 190$ K³⁹⁻⁴¹), may act as a suitable preserving formulation. It is evident that cryopreservation efficiency can be improved when multi-component cryoprotectants, such as, trehalose/proline,⁴² glucose/glycerol,⁴³ trehalose/glycerol¹⁷ are utilized instead of single component alone.^{44,45}

It is well known that host solvent (CPA) molecules strongly affect the structure and dynamics of biomolecules and also play an important role to prevent intra- and extra-cellular ice crystallization.⁴⁶⁻⁴⁹ This crystallization process is strongly coupled to the microscopic interaction and dynamics of the host cryoprotectants solution.⁴¹ Moreover owing to inherent glassy nature of these cryoprotectants formulation, it can be anticipated that the intrinsically heterogeneous nature of these systems will exercise pronounced control over interaction and dynamics.⁵⁰⁻⁵⁷ Therefore, study of spatio-temporal heterogeneity in cryoprotectants solutions provides an opportunity to gain deeper knowledge of these technologically important media which may help in engineering new cryoprotectants for specific applications.

Dielectric and NMR relaxation measurements with glycerol/DMSO mixtures,⁵⁸ NMR relaxation measurements with propanol/glycerol mixtures,⁵⁹ sugar alcohols,⁶⁰ neutron scattering measurements with glycerol/trehalose mixtures⁶¹ etc. have been attempted to explore the inherent interaction and relaxation dynamics of cryoprotectants. A combined time-resolved fluorescence spectroscopy along with molecular dynamic (MD) simulations in trehalose/glycerol cryoprotectant solution in the temperature range $T=298$ to 353 K have reported strong spatio-temporal heterogeneity in solution (at far above the T_g of solution) and proposed that there could be an interconnection between dynamic heterogeneity and cryopreservation properties of such systems.⁴¹ Although relaxation dynamics in neat glucose has been followed via dielectric relaxation spectroscopy (DRS),⁶² and differential scanning calorimetry (DSC)⁶³ and other studies on interaction and dynamics in neat glycerol performed, no attempt has yet been made to systematically investigate the composite glucose/glycerol binary solution. This is somewhat surprising considering the fact that glucose/glycerol solution possesses a strong potential in cryopreservation.⁴³ These facts provide the necessary motivation for investigating the glucose/glycerol cryoprotectant solution via steady state and time-resolved fluorescence emission spectroscopic techniques. The existing solute-centric fluorescence

studies in glycerol^{41,64,65} will be supportive to explain the current fluorescence results in glucose/glycerol solutions.

To investigate the impact of glucose (Glu) concentration and temperature on solution phase interaction and dynamics and subsequently on spatio-temporal heterogeneity in the glucose/glycerol cryoprotectant solutions, we have employed four different Glu wt% (0, 5, 15 and 25 wt %) in solution in the temperature range $T = 283\text{-}343\text{ K}$. Note the maximum amount of glucose that is completely soluble in glycerol is 25wt%. We have employed two well-known non-reactive external dipolar probe solutes, coumarin 153 (C153) and coumarin 343 (C343), in our present spectroscopic measurements.^{41,64-74} We have selectively chosen these two solutes, (with different chemical nature) hydrophobic solute C153 and hydrophilic C343 to extract information regarding the nature of interaction and dynamics of these binary mixtures.

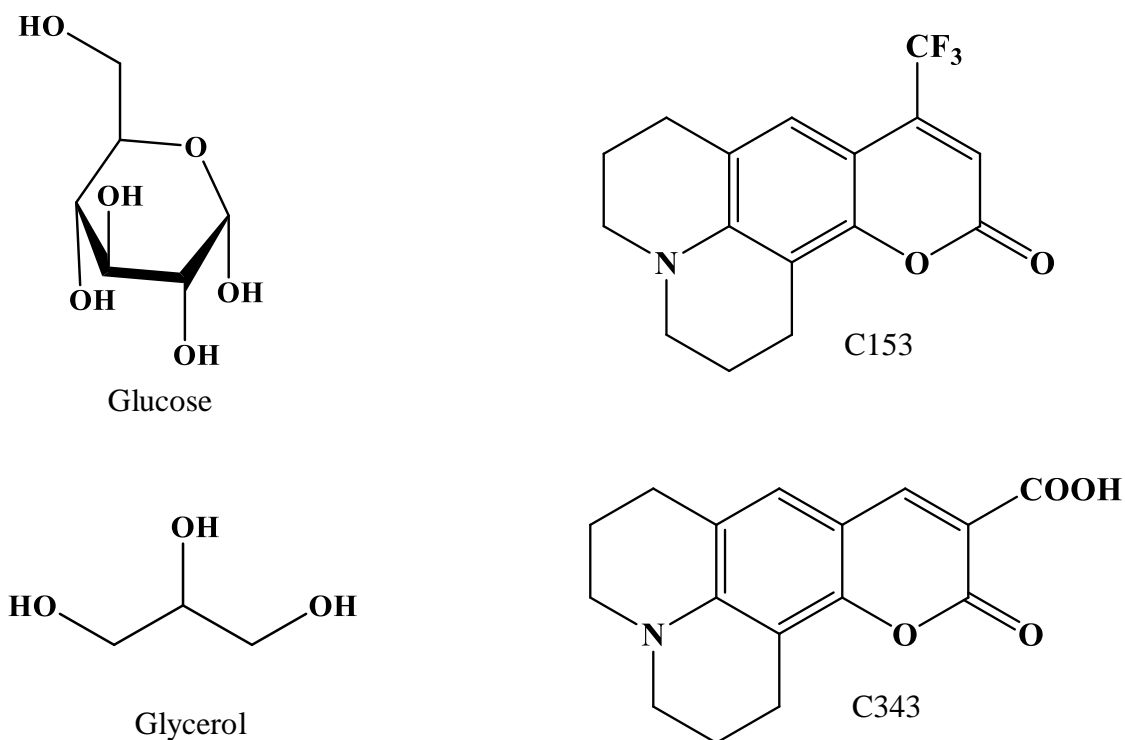
4.2 Experimental Details

4.2.1 Materials and Sample Preparation

D(+)-Glucose ($\geq 99.5\%$), glycerol ($\geq 99\%$), coumarin 153 (dye content 99%), coumarin 343 (dye content 97%) were purchased from Sigma Aldrich and used without further purification. The chemical structures of glucose (Glu), glycerol (Gly), coumarin 153 (C153) and coumarin 343 (C343) are shown in Scheme 4.1. The cryoprotectant solutions of glucose (Glu) and glycerol (Gly) were prepared following the same strategy as depicted in chapter 3. For preparing 5 wt% Glu/Gly solution, required amounts of Glu and Gly were weighed in an airtight glass vial and heated on a hot plate fitted with magnetic stirrer at $\sim 333\text{ K}$ for 3 hrs at 400 rpm to get a transparent colourless solution. Similarly, 15wt% and 25wt% Glu solutions were prepared by heating at 343 K for 3 hours and at 353 K for 4 hours, respectively. As these solutions are highly viscous in nature, fluorophore dyes (C153/C343) were preloaded in glass vials before weighing Glu and Gly to prepare solutions for UV-Vis absorption and fluorescence measurements. This ensured complete dissolution of dye molecules in these solutions. Concentrations of these dyes (C153 or C343) maintained in the solutions were $\leq 10^{-5}\text{ M}$.

4.2.2 Density and Viscosity Coefficient Measurements

Temperature dependent densities (ρ) and viscosity coefficients (η) of the Glu/Gly solutions were measured by using an automated temperature-controlled density and sound velocity analyzer (Anton Paar, model DSA 5000) and automated micro viscometer (AMVn, Anton Paar), respectively.^{41,73} Measured η values are summarized in Table 4.1.



Scheme 4.1: Chemical structures of glucose (Glu), glycerol (Gly), coumarin 153 (C153) and coumarin 343 (C343).

Table 4.1: Temperature dependent viscosity coefficients (η /cP) values of Glu/Gly solutions at various Glu concentrations.

T/K	Viscosity coefficients (η /cP) of Glu/Gly solutions			
	0 wt%	5 wt% Glu	15 wt% Glu	25 wt% Glu
293	1507	2143		
303	634	876	1586	
313	298	399	685	1446
318	211	280	467	954
323	153	201	327	647
328	114	148	236	448
333	87	111	172	317
338	67	84	129	230
343	53	66	98	170

4.2.3 Data Collection and Analysis for Steady State UV-Vis Absorption and Fluorescence Emission Measurements

UV-Visible spectrophotometer (UV-2600, Shimadzu) and fluorimeter (Fluorolog, Jobin-Yvon, Horiba) were used for recording steady state absorption and fluorescence emission spectra, respectively.^{69,70} Peltier temperature controller (accuracy ± 0.5 K) was used to perform temperature dependent measurements. The standard spectral analysis procedure was followed to determine spectral frequencies.^{75,76} The typical instrumental resolution for the determined spectral frequencies and spectral widths (full width at half maxima, FWHM) were within ± 200 cm^{-1} . Detailed description of the steady state UV-Vis absorption and fluorescence techniques are same as discussed in chapter 2.

4.2.4 Data Collection and Analysis for Time-Resolved Fluorescence Emission Spectra

Time-resolved fluorescence measurements⁷⁷ were performed with a time-correlated single-photon counting (TCSPC) set-up (LifeSpec-ps) from Edinburgh Instruments (Livingston, U.K.).⁷⁸ 409 nm laser excitation source was used to excite C153 or C343, dissolved in the cryoprotectant solutions using an excitation slit of 2 nm. Magic angle (54.7°) intensity decay at 409 nm of a scattering medium (water) after excitation by 409 nm laser that produced the FWHM of the instrument response function (IRF) ~ 85 ps. Temperature was controlled via a Julabo temperature controller (accuracy ± 1 K). Lifetime emission decays (magic angle intensity decays) were recorded at the peak wavelength of corresponding steady state fluorescence emission spectrum for both the solutes (C153 and C343). Data collection and analysis for Stokes shift dynamics and fluorescence anisotropy were performed as described in chapter 2 and references.^{67,79-81}

4.3 Results and Discussion

4.3.1. Steady State UV-Vis Absorption and Fluorescence Studies

4.3.1.1 Impact of Temperature

Figure 4.1 shows representative temperature-dependent absorption and emission spectra of C153 and C343 at 25 wt % Glu in Glu/Gly mixture. Temperature dependent changes in spectral peak frequencies ($\langle \nu_{em} \rangle$) and widths (FWHM, Γ_{em}) of both C153 and C343 dissolved in Glu/Gly cryoprotectant solutions are presented in Figure 4.2 and Figure A.b.1 (see Appendix), respectively. Note that for both the probe solutes, spectral features are somewhat sensitive (~ 100 - 500 cm^{-1} shift) to temperature variation in the range of $T = 283$ - 333 K. Though spectral

features are mildly temperature sensitive, the temperature dependence of absorption peak frequencies are found to be weaker than that of emission frequencies and they (absorption and fluorescence emission) exhibit opposite temperature dependencies. This is because temperature induced decrease of medium static dielectric constant (ϵ_s) (ϵ_s values are provided in Table 3.2 in chapter 3) is manifested in the slightly blue-shift of absorption spectra. On the other hand, red shift of fluorescence emission spectra reflects that fluorescence occurs from more solvent relaxed environment with increasing temperature (decreasing medium viscosity). Similar temperature impact on absorption and fluorescence emission spectra has been reported in trehalose/glycerol cryoprotectants⁴¹ and high viscous deep eutectic solvents⁸². Note, temperature-induced emission red-shift of C153 ($\sim 500 \text{ cm}^{-1}$) is larger than that of C343 ($\sim 300 \text{ cm}^{-1}$) for 60 K temperature change, observed in 25 wt% Glu solution. Because of different chemical nature of C153 (hydrophobic) and C343 (hydrophilic), it is quite expected that they would prefer to reside in different regions inside these solutions and respond differently to solution temperature variation.^{69,71} To understand the nature of these different regions probed by C153 and C343, we have successively varied Glu concentration in the Glu/Gly cryoprotectant solutions.

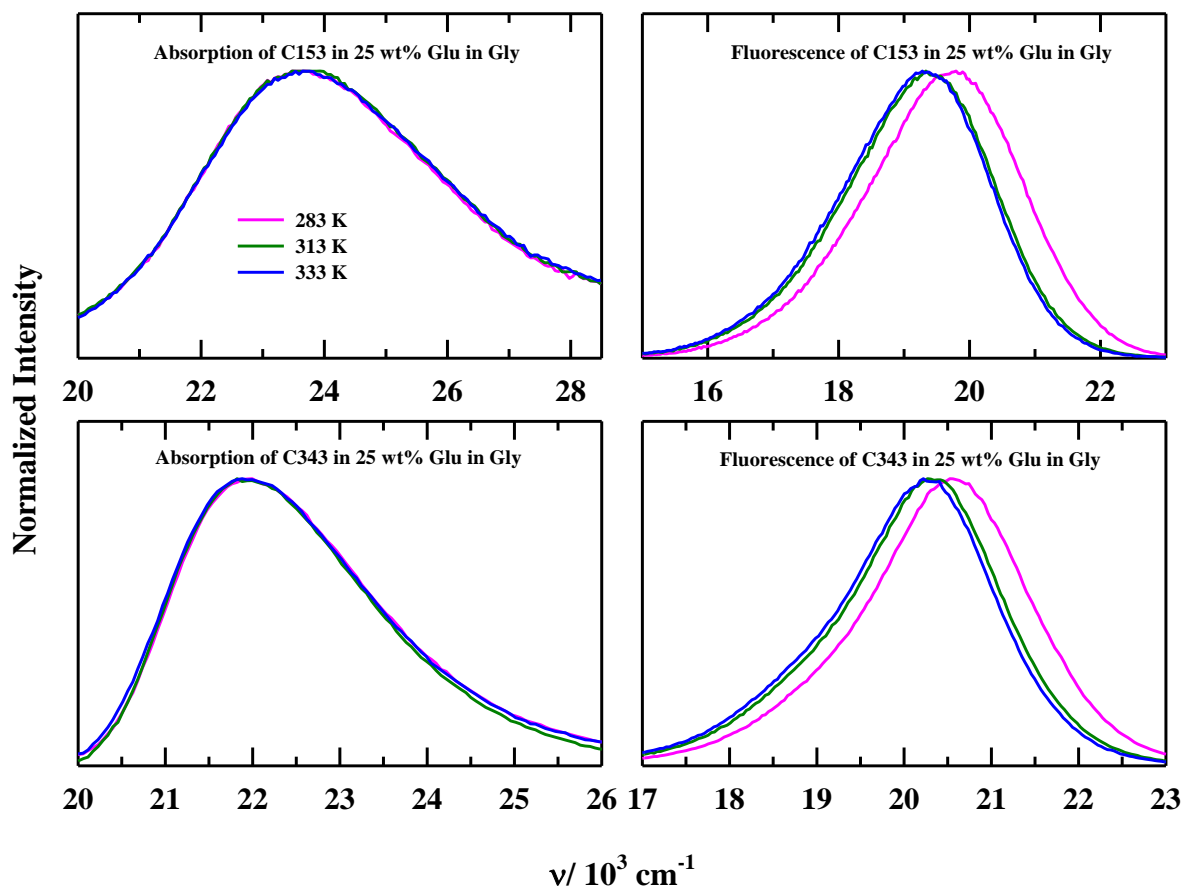


Figure 4.1: Temperature dependent steady state absorption (left panels) and fluorescence emission spectra (right panels) of C153 (upper panels) and C343 (lower panels) at 25 wt% of Glu in Glu/ Gly solutions. All presentations are colour-coded. Each of this emission spectrum has been recorded after excitation at the peak wavelength of the corresponding absorption spectrum.

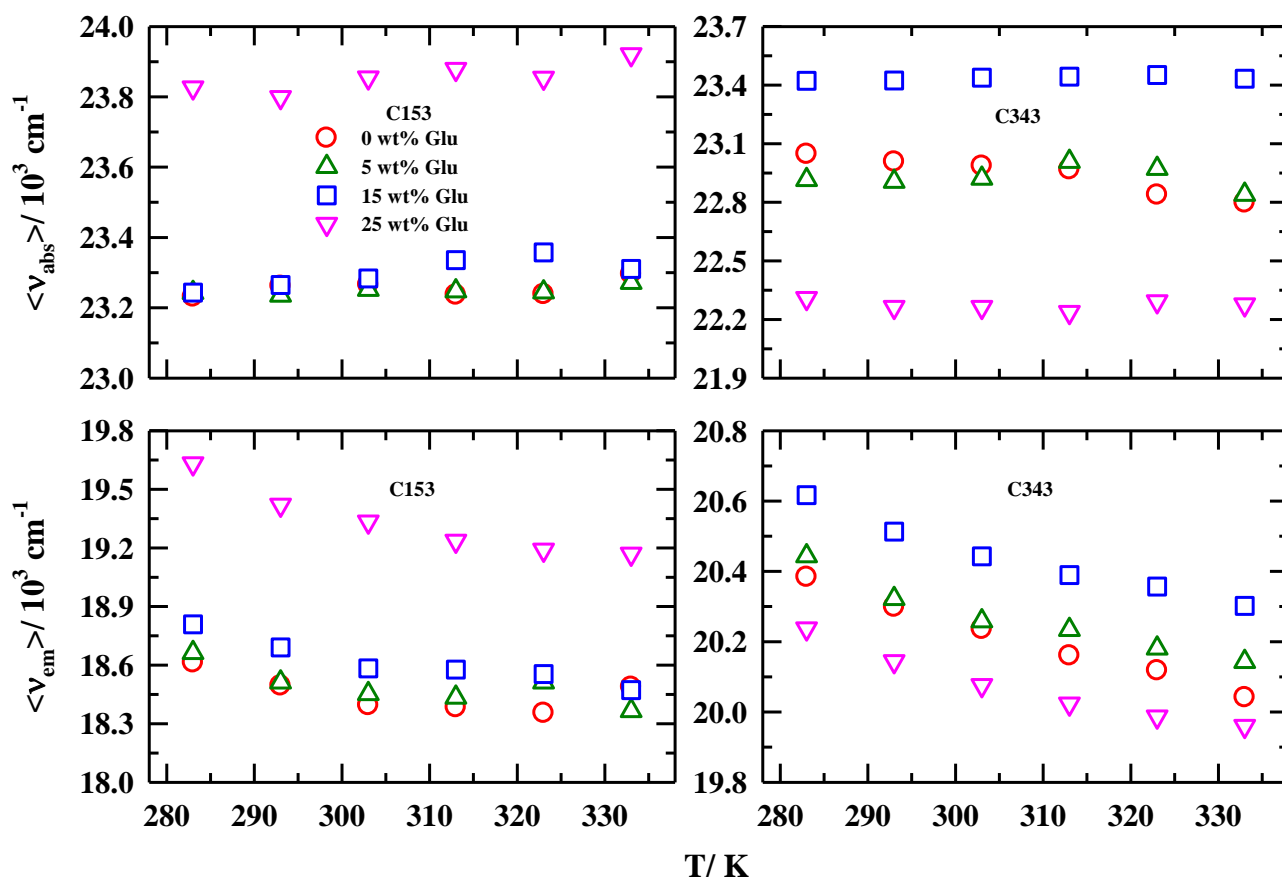


Figure 4.2: Temperature dependent steady state absorption (upper panels) and fluorescence emission peak average frequencies (lower panels) ($\langle \nu_{em} \rangle$) of C153 (left panels) and C343 (right panels) dissolved in Glu/ Gly solutions. All representations are colour-coded.

4.3.1.2 Glu Concentration Dependence

Figure 4.3 represents the absorption and emission spectra of C153 and C343 in Glu/Gly solutions at 293 K. Both the dye molecules report substantial change in absorption and emission spectral features with variation of Glu concentration in binary mixtures. Approximately 1000 cm^{-1} blue shift in the absorption and the emission peak frequencies of C153 have been observed in 25 wt% Glu containing solution compared to neat Gly. This is in contrast to the observation for the other dye, C343, where a non-monotonic dependence with Glu concentration has been registered. Note, both the components (Glu and Gly) of present cryoprotectants solutions possess multiple hydroxyl groups along with hydrophobic backbone. Therefore, with increasing Glu concentration in solution, both hydrophobic and hydrophilic rich microscopic domains are expected to emerge. Owing to hydrophobic nature, the spectral characteristic of dipolar solute C153 is expected to probe predominantly the hydrophobic regions of Glu/Gly

solutions while C343 locates itself inside the hydrophilic domains. The apparent shift of C153 and C343 absorption and emission peak positions in Gly and 25wt% Glu solution, shown in Figure 4.4, again emphasizes on Glu concentration induced modification of microscopic solution structure. Presence of such different microscopic environments in Glu/Gly cryoprotectant solutions can be explored further via monitoring the excitation wavelength dependent fluorescence emission of C153 and C343.

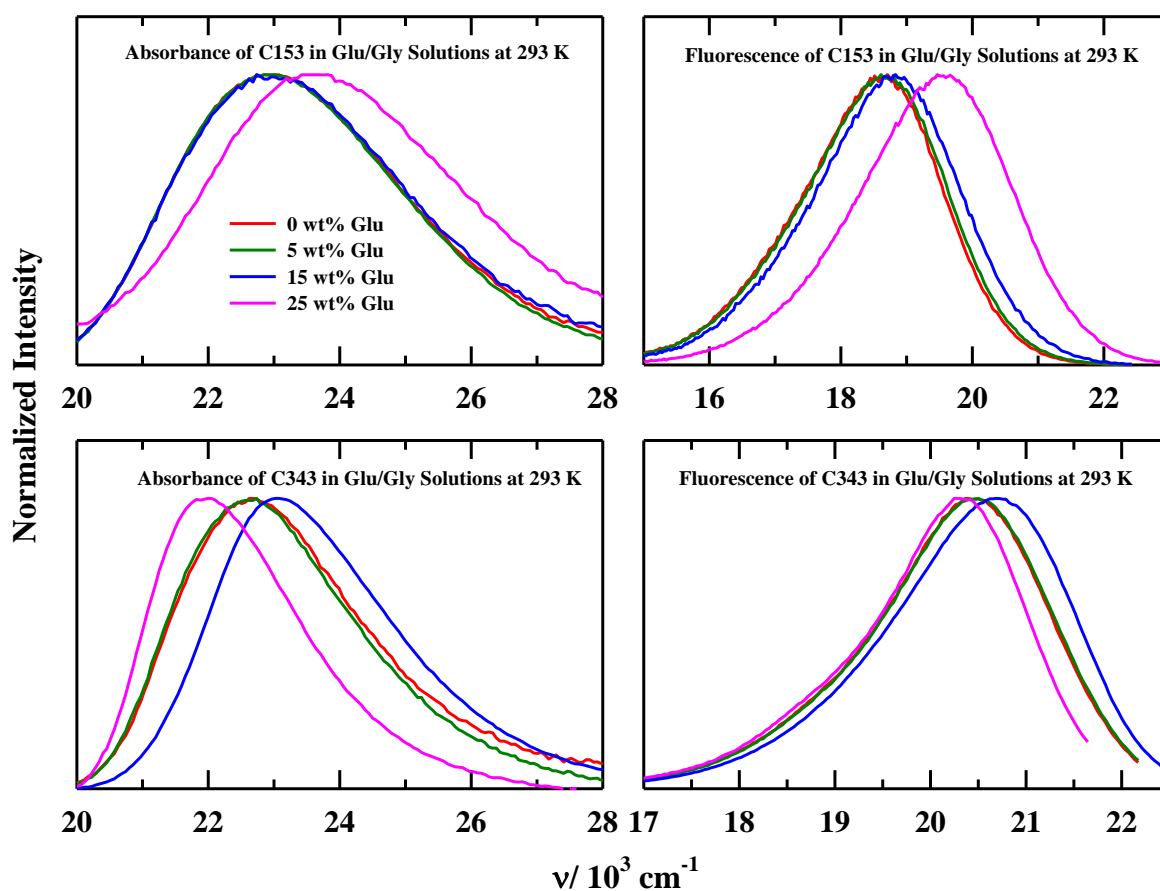


Figure 4.3: Steady state absorption (left panels) and fluorescence spectra (right panels) of C153 (upper panels) and C343 (lower panels) at different wt% of Glu in Glu/Gly solutions at 293 K. All presentations are colour-coded. Each of this emission spectrum has been recorded after excitation at the peak wavelength of the corresponding absorption spectrum.

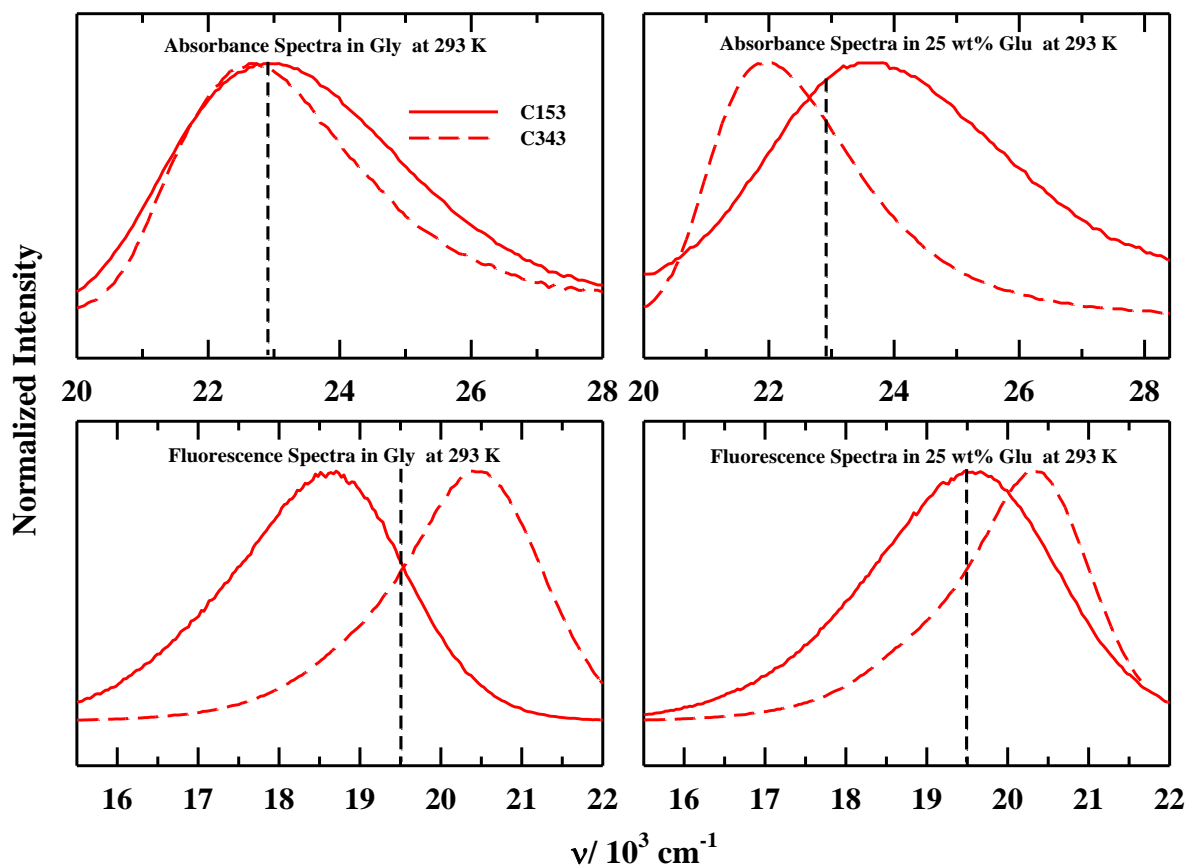


Figure 4.4: Steady state absorption (upper panels) and fluorescence spectra (lower panels) of C153 and C343 dissolved in neat Gly (left panels) and 25 wt% Glu in Glu/ Gly solutions (right panels) at 293 K. All presentations are colour-coded.

$$\lambda_{exc}$$

4.3.1.3 Spatial Heterogeneity in Glu/Gly Solutions

Presence of microscopic spatial heterogeneity has often been monitored via exciting the dissolved probe at various wavelengths (λ_{exc}) across its absorption spectrum.^{83,84} Figure 4.5 represents λ_{exc} dependent shift of fluorescence emission frequencies and changes in the corresponding FWHMs of C153 and C343 in Glu/Gly solutions under study. Shift of emission frequency for either of solutes C153/C343 with excitation energy (induced $\sim 200\text{-}600\text{ cm}^{-1}$ red shift for C153 and for C343 it is $300\text{-}700\text{ cm}^{-1}$) indicates that spatial inhomogeneity increases with increasing Glu concentration in the solutions. Temperature induced λ_{exc} dependent total shift of emission frequency and FWHM is shown in Figure 4.6. This results

reveal that irrespective of the nature of environment occupied by the C153/C343, the Glu/Gly cryoprotectants solutions are spatial heterogeneous and it is highest in presence of 25 wt% Glu (highest Glu wt% considered in this work). Similar result was reported for trehalose/glycerol cryoprotectants where heterogeneity was found to increase with gradual increase of trehalose concentration.⁴¹ Note the induced shift of ν_{em} is a manifestation of competition between fluorescence lifetime ($\langle \tau_{life} \rangle$) of a dissolved fluorophore probe and the inter-conversion timescales of different solvation environments surrounding the probe molecules. This heterogeneous picture of a solution cannot be registered by a dissolved probe with too short or too long $\langle \tau_{life} \rangle$ compared to the inter-conversion timescale of different solvation environments.^{70,73,82,85} Therefore, lifetime of the probe solutes (C153 and C343) in these Glu/Gly solutions is important to get an idea about persistent time of the heterogeneous domains in the medium.

Subsequently, excited state fluorescence lifetimes, $\langle \tau_{life} \rangle$, of C153 and C343 in this Glu/Gly cryoprotectants solutions have been measured. Measured lifetime data summarized in Table A.b.2 (Appendix) indicates that $\langle \tau_{life} \rangle$ of C153 varies substantially with temperature and composition of Glu/Gly solutions where as no significant change has been registered for C343. Similar $\langle \tau_{life} \rangle$ variation of these two probes (C153 and C343) was reported in Glucose based DES.^{72,73} Note the $\langle \tau_{life} \rangle$ of C153 and C343 summarized in Tables A.b.2 (Appendix) are ~ 2 - 4 ns and ~ 3 ns, respectively which suggest few-ns inter-conversion timescale for solvation structure surrounding the probe molecules in this Glu/Gly solutions. Next, pico-second resolved fluorescence technique is employed to investigate the temporal behaviour of this cryoprotectants solution.

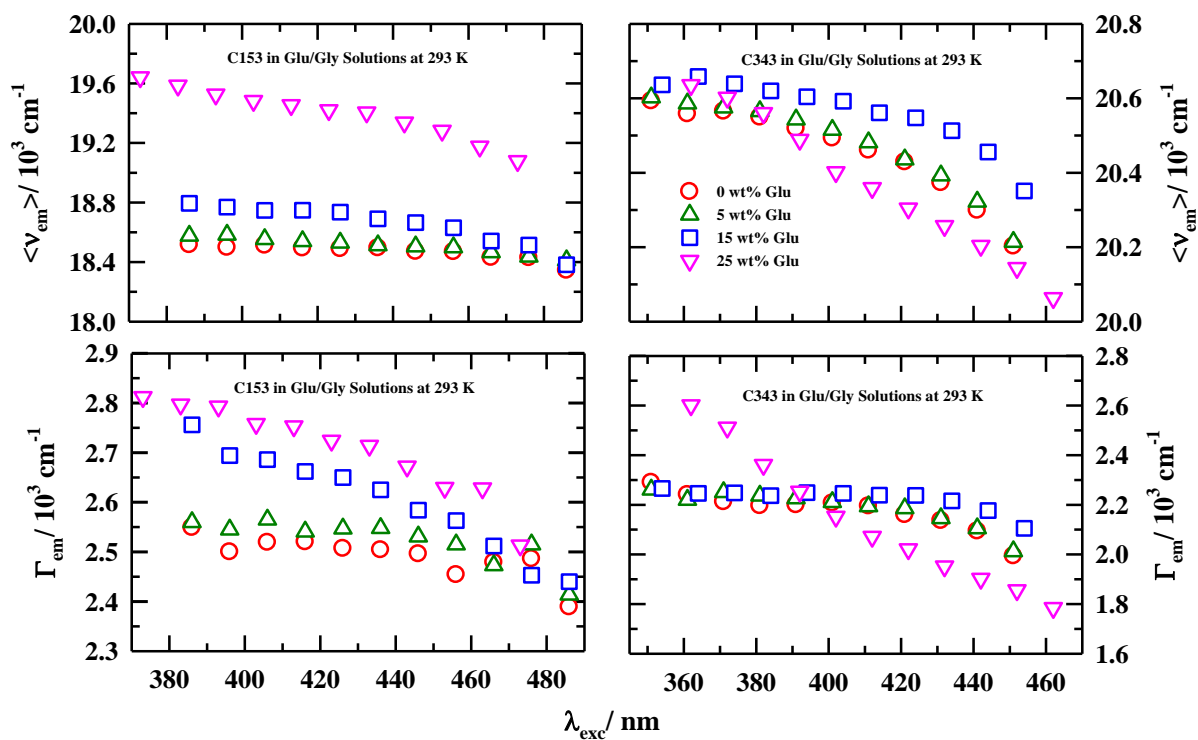


Figure 4.5: Excitation wavelength dependence (λ_{exc}) of steady state fluorescence emission average peak frequencies, $\langle \nu_{em} \rangle$ (upper panels) and spectral widths (FWHM), Γ_{em} (lower panels) of C153 (left panels) and C343 (right panels) at different wt% of Glu in Glu/Gly solutions at 293 K, respectively. All representations are colour-coded.

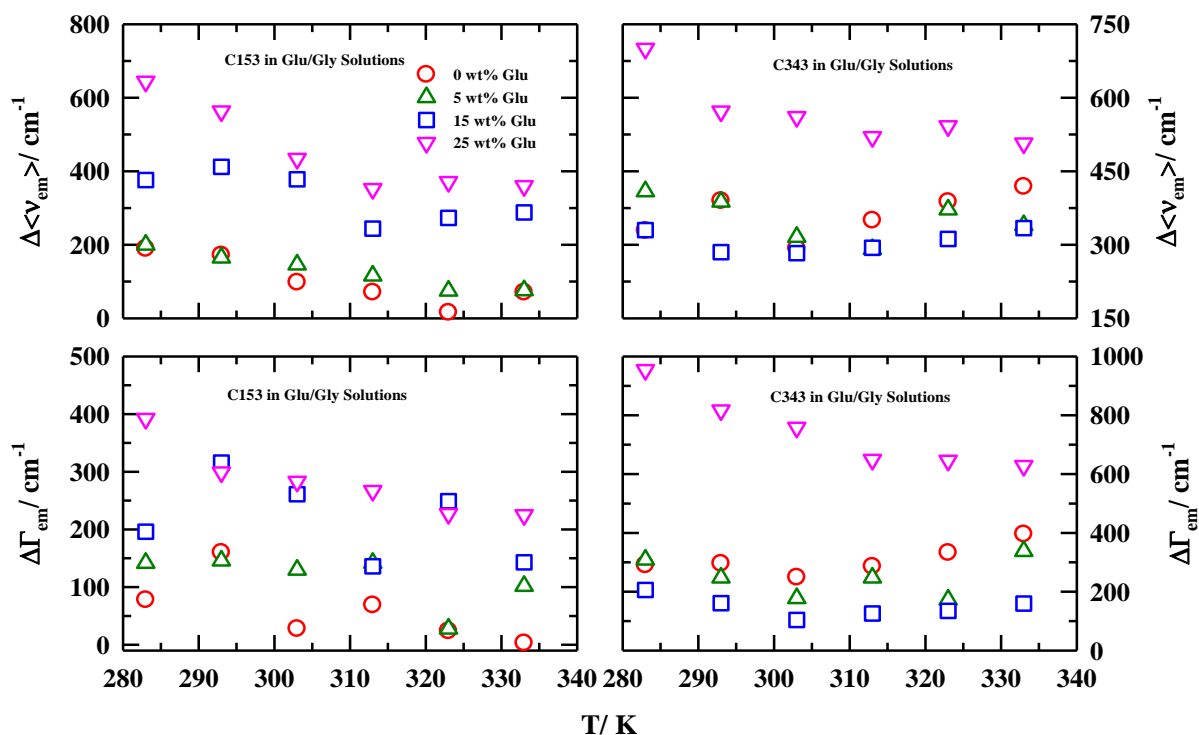


Figure 4.6: Temperature-induced λ_{exc} dependent total shifts of emission frequency (upper panels) and FWHM (lower panels) of C153 (left panels) and C343 (right panels) in Glu/ Gly solutions. All representations are colour-coded.

4.3.2 Time-Resolved Fluorescence Measurements

4.3.2.1 Stokes Shift Dynamics

Representative fluorescence intensity decays at blue and red end wavelength with respect to the steady state fluorescence emission peak wavelength for each of the dye molecules dissolved in 25 wt% Glu in Glu/Gly solution at 293 K are shown in Figure A.b.3. For both the dyes, only decay at blue-end wavelength and growth followed by decay at the red-end wavelength have been observed. This is a hallmark of dynamic Stokes shift of a dissolved dipolar solute probe because of the host particle rearrangement in response to the laser-induced sudden change in the charge distribution of the solute. Figure 4.7 is the representative time-resolved emission

spectra (TRES) of C343 and C153 in the Glu/Gly solutions at 293 K. The corresponding steady state emission spectra are also shown in each of the respective panels. Note the steady state emission spectra are blue shifted with respect to the emission spectrum taken at $t=\infty$ which indicates that steady state emission spectra recorded in these solutions have arisen from excited solutes that possessed incompletely solvent-relaxed configurations.

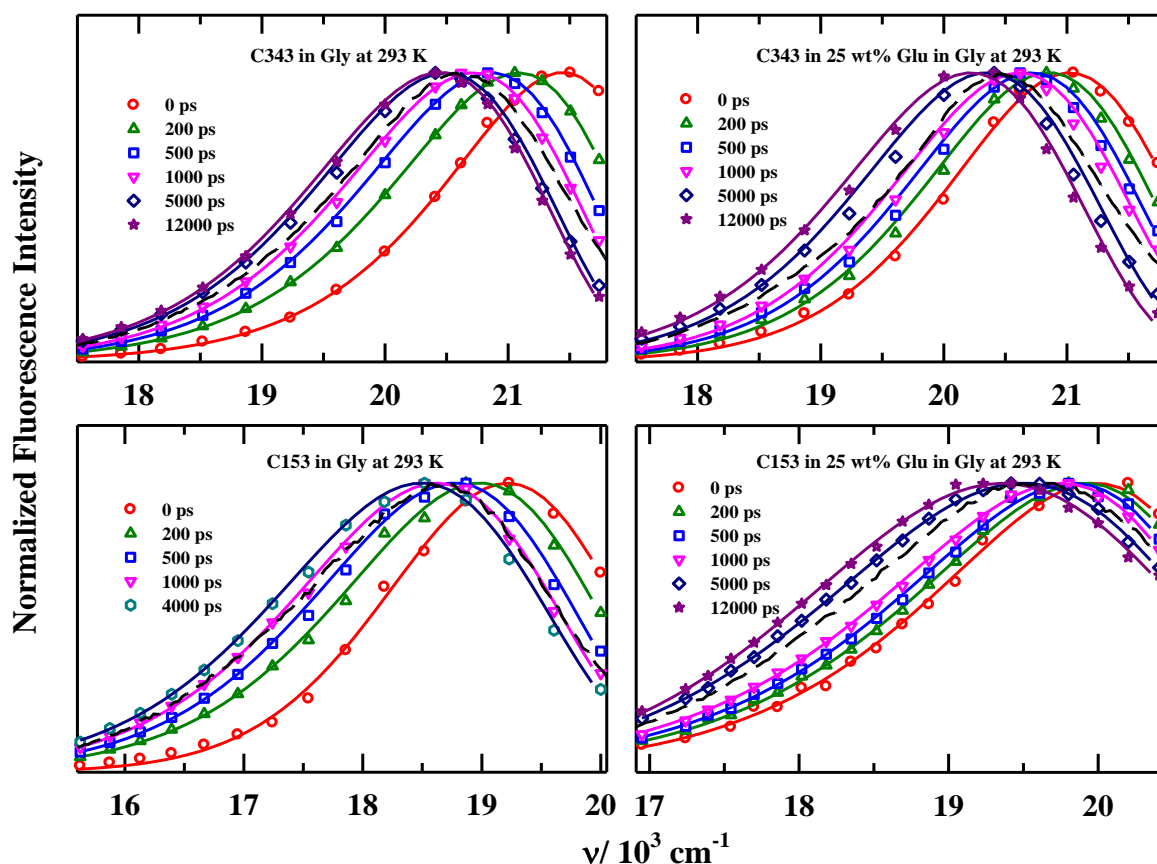


Figure 4.7: Representative constructed time-resolved emission spectra (TRES) of C343 (upper panels) and C153 (lower panels) dissolved in Glu/Gly solutions for different time intervals at 293 K. The corresponding steady state emission spectra of C343/C153 in these solutions are shown as dashed lines in each of the respective panels. All representations are colour-coded.

Glu and Gly have multiple hydroxyl groups ($(-OH)_n$) and in solution these hydroxyl groups participate in extensive intra and inter-species hydrogen bonding. The collective intermolecular vibration and libration modes of H-bonded systems are known to contribute to the ultrafast sub-picosecond polar solvation response.⁸⁶⁻⁸⁸ Thus the solvation response observed using present ps-resolved set-up does not represent complete detection of the total Stokes shift

dynamics in these systems. Table 4.2 summarizes the total dynamic Stokes shift of C153/C343 detected ($\Delta\nu_{obs}^t$) in these solutions from the present measurements and the corresponding estimated total dynamic Stokes shift ($\Delta\nu_{est}^t$) via a well-known approximate method⁸⁹. Because of broad temporal resolution employed, we have missed nearly 30-50% of the total dynamic Stokes shift. Since the density Glu/Gly solutions ($\sim 1.3 \text{ gcm}^{-3}$) are higher than the nonpolar reference solvent (hexane, density $\sim 0.7 \text{ gcm}^{-3}$), the actual missing portion may vary^{90,91} from the values shown in Table 4.2. Overestimation of slow-time component is expected due to missing of total dynamic Stokes shift as observed earlier in ionic liquids.^{84,92,93} Nevertheless the solvation dynamic response captured in the present measurements will provide a qualitative and useful information of medium dynamics.

Glu concentration dependent solvation response functions ($S(t)$), determined from the peak frequencies of time dependent emission spectrum, of C343/C153 in these Glu/Gly solutions at 293 K are shown in Figure 4.8. Representative temperature dependent solvation response functions are represented in Figure A.b.4. The decay fit parameters are summarized in Table 4.3. Solvation response functions of C153 are characterized by a few-100 ps and a slower multi-ns time component. This slower component dominates with increasing Glu concentration in the solution. $S(t)$ decay for other probe, C343 is characterized by a faster ~ 100 -300 ps component, a sub-ns component and a slower one, ~ 3 -6 ns component. A number of time-resolved fluorescence studies reported solvation timescales for C153 (~ 1100 ps) and C343 (~ 700 ps) in neat Gly (at $T \sim 295$ K) quite close to the solvation time obtained in our present measurements.^{64,65} Note DR measurements in the same Glu/Gly cryoprotectant solutions report average DR timescales ($\langle\tau_{DR}\rangle$), shown in Table 3.2 (see chapter 3), close to $\langle\tau_s\rangle$ of C343 and C153 (for 25 wt% Glu at 303 K: $\tau_{DR} = 2139$ ps, $\langle\tau_s\rangle^{C153} = 1842$ ps, $\langle\tau_s\rangle^{C343} = 1913$ ps) although the individual relaxation times and the corresponding amplitudes (τ_i, a_i) are different (as expected) from those found in solvation dynamics studies. Interestingly, $\langle\tau_s\rangle$ for C343 in these solutions are slightly longer than that of C153. Moreover, a long 3-5 ns time-component in solvation response of C343 has been found to persist irrespective of solution temperature and composition which is absent for C153 in lower Glu concentration regime (≤ 15 wt% Glu). Strong solute (C343)-medium interaction because of ionic nature of this probe is possibly the reason for such a slow component with 3-5 ns timescale.

Table 4.2: Magnitudes of estimated (Δv_{est}^t), observed (Δv_{obs}^t) and missing portion of the total dynamic Stokes shift of C343 and C153 at different wt% of Glu in Glu/Gly solutions.

C343 in Glu/Gly Solutions			
T/K	$\Delta v_{est}^t / \text{cm}^{-1}$	$\Delta v_{obs}^t / \text{cm}^{-1}$	% Missed
C343 in Gly			
283	1904	1044	45
293	1833	1003	45
303	1846	944	49
313	1791	820	54
323	1620	755	53
C343 in 5 wt% Glu			
283	1781	1115	37
293	1812	986	46
303	1786	946	47
313	1879	890	53
323	1856	808	56
333	1682	744	56
C343 in 15 wt% Glu			
283	2181	1052	52
293	2205	1003	54
303	2218	948	57
313	2229	877	60
323	2229	831	63
333	2228	742	67
C343 in 25 wt% Glu			
283	1268	792	38
293	1337	800	40
303	1352	783	42
313	1312	705	46
323	1351	655	52
333	1347	590	56
C153 in Glu/Gly Solutions at 293 K			
wt% Glu	$\Delta v_{est}^t / \text{cm}^{-1}$	$\Delta v_{obs}^t / \text{cm}^{-1}$	% Missed
0	1085	725	33
5	1049	681	35
15	740	571	23
C153 in 25 wt% Glu			
283	666	646	3
293	918	625	32
303	1014	595	41
313	1106	546	51
323	944	447	53
333	1005	431	57

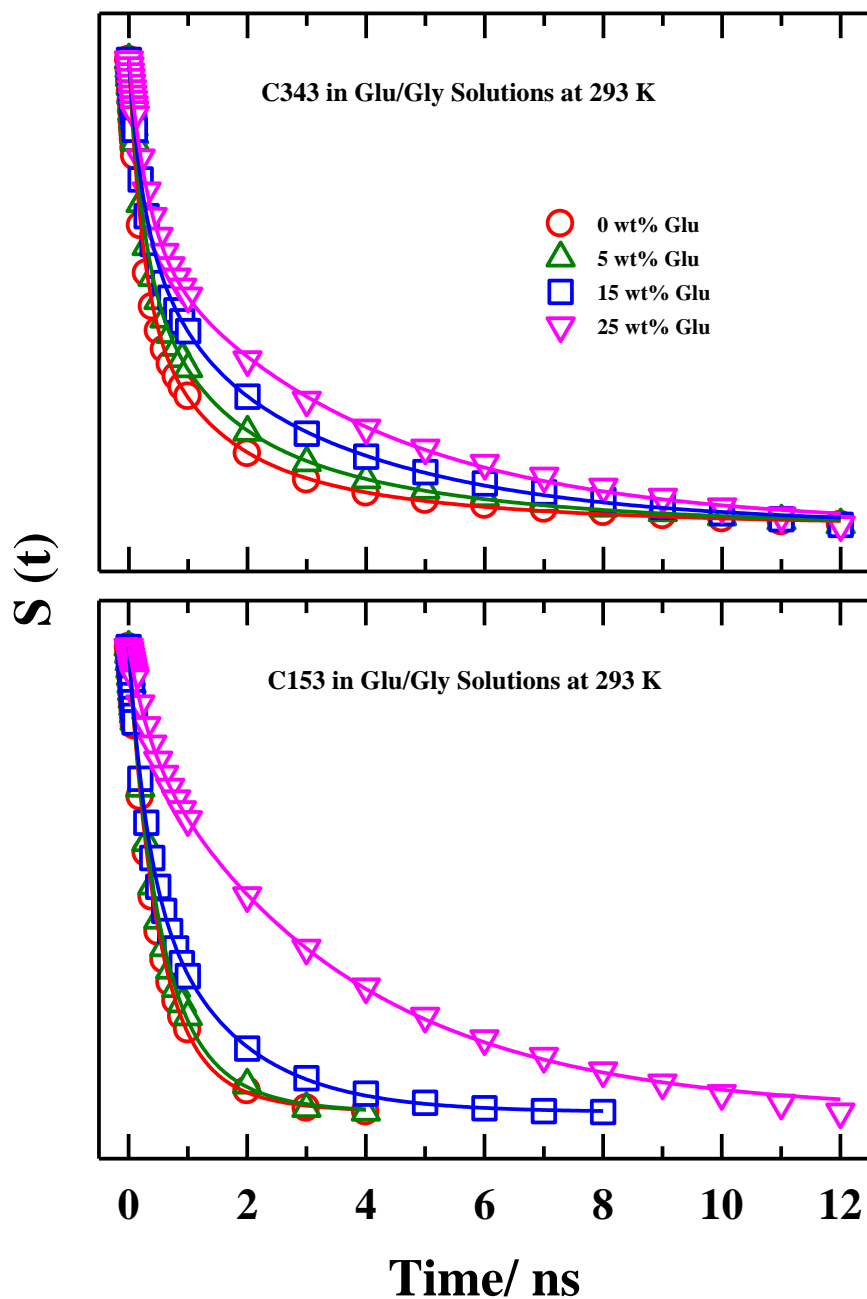


Figure 4.8: Solvation response function ($S(t)$) decays for C343 (upper panel) and C153 (lower panel) at different wt% of Glu in Glu/Gly at 293 K. Experimental data for $S(t)$ are shown by circles; solid lines passing through the data represent the fits. All presentations are colour-coded.

Table 4.3: Temperature dependent decay characteristics of solvation response function ($S(t)$) of C343 and C153 at various wt% of Glu in Glu/Gly.^a

T/ K	a_1	τ_1 / ps	a_2	τ_2 / ps	a_3	τ_3 / ps	$\langle\tau_s\rangle$ / ps
C343 in Gly							
283	0.27	261	0.26	787	0.47	3330	1853
293	0.49	224	0.35	1090	0.16	4077	1155
303	0.54	138	0.38	682	0.08	4540	705
313	0.66	114	0.28	468	0.06	5232	512
323	0.49	61	0.45	188	0.06	3182	315
C343 in 5 wt% Glu							
283	0.16	138	0.32	522	0.52	3439	1985
293	0.40	234	0.34	1006	0.27	3775	1436
303	0.50	155	0.37	722	0.13	4475	933
313	0.60	103	0.33	488	0.08	4796	617
323	0.68	84	0.25	350	0.07	5349	514
333	0.76	67	0.17	254	0.07	6489	519
C343 in 15 wt% Glu							
283	0.33	310	-	-	0.67	3722	2606
293	0.27	209	0.28	742	0.45	3582	1877
303	0.41	176	0.36	826	0.24	3994	1307
313	0.53	156	0.31	712	0.16	4780	1059
323	0.59	100	0.29	466	0.13	5083	838
333	0.70	85	0.18	386	0.12	5151	730
C343 in 25 wt% Glu							
283	0.26	275	-	-	0.74	3981	3009
293	0.38	323	-	-	0.62	3724	2423
303	0.34	189	0.25	796	0.41	4016	1913
313	0.49	195	0.22	852	0.29	4157	1504
323	0.56	150	0.18	578	0.26	4541	1375
333	0.61	118	0.16	555	0.23	4900	1283
C153 in Glu/Gly Solutions at 293 K							
wt% Glu	a_1	τ_1 / ps	a_2	τ_2 / ps	a_3	τ_3 / ps	$\langle\tau_s\rangle$ / ps
0	0.79	453	0.21	1065	-	-	584
5	0.58	419	0.42	932	-	-	634
15	0.45	311	0.55	1456	-	-	943
C153 in 25 wt% Glu							
283	0.18	121	0.82	3942	-	-	3254
293	0.18	347	0.82	3694	-	-	3091
303	0.41	501	0.59	2774	-	-	1842
313	0.69	523	0.31	2383	-	-	1100
323	0.74	285	0.26	900	-	-	445
333	0.83	208	0.17	1129	-	-	364

^aIndividual amplitudes and time constants can be reproduced within $\pm 10\%$ of the reported values.

Next we explored the coupling between average solvation time for the hydrophilic solute, C343 and medium viscosity. Figure 4.9 describes the partial decoupling of the measured $\langle \tau_s \rangle$ of C343 and medium viscosity in Glu/Gly solutions in double logarithmic fashion. Fits going through the experimental data points denote fractional viscosity dependence of the type, $\langle \tau_s \rangle = A(\eta/T)^p$, with fractional p values, ~ 0.1 - 0.5 . Note for homogeneous systems one expects $p = 1$, which is hydrodynamic prediction. This substantial deviation of p from unity suggests pronounced decoupling of $\langle \tau_s \rangle$ from medium viscosity and may be interpreted as arising from strong temporal heterogeneity of these cryoprotectant solutions.^{41,50,72,73,82,85,94-100}

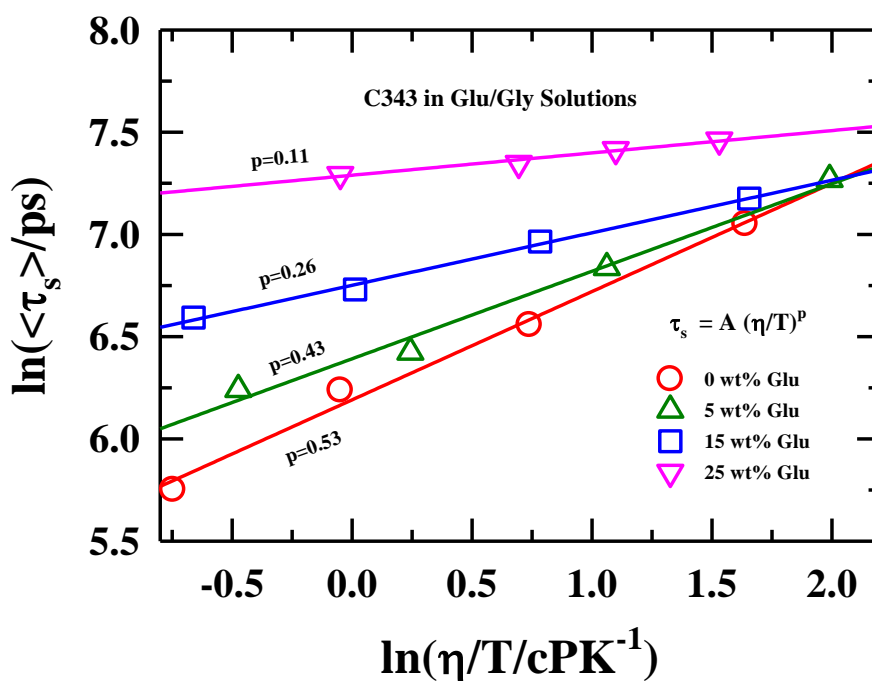


Figure 4.9: Temperature-reduced viscosity dependence (η/T) of average solvation time, $\langle \tau_s \rangle$, of C343 in Glu/Gly solutions. Solid lines passing through the data points represent fits. All presentations are colour-coded.

Viscosity decoupling has been further explored from the estimated activation energies associated with the temperature dependent solution viscosities and average solvation times of C343, shown in Figure 4.10. Clearly, these experimental quantities (η and $\langle \tau_s \rangle$) show

Arrhenius-type temperature dependencies. Note that the activation energy associated with viscosity, ($E_a^\eta \sim 60 \text{ kJmol}^{-1}$) is ~ 2 -5 times larger than those associated with $\langle \tau_s \rangle$.

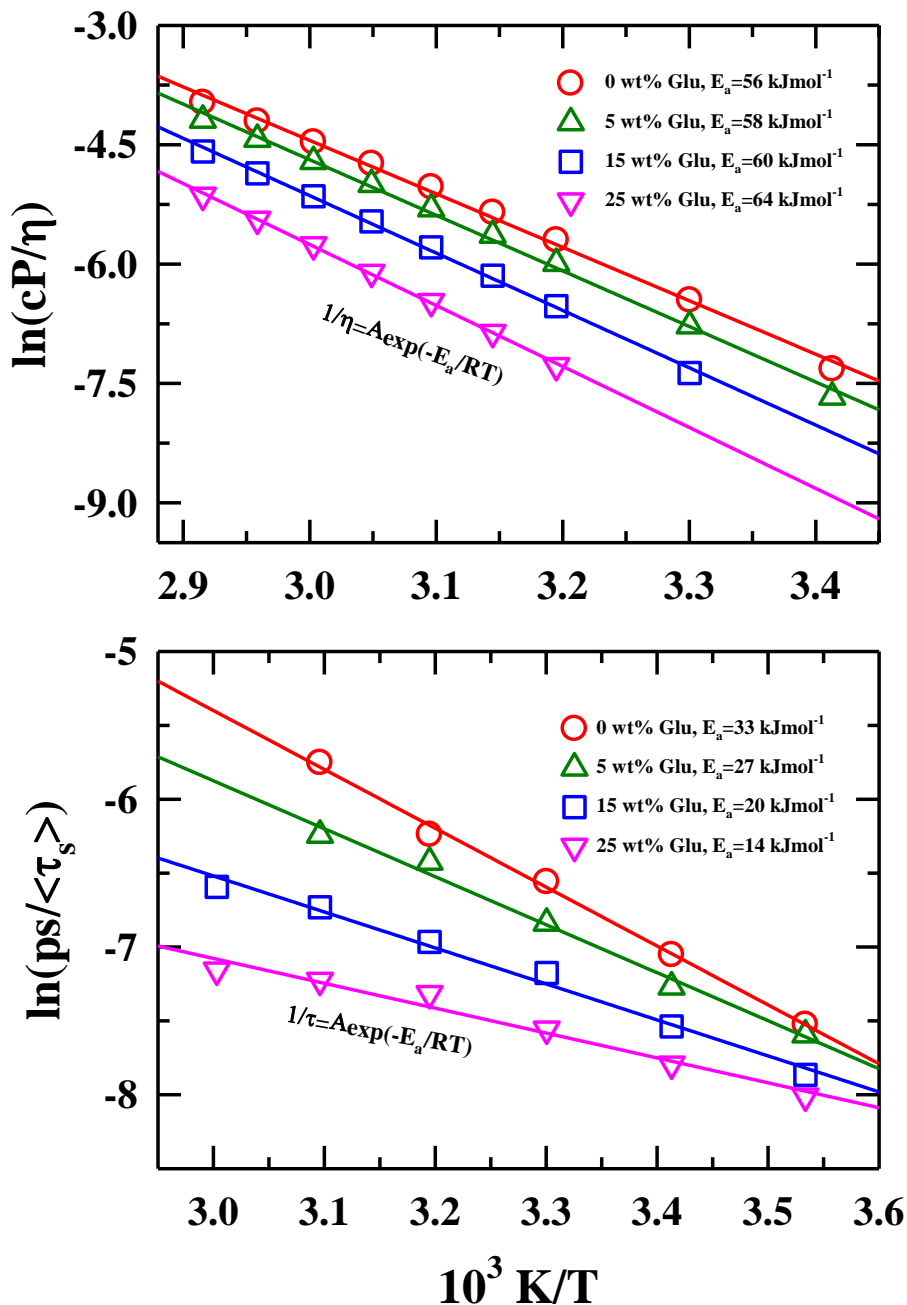


Figure 4.10: Arrhenius-type temperature dependencies of medium viscosity (upper panel) and average solvation time (lower panel) of C343 in Glu/Gly solutions. Solid lines passing through the experimental data points represent the fits. All are colour-coded.

4.3.2.2 Time-Resolved Fluorescence Anisotropy Studies

Time-resolved fluorescence anisotropy measurements of C343 and C153 in the Glu/Gly solutions were performed in order to explore the solute-medium frictional coupling. Representative fluorescence intensity decays of C343 and C153 at parallel and perpendicular polarizations (with respect to vertically polarized excitation) are represented in Figure A.b.5 (see Appendix). Rotational anisotropy ($r(t)$) decays and corresponding bi-exponential fits of C343 and C153 in two representative temperature are shown in Figure 4.11 while the residuals of respective fits are presented in Figure A.b.6 (see Appendix). Representative Glu concentration dependent $r(t)$ decays are shown in Figure A.b.7 (Appendix). Note pronounced non-exponential anisotropy decays for both the solutes. Temperature ($313 \leq T/\text{K} \leq 343$) and Glu concentration dependent bi-exponential $r(t)$ decay fit parameters are summarized in Table 4.4. These $r(t)$ decays are characterized by a fast timescale of ~ 100 ps and a dominant (~ 70 – 90%) slow component of multi-nanosecond time component. The average rotational times ($\langle \tau_{rot} \rangle$) become slower with increase of Glu wt% and decrease of solution temperature due to increase of medium viscosity.

Figure 4.12 describes the medium viscosity decoupling of solutes (C153 and C343) $\langle \tau_{rot} \rangle$ in a similar fashion considered for solvation time. Note, for both the solutes, fractional viscosity dependence of $\langle \tau_{rot} \rangle$ with $p < 1$ has been observed in all these solutions which again indicates about strongly temporal heterogeneity of solutions. Fractional viscosity dependence of solute rotation becomes more pronounced with increasing Glu wt% in the solutions and this dependence is more pronounced for C343 than C153. Next, we compare the measured rotation times with the hydrodynamic predicted rotation times from modified Stokes-Einstein-Debye (SED) relation, $\tau_{rot} = \frac{V\eta}{k_B T} fC$ employing stick and slip boundary limit for both C153 (volume of C153 (V) = 246 \AA^3 , shape factor (f) = 1.71, $C = 1$ (stick) and 0.24 (slip))⁸¹ and C343 ($V = 243 \text{ \AA}^3$, $f = 1.99$, $C = 1$ (stick) and 0.18 (slip))¹⁰¹, shown in Table A.b.8 (Appendix) and Figure 4.12. Interestingly, $\langle \tau_{rot} \rangle$ of these solutes shows sub-slip behaviour in the high viscous region. The departure from hydrodynamic prediction in the more viscous region may arise from non-Brownian moves such as angular jump.^{73,102-104} Such non-Brownian moves experience significantly less friction than predicted from the macroscopic viscosity, which results deviation of $\langle \tau_{rot} \rangle$ from hydrodynamic predictions. Fractional viscosity dependence in

concomitant with sub-slip rotation motion indicates that these Glu/Gly cryoprotectants solutions are dynamically heterogeneous and this heterogeneity intensified with Glu concentration.

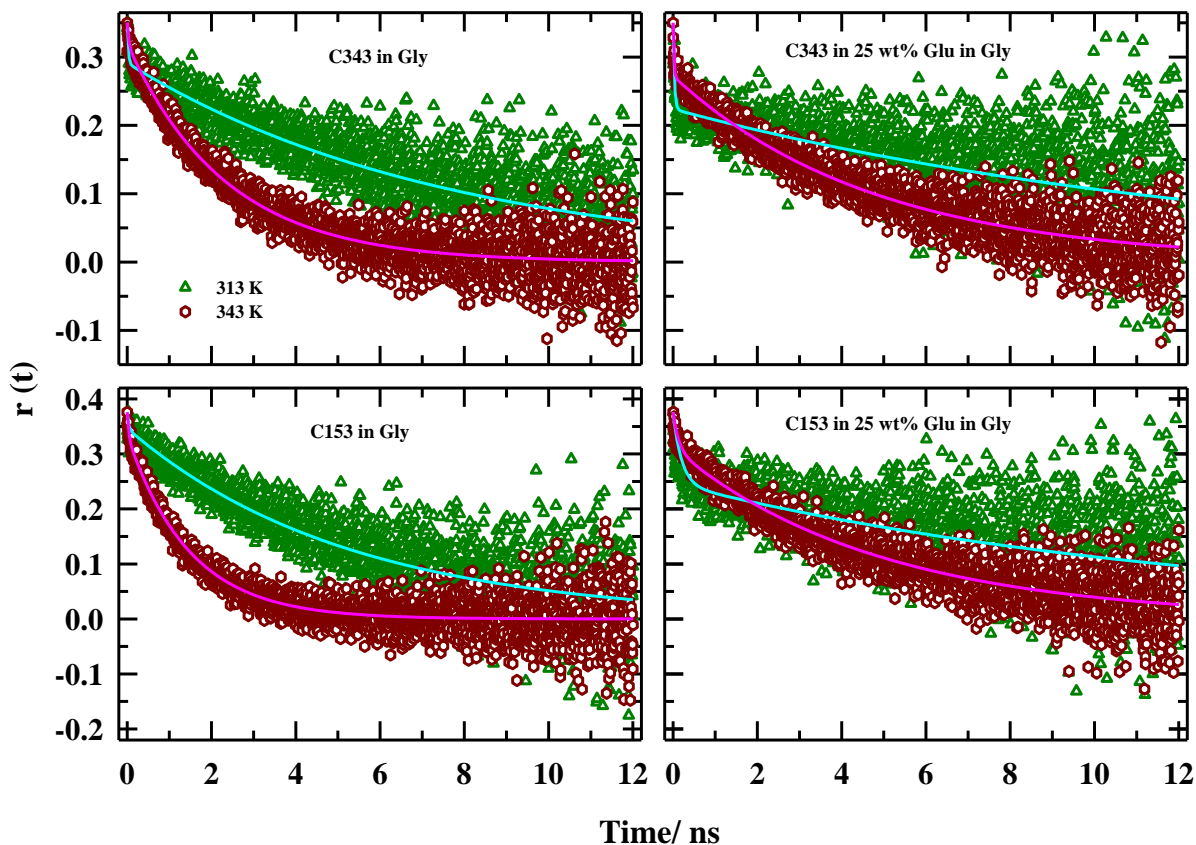


Figure 4.11: Rotational anisotropy ($r(t)$) decays of C343 (upper panels) and C153 (lower panels) in Gly (left panels) and 25 wt% Glu in Gly (right panels) at two representative temperatures. Symbols represent the experimental data points while lines passing through the experimental data points are biexponential fits. All representations are colour-coded.

Table 4.4: Temperature dependent $r(t)$ decay fit parameters of C343 and C153 at various wt% of Glu in Glu/Gly.^o

A: C343						B: C153				
T/ K	a_1	τ_1 / ps	a_2	τ_2 / ps	$\langle \tau_{rot} \rangle$ / ps	a_1	τ_1 / ps	a_2	τ_2 / ps	$\langle \tau_{rot} \rangle$ / ps
Gly						Gly				
313	0.17	25	0.83	7610	6321	0.08	33	0.92	5236	4820
318	0.19	28	0.81	5794	4698	0.04	33	0.96	4500	4320
323	0.16	26	0.84	5081	4272	0.07	33	0.93	3855	3588
328	0.09	29	0.91	4184	3810	0.06	33	0.94	2795	2630
333	0.11	32	0.89	4027	3588	0.05	33	0.95	2333	2218
338	0.16	28	0.84	3155	2654	0.10	33	0.90	1997	1800
343	0.09	37	0.91	2340	2133	0.11	36	0.89	1480	1321
5 wt% Glu						5 wt% Glu				
313	0.20	29	0.80	7994	6407	0.16	27	0.84	5945	4998
318	0.18	38	0.82	7158	5876	0.15	24	0.85	4653	3959
323	0.13	33	0.87	5945	5175	0.15	26	0.85	4344	3696
328	0.17	24	0.83	5173	4298	0.17	27	0.83	3493	2904
333	0.11	51	0.89	4244	3783	0.16	66	0.84	3122	2633
338	0.17	40	0.83	3224	2683	0.16	33	0.84	2217	1867
343	0.17	38	0.83	3098	2578	0.13	42	0.87	1734	1514
15 wt% Glu						15 wt% Glu				
313	0.21	20	0.79	9276	7333	0.15	20	0.85	8026	6825
318	0.14	20	0.86	8143	7006	0.09	26	0.91	5963	5429
323	0.18	20	0.82	7452	6114	0.10	20	0.90	4623	4163
328	0.21	20	0.79	7027	5556	0.13	30	0.87	4299	3744
333	0.09	32	0.91	5206	4740	0.08	34	0.92	3827	3536
338	0.15	32	0.85	5008	4261	0.10	100	0.90	3438	3104
343	0.13	64	0.87	4354	3796	0.08	49	0.92	2467	2273
25 wt% Glu						25 wt% Glu				
313	0.36	30	0.64	13495	8648	0.35	200	0.65	12853	8424
318	0.23	44	0.77	10638	8202	0.31	200	0.69	9597	6684
323	0.30	27	0.70	10730	7519	0.19	77	0.81	7435	6037
328	0.20	37	0.80	8333	6674	0.16	78	0.84	6649	5598
333	0.19	48	0.81	7123	5578	0.16	50	0.84	6207	5522
338	0.18	37	0.82	6510	5345	0.18	70	0.82	5580	4588
343	0.22	19	0.78	4757	3716	0.17	128	0.83	4854	4051

^oIndividual amplitudes and time constants can be reproduced within $\pm 10\%$ of the reported values.

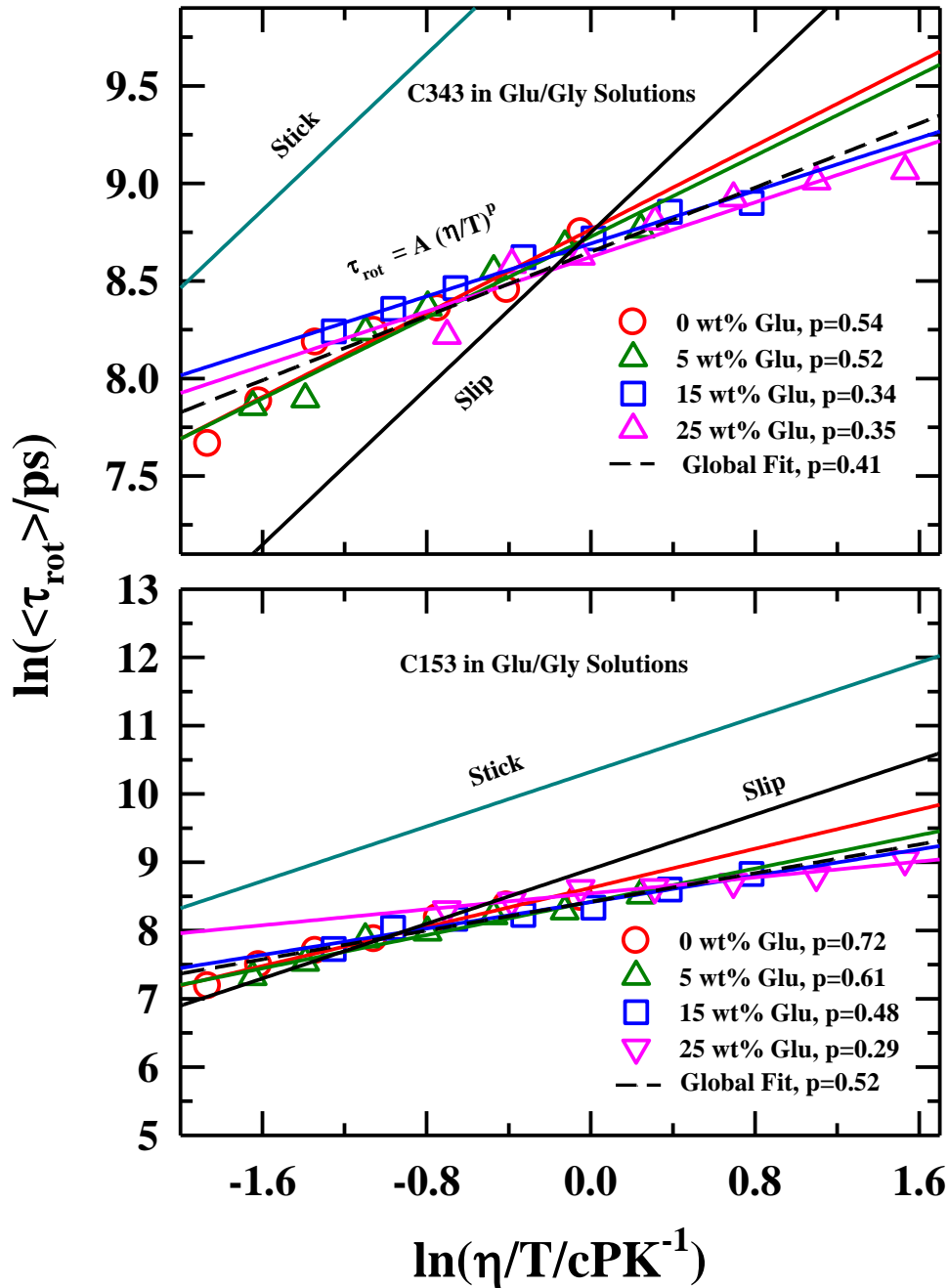


Figure 4.12: Temperature-reduced viscosity (η/T) dependence of average rotation time, $\langle \tau_{rot} \rangle$, of C343 (upper panel) and C153 (lower panel) at various wt% of Glu in Glu/Gly solutions. Solid lines passing through the experimental data points represent fits. Different colours have been used for various wt% of Glu.

Subsequently the activation energies associated with solutes rotation (E_a^{rot}) in these Glu/Gly cryoprotectant solutions have been determined from the temperature dependent measurements.

Arrhenius-type temperature dependence has been found for rotational relaxations of both the solutes, shown in Figure 4.13. The estimated activation energies (E_a^{rot}) for each solutes are presented in the respective panel of Figure 4.13. These E_a^{rot} for C153 and C343 are ~ 2-3 times smaller than that of E_a^η that further supports to the solute-medium viscosity decoupling, observed via fractional p value in Glu/Gly solutions. Note, the difference in activation energy (E_a^{rot}) between C153 and C343 rotation. The extent of decoupling is regulated by the nature of solute-medium which may originate from two sources: different chemical nature of the solutes (C153 and C343) and the nature of the local environments experienced by the individual solutes dissolved in Glu/Gly cryoprotectant solutions.

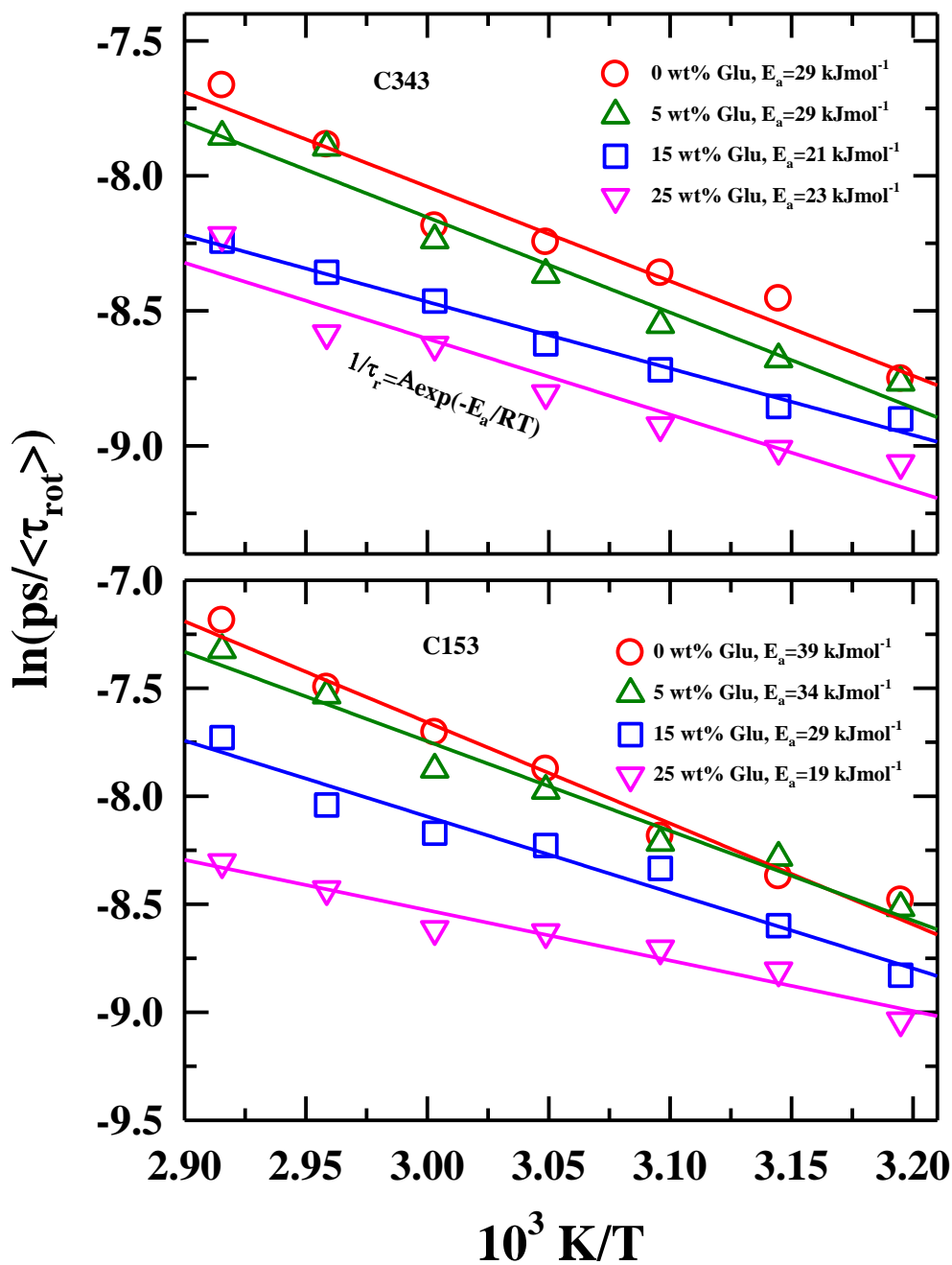


Figure 4.13: Arrhenius-type temperature dependencies of C343 (upper panel) and C153 rotation (lower panel) and the estimated activation energies at various wt% of Glu in Glu/Gly solutions. Solid lines passing through the experimental data points represent fits. Different colours have been used for various wt% of Glu.

4.4 Conclusion

To summarize, spectroscopic study indicates strong spatio-temporal heterogeneity in cryoprotectant mixtures made of glucose and glycerol. Strong signature of spatial heterogeneity has been detected via the excitation wavelength dependent fluorescence emission peak shift with both the solute (C153 and C343) having lifetime ~ 3 -5 ns. Highly non-exponential fluorescence anisotropy decay with two widely different time scales (~ 100 ps and several nanoseconds) have been observed for both solutes. Strong signature of temporal heterogeneity has been found via a pronounced fractional viscosity dependence of $\langle \tau_{rot} \rangle$ of C153 and C343 in these highly viscous Glu/Gly solutions. Dynamic Stokes shift measurements have revealed fraction power ($p = 0.1$ - 0.5 , much less than unity) dependence of $\langle \tau_s \rangle$ on medium viscosity. It is quite interesting to observe that the signature of medium spatio-temporal heterogeneity is registered by both the neutral and charged dipolar solutes and this heterogeneity increases significantly upon increasing Glu concentration in solution. MD simulation studies with realistic interaction potentials are required to further understand the anomalous motional features of the medium particles and consequent spatio-temporal heterogeneity of these cryoprotectant solutions.

References

1. B. J. Fuller, *CryoLetters* **25**, 375 (2004).
2. J. E. Lovelock, *Proc. R. Soc. Med.* **47**, 60 (1954).
3. S. Phadtare, *Curr. Issues. Mol. Biol.* **6**, 125 (2004).
4. C. Krembs, H. Eicken, K. Junge and J. Deming, *Deep Sea Res. Part I Oceanogr. Res. Pap.* **49**, 2163 (2002).
5. J. Costanzo, R. Lee and P. H. Lortz, *J. Exp. Biol.* **181**, 245 (1993).
6. M. F. Thomashow, *Annu. Rev. Plant Biol.* **50**, 571 (1999).
7. D. J. Von Willert, B. M. Eller, M. J. A. Werger and E. Brinckmann, *Vegetatio* **90**, 133 (1990).
8. M. Alberdi, L. A. Bravo, A. Gutiérrez, M. Gidekel and L. J. Corcuera, *Physiol. Plant.* **115**, 479 (2002).
9. A. Amtmann, H. J. Bohnert and R. A. Bressan, *Plant Physiol.* **138**, 127 (2005).
10. M. R. Michaud and D. L. Denlinger, *J. Comp. Physiol. B* **177**, 753 (2007).
11. C. Verde, D. Giordano and G. di Prisco, *IUBMB life* **60**, 29 (2008).
12. D. Pegg, *Semin. Reprod. Med.* **20**, 005 (2002).
13. C. Paiva and A. D. Panek, *Biotechnol Annu Rev* **2**, 293 (1996).
14. J. Auh, H. G. Lee, J. Kim, J. Kim, H. Yoon and K. H. Park, *J. Food Sci.* **64**, 418 (1999).
15. J. Kapla, B. Stevansson and A. Maliniak, *J. Phys. Chem. B* **120**, 9621 (2016).
16. C. Olsson, H. n. Jansson and J. Swenson, *J. Phys. Chem. B* **120**, 4723 (2016).
17. M. T. Cicerone and C. L. Soles, *Biophys. J.* **86**, 3836 (2004).
18. T. Eto, R. Takahashi, T. Kamisako, K. Hioki and Y. Sotomaru, *Cryobiology* **68**, 147 (2014).
19. M. ZA, N. WN and S. A. MN, *Czech J. Anim. Sci.* **60**, 10 (2015).
20. C. Polge, A. U. Smith and A. S. Parkes, *Nature* **164**, 666 (1949).
21. C. J. Hunt, *Transfus. Med. Hemother.* **38**, 107 (2011).
22. F. d. L. Janz, A. d. A. Debes, R. d. C. Cavaglieri, S. A. Duarte, C. M. Romão, A. F. Morón, M. Zugaib and S. P. Bydlowski, *J. Biomed. Biotechnol.* **2012** (2012).
23. S. Barun, *The Beats Nat Sci* **2**, 1 (2015).
24. W. F. Rall and G. M. Fahy, *Nature* **313**, 573 (1985).
25. B. S. Chang, R. M. Beauvais, A. Dong and J. F. Carpenter, *Arch. Biochem. Biophys.* **331**, 249 (1996).
26. J. Buitink, I. J. van den Dries, F. A. Hoekstra, M. Alberda and M. A. Hemminga, *Biophys. J.* **79**, 1119 (2000).

27. A. Simperler, A. Kornherr, R. Chopra, P. A. Bonnet, W. Jones, W. D. S. Motherwell and G. Zifferer, *J. Phys. Chem. B* **110**, 19678 (2006).
28. F. Franks, *J. Solution Chem.* **24**, 1093 (1995).
29. L. Slade, H. Levine and J. E. Kinsella, Kinsella, J. Ed (1995).
30. C. A. Angell, R. D. Bressel, J. L. Green, H. Kanno, M. Oguni and E. J. Sare, *Water in Foods*, 115 (1994).
31. J. L. Green, J. Fan and C. A. Angell, *J. Phys. Chem.* **98**, 13780 (1994).
32. L. N. Bell, M. J. Hageman and L. M. Muraoka, *J. Pharm. Sci.* **84**, 707 (1995).
33. R. H. M. Hatley, *Pharm. Dev. Technol.* **2**, 257 (1997).
34. S. L. Shamblin, X. Tang, L. Chang, B. C. Hancock and M. J. Pikal, *J. Phys. Chem. B* **103**, 4113 (1999).
35. W. Wang, *Int. J. Pharm.* **203**, 1 (2000).
36. L. M. Crowe, D. S. Reid and J. H. Crowe, *Biophys. J.* **71**, 2087 (1996).
37. J. H. Crowe, J. F. Carpenter and L. M. Crowe, *Annu. Rev. Physiol.* **60**, 73 (1998).
38. G. Caliskan, A. Kisliuk, A. M. Tsai, C. L. Soles and A. P. Sokolov, *J. Non-Cryst. Solids* **307**, 887 (2002).
39. W. Zheng and S. L. Simon, *J. Chem. Phys.* **127**, 194501 (2007).
40. C. Moynihan, S. Crichton and S. Opalka, *J. Non-Cryst. Solids* **131**, 420 (1991).
41. S. Indra and R. Biswas, *J. Phys. Chem. B* **120**, 11214 (2016).
42. A. S. Rudolph and J. H. Crowe, *Cryobiology* **22**, 367 (1985).
43. M. De los Reyes, L. Saenz, L. Lapierre, J. Crosby and C. Barros, *Vet. Rec.* **151**, 477 (2002).
44. F. Guo and J. M. Friedman, *J. Phys. Chem. B* **113**, 16632 (2009).
45. L. M. Sasnoor, V. P. Kale and L. S. Limaye, *Transplantation* **80**, 1251 (2005).
46. P. W. Fenimore, H. Frauenfelder, B. H. McMahon and R. D. Young, *Proc. Natl. Acad. Sci.* **101**, 14408 (2004).
47. C. R. Herbers, D. Sauer and M. Vogel, *J. Chem. Phys.* **136**, 03B616 (2012).
48. V. Bianco, S. Iskrov and G. Franzese, *J. Biol. Phys.* **38**, 27 (2012).
49. X. Pan and C. E. Glatz, *Cryst. Growth Des.* **2**, 45 (2002).
50. M. D. Ediger, *Annu. Rev. Phys. Chem.* **51**, 99 (2000).
51. I. Chang and H. Sillescu, *J. Phys. Chem. B* **101**, 8794 (1997).
52. E. R. Weeks, J. C. Crocker, A. C. Levitt, A. Schofield and D. A. Weitz, *Science* **287**, 627 (2000).
53. W. K. Kegel and A. van Blaaderen, *Science* **287**, 290 (2000).
54. C. Bennemann, C. Donati, J. Baschnagel and S. C. Glotzer, *Nature* **399**, 246 (1999).

55. A. I. Mel'cuk, R. A. Ramos, H. Gould, W. Klein and R. D. Mountain, *Phys. Rev. Lett.* **75**, 2522 (1995).
56. C. Donati, J. F. Douglas, W. Kob, S. J. Plimpton, P. H. Poole and S. C. Glotzer, *Phys. Rev. Lett.* **80**, 2338 (1998).
57. A. Anopchenko, T. Psurek, D. VanderHart, J. F. Douglas and J. Obrzut, *Phys. Rev. E* **74**, 031501 (2006).
58. M. Flämig, L. Gabrielyan, R. Minikejew, S. Markarian and E. A. Rössler, *Phys. Chem. Chem. Phys.* **22**, 9014 (2020).
59. M. Pöschl and H. Hertz, *J. Phys. Chem.* **98**, 8195 (1994).
60. A. Döb, M. Paluch, H. Sillescu and G. Hinze, *Phys. Rev. Lett.* **88**, 095701 (2002).
61. R. Busselez, R. Lefort, M. Guendouz, B. Frick, O. Merdrignac-Conanec and D. Morineau, *J. Chem. Phys.* **130**, 214502 (2009).
62. K. Kaminski, E. Kaminska, K. Adrjanowicz, Z. Wojnarowska, P. Włodarczyk, K. Grzybowska, M. Dulski, R. Wrzalik and M. Paluch, *Phys. Chem. Chem. Phys.* **12**, 723 (2010).
63. S. Vyazovkin and I. Dranca, *Pharm. Res.* **23**, 2158 (2006).
64. S. Koley, H. Kaur and S. Ghosh, *Phys. Chem. Chem. Phys.* **16**, 22352 (2014).
65. H. Kaur, S. Koley and S. Ghosh, *J. Phys. Chem. B* **118**, 7577 (2014).
66. M. Maroncelli and G. R. Fleming, *J. Chem. Phys.* **86**, 6221 (1987).
67. M. L. Horng, J. A. Gardecki, A. Papazyan and M. Maroncelli, *J. Phys. Chem.* **99**, 17311 (1995).
68. K. Mukherjee, A. Barman and R. Biswas, *J. Mol. Liq.* **222**, 495 (2016).
69. K. Kumbhakar, B. Saha, P. De and R. Biswas, *J. Phys. Chem. B* **123**, 11042 (2019).
70. K. Kumbhakar, E. Tarif, K. Mukherjee and R. Biswas, *J. Mol. Liq.* **290**, 111225 (2019).
71. E. Tarif, B. Saha, K. Mukherjee, P. De and R. Biswas, *J. Phys. Chem. B* **123**, 5892 (2019).
72. E. Tarif, J. Mondal and R. Biswas, *J. Mol. Liq.* **303**, 112451 (2020).
73. E. Tarif, J. Mondal and R. Biswas, *J. Phys. Chem. B* **123**, 9378 (2019).
74. E. Tarif, K. Mukherjee, K. Kumbhakar, A. Barman and R. Biswas, *J. Chem. Phys.* **151**, 154902 (2019).
75. R. Biswas, J. Lewis and M. Maroncelli, *Chem. Phys. Lett.* **310**, 485 (1999).
76. J. Lewis, R. Biswas, A. Robinson and M. Maroncelli, *J. Phys. Chem. B* **105**, 3306 (2001).
77. T. Pradhan and R. Biswas, *J. Phys. Chem. A* **111**, 11514 (2007).
78. T. Pradhan, P. Ghoshal and R. Biswas, *J. Phys. Chem. A* **112**, 915 (2008).
79. T. Pradhan, P. Ghoshal and R. Biswas, *J. Chem. Sci.* **120**, 275 (2008).

80. N. Sarma, J. M. Borah, S. Mahiuddin, H. A. R. Gazi, B. Guchhait and R. Biswas, *J. Phys. Chem. B* **115**, 9040 (2011).
81. M. L. Horng, J. A. Gardecki and M. Maroncelli, *J. Phys. Chem. A* **101**, 1030 (1997).
82. B. Guchhait, S. Das, S. Daschakraborty and R. Biswas, *J. Chem. Phys.* **140**, 104514 (2014).
83. Z. Hu and C. J. Margulis, *Proc. Natl. Acad. Sci.* **103**, 831 (2006).
84. A. Samanta, *J. Phys. Chem. B* **110**, 13704 (2006).
85. B. Guchhait, S. Daschakraborty and R. Biswas, *J. Chem. Phys.* **136**, 174503 (2012).
86. R. Jimenez, G. R. Fleming, P. V. Kumar and M. Maroncelli, *Nature* **369**, 471 (1994).
87. B. Bagchi and R. Biswas, *Adv. Chem. Phys.* **109**, 207 (1999).
88. B. Bagchi and R. Biswas, *Acc. Chem. Res.* **31**, 181 (1998).
89. R. S. Fee and M. Maroncelli, *Chem. Phys.* **183**, 235 (1994).
90. A. Das and R. Biswas, *J. Phys. Chem. B* **119**, 10102 (2015).
91. N. Subba, E. Tarif, P. Sen and R. Biswas, *J. Phys. Chem. B* **124**, 1995 (2020).
92. X. X. Zhang, M. Liang, J. Hunger, R. Buchner and M. Maroncelli, *J. Phys. Chem. B* **117**, 15356 (2013).
93. X. X. Zhang, M. Liang, N. P. Ernsting and M. Maroncelli, *J. Phys. Chem. B* **117**, 4291 (2013).
94. H. Sillescu, *J. Non-Cryst. Solids* **243**, 81 (1999).
95. M. D. Ediger, C. A. Angell and S. R. Nagel, *J. Phys. Chem.* **100**, 13200 (1996).
96. I. Chang, F. Fujara, B. Geil, G. Heuberger, T. Mangel and H. Sillescu, *J. Non-Cryst. Solids* **172**, 248 (1994).
97. C. T. Moynihan, *J. Phys. Chem.* **70**, 3399 (1966).
98. C. Angell, *J. Chem. Phys.* **46**, 4673 (1967).
99. D. Chakrabarti and B. Bagchi, *Phys. Rev. Lett.* **96**, 187801 (2006).
100. B. Guchhait, H. Al Rasid Gazi, H. K. Kashyap and R. Biswas, *J. Phys. Chem. B* **114**, 5066 (2010).
101. G. B. Dutt and T. K. Ghanty, *J. Phys. Chem. B* **107**, 3257 (2003).
102. M. F. Shlesinger, G. M. Zaslavsky and J. Klafter, *Nature* **363**, 31 (1993).
103. J. Habasaki and K. L. Ngai, *J. Chem. Phys.* **129**, 194501 (2008).
104. Z. Hu, X. Huang, H. V. R. Annapureddy and C. J. Margulis, *J. Phys. Chem. B* **112**, 7837 (2008).

Chapter 5

Solvent Dependent Relaxation Dynamics in Lithium Ion Battery Electrolytes: Coupling to Medium Friction

5.1 Introduction

Recent efforts are being increasingly focused on research and development of new materials that would possess potential for addressing the energy challenges ahead. Exotic and useful materials for rechargeable batteries are considered as important members in this domain.¹⁻⁵ Electrolytes are the key ingredients for electrochemical devices. In spite of diversity in applications, for example, batteries, capacitors, fuel cells etc., they execute the same role: transfer of charge by the charge carrier (ions in electrolyte medium) between pair of electrodes.⁶ Medium impact through frictional resistance on ion transport, which is at the heart of developing such energy storage devices, largely governs their suitability in storage and supply-on-demand applications. Another factor that dictates medium choice is the magnitude of static dielectric constant (ϵ_s) because solvents with large ϵ_s facilitate electrolyte dissociation. Solutions of lithium salts, for example, lithium perchlorate (LiClO_4), lithium fluoroborate (LiBF_4), lithium trifluoromethanesulfonate (LiCF_3SO_3), in propylene carbonate (PC), ethylene carbonate (EC), and dimethyl carbonate (DMC) or their mixtures have immense potential in industrial applications in rechargeable lithium ion batteries.^{6,7}

Here our primary goal is to decode the structure-dynamic relationship of such electrolyte system, a thorough understanding of which is essential for further applications of these media in energy storage and supply devices. In our investigation we have considered electrolyte solutions of LiClO_4 (sometime termed as ‘electrolyte system’ or even simply as ‘electrolytes’) in two widely used non-aqueous aprotic solvents, PC and EC, and their binary mixtures. This is to explore the impact of EC as cosolvent on ion-transport (conductivity) and its connection to structure and dynamics of electrolyte medium because EC is known to be an efficient cosolvent in rechargeable lithium-ion battery electrolytes.^{6,8,9} These two solvents are characterized by high dielectric constants, high flash points, large dipole moments, high boiling points (see Table 5.1)^{6,10} etc. which make them excellent media for the construction of Li-ion battery electrolytes. Several investigations have been carried out so far to elucidate the

interaction and dynamics of Li-salt solutions in these solvents or their mixtures employing different spectroscopic techniques such as infrared (IR), nuclear magnetic resonance (NMR), Raman spectroscopy etc.¹¹⁻¹⁵ A few studies have already explored solute-centred non-reactive dynamics, via fluorescence-based techniques, in Li-salt solutions in neat polar solvents¹⁶⁻¹⁸ though similar examinations employing binary solvent mixtures are very limited¹⁹. On this perspective, the present investigations not only provide information about structural and dynamic behaviour of these individual Li-ion battery electrolytes but also augment the understanding of dynamic behaviour of Li-salt in binary solvent mixtures. Pre-peak, often considered as a signature of long range spatial correlation, along with main peak have been observed in several solutions of Li-salt via small angle X-ray scattering (SAXS),²⁰ molecular dynamics (MD) simulation,^{21,22} quasi-elastic neutron scattering (QENS),²³ and neutron diffraction with isotopic substitution (NDIS)²⁴. Moreover, it has been found that the solution structure as well as the dynamics of the medium strongly depends on the salt concentration (here LiClO₄).^{25,26} However, several dynamical aspects regarding the frictional profiles relevant to charge transport in neat EC and PC, and those in their binary mixtures are still not understood. These two solvents, individually strongly polar liquids with a significant difference in ϵ_0 but not so much in η , offer a unique opportunity to decode the solvent polarity effects on friction that associates with ion transport.

In this work, we have investigated the structural and dynamical aspects of [9.795{xEC+(1-x)PC}+0.869LiClO₄], where x represents mole fraction of EC. This has been done via the steady state and the time-resolved fluorescence spectroscopic measurements, employing fluorescent solute probes that differ strongly in their excited state average lifetimes. We have considered (PC+EC)/ LiClO₄ mole ratio fixed at ~ 11.3 , which corresponds to $\sim 1\text{M}$ LiClO₄. This is the optimal LiClO₄ concentration that relates to the maximum value of DC conductivity in the medium.²⁵ The used fluorescent probe molecules are coumarin 153 (C153) ($\langle\tau_{\text{life}}\rangle \sim 3\text{-}5\text{ ns}$)²⁷⁻³⁵ and trans-2-[4-(dimethylamino)styryl]-benzothiazole (trans-DMASBT) ($\langle\tau_{\text{life}}\rangle \sim 0.5\text{ ns}$)^{36,37}. Note this difference in probe lifetimes allow these probes to separately report faster and slower density fluctuations that are present in these media.

Table 5.1: Physical properties^a of EC and PC.

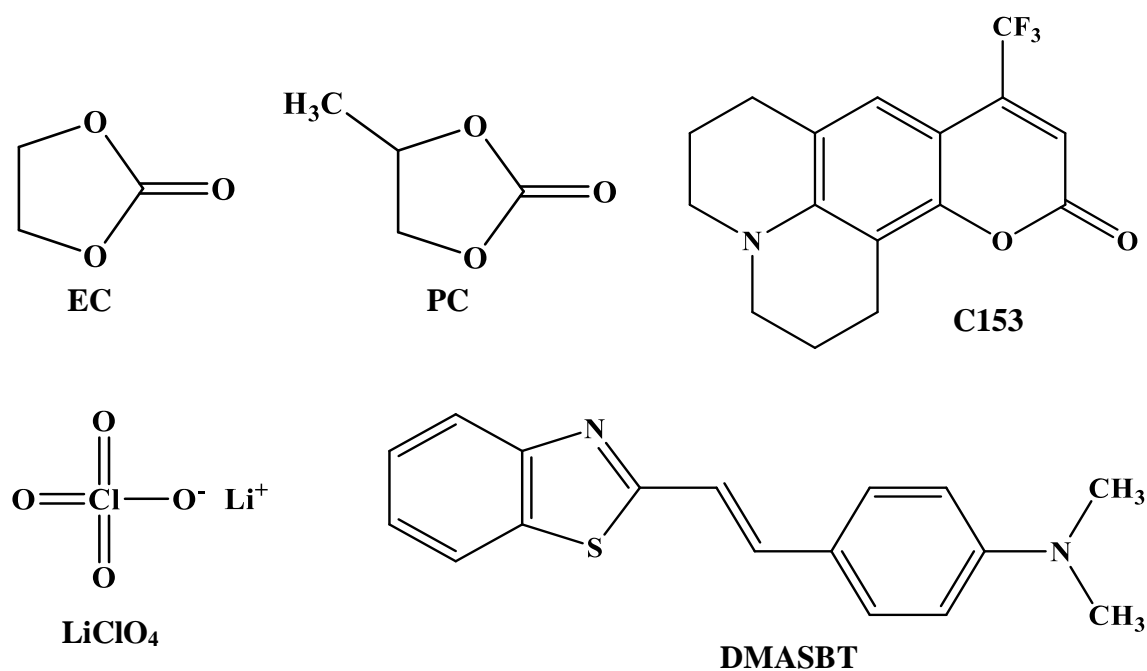
Solvent	Melting Point (T_m /K)	Boiling Point (T_b /K)	Flash Point (T_f /K)	Dipole moment/ Debye	Dielectric Constant (ϵ_s)
EC	309.4	521	433	4.61	89.78 ^c
PC	224.2	515	405	4.81	64.92 ^d

^aRef. 6, 10, ^cat 313 K, ^dat 298 K

5.2 Experimental Details

5.2.1 Materials

Lithium perchlorate (99 %, Alfa Aesar) was vacuum dried prior to use. Ethylene carbonate (EC, 99%, Alfa Aesar), propylene carbonate (PC, 99.7%, Sigma Aldrich), coumarin 153 (C153, Sigma Aldrich), trans-DMASBT (henceforth abbreviated as DMASBT, Sigma Aldrich) were used as received without any further purification. The chemical structures of these materials are provided in Scheme 5.1.

**Scheme 5.1:** Chemical structures of EC, PC, LiClO₄, C153 and DMASBT

5.2.2 Sample Preparation

Molten EC was prepared by gently heating solid EC at 310 K in a controlled environment. Required amount of PC and molten EC (in liquid state) were weighed and mixed in an air-tight glass vial to prepare the binary mixture of neat organic solvents of composition, $[9.795\{x\text{EC}+(1-x)\text{PC}\}]$. In this composition 9.795 mole (EC+PC) was taken and mole fraction of EC was denoted by 'x'. For the preparation of electrolyte solutions of composition, $[9.795\{x\text{EC}+(1-x)\text{PC}\}+0.869\text{LiClO}_4]$ (in this composition of electrolyte solution 0.869 mole LiClO_4 was dissolved in 9.795 mole of (EC+PC) binary solvent mixture), required amount of lithium perchlorate (LiClO_4) was dissolved in the binary solvent mixture, $[9.795\{x\text{EC}+(1-x)\text{PC}\}]$. Proper care was taken to ensure complete dissolution of the added electrolyte and to avoid moisture absorption. All these experimental solutions were prepared at room temperature. Optical measurements of these solutions were performed as follows: 2-3 μL of freshly prepared solutions of C153 in hexane (carrier solvent) was taken in a quartz cuvette of 1 cm optical path length. The carrier solvent was then evaporated off by gently blowing hot air around the outer surface of the cuvette. Approximately 2.5-3 mL of sample solution was then poured into the cuvette. In different measurements, a few crystals of DMASBT were directly added to sample solution taken in a quartz cuvette. Proper care was taken to ensure the complete dissolution of DMASBT. Concentrations of C153/ DMASBT in each of these samples were maintained at $\leq 10^{-5}$ M. All temperature dependent measurements were performed after ensuring thermal equilibration for each solution before data collection.

5.2.3 Measurements of Density and Viscosity Coefficients

Measurements of solution densities (ρ) and viscosity coefficients (η) were performed by using an automated temperature-controlled density-cum-sound analyzer (Anton Paar, model DSA 5000) and automated micro viscometer (AMVn, Anton Paar), respectively.^{19,36} Experimentally measured η and ρ values are provided in Table 5.2 and Table A.c.1 (see Appendix A.c) respectively.

5.2.4 Conductivity Measurements

Conductivity of the electrolyte solutions were measured by a bench-top multi-parameter electrochemical meter (SESHIN BIOTECH, Model: ECM-610). Experimental measured conductivity values are provided in Table 5.3.

5.2.5 Data Collection and Analysis for Steady State Optical Measurements

Steady state absorption and fluorescence emission spectra were recorded by using a UV-Visible spectrophotometer (UV-2600, Shimadzu), and a fluorimeter (Fluorolog, Jobin-Yvon, Horiba), respectively. Temperature was controlled by using a Peltier temperature controller. Steady-state absorption spectra were recorded at 2-nm slit width and fluorescence spectra collected using 2-nm slits at both the excitation and emission ends. Spectra were solvent blank subtracted and processed according to the standard spectral analysis procedure to estimate spectral frequencies and full-widths-at-half-maxima (FWHM).^{27,38-41} The typical error bar for the determined spectral frequencies was $\pm 200 \text{ cm}^{-1}$. Details of measurements technique are the same as discussed in chapter 2.

5.2.6 Data Collection and Analysis for Time-Resolved Fluorescence Emission Spectra

Time-resolved fluorescence measurements were performed with a time-correlated single-photon counting (TCSPC) setup as described in chapter 2 and references.^{27,29,42-44}

Table 5.2: Temperature dependent viscosity coefficients (η) of the solvent mixture [9.795{xEC+(1-x)PC}] and electrolyte solutions [9.795{xEC+(1-x)PC}+0.869LiClO₄].

T/ K	Viscosity (η /cP) of [9.795{xEC+(1-x)PC}]					
	x _{EC} = 0	x _{EC} = 0.204	x _{EC} = 0.409	x _{EC} = 0.613	x _{EC} = 0.817	x _{EC} = 1
293	2.81	2.83	2.85	2.78	2.81	-
298	2.46	-	-	-	-	-
303	2.24	-	-	-	-	-
308	2.09	-	-	-	-	-
313	1.88	-	-	-	-	2.00
318	1.74	-	-	-	-	1.77
T/ K	Viscosity (η /cP) of [9.795{xEC+(1-x)PC}+0.869LiClO ₄]					
	x _{EC} = 0	x _{EC} = 0.204	x _{EC} = 0.409	x _{EC} = 0.613	x _{EC} = 0.817	x _{EC} = 1
293	9.37	9.42	9.71	9.60	9.96	10.00
298	8.08	8.10	8.35	8.26	8.55	8.62
303	7.04	7.06	7.25	7.18	7.44	7.50
308	6.20	6.20	6.37	6.32	6.53	6.57
313	5.48	5.49	5.64	5.60	5.78	5.82
318	4.90	4.91	5.03	5.00	5.16	5.20

Table 5.3: Experimental DC conductivity (κ) for three x_{EC} in $[9.795\{x_{EC}+(1-x)PC\}+0.869LiClO_4]$ at $300\pm 1K$.

[9.795{x _{EC} +(1-x)PC}+0.869LiClO ₄]		
x_{EC}	Conductivity (κ /mScm ⁻¹)	Viscosity (η /cP) at 298K
0	5.57	8.08
0.613	6.65	8.26
1	7.07	8.62

5.3 Results and Discussion

5.3.1 Steady State Spectral Characteristics

Steady state absorption and emission spectra of C153 in EC, PC, their binary mixture, and in LiClO₄ solutions of each of them are shown in Figure 5.1. Notice that absorption and emission spectra of C153 in these neat media do not show any solvent dependence although ϵ_0 of EC is ~30% larger than that for PC (see Table 5.1). This is because the reaction field,³⁹ $RF = \frac{\epsilon_0 - 1}{\epsilon_0 + 2} - \frac{n_D^2 - 1}{n_D^2 + 2}$, is the same (~0.7) for both these solvents, indicating the nuclear polarizability associated with solvent reorganization around a dipolar solute is not different for these two neat solvents. However, red shift in both absorption and emission spectra has been observed upon addition of LiClO₄ in these neat solvents and their binary mixtures. Electrolyte-induced spectral red shift has already been observed for other pure solvents^{16,45,46} and binary mixtures,¹⁹ and attributed to the additional stabilization because of probe-ion (dipole-ion) interaction.¹⁷ Similar observation has been made for DMASBT spectra in these solutions, shown in Figure. A.c.2 (see Appendix).

Composition dependent absorption and emission spectral frequencies and widths (FWHMs) of C153 at 293 K in binary solvent mixture, $[9.795\{x_{EC}+(1-x)PC\}]$ and in the electrolyte system, $[9.795\{x_{EC}+(1-x)PC\}+0.869LiClO_4]$, are shown in Figure 5.2. Numerical values of these spectral features are summarized in Table A.c.3 (Appendix). Addition of electrolyte (~1 M) in the binary mixture leads to a red-shift of approximately 500 cm⁻¹ in both the absorption and emission spectra of C153 throughout the composition. This red-shift occurs with concomitant broadening and narrowing (although limited to ~250 cm⁻¹) of the absorption and emission spectra respectively. This spectral red-shift with broadening for absorption and narrowing for emission has been observed earlier for neat solvents with C153 as probe solute.²⁷ Temperature dependent absorption and emission measurements in the range T(K)=293 -318, shown in

Chapter 5

Figure A.c.4 (Appendix), do not reflect any peak shift with temperature, suggesting the interaction between the probe solute and the surround environment remains insensitive to the solution temperature.⁴⁷ Note this insignificant impact of temperature in this range on the steady state absorption and emission spectra of C153 in electrolyte solutions renders validity to the comparison shown in Figure 5.1 and Figure 5.2 where spectra in neat EC were recorded at 313 K while in other media at 293 K.

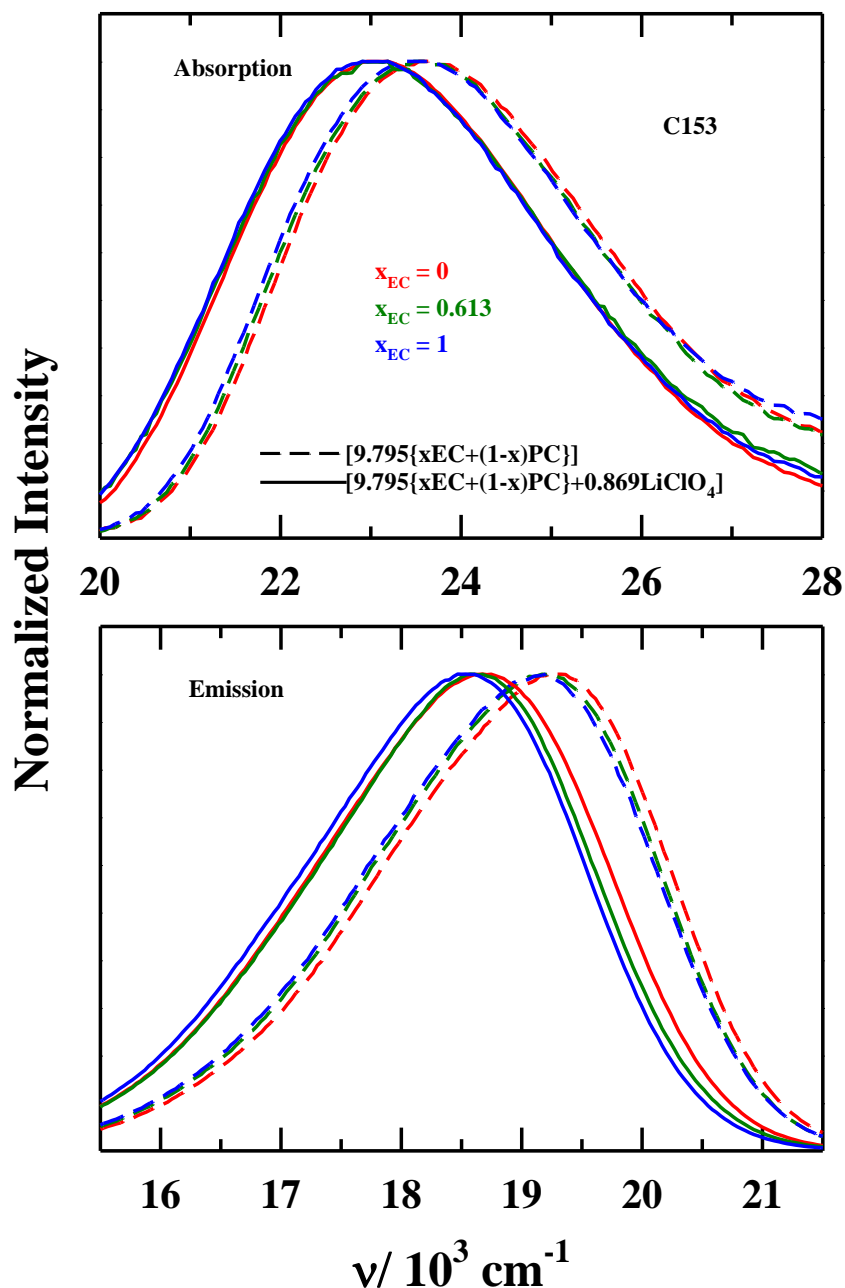


Figure 5.1: Steady state absorption (upper panel) and emission spectra (lower panel) of C153 at three different mole fractions of EC (x_{EC}) in the binary solvent mixture, $[9.795\{x_{\text{EC}}+(1-x)\text{PC}\}]$, and in the electrolyte solutions, $[9.795\{x_{\text{EC}}+(1-x)\text{PC}\}+0.869\text{LiClO}_4]$ at 293 K, and corresponding spectrum in neat EC at 313 K. All presentations are colour-coded. Each of these emission spectra was recorded after excitation at the peak wavelength of the corresponding absorption spectrum.

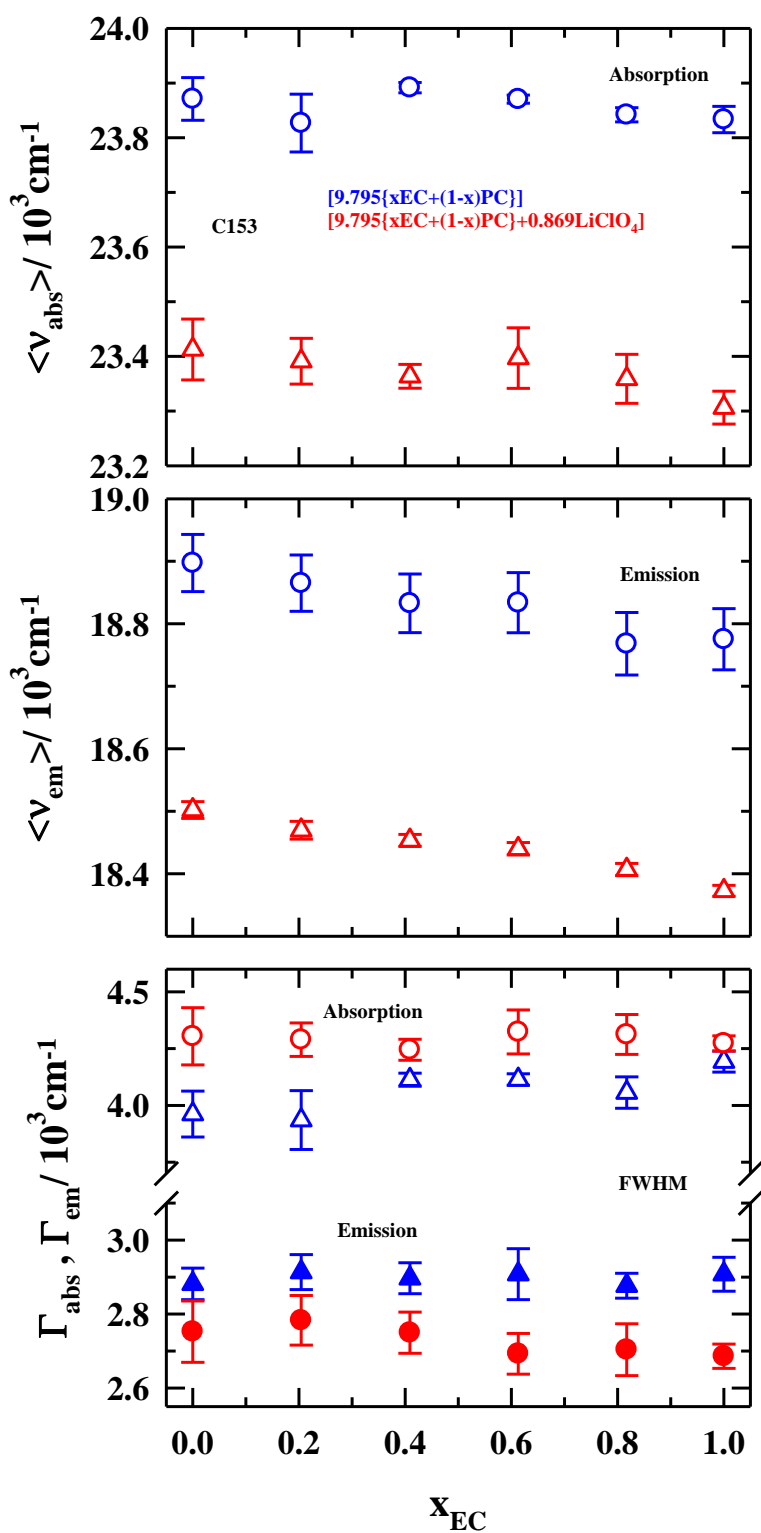


Figure 5.2: Absorption (upper panel) and emission frequencies (middle panel) and spectral widths (FWHMs) (lower panel) for C153 at various EC mole fractions in binary solvent mixture, [9.795{xEC+(1-x)PC}] and electrolyte solutions, [9.795{xEC+(1-x)PC}+0.869LiClO₄] at 293 K. For neat EC, $T=313$ K. All representations are colour-coded.

SAXS, QENS as well as simulation studies of electrolyte solutions of Li⁻ salt suggested presence of mesoscopic structures.²⁰⁻²⁴ The existence of such ion-induced micro-domains or inhomogeneous density distributions in the present systems (electrolyte concentration ~1M), can be investigated by following the excitation wavelength (λ_{exc}) dependence of the fluorescence emission from a dissolved probe solute.⁴⁷⁻⁵² This has been done by monitoring the λ_{exc} dependence of the emission spectral frequencies (ν_{em}) of both DMASBT and C153 in [9.795{xEC+(1-x)PC}] and [9.795{xEC+(1-x)PC}+0.869LiClO₄] solutions. Results from these measurements, shown Figure 5.3, indicate a weak dependence of ν_{em} (red-shift by ~300 cm⁻¹) on λ_{exc} for C153 in presence and absence of electrolyte in these solutions. For DMASBT, in contrast, this dependence in presence of electrolyte is stronger with a shift of ~700 cm⁻¹, although much weaker dependence is found in the absence of electrolyte. These emission energy shifts accompany a band narrowing of ~200 cm⁻¹, suggesting a qualitative similarity in polarity-induced red-shift in emission peak frequency along with band narrowing between common solvents²⁷ and these electrolyte solutions.

Now the question is why do we see λ_{exc} dependence of ν_{em} for DMASBT in electrolyte solutions but not for C153? Also, what does the λ_{exc} dependence of DMASBT in the presence of electrolyte and no-dependence in the absence of electrolyte in these solution suggest? It is known^{50,51} that if interconversion among different solvation environments (surrounding the dissolved probes) is much faster than the average fluorescence lifetime of the probe, the emission energy will report only a unique, dynamically averaged out, completely solvent-relaxed environment. Otherwise, the fluorescence emission will occur from differently solvated states of the probe molecules, rendering λ_{exc} dependence of ν_{em} . As observed earlier,^{36,37,53} the short lifetime of DMASBT in common solvents³⁷ and in these solutions ($\langle \tau_{life} \rangle \sim 0.2$ ns, see Table A.c.5A, Appendix) is the key for observing λ_{exc} dependent ν_{em} for [9.795{xEC+(1-x)PC}+0.869LiClO₄] solutions. These results, therefore, suggest that the heterogeneous solvation environments ('micro-domains') that surround DMASBT in electrolyte solutions of these solvents persist approximately for sub-nanosecond duration. Effects of temperature on λ_{exc} dependence of ν_{em} for DMASBT, entering through the increased rate of interconversion (and thus 'homogenization') of differing solvation environments, are shown in Figure 5.4. Note

the magnitude of total shift in ν_{em} remains nearly unchanged ($\sim 700 \text{ cm}^{-1}$) for the temperature range studied, 293 – 318 K. This near-constancy of λ_{exc} -induced total emission shift is counter-intuitive and may originate from competing intra-molecular processes in DMASBT³⁷. Further experimental and computational study is therefore warranted to fully understand the medium influence on temperature dependent excited state intra-molecular dynamics of DMASBT in solutions.

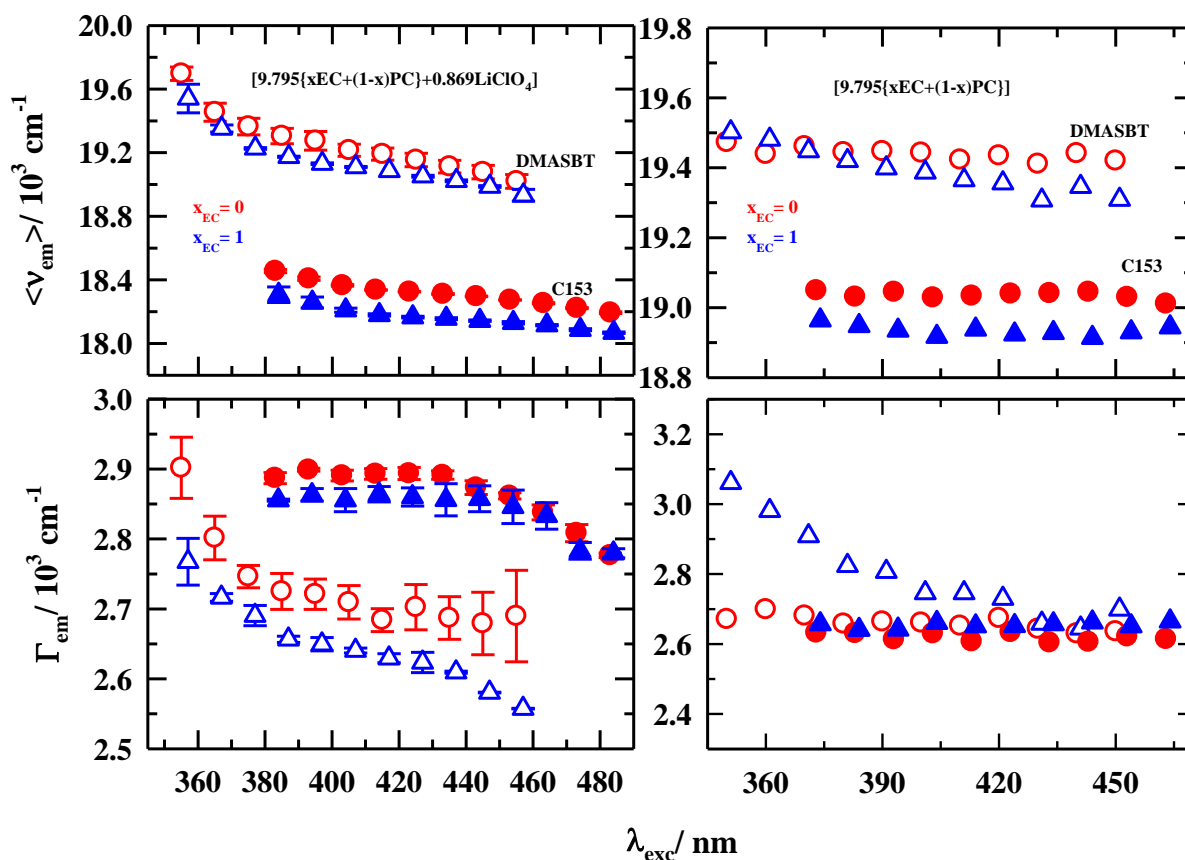


Figure 5.3: Excitation wavelength dependence (λ_{exc}) of steady state fluorescence emission frequency, $\langle \nu_{em} \rangle$ (upper panels) and spectral width (FWHM), Γ_{em} (lower panels) of DMASBT and C153 at two mole fractions of EC in $[9.795\{x\text{EC}+(1-x)\text{PC}\}]$ (right panel) and $[9.795\{x\text{EC}+(1-x)\text{PC}\}+0.869\text{LiClO}_4]$ (left panel) at 293 K, respectively. All representations are colour-coded.

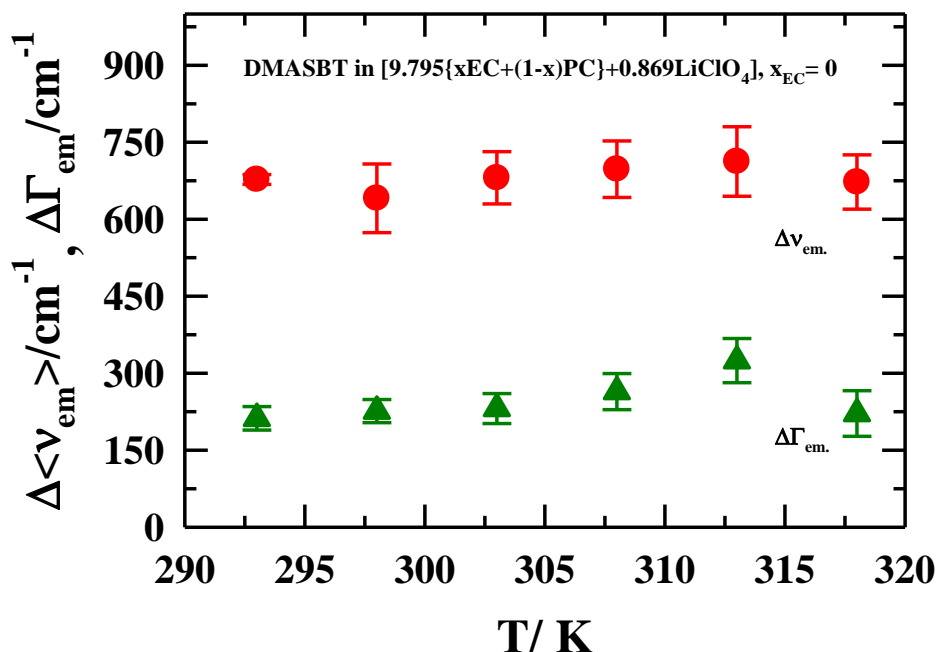


Figure 5.4: Representative temperature-dependent excitation wavelength (λ_{exc}) induced total emission shift ($\Delta \langle \nu_{em} \rangle$), and total change in width ($\Delta \Gamma_{em}$) of DMASBT in [9.795{xEC+(1-x)PC}+0.869LiClO₄] with $x_{EC}=0$, where $\Delta x(T) = x(T, \lambda_{exc,b}) - x(T, \lambda_{exc,r})$, $x = \langle \nu_{em} \rangle$ or Γ_{em} . $\lambda_{exc,b}$ and $\lambda_{exc,r}$ are the shortest (bluest) and longest (most red) excitation wavelengths respectively. We have considered λ_{exc} from 360 nm (bluest) to 460 nm (most red) for DMASBT whereas from 380 nm (bluest) to 480 nm (most red) for C153 at 10 nm interval. The bluest and most red λ_{exc} are -50 and +50 nm with respect to the individual peak wavelengths of the absorption spectra (λ_{abs}^{max}). All presentations are colour-coded.

5.3.2 Time-Resolved Measurements: Lifetime and Dynamic Stokes Shift

Because the average fluorescence lifetime ($\langle \tau_{life} \rangle$) of DMASBT depends both on solvent polarity and viscosity, and exhibits fractional viscosity dependence (that is, $\langle \tau_{life} \rangle \propto \eta^p$ with $p < 1$) in non-polar solvents,³⁷ we explored the impact of solution composition and temperature on DMASBT lifetime in these electrolyte solutions. Representative temperature and composition dependent fluorescence emission decays are shown in Figure 5.5 along-with bi-exponential fits. Fit parameters and $\langle \tau_{life} \rangle$ obtained from them are summarized in Table A.c.5A (Appendix). Temperature and viscosity dependence of $\langle \tau_{life} \rangle$ for DMASBT are displayed in

Figure 5.6. Similar results for C153 in these solutions are provided in Table A.c.5B and Figure A.c.6 (Appendix). Dependences shown in Figure 5.6 indicate that for DMASBT $\langle \tau_{\text{life}} \rangle$, ranging between ~ 100 - 200 ps, decreases with temperature and exhibits a fractional viscosity dependence, $\langle \tau_{\text{life}} \rangle \propto (\eta/T)^p$ with $p \sim 0.8$. Note this value of p is larger than that reported ($p \sim 0.5$) earlier from pressure dependent studies with DMASBT in non-polar solvents.³⁷ This difference is a reflection of the polarity dependence of the isomerisation barrier that separates the radiative *trans* form from the non-radiative *cis* in its excited state.

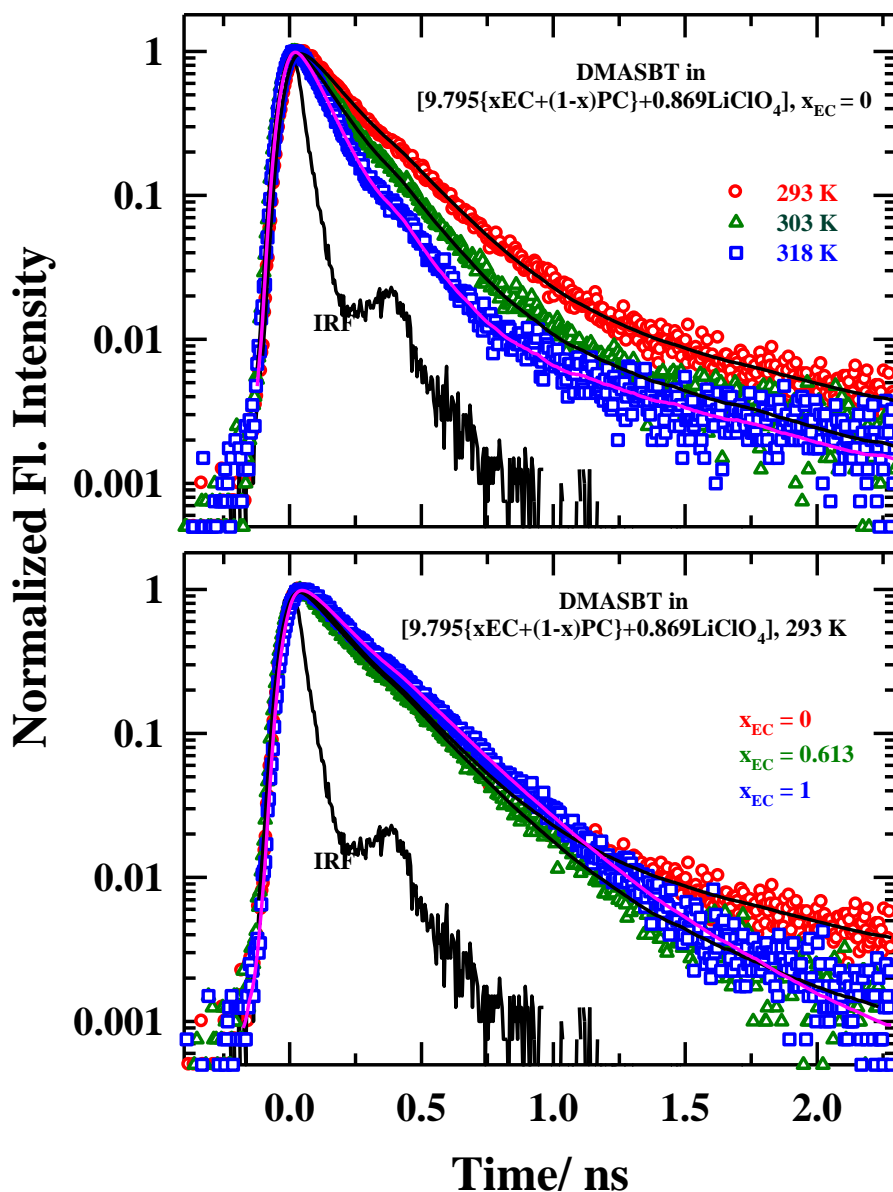


Figure 5.5: Temperature (upper panel) and composition (lower panel) dependent fluorescence emission decays of DMASBT in $[9.795\{x_{\text{EC}}+(1-x)\text{PC}\}+0.869\text{LiClO}_4]$. All representations are colour-coded.

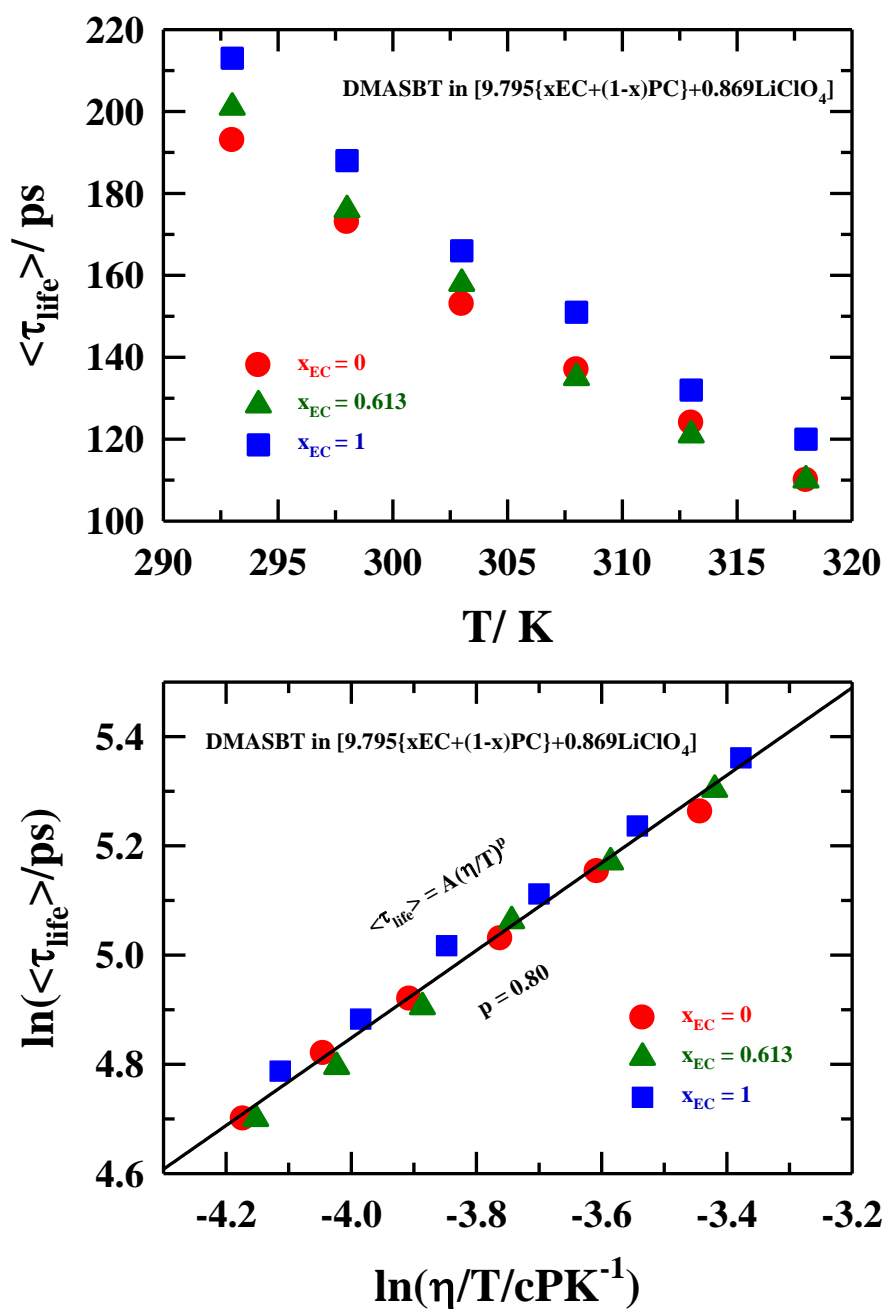


Figure 5.6: Temperature dependent (upper panel) and temperature-reduced viscosity (η/T) (lower panel) dependent average lifetime ($\langle \tau_{\text{life}} \rangle$) of DMASBT at three x_{EC} in $[9.795\{x_{\text{EC}}+(1-x)\text{PC}\}+0.869\text{LiClO}_4]$. All representations are colour-coded.

Next we explore the Stokes shift dynamics in electrolyte solutions by using the solvation probe C153. Fluorescence emission intensity decays collected at blue (490 nm) and red wavelength (640 nm) with respect to the peak wavelength of the corresponding steady state fluorescence emission spectrum of C153 dissolved in $[9.795\{x_{\text{EC}}+(1-x)\text{PC}\}+0.869\text{LiClO}_4]$ with $x_{\text{EC}} = 0$

solution are shown in Figure 5.7. Tri-exponential fits going through these data points, fit parameters, and instrument response function (black dotted lines) are shown in the same figure. A similar representation of intensity decay in $[9.795\{x_{EC}+(1-x)PC\}+0.869LiClO_4]$ with $x_{EC}=1$ is shown in Figure A.c.7 (Appendix). Decay only at the blue wavelength, and rise followed by decay at the red wavelength is a typical signature of relaxation of environment (Stokes shift dynamics) in response to the sudden excitation of the solute dipole.^{54,55} Representative time-resolved emission spectra (TRES) of C153 dissolved in $[9.795\{x_{EC}+(1-x)PC\}+0.869LiClO_4]$ with $x_{EC}=0$ solution are shown in Figure 5.8. The lines connecting the data points are generated from fits of the reconstructed data points to a log-normal line-shape function.³² Steady state emission spectrum of C153 in the same solution is shown by the dashed lines in the same figure. Note steady state emission spectrum is slightly blue shifted compared to time-resolved emission spectrum at $t = \infty$ i.e. when excited C153 is surrounded by completely polarisation-relaxed environment. Steady state emission from excited solute with incompletely relaxed solvent environment is responsible for the observed blue shift.

Table 5.4 summarizes the magnitudes of dynamic Stokes shift for C153 dissolved in $[9.795\{x_{EC}+(1-x)PC\}+0.869LiClO_4]$ and the estimated missing components⁵⁶ due to the limited time resolution employed in the present measurements. Estimated total dynamic Stokes shifts⁵⁶ are also provided in this table. Previously reported experimental studies on solvation dynamics of C153 in PC indicate presence of multi-exponential decay with a substantial ultrafast time component in the sub-hundred femtosecond regime.²⁷ It is therefore quite expected that in these electrolyte solutions faster solvation response (sub-10 ps) would contribute significantly. Results presented in Table 5.4 clearly indicate that present experimental set up with broad time resolution (FWHM of IRF ~ 85 ps) have missed nearly half of the total dynamic shift across the compositions considered.

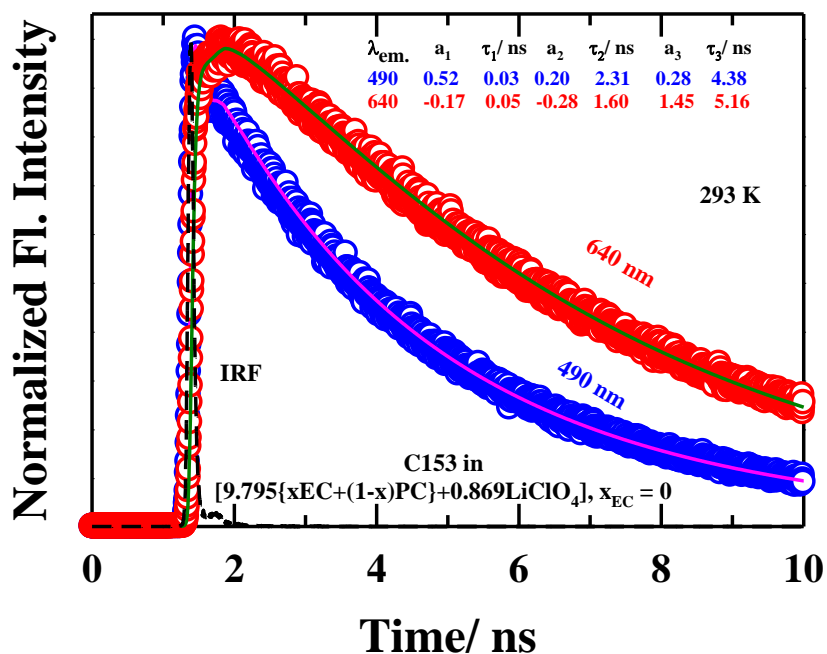


Figure 5.7: Representative time-dependent fluorescence intensity decays of C153 in [9.795{xEC+(1-x)PC}+0.869LiClO₄] with x_{EC}=0, collected at blue (490 nm) and red end (640 nm) wavelengths with respect to the peak wavelength of the corresponding steady state emission spectrum at 293 K. Experimental data are represented by circles; solid lines going through the data are fits. Black dashed lines depict the instrument response function. Multi-exponential decay fit parameters are shown in the inset. All representations are colour-coded.

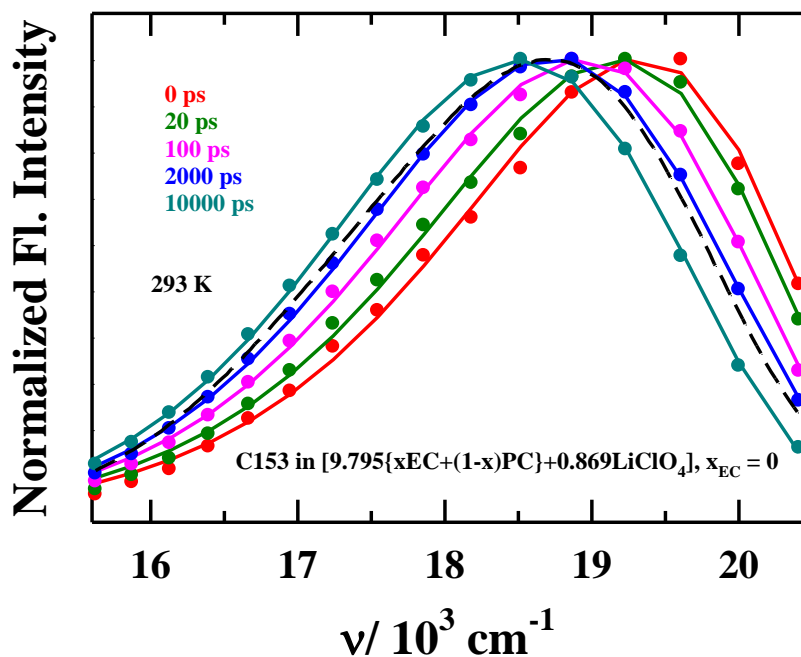


Figure 5.8: Representative constructed time-resolved emission spectra (TRES) of C153 in [9.795{x_{EC}+(1-x)PC}+0.869LiClO₄] with x_{EC}=0 for different time intervals at 293 K. The steady state emission spectrum of C153 in this solution is shown by the dashed lines. All representations are colour-coded.

Table 5.4: Magnitudes of estimated ($\Delta\nu_{\text{est}}^t$), observed ($\Delta\nu_{\text{obs}}^t$) and missing portion of the total dynamics Stokes shift for C153 in [9.795{x_{EC}+(1-x)PC}+0.869LiClO₄] at 293K.

x _{EC}	$\Delta\nu_{\text{est}}^t/10^3\text{cm}^{-1}$	$\Delta\nu_{\text{obs}}^t/10^3\text{cm}^{-1}$	% missed
0	1.49	0.75	50
0.204	1.52	0.82	46
0.409	1.53	0.87	43
0.613	1.55	0.75	52
0.817	1.56	0.72	54
1	1.58	0.73	54

Representative solvation response function ($S(t)$) obtained from the time-resolved emission spectra are shown in Figure 5.9. Decays shown in Figure 5.9 as well as at other x_{EC} are found to fit adequately to bi-exponential function. Associated fit parameters are summarized in Table 5.5. Note in this table that the composition dependent $S(t)$ decays are characterized by two nearly equal components: a relatively faster (sub-50 ps) component followed by a much slower (2-4 ns) one. The sub-50 ps component may originate from the relaxation of the free solvent molecules³² which are not complexed with the ions present in these electrolyte solutions.

Inspection of the dielectric relaxation data for pure PC at room temperature also support presence of such a timescale.⁵⁷ Translational diffusion of Li^+ ¹⁹ may also contribute to this relaxation component as the estimated translational diffusion time of Li^+ is \sim sub-100ps (see AppendixTable A.c.8). Next, what is the origin of the slow, nano-second component? Within the continuum model one can immediately think of the charge-density relaxation whose timescale could be estimated from the Maxwell relaxation time. The estimated Maxwell relaxation times¹⁷ (τ) for the collective translational mode of ions from the static dielectric constant and the DC conductivity in the electrolyte solution, [9.795{xEC+(1-x)PC}+0.869LiClO₄], at various EC mole fractions lie approximately in the 1 ns range. These estimated relaxation times are \sim 2.5-3.5 times shorter than the slowest S(t) relaxation times measured here. Therefore, the slowest mode of the dynamic Stokes shift of C153 in these electrolyte solutions might have originated from molecular processes that involve motions of both ions and solvent molecules.¹⁷ For this we consider the following probable sources: translational diffusion of (i) free solvent molecules, (ii) ClO_4^- ion diffusion, (iii) relaxation of cation-solvent composite species²⁵. Recent simulation study of electrolyte solutions containing LiBF_4 salt at low concentration suggests that the solvent molecules are so strongly bound to the cations that no particle exchange between the first and the second solvation shell of lithium ion could be observed in 100 ps timescale, whereas several such exchanges can take place for the anion within the same timescale.⁵⁸ It may therefore be plausible that the nanosecond component is arising from the solvent molecules that are bound to Li^+ . A relaxation peak around 100 MHz has been reported by dielectric relaxation studies of (PC+ LiClO_4) solutions,⁵⁹ providing further support to presence of nanosecond solvation timescale in these electrolyte solutions. Both the relaxation time constants and average solvation time ($\langle\langle\tau_s\rangle\rangle$), summarized in Table 5.5, become somewhat faster with increase of co-solvent, EC, in the electrolyte solution despite a mild increase of medium viscosity. Relatively faster rotational and translational movements due to smaller size of EC than PC may be a reason for this EC-induced decrease of solvation time.

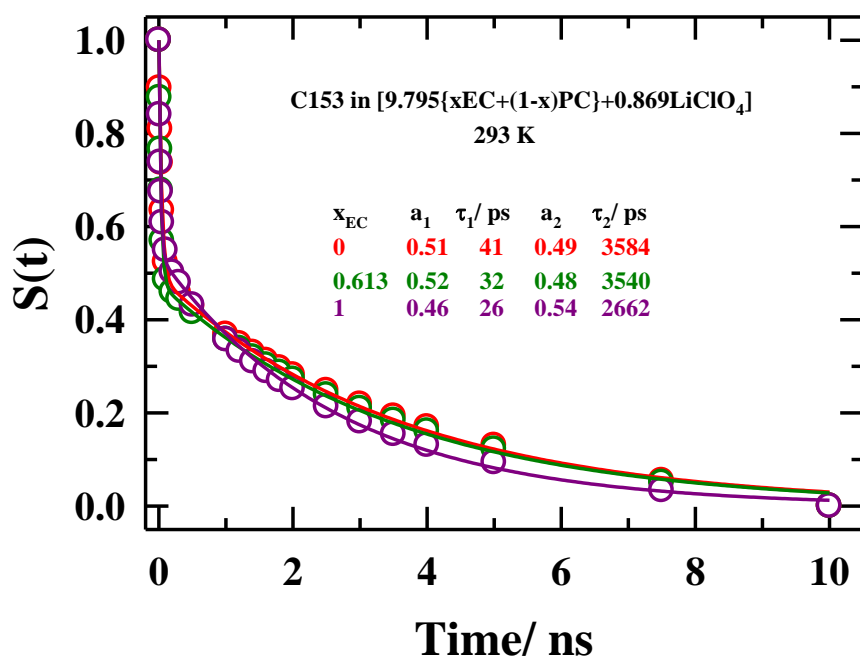


Figure 5.9: Solvation response functions ($S(t)$) for C153 at three x_{EC} in [9.795(x_{EC} +(1- x)PC)+0.869LiClO₄] at 293 K. Experimental data are shown by circles; solid lines through the data represent fits. Fit parameters are shown in the inset. All representations are colour-coded.

Table 5.5: Decay characteristics of solvation response function for C153 in [9.795{x_{EC}+(1- x)PC}0.869LiClO₄] at 293K.

x _{EC}	a ₁	τ ₁ /ps	a ₂	τ ₂ /ps	$\langle\tau_s\rangle$ /ps
0	0.51	41	0.49	3584	1775
0.204	0.53	34	0.47	3364	1599
0.409	0.55	34	0.45	3482	1586
0.613	0.52	32	0.48	3540	1716
0.817	0.49	43	0.51	3405	1758
1	0.46	26	0.54	2662	1449

5.3.3 Time-Resolved Anisotropy ($r(t)$) Measurements: Solute Rotation and Viscosity Coupling

Rotational anisotropy decay of C153 and DMASBT in [9.795{x_{EC}+(1- x)PC}] and [9.795{x_{EC}+(1- x)PC}+0.869LiClO₄], have been investigated within the temperature range $293 \leq T/K \leq 318$. Representative $r(t)$ decays showing the impact of electrolyte on rotation dynamics of these solutes are presented in Figure 5.10. As expected,⁶⁰ $r(t)$ decays become slower for both the solutes upon addition of electrolyte. However, the extent of slowing down

upon addition of electrolyte for C153 is nearly the same as the amount of increase in solution viscosity ($\eta_{\text{elec}}/\eta_{\text{solv}} \sim 3$, see Table 5.2), whereas that factor for DMASBT is double ($\langle \tau_{\text{rot}} \rangle^{\text{elec}} / \langle \tau_{\text{rot}} \rangle^{\text{solv}} \sim 6$). This indicates that electrolyte-induced lengthening of the rotation time for DMASBT is arising not only from the enhanced solution frictional resistance but also from the modulation of the isomerisation barrier³⁷ upon addition of electrolyte.

Parameters from fit to $r(t)$ decays for C153 and DMASBT collected at other compositions and temperatures are summarized in Table A.c.9 (Appendix). Data in this table suggest that anisotropy decays in these solutions are mostly bimodal for both the solutes in these electrolyte solutions. This reflects the non-Markovian nature of the underlying time-dependent medium friction exerted by the medium on the rotating solute. Note our measured $\langle \tau_{\text{rot}} \rangle$ for neat solvent (PC) is in good agreement with those reported earlier^{29,32}. Data shown in this table indicate that $\langle \tau_{\text{rot}} \rangle$ for both solutes decreases with increase of solution temperature.

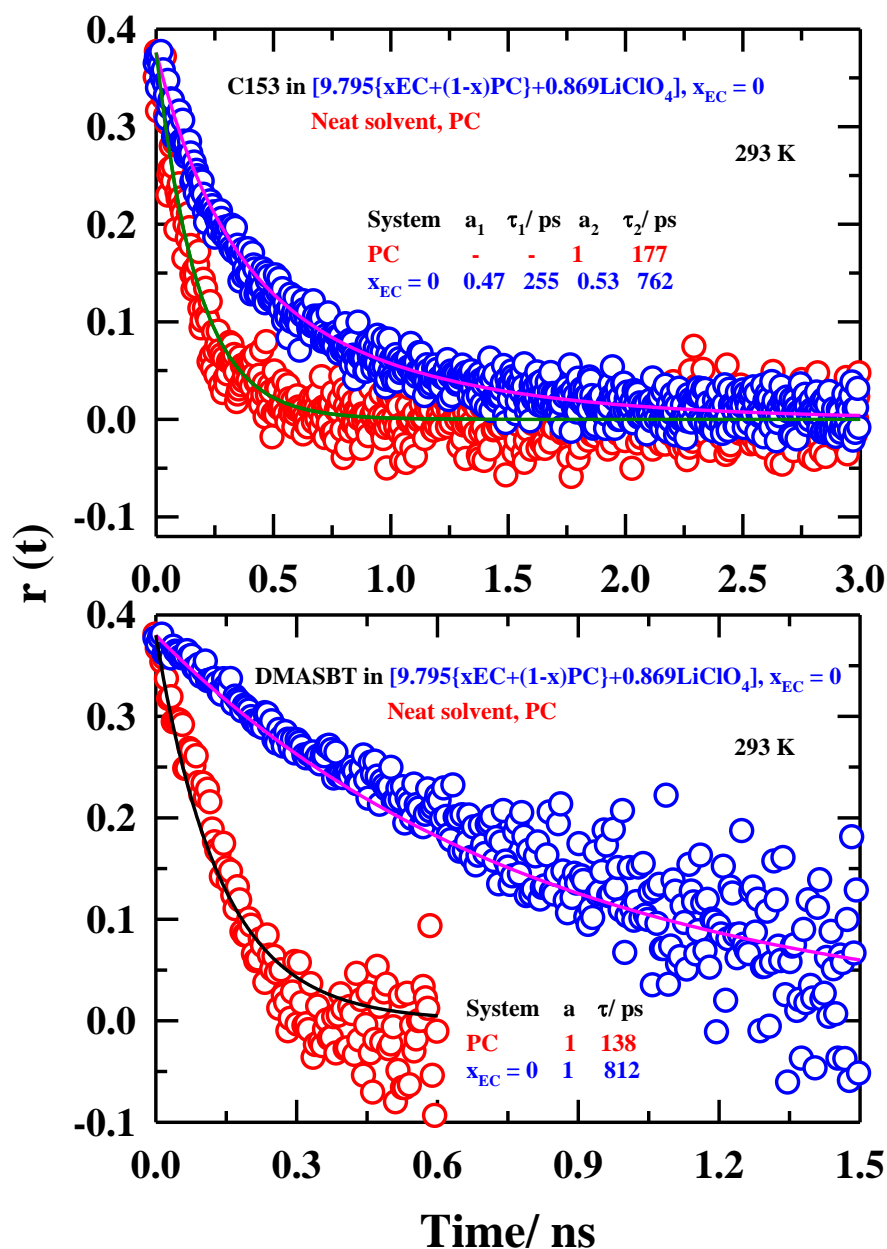


Figure 5.10: Representative fluorescence anisotropy decays, $r(t)$, for C153 (upper panel) and DMASBT (lower panel) in PC, [9.795{xEC+(1-x)PC}+0.869LiClO₄] with $x_{EC}=0$, solution at 293 K. Experimental data are shown by circles; solid lines through the data points represent fits. Fit parameters are shown in the inset. All representations are colour-coded.

We explore in Figure 5.11 the viscosity-coupling of $\langle \tau_{rot} \rangle$ for these solutes where $\langle \tau_{rot} \rangle$ values are shown as a function of temperature-reduced viscosity, (η/T) . Solid lines going through the data points depict dependence of the type, $\langle \tau_{rot} \rangle \propto (\eta/T)^p$. Note for C153 the value of the power is near-unity ($p=0.98$) whereas it is significantly lower than unity ($p=0.5-0.7$) for DMASBT.

Stokes-Einstein-Debye (SED) predictions,^{29,61-66} $\tau_{\text{rot}}^{\text{h}} = V \eta C f_s / k_B T$, (V and f_s being the volume and shape factor and C the solute-solvent coupling parameter) using $V = 246 \text{ \AA}^3$, $f_s = 1.71$, and $C = 0.24$ (slip boundary condition) and 1 (stick boundary condition) are shown in Figure A.c.10 (Appendix) which suggest that the measured rotation times for C153 fall between these two limits of hydrodynamic predictions. Interestingly, DMASBT rotation times in these solutions with differing EC concentrations, unlike for C153 where data coalesce into one single curve, exhibit disparate dependencies at different EC concentrations. The difference for DMASBT arises probably from the modulation of the isomerisation barrier with EC concentration because EC is more polar than PC. Note the p values at these EC concentrations are also different (0.62, 0.47 and 0.65). However, this variation in p values should not be interpreted too quantitatively; rather, it may be considered simply as an over-all reflection of a partial viscosity decoupling of DMASBT in these solutions with a fraction power ($p=0.6 \pm 0.1$), which is significantly less than unity. This qualitative consideration is necessary reminding the fact that DMASBT possesses a short lifetime ($\sim 100\text{-}200$ ps) and it participates in excited state isomerisation reaction while undergoing rotational diffusion. This in turn suggests that DMASBT might not be an appropriate dipolar probe to map the dynamic friction on a solute rotating in these media.

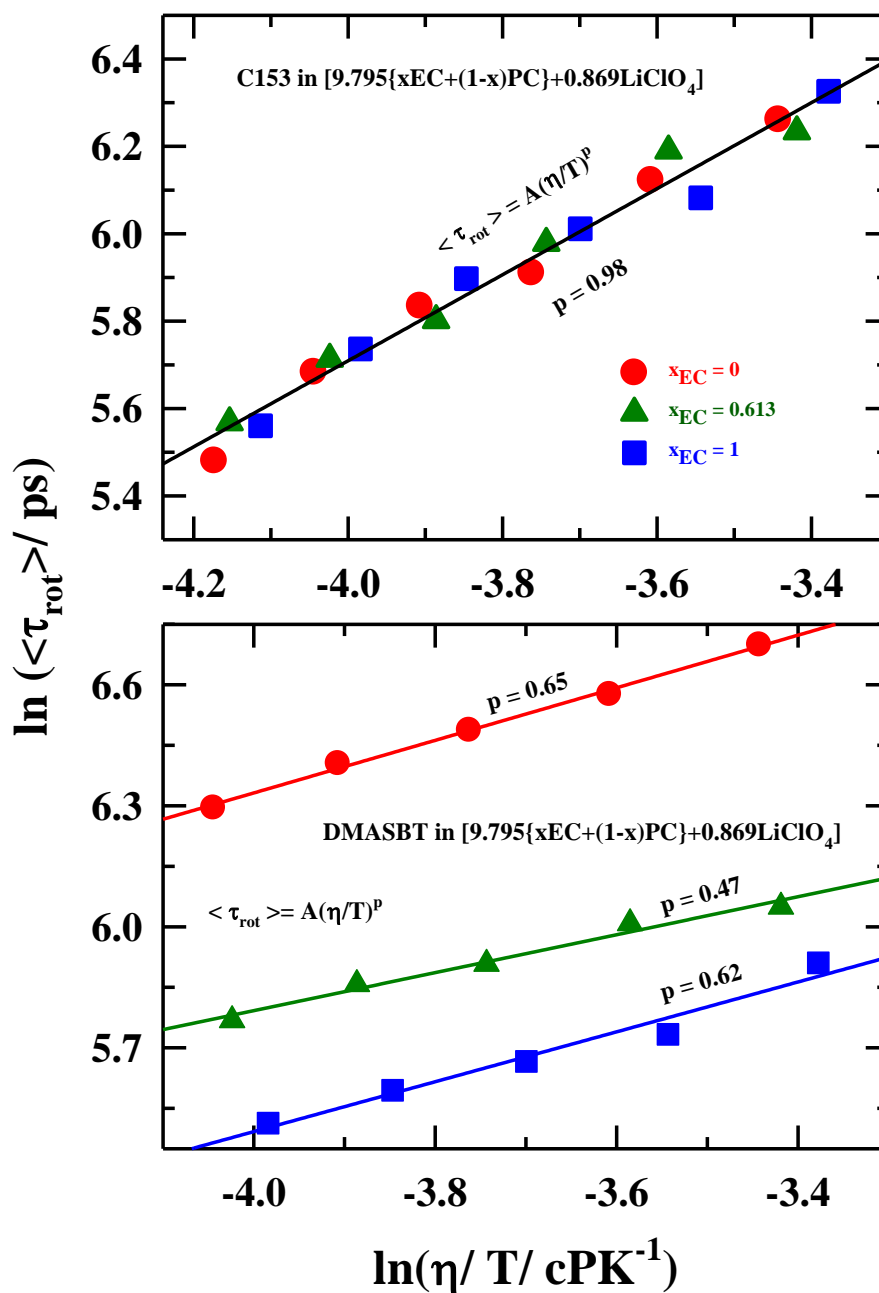


Figure 5.11: Temperature-reduced viscosity dependence (η/T) of average rotation time ($\langle \tau_{\text{rot}} \rangle$), of C153 (upper panel) and DMASBT (lower panel) in three mole fraction of EC in [9.795{xEC+(1-x)PC}+0.869LiClO₄]. Solid lines passing through the data points represent fits. Data at different EC mole fractions are colour-coded.

5.4 Conclusion

In summary, the heterogeneity aspect of the solvent mixture, $[9.795\{x\text{EC}+(1-x)\text{PC}\}]$, and the electrolyte system, $[9.795\{x\text{EC}+(1-x)\text{PC}\}+0.869\text{LiClO}_4]$, and solute-centred dynamics in them have been explored by using two fluorescent probes, C153 and DMASBT. These two probe solutes differ widely in their excited state lifetimes. Significant excitation wavelength dependent steady state fluorescence emission of DMASBT in electrolyte solutions supports the view of solution spatial heterogeneity with relatively faster inhomogeneity timescales (micro-domain persistence times) because such dependence is absent for C153. The magnitude of excitation wavelength induced total shift of emission frequency has been found to remain constant ($\sim 750\text{ cm}^{-1}$) for the temperature range studied, reflecting complex electrolyte effects on the photo-induced excited state cis-trans isomerisation reaction of DMASBT. Dynamic Stokes shift measurements using C153 in this electrolyte system at six different concentrations of EC report $\sim 700\text{-}900\text{ cm}^{-1}$ dynamic shifts with an estimated missing portion of $\sim 40\text{-}50\%$. Solvation and rotation dynamics measured using C153 have been found to be biphasic in these media. Temperature dependent rotation times for C153 suggests hydrodynamic viscosity coupling while those for DMASBT reflect strong fractional viscosity dependence. Megahertz-gigahertz dielectric relaxation measurements and computer simulation studies are necessary for further understanding of the structure and dynamics of these technologically important battery electrolyte systems.

References

1. M. Armand and J. M. Tarascon, *Nature* **451**, 652 (2008).
2. J. M. Tarascon and M. Armand, *Nature* **414**, 359 (2001).
3. Y. C. Lu, Z. Xu, H. A. Gasteiger, S. Chen, K. Hamad-Schifferli and Y. Shao-Horn, *J. Am. Chem. Soc.* **132**, 12170 (2010).
4. P. Simon and Y. Gogotsi, *Nat. Mater.* **7**, 845 (2008).
5. T. Ogasawara, A. Débart, M. Holzapfel, P. Novák and P. G. Bruce, *J. Am. Chem. Soc.* **128**, 1390 (2006).
6. K. Xu, *Chem. Rev.* **104**, 4303 (2004).
7. F. Croce, G. B. Appetecchi, L. Persi and B. Scrosati, *Nature* **394**, 456 (1998).
8. S. Tobishima, M. Arakawa, T. Hirai and J. Yamaki, *J. Power Sources* **26**, 449 (1989).
9. R. S. McMillan and M. W. Juzkow, *J. Electrochem. Soc.* **138**, 1566 (1991).
10. N. Peruzzi, P. L. Nostro, B. W. Ninham and P. Baglioni, *J. Solution Chem.* **44**, 1224 (2015).
11. B. Klassen, R. Aroca, M. Nazri and G. A. Nazri, *J. Phys. Chem. B* **102**, 4795 (1998).
12. L. Yang, A. Xiao and B. L. Lucht, *J. Mol. Liq.* **154**, 131 (2010).
13. E. Cazzanelli, P. Mustarelli, F. Benevelli, G. B. Appetecchi and F. Croce, *Solid State Ion.* **86**, 379 (1996).
14. H. L. Yeager and H. Reid, *J. Phys. Chem.* **80**, 850 (1976).
15. M. Takeuchi, Y. Kameda, Y. Umebayashi, S. Ogawa, T. Sonoda, S.-i. Ishiguro, M. Fujita and M. Sano, *J. Mol. Liq.* **148**, 99 (2009).
16. V. Ittah and D. Huppert, *Chem. Phys. Lett.* **173**, 496 (1990).
17. C. F. Chapman and M. Maroncelli, *J. Phys. Chem.* **95**, 9095 (1991).
18. J. A. Gardecki and M. Maroncelli, *Chem. Phys. Lett.* **301**, 571 (1999).
19. H. Al Rasidgazi, H. K. Kashyap and R. Biswas, *J. Chem. Sci.* **127**, 61 (2015).
20. L. Aguilera, S. Xiong, J. Scheers and A. Matic, *J. Mol. Liq.* **210**, 238 (2015).
21. K. Shimizu, A. A. Freitas, R. Atkin, G. G. Warr, P. A. FitzGerald, H. Doi, S. Saito, K. Ueno, Y. Umebayashi and M. Watanabe, *Phys. Chem. Chem. Phys.* **17**, 22321 (2015).
22. S. Kaur, A. Gupta and H. K. Kashyap, *J. Phys. Chem. B* **120**, 6712 (2016).
23. T. Yamaguchi, T. Yonezawa, K. Yoshida, T. Yamaguchi, M. Nagao, A. Faraone and S. Seki, *J. Phys. Chem. B* **119**, 15675 (2015).

24. T. Yamaguchi, K. Yoshida, T. Yamaguchi, Y. Kameda, K. Ikeda and T. Otomo, *J. Phys. Chem. B* **121**, 5355 (2017).
25. D. Battisti, G. A. Nazri, B. Klassen and R. Aroca, *J. Phys. Chem.* **97**, 5826 (1993).
26. K. Kondo, M. Sano, A. Hiwara, T. Omi, M. Fujita, A. Kuwae, M. Iida, K. Mogi and H. Yokoyama, *J. Phys. Chem. B* **104**, 5040 (2000).
27. M. L. Horng, J. A. Gardecki, A. Papazyan and M. Maroncelli, *J. Phys. Chem.* **99**, 17311 (1995).
28. R. Baumann, C. Ferrante, E. Kneuper, F.-W. Deeg and C. Bräuchle, *J. Phys. Chem. A* **107**, 2422 (2003).
29. M. L. Horng, J. A. Gardecki and M. Maroncelli, *J. Phys. Chem. A* **101**, 1030 (1997).
30. S. Indra and R. Biswas, *J. Chem. Phys.* **142**, 204501 (2015).
31. R. Karmakar and A. Samanta, *J. Phys. Chem. A* **106**, 4447 (2002).
32. M. Maroncelli and G. R. Fleming, *J. Chem. Phys.* **86**, 6221 (1987).
33. D. Roy, S. K. Mondal, K. Sahu, S. Ghosh, P. Sen and K. Bhattacharyya, *J. Phys. Chem. A* **109**, 7359 (2005).
34. H. Shirota and E. W. Castner Jr, *J. Chem. Phys.* **112**, 2367 (2000).
35. L. Reynolds, J. A. Gardecki, S. J. V. Frankland, M. L. Horng and M. Maroncelli, *J. Phys. Chem.* **100**, 10337 (1996).
36. B. Guchhait, S. Daschakraborty and R. Biswas, *J. Chem. Phys.* **136**, 174503 (2012).
37. M. Kondo, X. Li and M. Maroncelli, *J. Phys. Chem. B* **117**, 12224 (2013).
38. T. Pradhan and R. Biswas, *J. Phys. Chem. A* **111**, 11524 (2007).
39. R. Biswas, J. E. Lewis and M. Maroncelli, *Chem. Phys. Lett.* **310**, 485 (1999).
40. J. E. Lewis, R. Biswas, A. G. Robinson and M. Maroncelli, *J. Phys. Chem. B* **105**, 3306 (2001).
41. T. Pradhan and R. Biswas, *J. Phys. Chem. A* **111**, 11514 (2007).
42. N. Sarma, J. M. Borah, S. Mahiuddin, H. A. R. Gazi, B. Guchhait and R. Biswas, *J. Phys. Chem. B* **115**, 9040 (2011).
43. T. Pradhan, P. Ghoshal and R. Biswas, *J. Chem. Sci.* **120**, 275 (2008).
44. S. K. Saha, P. Purkayastha, A. B. Das and S. Dhara, *J. Photochem. Photobiol. A Chem.* **199**, 179 (2008).
45. D. Huppert, V. Ittah and E. M. Kosower, *Chem. Phys. Lett.* **159**, 267 (1989).
46. R. Argaman and D. Huppert, *J. Phys. Chem. B* **104**, 1338 (2000).
47. A. Das and R. Biswas, *J. Phys. Chem. B* **119**, 10102 (2015).
48. P. K. Mandal, M. Sarkar and A. Samanta, *J. Phys. Chem. A* **108**, 9048 (2004).

Chapter 5

49. S. Indra and R. Biswas, *J. Phys. Chem. B* **120**, 11214 (2016).
50. A. Samanta, *J. Phys. Chem. B* **110**, 13704 (2006).
51. Z. Hu and C. J. Margulis, *Proc. Natl. Acad. Sci.* **103**, 831 (2006).
52. K. Mukherjee, A. Barman and R. Biswas, *J. Mol. Liq.* **222**, 495 (2016).
53. B. Guchhait, S. Das, S. Daschakraborty and R. Biswas, *J. Chem. Phys.* **140**, 104514 (2014).
54. B. Guchhait and R. Biswas, *J. Chem. Phys.* **138**, 114909 (2013).
55. B. Guchhait, H. Al Rasid Gazi, H. K. Kashyap and R. Biswas, *J. Phys. Chem. B* **114**, 5066 (2010).
56. R. S. Fee and M. Maroncelli, *Chem. Phys.* **183**, 235 (1994).
57. J. Barthel, K. Bachhuber, R. Buchner, J. Gill and M. Kleebauer, *Chem. Phys. Lett.* **167**, 62 (1990).
58. J. C. Soetens, C. Millot and B. Maigret, *J. Phys. Chem. A* **102**, 1055 (1998).
59. T. Yamaguchi, M. Hayakawa, T. Matsuoka and S. Koda, *J. Phys. Chem. B* **113**, 11988 (2009).
60. A. Pal, G. Dass and A. Kumar, *J. Chem. Eng. Data* **43**, 738 (1998).
61. B. Bagchi, *Molecular Relaxation in Liquids* (Oxford University Press. New York, 2012).
62. J. L. Dote, D. Kivelson and R. N. Schwartz, *J. Phys. Chem.* **85**, 2169 (1981).
63. A. Das, R. Biswas and J. Chakrabarti, *J. Phys. Chem. A* **115**, 973 (2011).
64. A. Das, R. Biswas and J. Chakrabarti, *Chem. Phys. Lett.* **558**, 36 (2013).
65. H. Jin, G. A. Baker, S. Arzhantsev, J. Dong and M. Maroncelli, *J. Phys. Chem. B* **111**, 7291 (2007).
66. C. M. Hu and R. Zwanzig, *J. Chem. Phys.* **60**, 4354 (1974).

Chapter 6

Use of Translational-Rotational Decoupling for Development of New Energy Materials: A Representative Study with Polymer Gel Electrolytes

6.1 Introduction

Carrying energy in capsules for communication and data transfer in real time has been the signature for this electronics-driven era. Tremendous development in portable electronic gadgets, for example, mobile phones, electronic notebooks, cameras, medical devices and many others have boosted the demand for efficient and safe energy storage devices.¹⁻³ Rechargeable lithium-ion (Li-ion) battery serves the need of energy storage devices extensively.⁴ Electrolyte media is one of the critical components in such devices. High ionic conductivity (10^{-3} - 10^{-2} Scm^{-1}), good thermal and mechanical stability, wide electrochemical window, good contacts with electrodes, non-toxicity, high flash point, low cost etc. are fundamental requirements of a good electrolyte medium for energy storage purpose.⁴⁻⁶ Three types of electrolytes - liquid electrolytes (electrolyte salt dissolved in organic solvents),^{6,7} solid polymer electrolytes (electrolyte salt in polymer material)⁸⁻¹⁰ and polymer gel electrolytes (consist of salt, organic solvent and polymer)¹¹⁻¹³—have traditionally been used in rechargeable Li-ion batteries. A major drawback of the liquid electrolytes is the risk of leakage and formation of lithium dendrite in solution.¹⁴ Although these issues may be tackled via using solid polymer electrolytes, it introduces complications arising from low conductivity (10^{-8} - 10^{-5} Scm^{-1}) and poor electrode contacts.¹⁴ Polymer gel electrolyte (PGE) solutions can, on the other hand, simultaneously provide high ionic conductivity and high mechanical strength. These properties render PGE as promising candidates for usage in various electrochemical devices that include rechargeable Li-ion battery, super capacitors, dye-sensitized solar cells, fuel cells etc.¹²⁻¹⁷

PGE is formed by adding a polymer material in liquid electrolyte. Proper selection of individual components in polymer gel electrolytes is extremely important. Poly(ethylene oxide) (PEO), poly(propylene oxide) (PPO), poly(acrylonitrile) (PAN), poly(methyl methacrylate) (PMMA), poly(vinyl chloride) (PVC), poly(vinylidene fluoride) (PVdF) etc. are common examples of polymer moieties used in PGE.^{12,13} Solutions of lithium salts, like lithium perchlorate (LiClO_4), lithium fluoroborate (LiBF_4), lithium trifluoromethanesulfonate (LiCF_3SO_3) in highly polar

(high dielectric constant, ϵ_s) and low viscous organic solvents, such as, propylene carbonate (PC), ethylene carbonate (EC), dimethyl carbonate (DMC) or their mixtures can serve the purpose of suitable liquid electrolyte medium in rechargeable lithium batteries.^{6,18} Microscopic dynamics of the solvent and the polymer matrix investigated in a polymer gel electrolytes (LiClO₄/PC/EC/PMMA)¹⁹ via photon correlation spectroscopy (PCS) have revealed a complicated dynamical response with a faster diffusive process closely connected to the ion conductivity, whereas the polymer segmental motion was found to be nearly completely decoupled from the ion conductivity. This observation supports the unique characteristic of polymer gel electrolyte (PGE): simultaneously provide high ionic conductivity and high mechanical strength.

Polymer gel electrolytes are thus fast becoming interesting and emerging field of research. Extensive investigations is essential for development and achieving better design and more efficient performance in application-based usage. Exploring interaction, structure and dynamics in the molecular level of polymer gel electrolyte would help to tune and design efficient materials which is expected to satisfy partially the ever-increasing demand for more reliable and benign electrolytes for different energy storage devices. In this work, we have prepared a polymer gel electrolyte by taking the (PC+LiClO₄) solution as liquid electrolyte and polypropylene glycol of number-averaged molecular weight 425 (PPG425) to investigate the microscopic interaction, structure and dynamics. Impact of medium viscosity, a macroscopic solution property, on relaxation dynamics has been investigated via following solute and solvent dynamics. PPG is a lower homolog of poly(propylene oxide) (PPO). Being a ternary mixture, behaviour of polymer gel electrolyte is quite complex. Thus a prior knowledge of interaction and dynamics of the individual constituents of PGE as well as their binary mixtures will be quite beneficial to describe adequately the same in complex PGE systems. A number of investigations have been carried out to elucidate the solution structure and dynamics of PC and (PC+LiClO₄) systems using different spectroscopic measurement techniques.²⁰⁻²⁵ Earlier investigations on this liquid electrolyte reported that solution dynamics vary significantly with salt concentration in the system.^{26,27} The conductivity of a pure polymer electrolyte is closely linked to the polymer segmental mobility^{10,28,29} and this is why the conductivity of pure polymer electrolyte is much lower than the conductivity of liquid electrolytes. Our ultimate goal is to combine two features in a proposed system: high mechanical and chemical stability of pure polymer electrolyte and high conductivity of liquid electrolyte in a target polymer gel electrolyte.

Recently, several attempts have been made to understand structure and dynamics of polymer gel electrolyte systems using various polymer molecules.^{13,19,30-32} It is noteworthy that conductivities of these polymer gel electrolytes are much higher than the corresponding pure polymer electrolyte systems. QENS study of a polymer gel electrolyte system, containing PMMA, have revealed the information on both the spatial and the temporal behaviours of the investigated system and proposed two dynamical processes in the picosecond-nanosecond range: a faster one of rotational character (in short range very similar to liquid) and a slower one of translational character (observed in long range, $> 5\text{\AA}$, spatially constrained by polymer matrix).³² Moreover, the QENS investigation estimated the heterogeneity length scale $\sim 5\text{-}20\text{\AA}$ for the same polymer gel electrolyte system which arises due to the polymer matrix. The complex dynamics observed in PGEs warrants a systematic investigation to understand the interaction and friction profile that dictates the foundation of these materials in application: efficient transportation of charge between electrodes. This work is an attempt to explore the friction imparted on short range (rotation) and long range diffusion (translation) through PGE solution. We are also interested to examine the effects of a polymer, PPG, on interaction and dynamics of (PC+LiClO₄) liquid electrolytes by time resolved fluorescence spectroscopic technique.

To conduct our investigation, we have performed the fluorescence Stokes shift dynamics and rotational and translational relaxation of an external dipolar solute, coumarin 153³³⁻³⁷ in a polymer gel electrolyte composite, composed of PC, LiClO₄ and PPG (number average molecular weight = 425). A set of PGEs with composition, [(PC+LiClO₄)+wt%PPG] have been considered for the current investigation by varying the relative wt% of $\sim 1\text{ M}$ LiClO₄/PC and PPG. The reason behind the selection of this specific LiClO₄ concentration is: close to this LiClO₄ concentration ($\sim 1.3\text{ M}$) DC conductivity reaches to a maximum value.²⁶ Medium frictional profile has been explored extensively via following solvent relaxation and monitoring solute (here C153) rotational and translational dynamics. The solute medium dynamical coupling is an interesting aspect to look into, given that the celebrated Walden rule is not valid in this type of systems.³¹

6.2 Experimental Details

6.2.1 Materials and Sample Preparation

Lithium perchlorate (LiClO₄) (99% Alfa Aesar) was vacuum dried prior to use. Poly(propylene glycol) of number averaged molecular weight 425 (PPG425, henceforth abbreviated as PPG)

and propylene carbonate (PC) were used as received (Sigma-Aldrich). Laser grade coumarin 153 and trans-2-[4-[(dimethylamino)styryl]benzothiazole (DMASBT) were used as received (Sigma Aldrich). The chemical structures of these materials are provided in Scheme 6.1. Required amount of LiClO₄ was dissolved in PC in an airtight glass vial to prepare (PC+LiClO₄) liquid electrolyte of predefined composition (PC/LiClO₄ molar ratio fixed at ~11.3, ~ 1 M LiClO₄). Proper care was taken to ensure complete dissolution of the added electrolyte and to avoid moisture absorption. The polymer gel electrolytes, [(PC+LiClO₄)+wt%PPG] where 0 ≤ wt%PPG ≤ 100, were prepared by dissolving required amount of PPG in freshly prepared (PC+LiClO₄) solution. All these [(PC+LiClO₄)+wt%PPG] solutions are transparent and colourless. For UV-visible absorption and fluorescence measurements, 2-3 mL sample solution was poured in a quartz cuvette preloaded with dye, C153 or DMASBT.²⁵ Proper care was taken to ensure the complete dissolution of dye in the sample. Concentration of C153 and DMASBT in each of these samples was maintained at ≤ 10⁻⁵ M. Sufficient time was allowed for achieving thermal equilibrium for each sample before measurement.

6.2.2 Density and Viscosity Coefficients Measurements

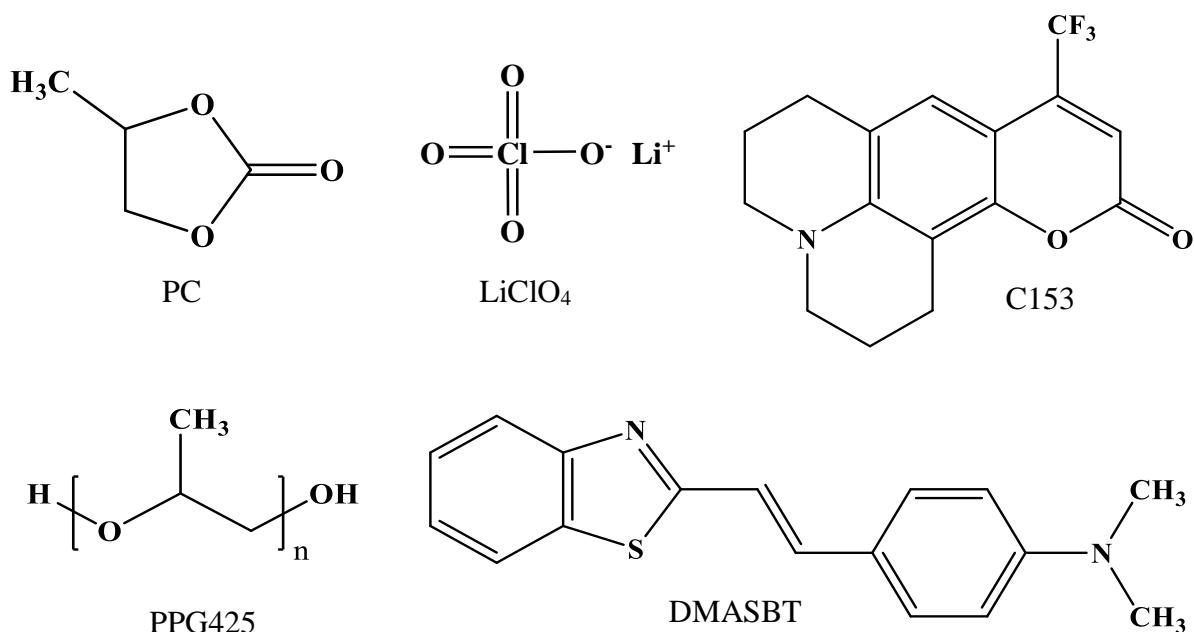
Density (ρ) and viscosity coefficients (η) were measured by using an automated temperature-controlled density meter (Anton Paar, model DSA 5000) and micro viscometer (AMVn, Anton Paar), respectively. Measured density and viscosity coefficient values are summarized in Table A.d.1 (Appendix).

6.2.3 Conductivity Measurements

Conductivity of the polymer gel electrolyte systems were measured by a Bench-top multi-parameter electrochemical meter (SESHIN BIOTECH, Model: ECM-610). All the conductivity data were collected at room temperature (~300 K). Experimentally measured conductivity values are provided in Table 6.1.²⁵

Table 6.1: DC conductivity, κ (mScm⁻¹), in [(PC+LiClO₄)+wt%PPG] at ~ 300 K.

wt% PPG	κ / mScm ⁻¹
0	5.30
10	4.95
20	4.44
30	3.22
40	2.17
50	1.39
60	0.85



Scheme 6.1: Chemical structures of PC, LiClO_4 , PPG425, C153 and DMASBT.

6.2.4 Differential Scanning Calorimetry (DSC) Measurements

Differential scanning calorimetry measurements were performed with TA Instruments Q2000 to determine the glass transition temperature of polymer gel electrolytes. The samples were taken in a hermetically sealed aluminium pan ($40 \mu\text{l}$, Tzero, TA Instruments) to prevent evaporation during the measurements.

6.2.5 Steady State Measurements and Spectral Analysis

Steady state absorption and fluorescence emission spectra were recorded by using a UV-Vis spectrophotometer (UV-2600, Shimadzu), and a fluorimeter (Fluorolog, Jobin-Yvon, Horiba), respectively. A Peltier temperature controller has been used to perform temperature controlled measurements (accuracy $\pm 0.5 \text{ K}$). Steady-state absorption spectra were taken at 2-nm slit and fluorescence spectra collected using 2-nm slits at both the excitation and emission ends. The standard spectral analysis procedure was then followed to estimate spectral frequencies and full-widths-at-half-maxima (FWHM).³⁷⁻⁴⁰ The typical error bar for the determined spectral frequencies was $\pm 200 \text{ cm}^{-1}$. Details of the steady state measurements technique are the same as discussed in chapter 2.

6.2.6 Time-Resolved Fluorescence Measurements and Data Analysis

Time-resolved fluorescence measurements⁴⁰ were performed with a time-correlated single-photon counting (TCSPC) system (LifeSpec-ps) from Edinburgh Instruments (Livingston, U.K.).^{41,42} A Julabo temperature controller was used in temperature dependent measurements (accuracy ± 1 K). Details of time-resolved fluorescence measurements are the same as described in chapter 2 and references.^{25,34,37}

6.2.7 Fluorescence Correlation Spectroscopy (FCS) Measurements and Data Analysis

6.2.7.1 FCS Theory

FCS measures the fluctuation of fluorescence intensity of fluorophore within a tiny observation volume.⁴³ The autocorrelation function of this fluorescence intensity fluctuation can be expressed as⁴³

$$G(\tau) = \frac{\langle \delta F(t) \delta F(t + \tau) \rangle}{\langle F(t) \rangle^2}, \quad (6.1)$$

where $\langle F(t) \rangle$ is the average fluorescence intensity, $\delta F(t)$ and $\delta F(t + \tau)$ are the magnitudes of fluorescence intensity fluctuation from the average value at time t and $t + \tau$, respectively. For a single diffusing species this autocorrelation function can be expressed as⁴³

$$G(\tau) = \frac{1}{N} \left(1 + \frac{\tau}{\tau_D} \right)^{-1} \left(1 + \frac{\tau}{w^2 \tau_D} \right)^{-0.5}, \quad (6.2)$$

where N is the average number of molecules diffusing through the observation volume, τ_D is the diffusion time and w is the geometric factor of the observation volume (i.e. the ratio of radius and the half-length of the depth of the observation volume). If the system contains two diffusing species then the autocorrelation function can be written as⁴³

$$G(\tau) = \frac{1}{(N_1 + N_2)^2} [N_1 D_1(\tau) + N_2 D_2(\tau)], \quad (6.3)$$

$$D_i(\tau) = \frac{1}{N} \left(1 + \frac{\tau}{\tau_{D_i}} \right)^{-1} \left(1 + \frac{\tau}{w^2 \tau_{D_i}} \right)^{-0.5}, \quad i=1,2 \quad (6.4)$$

6.2.7.2 FCS Measurements

FCS measurements have been carried out using a home-built confocal microscope set-up. For FCS study, the sample was placed on a cleaned glass coverslip of 0.17 mm thickness and was excited with a 405 nm pulsed diode laser (pulse width < 50 ps) with a repetition rate of 40 MHz through an oil-immersion objective (Zeiss, α PlanApo, 100x, NA 1.46). The fluorescence from

the sample was collected via the same objective and it was then passed through an appropriate dichroic mirror (Di01-R405-25X36, Semrock) and long-pass filter (BLP01-488R-25, Semrock) to finally get focused on a non-polarising 50:50 beam-splitter. After passing through the beam-splitter the fluorescence photons were recorded with two single-photon avalanche photodiode (τ -SPAD) detectors. The signal was then processed by PicoHarp-300 time correlated single photon counting (TCSPC) module (PicoQuant). The data acquisition was performed in time-tagged time-resolved (TTTR) mode with SymPhoTime 64 software.

In order to determine the confocal volume of the microscope set-up Rhodamine 6G (concentration ~ 10 nM in water) was used with a known diffusion coefficient value of $430 \pm 40 \mu\text{m}^2/\text{s}$ at 25°C .^{44,45} The confocal volume (V_{eff}) and the geometric factor (w) was found to be 0.001 femto-litre (fL) and 2.0, respectively. Data analyses of the recorded autocorrelation graphs [$G(\tau)$] of the samples were performed using the fit model described via Eqs. 6.2 - 6.4.

6.3 Results and Discussion

6.3.1 Steady State Fluorescence Measurements

Blue shift in steady state UV-Vis absorption and fluorescence emission spectra of C153 in the polymer gel electrolytes [(PC+LiClO₄)+wt%PPG] with increasing polymer content has been observed. Corresponding absorption and emission spectra at 293K is shown in Figure 6.1 and the polymer concentration dependent absorption and emission peak frequencies are presented in Figure 6.2. A total of nearly 1000 cm^{-1} blue shift of absorption and emission frequencies for C153 upon increasing PPG concentration from 0 to 100 wt% in the above systems is an indication of lowering of medium polarity.³⁷ Here the polymeric substance is characterized by $\epsilon_s \sim 15$ at 293 K,⁴⁶ which is much lower than that ($\epsilon_s \sim 50$ ⁴⁷) for 1 M (PC+LiClO₄) solution. No impact of altering temperature within the range of $293 \leq T/\text{K} \leq 318$ on absorption and emission spectra of C153 in [(PC+LiClO₄)+wt%PPG] suggest the temperature induced insignificant modification of medium polarity. This is similar to what has already been observed in earlier study for 1M (PC+LiClO₄) solution.²⁵ A representative figure providing temperature dependent absorption and emission spectra of C153 in [(PC+LiClO₄)+60wt%PPG] is shown in Figure A.d.2 (see Appendix).

Further investigation on steady state fluorescence emission of C153 in these PGE systems after selectively exciting across the absorption band results minimal shift of emission frequency as

well as FWHM with excitation wavelength (λ_{exc}). Such monitoring of emission frequency as a function of excitation wavelength is routinely done to investigate spatial heterogeneity in a given system.⁴⁸ Similar study using a different fluorescent probe, DMASBT, having excited state lifetime ($\langle\tau_{life}\rangle$) much faster⁴⁹ than C153, shows a emission frequency shift of ~500-700 cm^{-1} towards lower energy with concomitant lowering of FWHM ~300-400 cm^{-1} with increasing λ_{exc} . The change in fluorescence emission frequency and FWHM of C153 and DMASBT in 60 and 100 wt% PPG (neat PPG) systems at 293K with λ_{exc} is represented in Figure 6.3. These observations indicate that spatially distributed domains in these PGEs interconvert among themselves in a timescale longer or comparable with $\langle\tau_{life}\rangle$ of DMASBT and much faster than the $\langle\tau_{life}\rangle$ of C153 ($\langle\tau_{life}\rangle$ of C153 and DMASBT in [(PC+LiClO₄)+wt%PPG] are provided in Table 6.2).^{25,50}

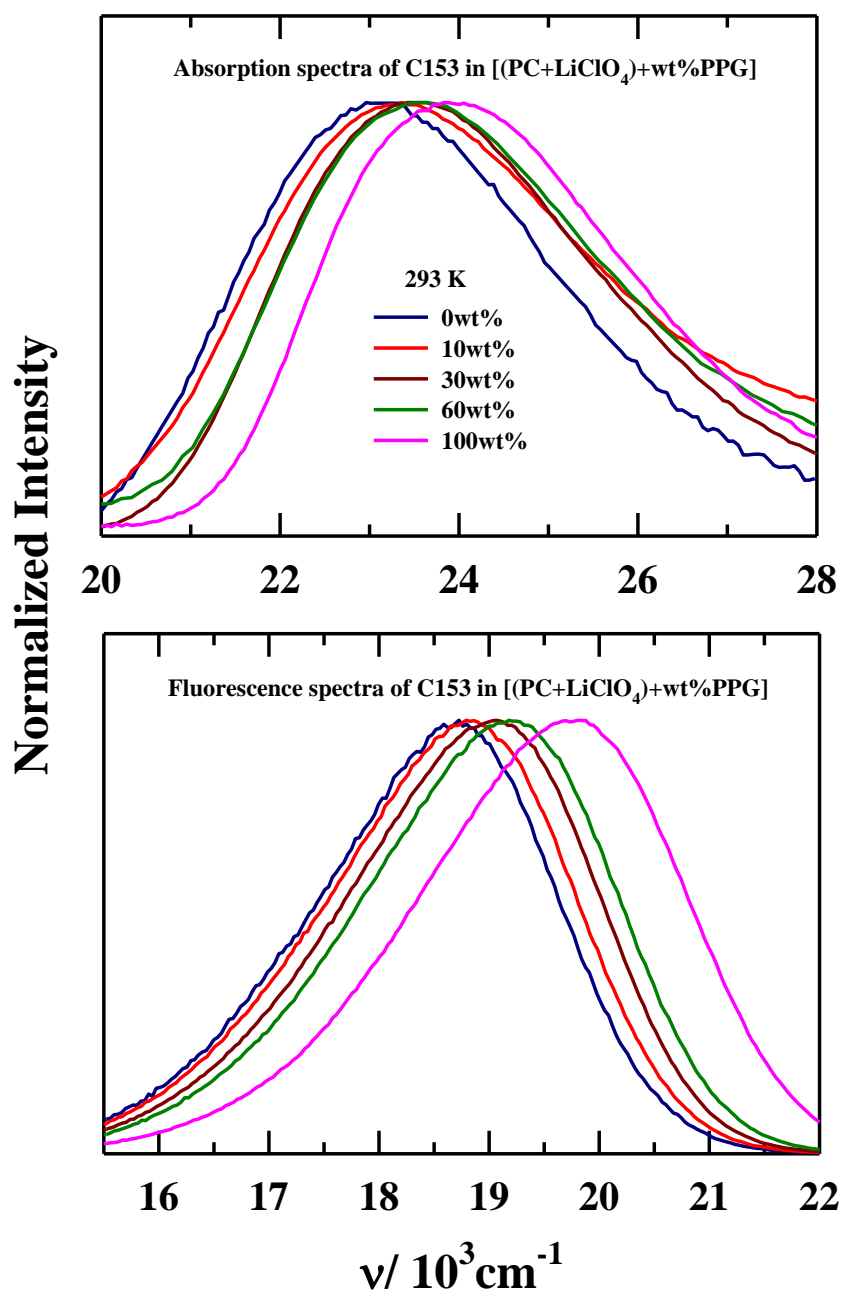


Figure 6.1: Steady state absorption (upper panel) and emission spectra (lower panel) of C153 at different wt% of PPG in the polymer gel electrolytes, [(PC+LiClO₄)+wt%PPG], at 293 K. All presentations are colour-coded. Each of this emission spectrum was recorded after excitation at the peak wavelength of the corresponding absorption spectrum.

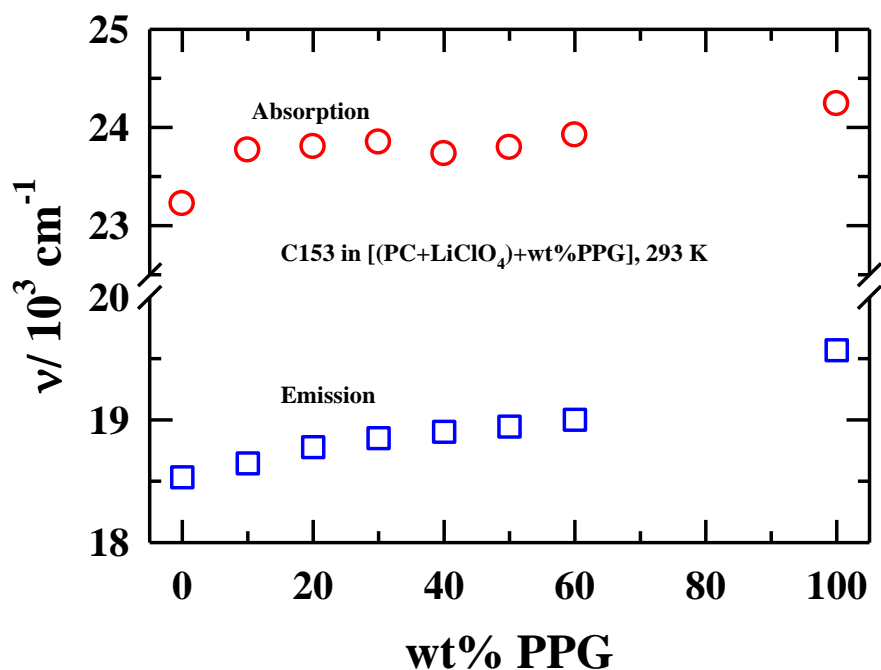


Figure 6.2: Absorption and emission frequencies of C153 at different wt% of PPG in the polymer gel electrolytes, [(PC+LiClO₄)+wt%PPG], at 293 K. All representations are colour-coded.

The λ_{exc} dependent total shift in emission peak frequency and FWHM of DMASBT in these electrolyte systems increases mildly ($\sim 150 \text{ cm}^{-1}$) with increasing temperature from 293 to 318 K as observed in earlier work in lithium ion battery electrolytes.²⁵ A representative figure indicating temperature induced λ_{exc} dependent total shift of emission frequency and FWHM is shown in Figure 6.4. This is quite surprising because increased temperature leads to better homogenization of spatially distributed domains and thus λ_{exc} dependent total shift decreases. The probable causes for this unconventional result are: the relative competition between temperature induced $\langle \tau_{life} \rangle$ of DMASBT in these electrolyte solutions and persistent time of solution's heterogeneous domains continues to govern the photo-selection for the temperature regime $T=293\text{-}318 \text{ K}$. Complex solution effects on excited state trans-cis photo-isomerisation of DMASBT may also be responsible for mild λ_{exc} dependent total shift of emission peak frequency and the corresponding FWHM.

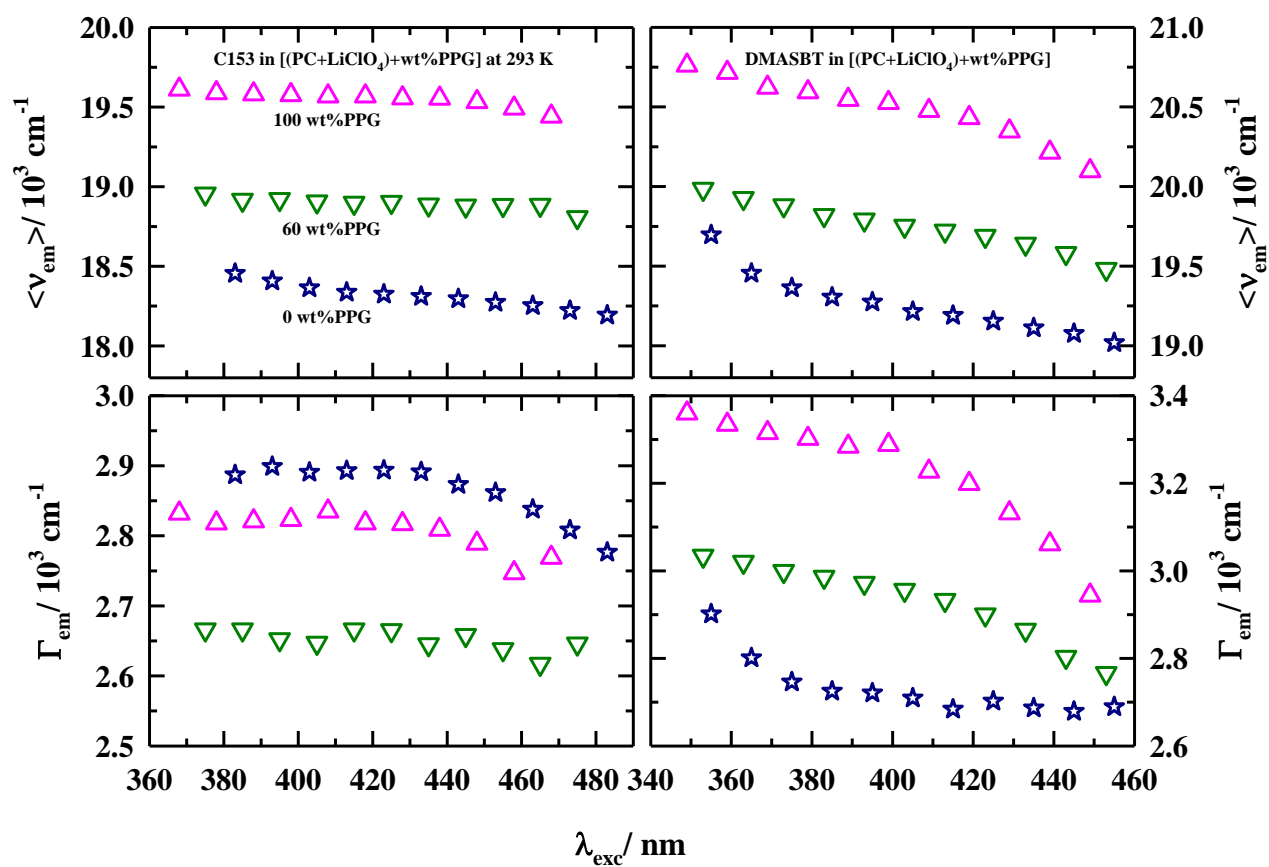


Figure 6.3: Excitation wavelength dependence (λ_{exc}) of steady state fluorescence emission frequency, $\langle \nu_{em} \rangle$ (upper panels) and spectral width (FWHM), Γ_{em} (lower panels) of C153 (left panels) and DMASBT (right panels) for three compositions in [(PC+LiClO₄)+wt%PPG] at 293 K. All representations are colour-coded.

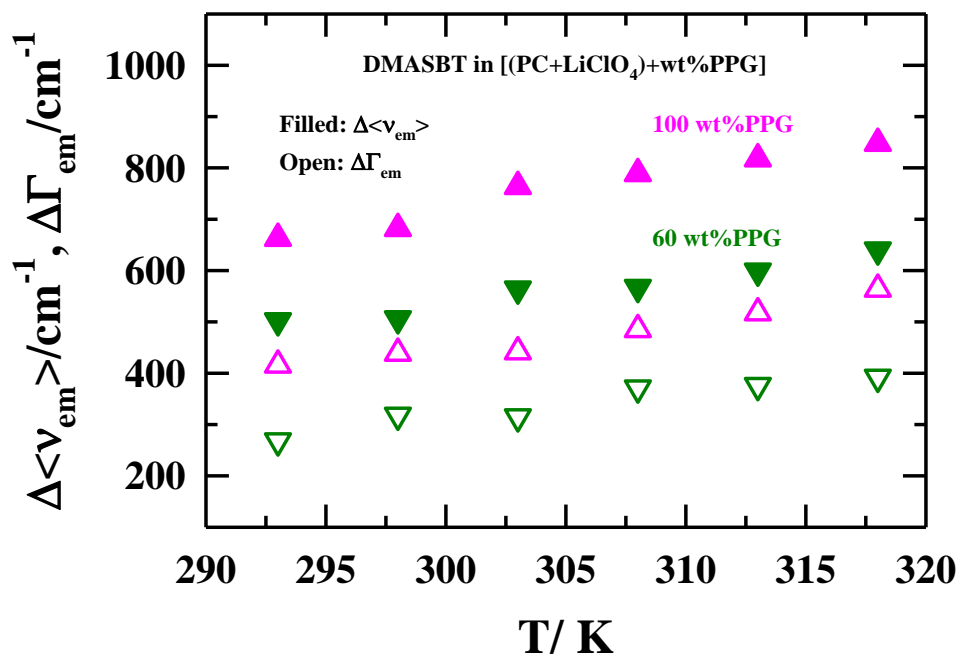


Figure 6.4: Temperature induced λ_{exc} dependent total shift of emission frequency and FWHM of DMASBT at two compositions in [(PC+LiClO₄)+wt%PPG] respectively. All representations are colour-coded.

6.3.2 Time-Resolved Fluorescence Measurements

Lifetimes of C153 and DMASBT in the [(PC+LiClO₄)+wt% PPG] were determined from multi-exponential fits of magic angle (54.7°) fluorescence decay. Corresponding average lifetimes, $\langle \tau_{life} \rangle$, are summarized in Table 6.2.

Table 6.2: Average lifetimes of C153 and DMASBT at various wt% of PPG in [(PC+LiClO₄)+wt% PPG].

wt% of PPG [(PC+LiClO ₄)+wt% PPG]	$\langle \tau_{life} \rangle$ of C153/ ns						$\langle \tau_{life} \rangle$ of DMASBT/ ns
	293 K	298 K	303 K	308 K	313 K	318 K	293 K
0	5.04	5.08	5.03	4.91	5.30	4.88	0.16
10	4.24	4.19	4.23	4.11	4.41	4.45	0.24
20	3.97	4.31	4.22	3.79	3.93	4.29	0.18
30	4.13	4.49	4.55	4.44	4.52	4.49	0.18
40	5.07	4.94	5.03	5.02	5.09	5.03	0.16
50	4.35	4.46	4.06	4.09	4.40	4.24	0.18
60	4.44	4.30	4.33	4.22	4.44	4.60	0.17
100	4.30	4.38	4.37	4.40	4.57	4.28	0.19

6.3.2.1 Stokes Shift Dynamics

Picosecond-resolved fluorescence decay measurements of C153 at magic angle (54.7°) have been performed to explore the solution dynamics via dynamic Stokes shift. The representative fluorescence transients of C153, recorded at 293 K, in these PGEs with 60 wt% PPG, having signature of Stokes shift dynamics: only decay at the blue end wavelength and rise followed by decay at the red wavelength with respect to steady state emission peak wavelength are shown in Figure A.d.3 (Appendix). Figure 6.5 is the representative time-resolved emission spectra (TRES) of C153 in these solutions with 60 wt% PPG. The corresponding steady state emission spectra are also shown in the same figure. Note the steady state emission spectrum in each of the solutions is not the representative of emission of C153 molecules from completely relaxed solvation configuration because it is $\sim 200 \text{ cm}^{-1}$ blue shifted compared to emission spectrum at $t=\infty$. Similar observation was also found earlier in some viscous electrolyte solutions.^{25,51}

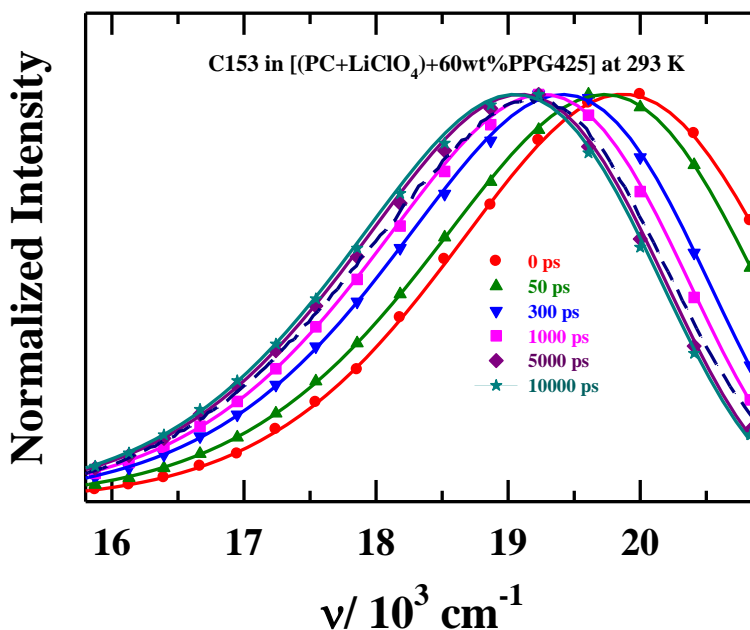


Figure 6.5: Representative constructed time-resolved emission spectra (TRES) of C153 with 60 wt% in [(PC+LiClO₄)+wt%PPG] for different time intervals at 293 K. The steady state emission spectrum of C153 in this solution is shown as dashed lines in the same figure. All representations are colour-coded.

Table 6.3 summarizes the total dynamic Stokes shift of C153 detected ($\Delta\nu_{obs}^t$) in these solutions from the present measurements and corresponding estimated total dynamic Stokes shift ($\Delta\nu_{est}^t$) by following a well-known approximate method.⁵² We have missed ~ 40-50% of total dynamic Stokes shift which are primarily arising from the faster dynamics of the constituent components in PGEs, and is beyond our present experimental time-resolution (FWHM of IRF ~ 85 ps) even after iterative deconvolution.⁵³ Ultrafast fluorescence study of C153 in PC³⁷ reported solvation time ~ 2 ps at 295 K. With increase of polymer (PPG) amount in the medium, the missed portion of dynamic Stokes shift decreases. Probably, PPG induced increase of medium viscosity is responsible for larger detection of total dynamic Stokes shift.

Table 6.3: Magnitudes of estimated ($\Delta\nu_{est}^t$), observed ($\Delta\nu_{obs}^t$) and missing portion of the total dynamic Stokes shift of C153 at various wt% of PPG in [(PC+LiClO₄)+wt%PPG].

wt% PPG in [(PC+LiClO ₄)+wt%PPG]	$\Delta\nu_{est}^t / \text{cm}^{-1}$	$\Delta\nu_{obs}^t / \text{cm}^{-1}$	% Missed
0	1400	606	57
10	1805	685	62
20	1618	591	63
30	1626	597	63
40	1435	712	50
50	1442	735	49
60	1527	819	46
100	1333	1210	9

The representative decay of solvation response functions, $S(t)$, determined from the peak frequencies of time dependent emission spectrum of C153 in these PGEs at 293 K are shown in Figure 6.6. Corresponding fit parameters are summarized in Table 6.4. The $S(t)$ decays show bi- or tri-exponential kinetics depending upon polymer concentration. In the absence of polymer in the PGEs, among the two solvation time components of C153, summarized in Table 6.4, the faster sub-50 ps arises from the dynamics of free solvent molecules (i.e. unbound with ion) while ion dynamics in the vicinity of excited solute contribute to the slower few-ns time components.^{25,54} Although medium viscosity increases with increasing the polymer concentration in solutions, the average solvation time, $\langle\tau_s\rangle$, decreases. The faster dynamics of terminal hydroxyl and/ or ether group present in polymer chain of PPG425 may be responsible for shortening of $\langle\tau_s\rangle$. Earlier study on ps-resolved Stokes shift dynamics of C153 in polyethylene glycol (PEG300) have reported bi-exponential dynamics with sub-100 ps and ~1 ns time components with $\langle\tau_s\rangle \sim 350$ ps.⁵⁵ The presence of additional methyl side group in PPG425 is believed to be responsible for lengthening of these time components (Table 6.4). Dielectric relaxation studies have reported that presence of additional methyl side group dominates over the increasing chain length of the polymers in lengthening of relaxation dynamics.⁵⁶ Dielectric relaxation of PPG425 in the GHz region reported a timescale ~ 440 ps at 293 K.⁴⁶ Collective inter and intra molecular H-bond relaxation mode of terminal –OH group in ethylene glycol based polymers was considered to be responsible for low-frequency dispersion mode of dielectric relaxation while segmental motion of C–O–C group resulted the ~ 100 ps component.⁵⁷ Therefore, intra and intermolecular H-bond dynamics among terminal

–OH group in PPG are expected to contribute in the slowest time (~ 2 ns) obtained in Stokes shift dynamics in neat PPG.

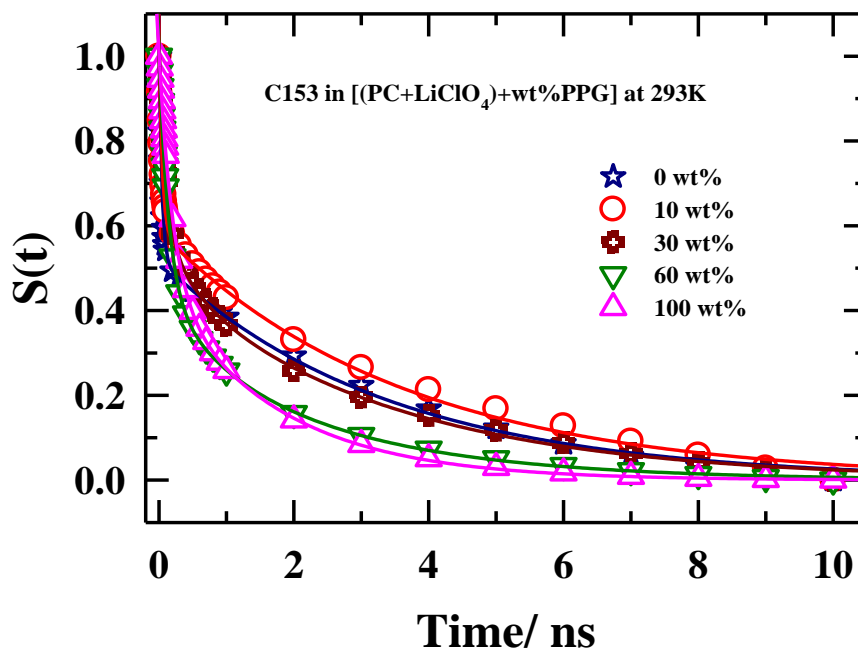


Figure 6.6: Solvation response functions ($S(t)$) decays of C153 at various wt% of PPG in [(PC+LiClO₄)+wt%PPG] at 293 K. Experimental data for $S(t)$ are shown by circles; solid lines passing through the data represent the fits. All presentations are colour-coded.

Table 6.4: Decay characteristics of solvation response function of C153 at various wt% of PPG in [(PC+LiClO₄)+wt%PPG] at 293 K.

wt% PPG	^m a_1	ⁿ τ_1 /ps	a_2	τ_2 /ps	a_3	τ_3 /ps	$\langle \tau_s \rangle$ /ps
0	0.48	42	-	-	0.52	3351	1763
10	0.36	38	0.08	333	0.56	3828	2184
20	0.41	46	0.11	379	0.48	3534	1757
30	0.39	98	0.13	479	0.48	3358	1712
40	0.40	74	0.25	352	0.35	3044	1183
50	0.48	118	0.17	529	0.35	2778	1119
60	0.54	141	0.13	816	0.33	2585	1035
100	0.54	209	0.46	1747	-	-	916

^{m,n} The reported individual amplitudes and time constants can be reproduced within $\pm 10\%$ of the reported values.

Figure 6.7 describes the viscosity coupling of solution dynamics at various polymer concentrations in the PGEs via dependence of experimentally obtained $\langle \tau_s \rangle$ of C153 and medium viscosity at 293 K in double logarithmic fashion. The fit going through the data points shows fractional viscosity dependence of the type, $\langle \tau_s \rangle = A \left(\frac{\eta}{T} \right)^p$, with a negative p value having magnitude ~ 0.5 . The significant decoupling of $\langle \tau_s \rangle$ of C153 with medium viscosity suggests that these polymer gel electrolytes (PGEs) are strongly temporal heterogeneous⁵¹.

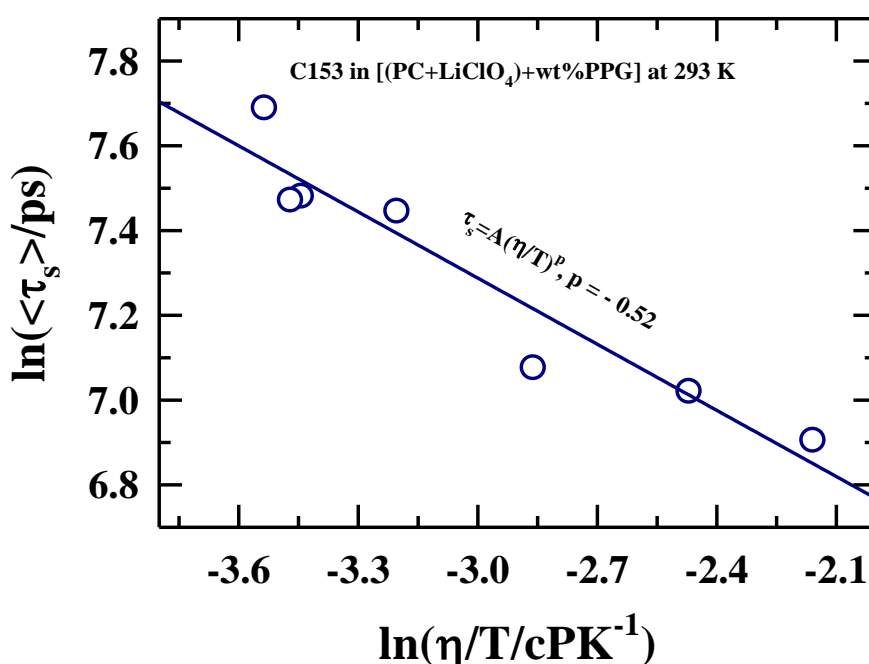


Figure 6.7: Temperature reduced viscosity dependence $\left(\frac{\eta}{T} \right)$ of average solvation time, $\langle \tau_s \rangle$, of C153 in [(PC+LiClO₄)+wt%PPG] at 293 K. Solid lines passing through the data points represent the fit.

6.3.2.2. Time-Resolved Fluorescence Anisotropy: Rotational Diffusion of Solute

Time-resolved fluorescence anisotropy measurements of C153 in these polymer gel electrolyte systems have been performed to explore the coupling between the solute's rotational diffusion and the medium viscosity. Representative fluorescence intensity decay at different emission polarization (0° & 90°) with respect to vertical excitation polarization of C153 in [(PC+LiClO₄)+wt%PPG] with 60 wt% PPG is shown in Figure A.d.4 (Appendix). A

representative fluorescence anisotropy decay, $r(t)$, at 60 wt% PPG and the corresponding bi-exponential fit is provided in Figure 6.8. Corresponding residuals of fits are also shown in this figure. The experimentally observed $r(t)$ decay fit parameters in these systems at different temperatures are summarized in Table 6.5. All these anisotropy decays are well described by a sum of two exponentials characterized by a fast (~ 100 - 200 ps) and a slow (~ 500 - 1000 ps) time constants with both possessing substantial amplitudes. Biexponential $r(t)$ decay is a reflection of non-Markovian rotational moves and suggests that the solute's rotational diffusion in these media haven't taken place by via Debye rotations through temporally uncorrelated stochastic small orientation moves.³⁴

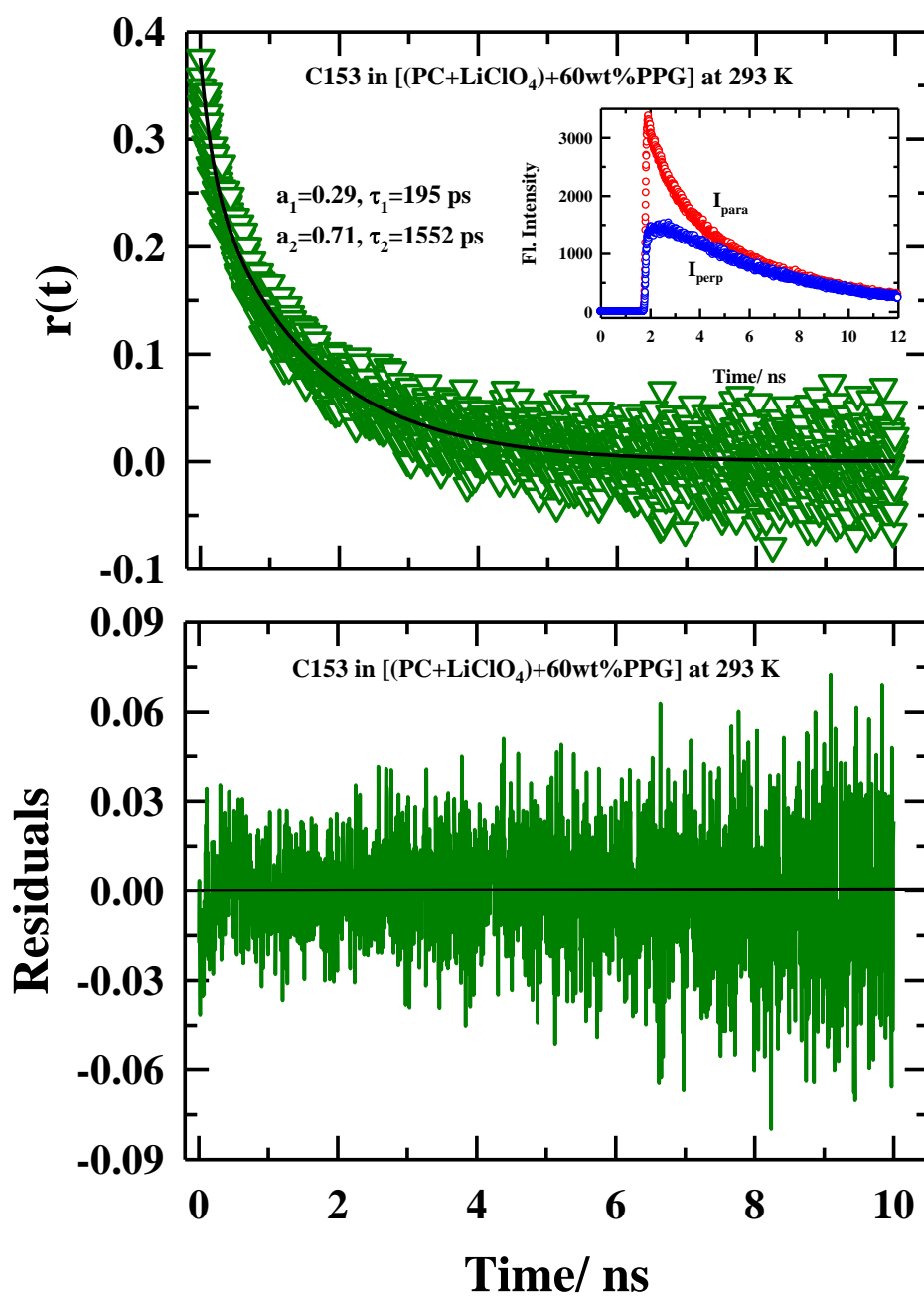


Figure 6.8: Representative fluorescence anisotropy decays, $r(t)$ (upper panel) of C153 in [(PC+LiClO₄)+60wt%PPG] at 293 K. Experimental data are denoted by circles and solid line passing through them represents biexponential fit. Fit parameters are shown in the inset. Corresponding residuals for $r(t)$ decay fit is shown in the lower panel.

Table 6.5: Temperature dependent decay characteristics of fluorescence anisotropy ($r(t)$) of C153 at various wt% of PPG in [(PC+LiClO₄)+wt%PPG]. Experimental measured viscosity coefficients (η) of these solutions are also summarized in this table.

Systems	T/K	^m a_1	ⁿ τ_1 /ps	a_2	τ_2 /ps	$\langle \tau_{rot} \rangle$ /ps	η /cP
PC+LiClO ₄	293	0.56	160	0.44	982	519	9.37
	298	0.53	174	0.47	846	490	8.08
	303	0.55	114	0.45	739	394	7.04
	308	0.61	155	0.39	702	366	6.19
	313	0.60	113	0.40	614	312	5.48
	318	0.58	124	0.42	490	276	4.90
PC+LiClO ₄ +10wt% PPG	293	0.48	190	0.52	788	504	8.54
	298	0.55	231	0.45	726	454	7.35
	303	0.55	172	0.45	650	386	6.40
	308	0.62	199	0.38	582	344	5.63
	313	0.66	168	0.34	563	301	5.02
	318	0.75	184	0.25	509	265	4.50
PC+LiClO ₄ +20wt% PPG	293	0.55	239	0.45	838	510	9.12
	298	0.56	196	0.44	695	417	7.77
	303	0.61	203	0.39	646	377	6.73
	308	0.69	211	0.31	613	336	5.88
	313	0.73	165	0.27	597	282	5.19
	318	0.76	163	0.24	567	261	4.62
PC+LiClO ₄ +30wt% PPG	293	0.39	221	0.61	819	588	11.91
	298	0.40	179	0.60	682	483	9.95
	303	0.42	136	0.58	587	398	8.47
	308	0.50	174	0.50	551	364	7.29
	313	0.60	180	0.40	523	317	6.33
	318	0.63	127	0.37	492	262	5.56
PC+LiClO ₄ +40wt% PPG	293	0.35	119	0.65	950	656	16.77
	298	0.43	141	0.57	929	593	13.76
	303	0.46	138	0.54	839	514	11.46
	308	0.54	192	0.46	766	456	9.70
	313	0.59	161	0.41	693	380	8.28
	318	0.61	136	0.39	680	348	7.18
PC+LiClO ₄ +50wt% PPG	293	0.32	178	0.68	1251	909	24.80
	298	0.38	195	0.62	1139	782	19.83
	303	0.36	140	0.64	889	616	16.17
	308	0.46	224	0.54	826	548	13.38
	313	0.48	179	0.52	732	468	11.22
	318	0.52	148	0.48	655	391	9.59
PC+LiClO ₄ +60wt% PPG	293	0.29	195	0.71	1552	1161	33.84
	298	0.32	210	0.68	1342	977	26.56
	303	0.38	164	0.62	1140	772	21.21
	308	0.41	160	0.59	975	642	17.28
	313	0.41	193	0.59	821	566	14.25
	318	0.41	146	0.59	683	464	11.93
	293	0.25	155	0.75	3256	2481	98.31

PPG	298	0.24	211	0.76	2595	2023	70.79
	303	0.29	146	0.71	2051	1499	52.72
	308	0.29	175	0.71	1712	1266	40.10
	313	0.34	146	0.66	1394	970	31.22
	318	0.39	189	0.61	1314	875	24.81

^{m,n} The reported individual amplitudes and time constants can be reproduced within $\pm 10\%$ of the reported values.

With increasing polymer concentration and decreasing temperature, the average rotational correlation time, $\langle \tau_{rot} \rangle$, increases. The same is true for the medium viscosity as well. Although experimentally measured $\langle \tau_{rot} \rangle$ increases with the increase of viscosity, partial decoupling of $\langle \tau_{rot} \rangle$ from viscosity is prominent. For example, the viscosity of [(PC+LiClO₄)+60wt% PPG] is ~4 times higher than that of the solution with 10 wt% PPG but $\langle \tau_{rot} \rangle$ for C153 is only ~ 2.3 times longer in the former than the latter. Figure 6.9 describes the medium viscosity coupling of the solute's rotational diffusion via $\langle \tau_{rot} \rangle = A(\eta/T)^p$ in a double logarithmic scale. The predicted stick and slip limit values of $\langle \tau_{rot} \rangle$ have been calculated by using the modified Stokes-Einstein-Debye (SED) equation, $\langle \tau_{rot} \rangle = \frac{V\eta f C}{k_B T}$. In this relation, solute (C153) volume $V = 246 \text{ \AA}^3$; shape factor $f = 1.71$; and the coupling constant $C = 1$ (for stick) and 0.24 (for slip). These calculated hydrodynamic rotation times at different temperatures are also shown in the same figure. All the experimental $\langle \tau_{rot} \rangle$ values lie in between the stick and the slip predicted rotation times.

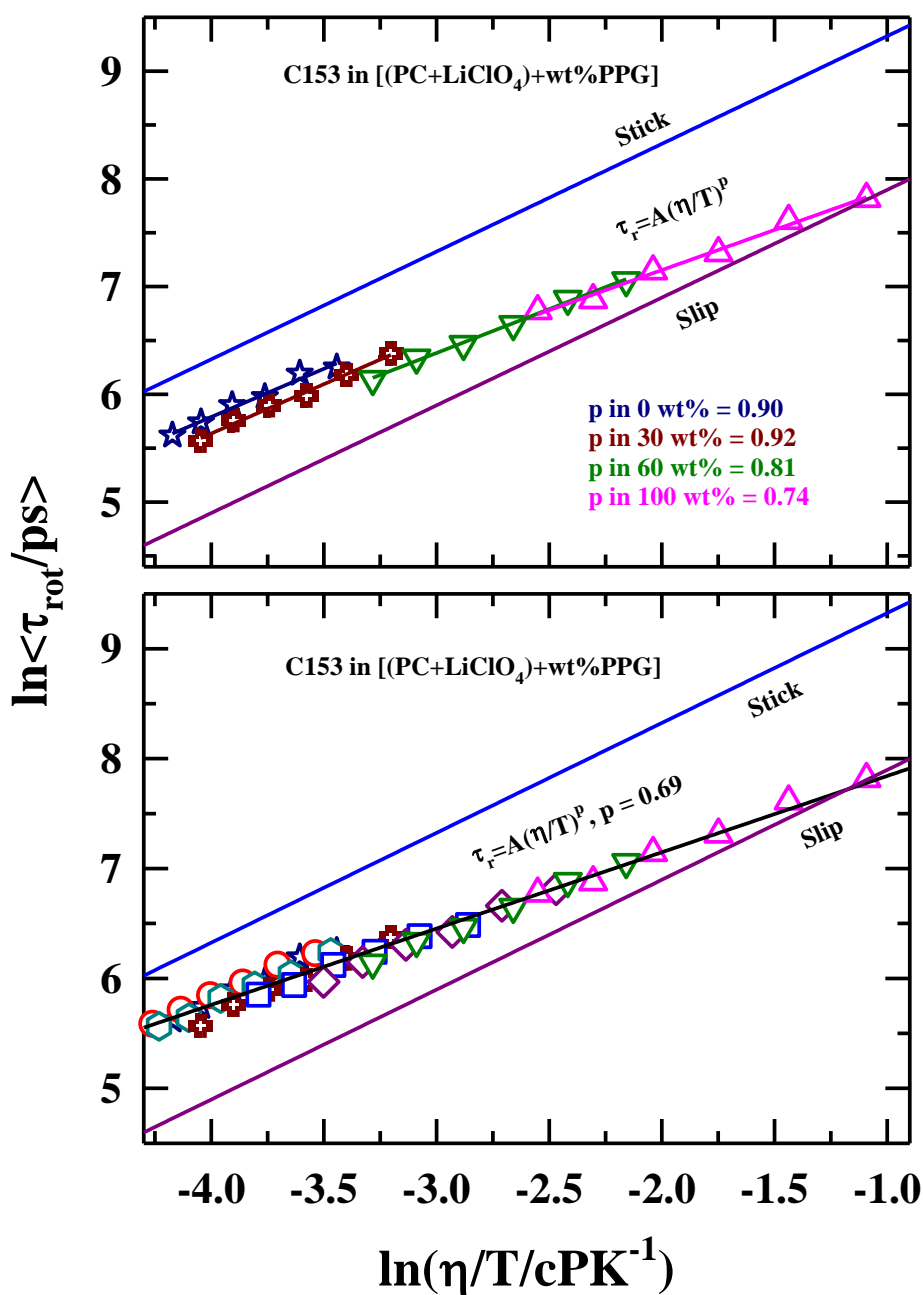


Figure 6.9: Temperature-reduced viscosity $\left(\frac{\eta}{T}\right)$ dependence of average rotation time, $\langle\tau_{rot}\rangle$, of C153 at various wt% of PPG in [(PC+LiClO₄)+wt%PPG] (upper panel). Solid lines passing through the data points represent fits. Different colours have been used to denote different wt% of PPG in the solution. The lower panel represents the global fit of η/T dependence with $\langle\tau_{rot}\rangle$ of C153 in [(PC+LiClO₄)+wt%PPG].

Fractional viscosity coupling of $\langle \tau_{rot} \rangle$ with $p < 1$ is observed in all these solutions. Note, in the upper panel of Figure 6.9, where the η changes due to change of temperature, the value of p varies from 0.9 to 0.7 as polymer concentration increases from 0 to 100 wt% in [(PC+LiClO₄)+wt%PPG]. A global fit of all the collected data (that include all temperature and all wt% of PPG considered), shown in the lower panel of this figure, results $p = 0.69$. The fractional p value suggests a presence of significant temporal heterogeneity in these polymer gel electrolytes.

To further explore the coupling of medium viscosity with solute (C153) rotation, activation energy associated with medium viscosity (E_a^η) and solute rotation (E_a^{rot}) have been determined via analysing the Arrhenius-type temperature dependencies of the measured η and $\langle \tau_{rot} \rangle$ in the temperature range, $T = 293$ to 318 K. The obtained activation energies (E_a^η and E_a^{rot}) in these polymer gel electrolytes are summarized in Table 6.6. Note, at the lower polymer concentration regime, E_a^η are quite close to E_a^{rot} , signifying the solute rotation in this limit is totally dictated by the medium viscosity. At the higher polymer concentration regime, on the other hand, $E_a^{rot} < E_a^\eta$, suggesting a partial decoupling of solute rotation from medium viscosity in this limit.

Table 6.6: Activation energy associated with medium viscosity and rotational diffusion of C153 at various wt% of PPG in [(PC+LiClO₄)+wt%PPG].

wt% PPG in [(PC+LiClO ₄)+wt%PPG]	E_a^η /kJmol ⁻¹ K ⁻¹	E_a^{rot} /kJmol ⁻¹ K ⁻¹
0	20.09	20.28
10	19.83	20.19
20	21.03	20.56
30	23.56	23.90
40	26.29	20.46
50	29.46	26.02
60	32.29	28.39
100	42.61	33.63

6.3.3 Fluorescence Correlation Spectroscopy: Translational Diffusion of Solute

To have a comprehensive understanding about medium frictional profile, translational diffusion of C153 in the polymer gel electrolytes have been explored via fluorescence correlation spectroscopy. Representative $G(\tau)$ of C153 dissolved in polymer gel electrolytes is shown in Figure 6.10. Normal single diffusion function has been found to describe the experimental $G(\tau)$, shown as solid lines in the same figure. The possibility of multiple diffusing species has also been verified. The comparison of mono- and bi-modal diffusion model to fit experimental $G(\tau)$ is represented in Figure 6.10 along with the residuals. No prominent difference between the two models leads us to consider the monomodal (also called normal single diffusion) function to describe the experimentally observed $G(\tau)$ of C153 in the present polymer gel electrolytes, [(PC+LiClO₄)+wt%PPG]. Change of $G(\tau)$ with gradual addition of PPG in this polymer gel electrolytes is shown in Figure 6.10 where the solid lines indicates normalized $G(\tau)$ fits. With the increase of polymer (PPG) concentration, the $G(\tau)$ decays become slower. Translational diffusion times ($\langle\tau_D\rangle$) extracted from fits are summarized in Table 6.7B along with the medium viscosities.

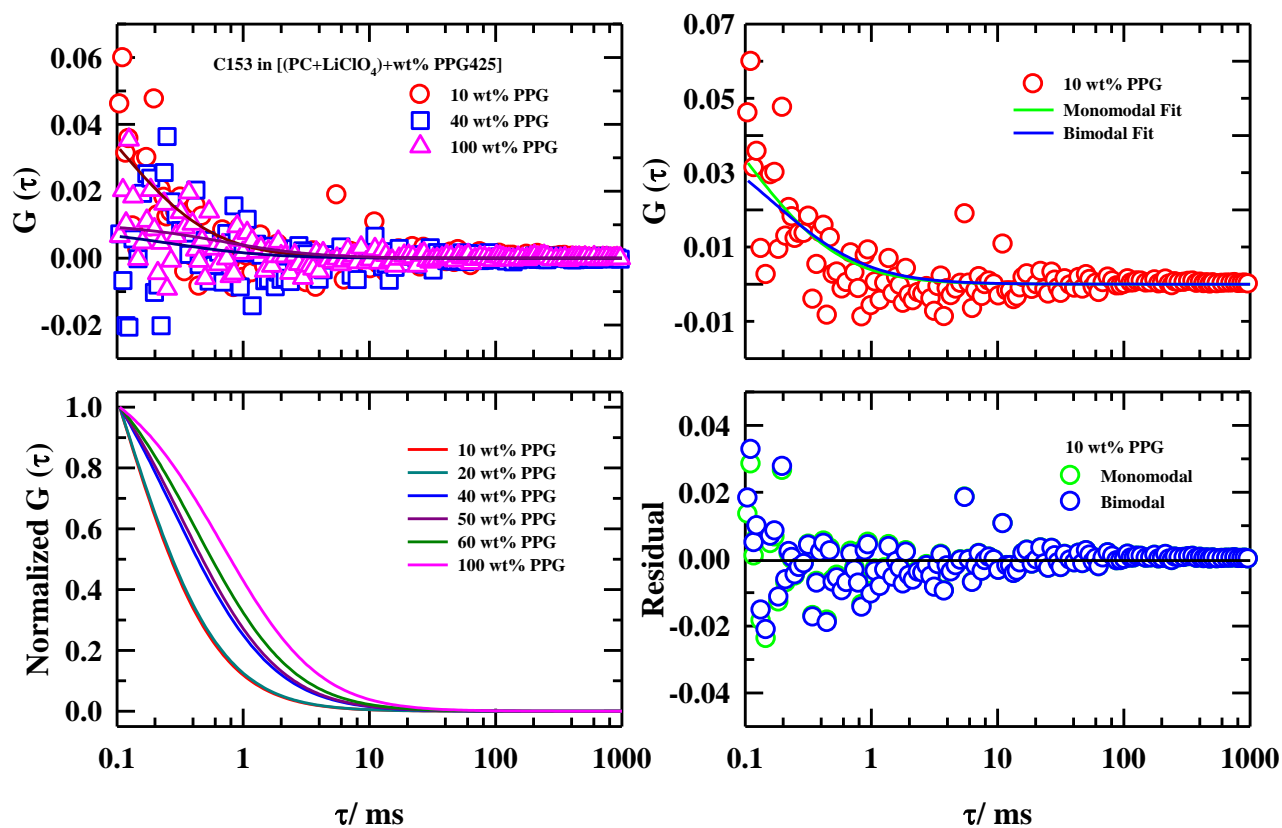


Figure 6.10: Fluorescence autocorrelation $G(\tau)$ of C153 in [(PC+LiClO₄)+wt%PPG] at 293 K. Upper left panel: Coloured symbols represent $G(\tau)$ data points while solid lines passing through the data points depict the normal single diffusion fits. Upper right panel: A representative comparison between monomodal and bimodal fit of $G(\tau)$ data for C153 dissolved in 10 wt% PPG425 in [(PC+LiClO₄)+wt%PPG]. Lower right panel: Comparison of residuals between monomodal and bimodal fit of $G(\tau)$ data for C153 dissolved in 10 wt% PPG425 in [(PC+LiClO₄)+wt%PPG]. Lower left panel: Normalized autocorrelation fits (normal single diffusion) of C153 at various wt% of PPG in [(PC+LiClO₄)+wt%PPG]. Different colours have been used for various wt% of PPG.

Rotational diffusion times, discussed in the earlier section for fluorescence anisotropy measurements of C153 in this electrolyte system, have been found to show fractional (~ 0.7) power dependence on medium viscosity. The fractional power (here p) dependence of translational diffusion time, $\langle \tau_D \rangle$, with temperature-reduced medium viscosity (η/T) is shown in the lower panel of Figure 6.11 which indicates a p value of 0.6. As before, this is significantly

less than unity, and confirms the view that these systems are strongly temporally heterogeneous. However, this interpretation of fractional viscosity dependence is strongly conditioned to solute sphericity and solute-solvent size ratio, and therefore requires a re-confirmation via similar analysis of rotation times of the same solute in normal homogeneous small molecular solvents. This leads us to study the FCS of C153 in a set of normal solvents. A representative $G(\tau)$ data and monomodal fit through the data point of C153 in acetonitrile solvent is shown in upper panel of Figure 6.12 and the corresponding residual is provided in the middle panel of the same figure. Normalized monomodal fits through the $G(\tau)$ of C153 in a series of normal solvents with gradual increase of solvent viscosity is presented in the lower panel of Figure 6.12. Translational diffusion times obtained from the fits are provided in Table 6.7A. Furthermore, η/T coupling of $\langle\tau_D\rangle$ of C153 in these normal solvents results a fractional $p=0.86$, shown in the upper panel of Figure 6.12. Note here that in normal solvents also, η/T dependence of $\langle\tau_D\rangle$ is not perfectly following the hydrodynamic Stokes-Einstein (SE) relation (where $p=1$). Interestingly, the translational diffusion of non-spherical solute, rhodamine 6G (R6G), was also found to deviate from the SE prediction.^{58,59} Since the SE relation is based on the translational diffusion of a spherical solute in a solvent continuum, the nonspherical shape of C153 might be responsible for the observed fractional $p=0.86$ in normal solvents. Even with such a base line, $p\sim 0.6$ found for C153 translation in these polymer electrolyte solutions does indicate significant temporal heterogeneity in these media. This interpretation is in line with the findings for deeply super-cooled liquids, glass etc.⁶⁰⁻⁶⁶ Surprisingly, even ~ 100 K above their respective glass transition temperature (T_g), shown in Figure A.d.5 (see Appendix), the current PGEs exhibit such dynamical characteristics observed in super-cooled systems.

Table 6.7: Diffusion time, $\langle \tau_D \rangle$, obtained from normal single diffusion of C153 (A) dissolved in sets of normal solvents and (B) polymer gel electrolytes, [(PC+LiClO₄)+wt%PPG] at 293K.

A:Normal Solvents at 293 K			B:[(PC+LiClO ₄)+wt%PPG] at 293 K		
Solvents	η/cP	$\langle \tau_D \rangle/\mu s$	wt% PPG	η/cP	$\langle \tau_D \rangle/\mu s$
Acetonitrile	0.37	22±4	10	8.54	190±41
Ethanol	1.20	65±14	20	9.12	198±21
1-Propanol	2.20	100±22	40	16.77	307±26
1-Butanol	2.94	130±27	50	24.80	376±60
1-Hexanol	5.32	210±32	60	33.84	484±70
1-Octanol	9.01	370±48	100	98.31	807±95
1-Decanol	14.32	550±52			
Ethylene Glycol	20.81	700±92			

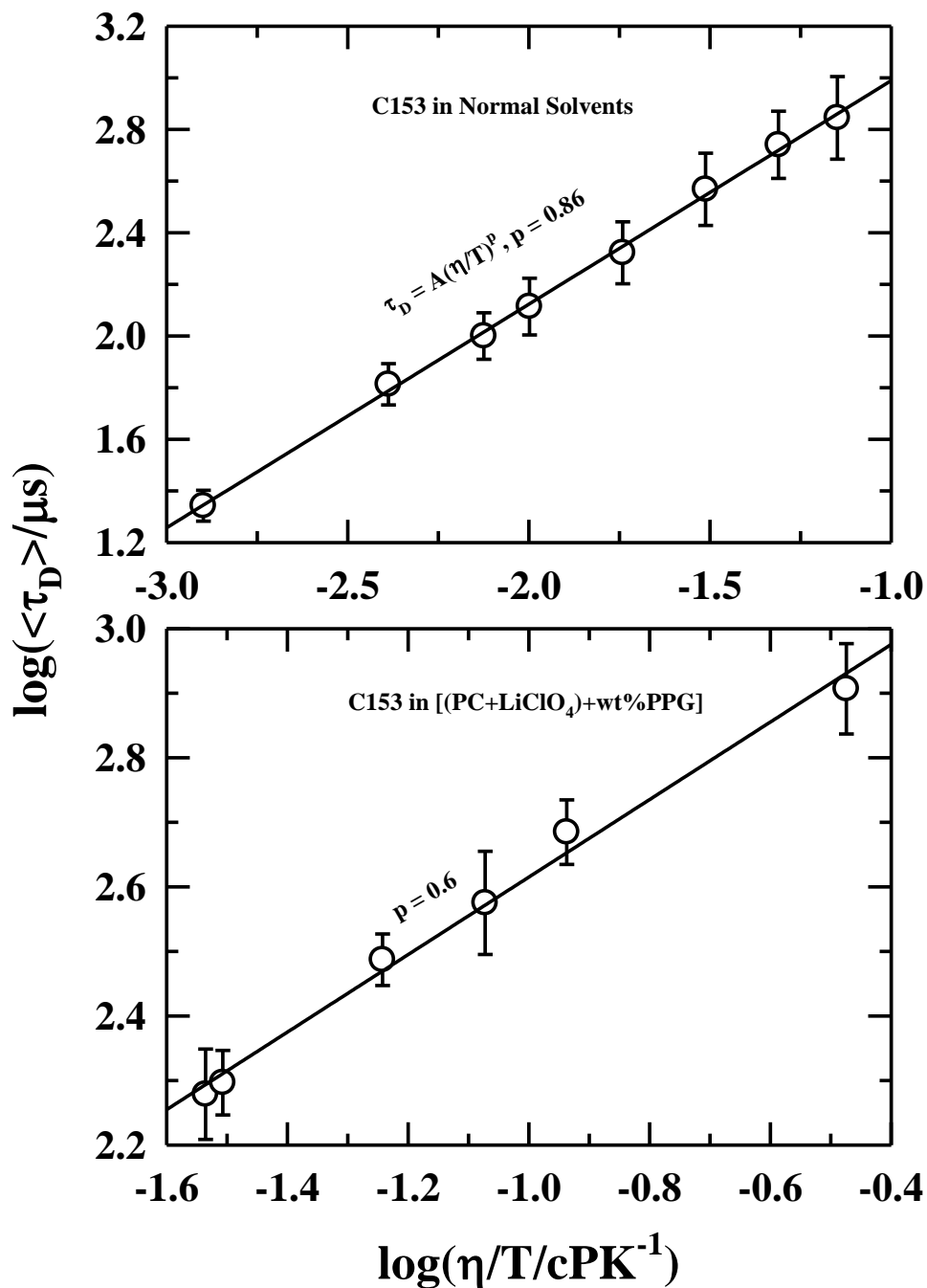


Figure 6.11: Temperature-reduced viscosity $\left(\frac{\eta}{T}\right)$ dependence of average translation time, $\langle\tau_D\rangle$, of C153 dissolved in normal solvents (upper panel) and in [(PC+LiClO₄)+wt%PPG] (lower panel). Solid lines passing through the data points represent the fits.

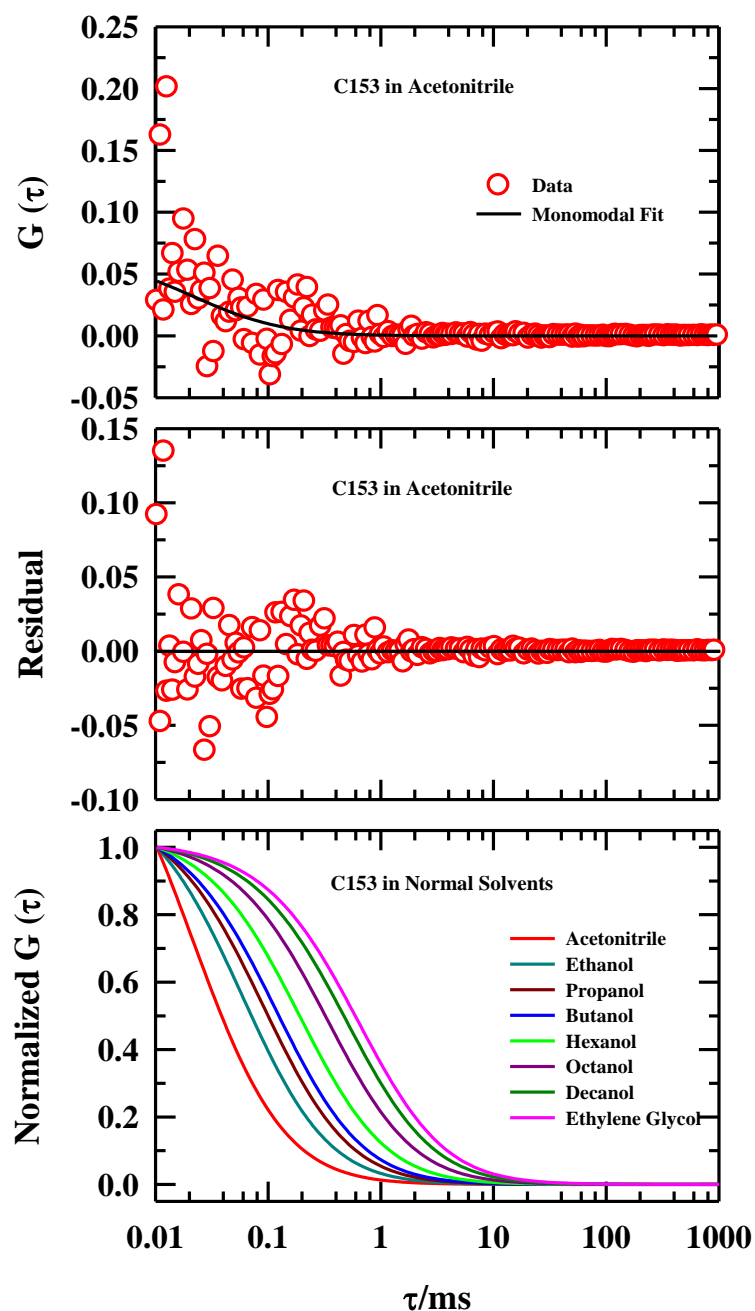


Figure 6.12: Upper panel: Representative fluorescence autocorrelation $G(\tau)$ of C153 in acetonitrile at 293K. Coloured symbols represent $G(\tau)$ data points while solid line passing through the data points depicts the normal single diffusion fits and corresponding residual is shown in middle panel. Lower panel: Normalized autocorrelation fits (normal single diffusion) of C153 in various normal solvents. Different colours have been used to indicate various solvents.

6.3.4 Translation-Rotation Decoupling

For deeply super-cooled liquids, it has been found that solute rotation decouples from solvent viscosity later than its translation.^{62,67-71} Thus fraction values obtained from rotation (p_{rot}) and translation (p_{tr}) should differ from each other with $p_{rot} > p_{tr}$. In the present polymer gel electrolytes, the rotational motion of external solute C153 exhibits fractional viscosity dependence with $p \sim 0.7$ (see Figure 6.9) and ~ 0.6 (Figure 6.11) for translational motion. Further investigations using NMR, MD simulation, dielectric relaxation etc. are needed to explore and understand the origin of such translation-rotation decoupling in various polymer gel electrolytes.

6.4 Conclusion

In summary, the above work presented here clearly depicts the viscosity decoupling of rotation and translation of C153 in the PPG based polymer gel electrolyte system. Excitation wavelength dependent fluorescence emission studies with a fast lifetime probe such as DMASBT suggests inhomogeneous density persistence timescale is rather fast and fall in the sub-nanosecond regime. The fractional viscosity dependence of the average rotation and translation diffusion times of C153 has been observed in the present PGEs. The p values deviate significantly from unity, suggesting substantial medium temporal heterogeneity. A negative viscosity coupling (opposite to C153 rotation and translation) of the average solvation time of C153 indicates C153 solvation is overwhelmingly dominated by local participation where medium viscosity finds no significant role. The appearance of a new time component in the solvation response function of C153 in these polymer containing systems and a close qualitative similarity of this timescale with a previously reported dielectric relaxation time in pure PPG re-establishes the impact of the polymer on solution dynamics of these polymer gel electrolytes. The decrease in average solvation time with increasing the relative wt% of polymer in [(PC+LiClO₄)+wt%PPG] polymer gel electrolytes (and hence increasing medium viscosity) signifies remarkable effect of polymer in the solvation dynamics of the photo-excited probe (C153) molecule. A signature of translation-rotation decoupling for solute motion has also been found. The translation-rotation decoupling and spatio-temporal heterogeneity are two important observations for these polymer gel electrolytes which may be intelligently used to realise their full application potential in various electro-chemical devices where ion-transport is the main focus.

References

1. H. Nishide and K. Oyaizu, *Science* **319**, 737 (2008).
2. J. R. Miller, *Science* **335**, 1312 (2012).
3. X. Yang, F. Zhang, L. Zhang, T. Zhang, Y. Huang and Y. Chen, *Adv. Funct. Mater.* **23**, 3353 (2013).
4. J. M. Taracson and M. Armand, *Nature* **414**, 359 (2001).
5. M. Armand and J. M. Tarascon, *Nature* **451**, 652 (2008).
6. K. Xu, *Chem. Rev.* **104**, 4303 (2004).
7. D. Aurbach, M. L. Daroux, P. W. Faguy and E. Yeager, *J. Electrochem. Soc.* **134**, 1611 (1987).
8. P. Carlsson, B. Mattsson, J. Swenson, L. M. Torell, M. Käll, L. Börjesson, R. L. McGreevy, K. Mortensen and B. Gabrys, *Solid State Ion.* **113**, 139 (1998).
9. K. M. Abraham and M. Alamgir, *J. Electrochem. Soc.* **137**, 1657 (1990).
10. W. Gorecki, P. Donoso, C. Berthier, M. Mali, J. Roos, D. Brinkmann and M. B. Armand, *Solid State Ion.* **28**, 1018 (1988).
11. O. Bohnke, G. Frand, M. Rezrazi, C. Rousselot and C. Truche, *Solid State Ion.* **66**, 97 (1993).
12. A. M. Stephan, *Eur. Polym. J.* **42**, 21 (2006).
13. J. Y. Song, Y. Y. Wang and C. C. Wan, *J. Power Sources* **77**, 183 (1999).
14. X. Cheng, J. Pan, Y. Zhao, M. Liao and H. Peng, *Adv. Energy Mater.* **8**, 1702184 (2018).
15. O. A. Ileperuma, *Mater. Technol.* **28**, 65 (2013).
16. J. Wu, Z. Lan, J. Lin, M. Huang, Y. Huang, L. Fan and G. Luo, *Chem. Rev.* **115**, 2136 (2015).
17. H. Yu, J. Wu, L. Fan, Y. Lin, K. Xu, Z. Tang, C. Cheng, S. Tang, J. Lin and M. Huang, *J. Power Sources* **198**, 402 (2012).
18. F. Croce, G. B. Appetecchi, L. Persi and B. Scrosati, *Nature* **394**, 456 (1998).
19. C. Svanberg, J. Adebahr, H. Ericson, L. Börjesson, L. M. Torell and B. Scrosati, *J. Chem. Phys.* **111**, 11216 (1999).
20. B. Klassen, R. Aroca, M. Nazri and G. A. Nazri, *J. Phys. Chem. B* **102**, 4795 (1998).
21. L. Yang, A. Xiao and B. L. Lucht, *J. Mol. Liq.* **154**, 131 (2010).

22. E. Cazzanelli, P. Mustarelli, F. Benevelli, G. B. Appetecchi and F. Croce, *Solid State Ion.* **86**, 379 (1996).
23. H. L. Yeager and H. Reid, *J. Phys. Chem.* **80**, 850 (1976).
24. H. L. Yeager, J. D. Fedyk and R. J. Parker, *J. Phys. Chem.* **77**, 2407 (1973).
25. K. Kumbhakar, E. Tarif, K. Mukherjee and R. Biswas, *J. Mol. Liq.* **290**, 111225 (2019).
26. D. Battisti, G. A. Nazri, B. Klassen and R. Aroca, *J. Phys. Chem.* **97**, 5826 (1993).
27. K. Kondo, M. Sano, A. Hiwara, T. Omi, M. Fujita, A. Kuwae, M. Iida, K. Mogi and H. Yokoyama, *J. Phys. Chem. B* **104**, 5040 (2000).
28. Z. Gadjourova, Y. G. Andreev, D. P. Tunstall and P. G. Bruce, *Nature* **412**, 520 (2001).
29. A. Triolo, V. Arrighi, R. Triolo, S. Passerini, M. Mastragostino, R. E. Lechner, R. Ferguson, O. Borodin and G. D. Smith, *Physica B Condens. Matter* **301**, 163 (2001).
30. P. Carlsson, R. Zorn, D. Andersson, B. Farago, W. S. Howells and L. Börjesson, *J. Chem. Phys.* **114**, 9645 (2001).
31. T. Yamaguchi, R. Matsui and S. Koda, *J. Phys. Chem. B* **117**, 7077 (2013).
32. D. Andersson, D. Engberg, J. Swenson, C. Svanberg, W. S. Howells and L. Börjesson, *J. Chem. Phys.* **122**, 234905 (2005).
33. R. Baumann, C. Ferrante, E. Kneuper, F. W. Deeg and C. Bräuchle, *J. Phys. Chem. A* **107**, 2422 (2003).
34. M. L. Horng, J. A. Gardecki and M. Maroncelli, *J. Phys. Chem. A* **101**, 1030 (1997).
35. R. Karmakar and A. Samanta, *J. Phys. Chem. A* **106**, 4447 (2002).
36. M. Maroncelli and G. R. Fleming, *J. Chem. Phys.* **86**, 6221 (1987).
37. M. L. Horng, J. A. Gardecki, A. Papazyan and M. Maroncelli, *J. Phys. Chem.* **99**, 17311 (1995).
38. R. Biswas, J. E. Lewis and M. Maroncelli, *Chem. Phys. Lett.* **310**, 485 (1999).
39. J. E. Lewis, R. Biswas, A. G. Robinson and M. Maroncelli, *J. Phys. Chem. B* **105**, 3306 (2001).
40. T. Pradhan and R. Biswas, *J. Phys. Chem. A* **111**, 11514 (2007).
41. T. Pradhan, P. Ghoshal and R. Biswas, *J. Phys. Chem. A* **112**, 915 (2008).
42. T. Pradhan, P. Ghoshal and R. Biswas, *J. Chem. Sci.* **120**, 275 (2008).
43. J. R. Lakowicz, *Principles of Fluorescence Spectroscopy* (Springer science & business media, 2013).
44. P. O. Gendron, F. Avaltroni and K. J. Wilkinson, *J. Fluoresc.* **18**, 1093 (2008).
45. G. Majer and J. P. Melchior, *J. Chem. Phys.* **140**, 094201 (2014).
46. A. V. Sarode and A. C. Kumbharkhane, *J. Mol. Liq.* **160**, 109 (2011).

47. T. Yamaguchi, M. Hayakawa, T. Matsuoka and S. Koda, *J. Phys. Chem. B* **113**, 11988 (2009).
48. A. Samanta, *J. Phys. Chem. B* **110**, 13704 (2006).
49. M. Kondo, X. Li and M. Maroncelli, *J. Phys. Chem. B* **117**, 12224 (2013).
50. B. Guchhait, S. Das, S. Daschakraborty and R. Biswas, *J. Chem. Phys.* **140**, 104514 (2014).
51. B. Guchhait, H. Al Rasid Gazi, H. K. Kashyap and R. Biswas, *J. Phys. Chem. B* **114**, 5066 (2010).
52. R. S. Fee and M. Maroncelli, *Chem. Phys.* **183**, 235 (1994).
53. N. Ito, S. Arzhantsev, M. Heitz and M. Maroncelli, *J. Phys. Chem. B* **108**, 5771 (2004).
54. C. F. Chapman and M. Maroncelli, *J. Phys. Chem.* **95**, 9095 (1991).
55. B. Guchhait and R. Biswas, *J. Chem. Phys.* **138**, 114909 (2013).
56. R. J. Sengwa, *J. Mol. Liq.* **108**, 47 (2003).
57. S. Schrödle, R. Buchner and W. Kunz, *J. Phys. Chem. B* **108**, 6281 (2004).
58. N. Subba, K. Polok, P. Piatkowski, B. Ratajska-Gadomska, R. Biswas, W. Gadomski and P. Sen, *J. Phys. Chem. B* **123**, 9212 (2019).
59. N. Subba, E. Tarif, P. Sen and R. Biswas, *J. Phys. Chem. B* **124**, 1995 (2020).
60. M. D. Ediger, C. A. Angell and S. R. Nagel, *J. Phys. Chem.* **100**, 13200 (1996).
61. C. A. Angell, *J. Chem. Phys.* **46**, 4673 (1967).
62. M. D. Ediger, *Annu. Rev. Phys. Chem.* **51**, 99 (2000).
63. H. Sillescu, *J. Non-Cryst. Solids* **243**, 81 (1999).
64. I. Chang, F. Fujara, B. Geil, G. Heuberger, T. Mangel and H. Sillescu, *J. Non-Cryst. Solids* **172**, 248 (1994).
65. C. T. Moynihan, *J. Phys. Chem.* **70**, 3399 (1966).
66. D. Chakrabarti and B. Bagchi, *Phys. Rev. Lett.* **96**, 187801 (2006).
67. C. A. Angell, K. L. Ngai, G. B. McKenna, P. F. McMillan and S. W. Martin, *J. Appl. Phys.* **88**, 3113 (2000).
68. J. C. Dyre, *Rev. Mod. Phys.* **78**, 953 (2006).
69. K. L. Ngai, *Relaxation and Diffusion in Complex Systems* (Springer Science & Business Media, 2011).
70. P. J. Griffin, A. L. Agapov and A. P. Sokolov, *Phys. Rev. E* **86**, 021508 (2012).
71. K. V. Edmond, M. T. Elsesser, G. L. Hunter, D. J. Pine and E. R. Weeks, *Proc. Natl. Acad. Sci.* **109**, 17891 (2012).

Chapter 7

Cloud Point Driven Dynamics in Aqueous Solutions of Thermoresponsive Copolymers: Are They Akin to Criticality Driven Solution Dynamics?

7.1 Introduction

Phase separation is a consequence of nucleation and growth with time.¹ The growth is a diffusion controlled process, and near the critical point (T_c) the mutual diffusion coefficient decreases asymptotically and approaches to zero.² The slowing down of nucleation and growth near T_c was observed in various systems including neat solvents,³ binary mixtures of molecular liquids,^{4,5} polymer solutions,⁶ etc. Divergence of correlation length and universality in static and dynamic critical behaviour⁷ near T_c are the hallmark of criticality. Different stimuli-responsive polymers are known to show hydrophilic-hydrophobic phase transition in aqueous medium.^{8,9} In this regard, stimuli-responsive polymers (also known as ‘smart’ polymers) could be a suitable system to exhibit such criticality owing to their inherent ability to respond to various external stimuli such as pH,^{10,11} temperature,^{12,13} light,^{14,15} redox potential,^{16,17} electric¹⁸ and magnetic fields.¹⁹

Amongst the smart polymers, thermoresponsive polymers are the most widely used as they can undergo a reversible phase transition as a function of temperature.¹² This facet allows them to act like unique smart polymers having “on-off” switchable feature through externally applied temperature.²⁰ These polymers possess a miscibility gap in their temperature-composition phase diagram in aqueous solutions. Accordingly, depending upon the appearance of miscibility gap either by increasing or decreasing temperature of polymer solutions, thermoresponsive polymers can be classified as those with a lower critical solution temperature (LCST), and another with upper critical solution temperature (UCST).²¹ LCST defined as the lowest temperature of the binodal phase diagram (or the coexistence curve). However, cloud point or phase transition temperature (T_{cp}) of thermoresponsive polymer refers to the temperature at which the polymer solution at a specific concentration undergoes a sharp and reversible transition from hydrophilic coil to hydrophobic globule state followed by formation of large aggregates of collapsed dehydrated polymer chains.^{22,23} Notably, the T_{cp} of a water-soluble amphiphilic copolymer relies on their hydrophilic/hydrophobic segment balance.²⁴ At

a temperature lower than T_{cp} , the polymer chains remain completely hydrated, and solubilized in water while a sudden change in solution behaviour occurs at elevated temperature as the interactions between hydrophobic units of polymer dominate over the hydrogen bonding between water and hydrophilic segments.²⁵ Consequently, the polymers no longer remain hydrated, and undergo a phase transition resulting in the formation of water-insoluble large polymeric aggregates.

Examples of well-known thermoresponsive LCST polymers include poly(*N*-isopropyl acrylamide) (PNIPAM),¹³ poly(*N,N*-diethyl acrylamide) (PDEAM),¹³ poly(*N*-vinylcaprolactam) (PNVCL),²⁶ poly[2-(dimethylamino)ethyl methacrylate] (PDMAEMA),²⁷ poly(ethylene oxide) (PEO),²⁸ etc. The size or polarity of side chains is known to impart a significant impact on LCST. For instance, the PEG (polyethylene glycol)-based polymers having different length of ethylene oxide side units represents diverse range of LCST values.²⁹ Additionally, the LCST of a polymer can also be manipulated by copolymerizing with a hydrophilic or hydrophobic monomer and controlling molecular weight.³⁰ Recently, PEG-based thermoresponsive macromolecules emerged as a potential candidate for biomedical applications since they are primarily composed of biocompatible neutral ethylene oxide segments which make them uncharged, nonimmunogenic, non-toxic and water-soluble.^{31,32} Because of such intriguing properties, PEG-based amphiphilic copolymers with tunable T_{cp} around body temperature become the most sought-after materials for different biomedical applications.³³

PEG-based thermoresponsive polymers, specifically random copolymers, were designed to achieve tunable T_{cp} around human body temperature by varying copolymer composition and chain length to make the copolymer micelles applicable for biomedical purposes.³⁴⁻³⁹ Majority of these works mainly focused on the synthesis of such copolymers to achieve on-demand morphology along with stimuli-responsive feature. However, understanding the structure, nature of interaction and relaxation dynamics of such kind of amphiphilic copolymers in aqueous media is critical for developing smart copolymers for targeted applications. Unfortunately, investigations along this line have remained largely unexplored so far. This observation has led us to investigate the interactions and relaxation dynamics in amphiphilic thermoresponsive random copolymers having miscibility gap depending on their concentration/ T_{cp} in aqueous media. More particularly, we have focused here on the impact of T_{cp} on solute-medium interaction, and explored whether the solution dynamics altered as T_{cp} is approached in a way reminiscent of that driven by critical solution temperature (T_c). For this

purpose, a series of thermosensitive water-soluble amphiphilic random copolymers comprised of methyl methacrylate (MMA) and poly(polyethylene glycol) monomethyl ether methacrylate (PEGMA) are taken. These series of thermoresponsive copolymers have been designed, synthesized and characterized by Prof. Priyadarsi De's group, IISER Kolkata, India.⁴⁰ MMA was integrated as a hydrophobic partner during the copolymerization to tune the T_{cp} of these copolymers between 298 K and 323 K. Steady state and time-resolved fluorescence spectroscopy have been employed to explore the interaction and aqueous solution dynamics of these copolymers employing two fluorescent dye molecules, coumarin 153 (C153, hydrophobic) and coumarin 343 (C343, hydrophilic). Further, a thorough and systematic investigation was performed to reveal the impact on solution structure and relaxation dynamics as T_{cp} is approached via the static and dynamic fluorescence measurements.

7.2 Experimental Details

7.2.1 Materials Sample Preparation for Fluorescence Measurements

Pyrene, coumarin 343 (C343) and coumarin 153 (C153) were purchased from Sigma Aldrich and used as received. Experimental solutions were prepared by mixing required amount of copolymers in Milli-Q water. Three different polymers⁴⁰ (P1, P2 and P3) with different number of hydrophobic (m) and hydrophilic (n) chain length (P1 (m=31, n=30), P2 (m=29, n=24), P3 (m=41, n=24)) were used in the current work. Aqueous copolymer mixture was then kept at lower temperature (with respect to T_{cp}) till complete dissolution of copolymer. The concentrations of experimental aqueous copolymer solutions were fixed at 2 mg/mL. Optical measurements of these solutions were performed as follows: 2-3 μ L of freshly prepared solutions of coumarin 153 (C153) in hexane was taken in a quartz cuvette of 1 cm optical path length. The nonpolar solvent was then evaporated off by uniformly blowing hot air around the outer surface of the cuvette. Approximately 2.5-3 mL of sample solution was poured into the cuvette with C153. In other set of measurements, a few crystals of C343 were added directly to solutions, shaken gently until complete dissolution. Concentration of C153/C343 in each of these samples was maintained at $\leq 10^{-5}$ M. Spectroscopic measurements were carried out in a humidity-controlled environment. The chemical structures of synthesized thermoresponsive copolymers, C153, C343 and pyrene are shown in Scheme 7.1.

7.2.2 Dynamic Light Scattering (DLS)

Dynamic light scattering (DLS) measurements were conducted with a Malvern Nano Zetasizer instrument (Malvern Instrument Ltd., Malvern, UK) equipped with a 4.0 mW He–Ne laser beam operating at $\lambda = 633$ nm at a scattering angle of 173° . All aqueous copolymer solutions were filtered through a $0.45 \mu\text{m}$ syringe filter prior to measurement. Temperature dependent DLS measurements were carried out for each copolymer at a fixed concentration of 2 mg/mL in water.

7.2.3 Density and Viscosity Coefficient Measurements

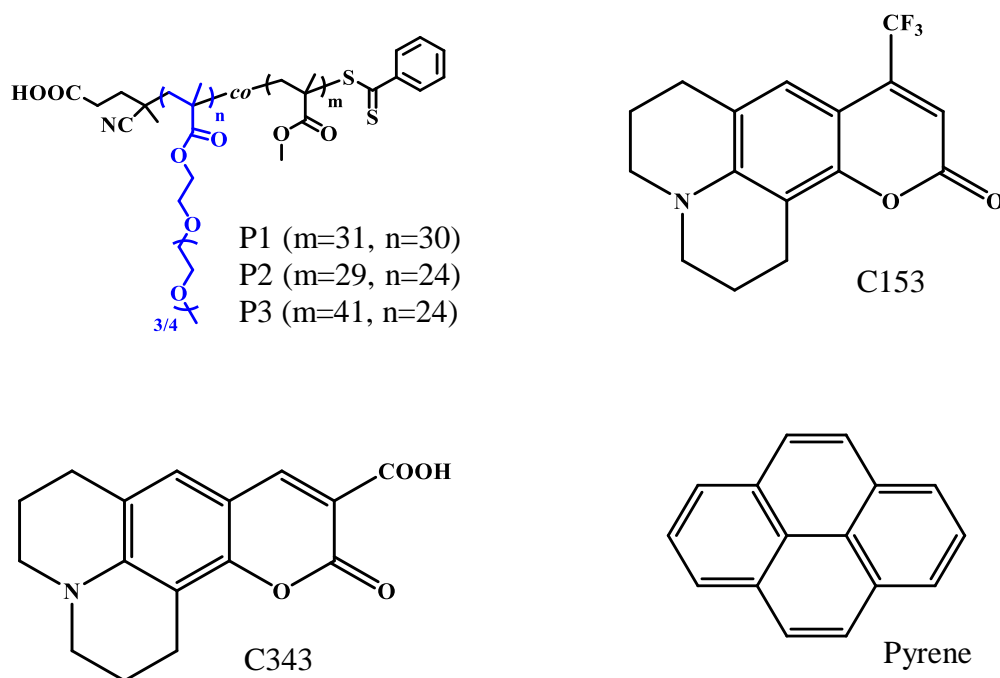
Densities (ρ) and viscosity coefficients (η) of the solutions were measured by using an automated temperature-controlled density-cum-sound analyzer (Anton Paar, model DSA 5000) and automated micro viscometer (AMVn, Anton Paar), respectively.^{41,42}

7.2.4 Data Collection and Analysis for Steady State Optical Measurements

UV-Visible spectrophotometer (UV-2600, Shimadzu), and a fluorimeter (Fluorolog, Jobin-Yvon, Horiba) were used for recording steady state absorption and fluorescence emission spectra, respectively.^{43,44} Temperature was controlled by using Peltier temperature controller (accuracy ± 0.5 K). Steady-state absorption spectra were taken at 2 nm slit width and fluorescence spectra were recorded using 2 nm slits at both the excitation and emission ends. The standard spectral analysis procedure was followed to determine spectral frequencies.^{45,46} The typical error bar for the determined spectral frequencies and spectral widths (full width at half maxima, FWHM) were $\pm 200 \text{ cm}^{-1}$. Details of the steady state measurements technique are the same as discussed in chapter 2.

7.2.5 Data Collection and Analysis for Time-Resolved Fluorescence Emission Spectra

Time-resolved fluorescence measurements⁴⁷ were performed with a time-correlated single-photon counting (TCSPC) system (LifeSpec-ps) from Edinburgh Instruments (Livingston, U.K.).^{48,49} Details of time-resolved fluorescence measurements are the same as described in chapter 2 and references.⁴⁹⁻⁵¹



Scheme 7.1: Chemical structure of P1-P3 polymers, C153, C343 and pyrene.

7.3 Results and Discussion

7.3.1 Determination of Critical Aggregation Concentration (CAC) of the Copolymers

Amphiphilic random copolymers are known to form self-assembled structures in water.^{52,53} As the synthesized P1-P3 are amphiphilic in nature having both hydrophilic (PEGMA) and hydrophobic (MMA) segments, we have studied the self-assembly characteristics of the copolymers in aqueous medium by fluorescence technique using pyrene as a fluorescent probe. The CAC values of these copolymers are determined from the emission spectra of pyrene in the aqueous medium with gradual increment of the polymer concentration.^{44,54} CAC values of P1-P3 have been calculated from the point of intersection of two slopes obtained from the plot of I_{391}/I_{370} versus the logarithm of the copolymer concentration as shown in Figure 7.1. The CAC values thus determined are 14, 2.5 and 2 mg/L for P1, P2 and P3 respectively. The decrease in CAC value with the increase of the hydrophobic MMA content in the copolymer can be attributed to the fact that a copolymer with larger hydrophobic/hydrophilic ratio aggregates in aqueous medium at a concentration lower than that for smaller hydrophobic/hydrophilic ratio.

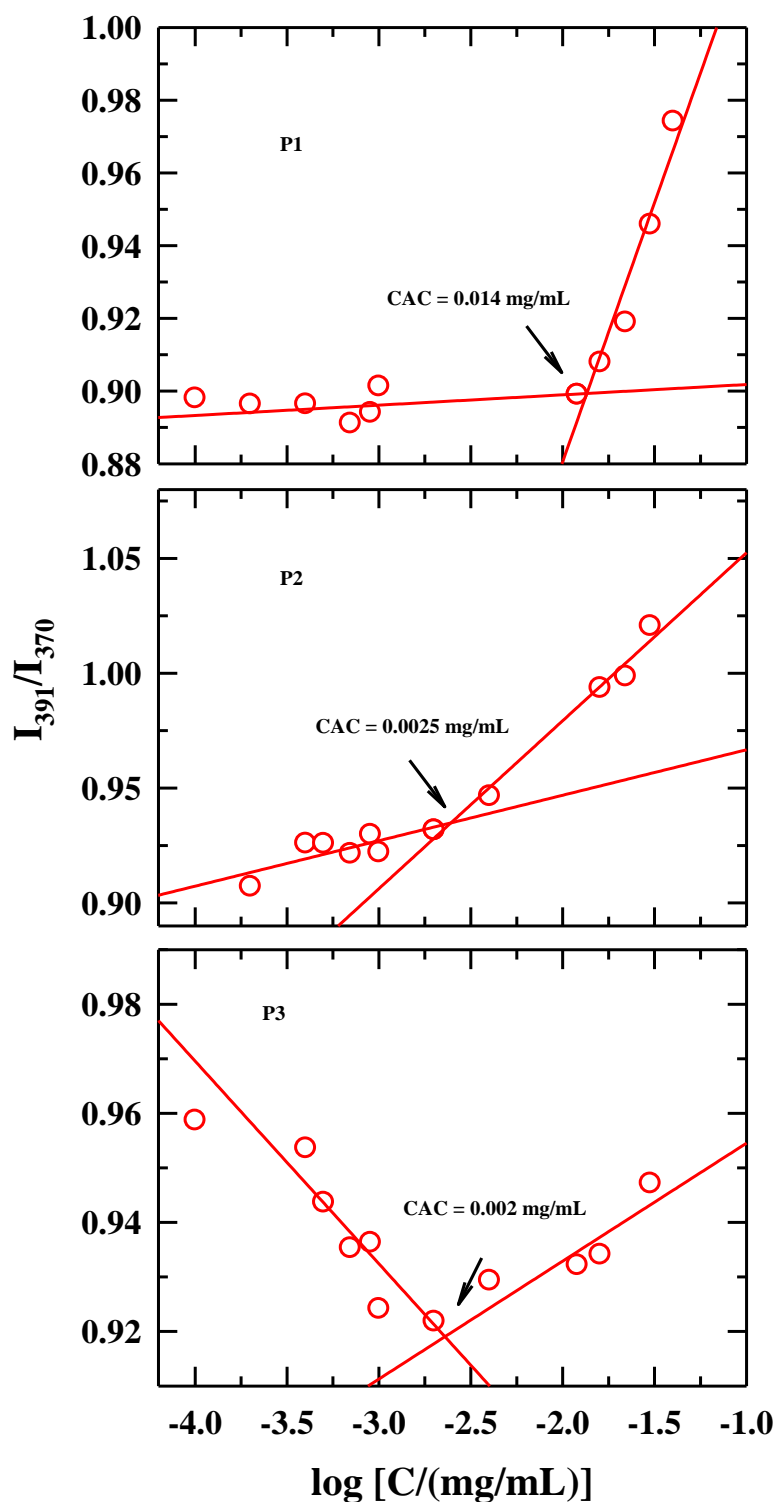


Figure 7.1: Polymer concentration dependent fluorescence emission intensity ratio, I_{391}/I_{370} , for pyrene in aqueous solutions of P1 (upper panel), P2 (middle panel) and P3 (lower panel). The intersection points, indicated by arrows, represent respective CAC values.

7.3.2 Cloud Point Temperature (T_{cp})

These random copolymers, P1-P3, are expected to show temperature induced phase transition behaviour as they consist of well-known thermosensitive PEGMA units. Hence, the turbidity measurements of P1-P3 have been carried out by monitoring the percentage of transmittance (% T) with increasing temperature using UV-Vis spectroscopy at 500 nm.⁵² The T_{cp} is considered as the temperature where % T is reduced to 50%.⁵⁴ Figure 7.2 indicates T_{cp} of these aqueous copolymer solutions are 323 K, 316 K and 301 K for P1, P2 and P3, respectively. As anticipated, T_{cp} of the copolymers decreases with the decrease of hydrophilic PEGMA content and increase of hydrophobic MMA units into the copolymers. These copolymers form transparent solutions in aqueous medium below their respective cloud point temperature and turn opaque (milky white) when temperatures of the solutions reach their respective T_{cp} or go beyond as the globules aggregate causing turbidity and large scale density fluctuations. However, the phase transition of P1-P3 showed a negligible hysteresis on changing temperature upward/downward (data not shown).

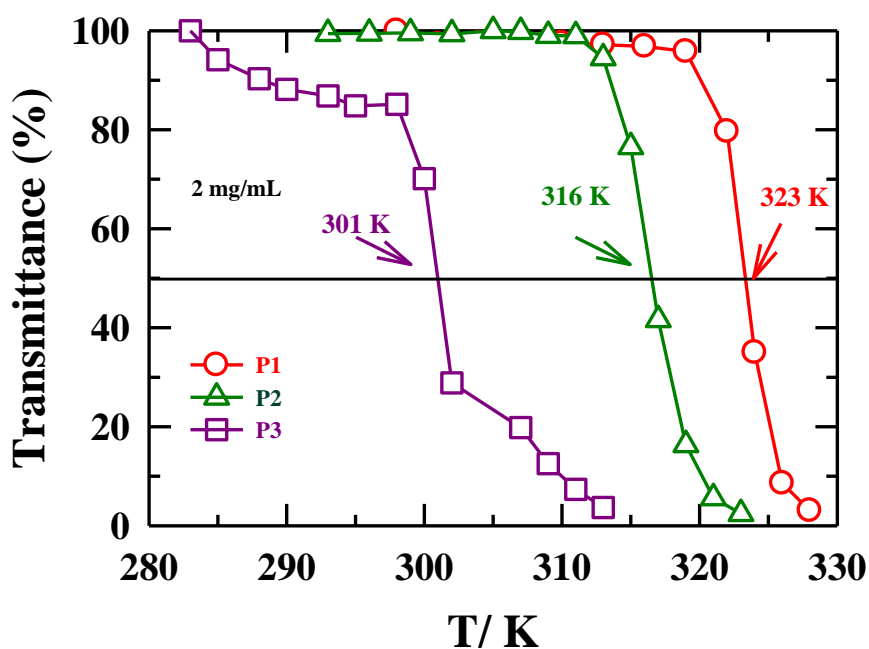


Figure 7.2: Temperature dependent transmittance % of aqueous solutions (2 mg/mL) of P1-P3. Arrows indicate cloud point temperature, T_{cp} .

In the subsequent step, the T_{cp} s of P1-P3 have also been determined by temperature-dependent DLS measurements. The DLS diagrams of the copolymer solutions (2 mg/mL) at variable

temperatures are presented in Figure 7.3. For P1, hydrodynamic diameter (D_h) is found to be in the range of <10 nm up to 318 K, but the particle size suddenly increases to ~500-800 nm at and above 323 K. It is clear that below T_{cp} the obtained D_h s are attributed to the single copolymer chain conformation.⁵⁵ On the other hand, when the temperature approaches to T_{cp} , large aggregated structures are formed. This is ascribed to the temperature driven phase separation of thermoresponsive copolymers in aqueous medium. Presence of smaller size particles than visible light wavelength range (400-800 nm) is responsible for transparent appearance (maximum of incident light transmit through the solution) of these aqueous solutions of P1-P3 in visible light below individual's (P1-P3) T_{cp} . The large size particles formed above T_{cp} is because of the loss of *H*-bonding between the polymer chains (PEGMA) and water, making the polymer solution opaque. A small deviation in T_{cp} determined from UV-Vis spectroscopy and DLS measurements can be explained by considering the fact that during heating of the copolymers some small particles are formed due to the gradual dehydration of the polymer which may simply be overlooked by UV-Vis spectroscopy.^{20,56}

To check whether this phase separation is akin to criticality driven concentration fluctuations or not, we have performed steady state and time-resolved fluorescence spectroscopic measurements of C153 and C343 in aqueous solutions of P1, P2 and P3 (Sec. 4.5 and 4.6). Impact of external solute (C153/C343, $\leq 10^{-5}$ M) on the T_{cp} of the aqueous copolymer solutions were investigated (shown in Figure A.e.1, Appendix A.e). A mild shift of T_{cp} indicates insignificant impact of the foreign solute on cloud point temperatures for these aqueous polymer solutions.

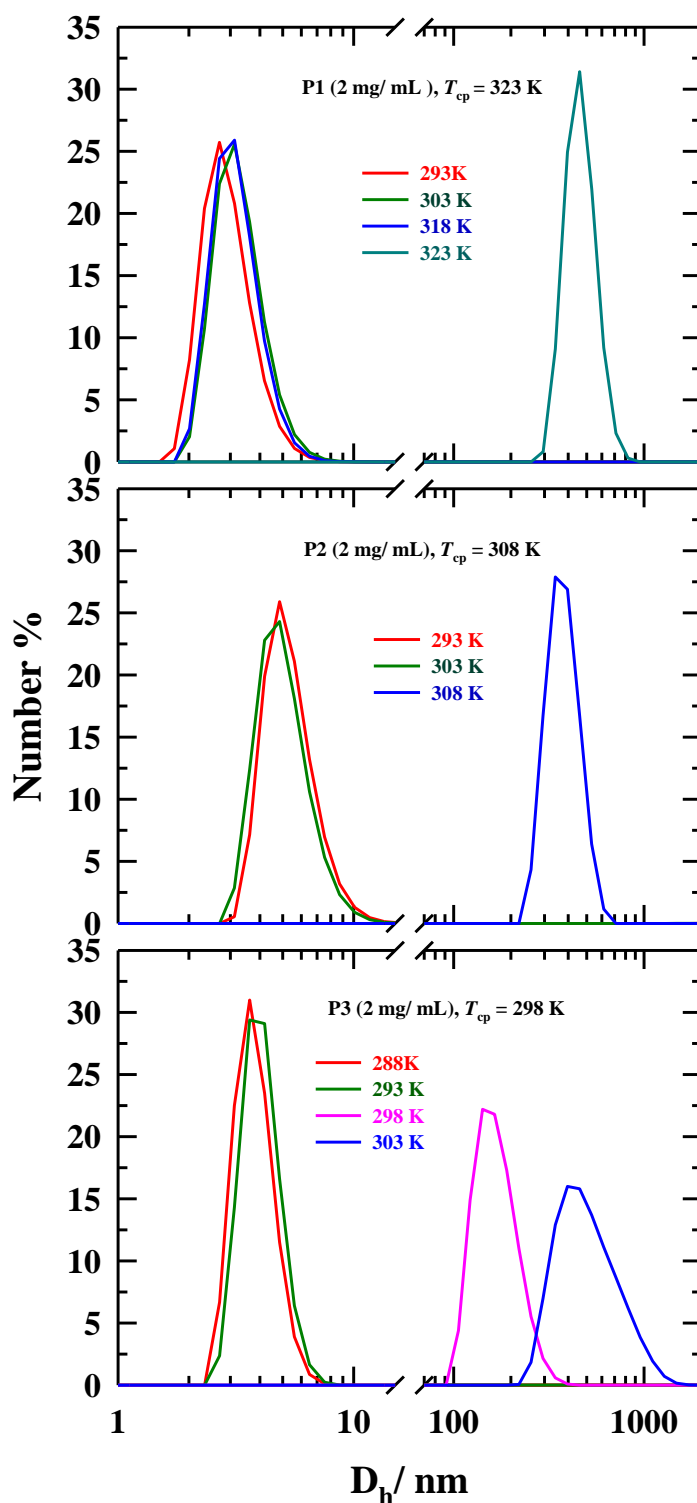


Figure 7.3: Particle size distributions of random copolymers: P1 (upper panel), P2 (middle panel) and P3 (lower panel) in aqueous medium (concentration = 2 mg/mL) below and above T_{cp} . All representations are colour-coded.

Figure 7.3 demonstrates the presence of larger particles with diameter more than 100 nm near or beyond T_{cp} suggesting the formation of larger aggregates through collapse of smaller aggregated structures at $T \geq T_{cp}$ (like coil to globule transition due to dehydration) without making polymer solutions appear cloudy at the onset stage. However, we have restricted the experimental temperatures nearly 5 K below the individual cloud point temperatures (T_{cp}) during the steady state and time-resolved spectroscopic measurements in order to avoid complications arising from the formation of larger particles.

7.3.3 Density and Viscosity Coefficient Measurements

The measured temperature-dependent densities and viscosity coefficients of three aqueous copolymer solutions are summarized in Table A.e.2 (see Appendix). Note that the densities and viscosity coefficients of these solutions are quite close to those for neat water.

7.3.4 Steady State UV-Vis Absorption and Fluorescence Emission Studies

Figure 7.4 represent the temperature dependent absorption and emission spectra of C153, and C343 in aqueous solution of P1. Corresponding spectra in P2 are shown in Figure A.e.3 (see Appendix). Note that for any given polymer solution, absorption and emission spectral characteristics of both C153 and C343 at temperatures away from T_{cp} are quite similar to those at a temperature nearest to the T_{cp} . The highest temperature in these spectroscopic measurements has been restricted below the T_{cp} s (to avoid complications due to phase separation), and emission spectrum recorded after exciting the sample at the wavelength of absorption maximum. These spectral features do not show any abrupt changes with temperature, suggesting a negligible role for T_{cp} in governing the temperature-dependent solute-medium interactions.

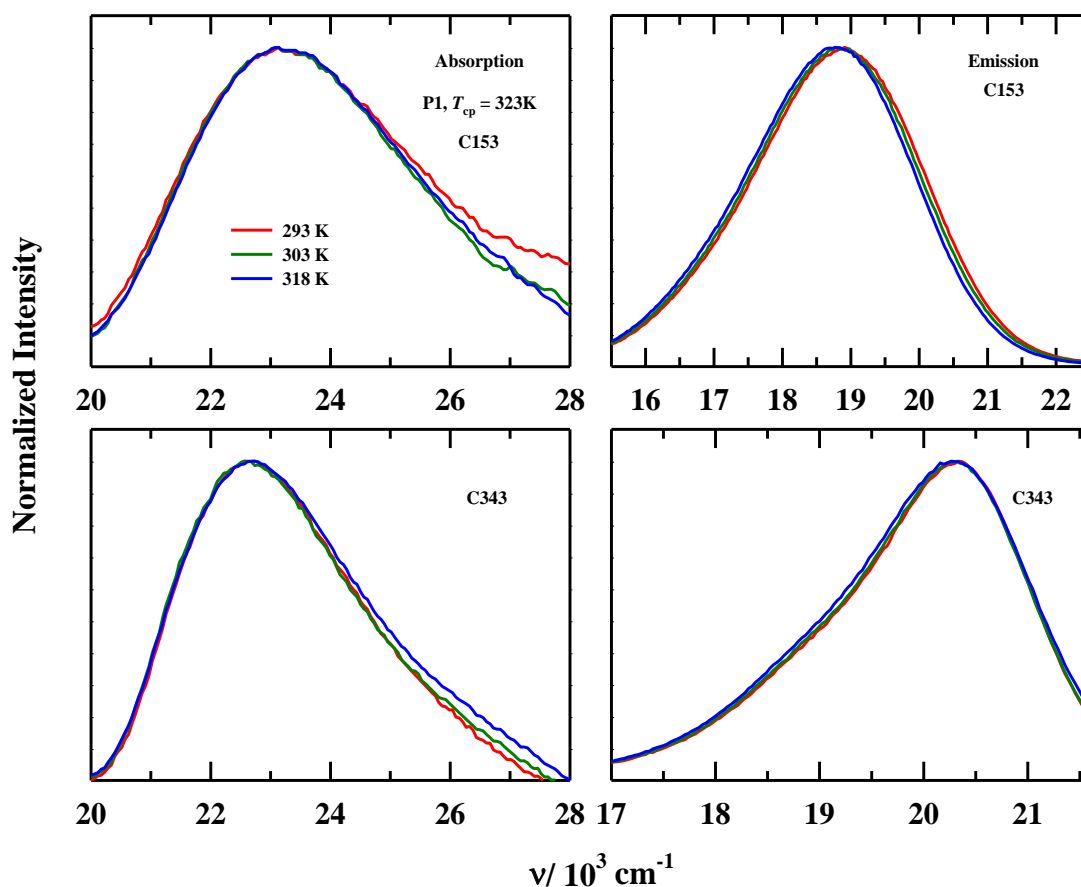


Figure 7.4: Representative temperature dependent UV-Vis absorption (left panels) and steady state fluorescence emission spectra (right panels) of C153 (upper panels), and C343 (lower panels) in aqueous solutions of P1. T_{cp} s are from DLS measurements. Each emission spectrum was recorded at the wavelength of absorption maximum (λ_{max}^{abs}) where λ_{max}^{abs} of C153 were ~ 432 nm and ~ 455 nm for C343. All representations are colour-coded.

We have investigated next the impact of hydrophilic/ hydrophobic unit ratio on steady state UV-Vis absorption and fluorescence emission spectra of C153 and C343 in these three aqueous copolymer (P1-P3) solutions. Representative absorption and emission spectra of C153 and C343 in aqueous solution of P1 to P3 are shown in Figure 7.5. Corresponding absorption and emission spectra in neat water are represented in this figure for comparison. Note the blue shift in emission frequency by ~ 500 - 1000 cm^{-1} for C153 in aqueous P1-P3 solutions compared to that in neat water. This suggests that local environments surrounding C153 in these solutions are less polar than that in neat water.⁵⁷ As the copolymers P1-P3 form self-assembly in aqueous solutions, the hydrophobic polar solute C153 prefers to locate at the interfacial region, which is less polar than bulk water. This interfacial location of C153 in aqueous solutions of self-

assembled structures has been indicated in several earlier studies that dealt with micellar solutions.^{44,58,59} As the hydrophilic/ hydrophobic ratio decreases from P1 to P3, the extent of blue shift increases, suggesting further decrease of polarity of the local environment surrounding C153. In contrast, absorption and emission spectra of C343 (Figure 7.5) in these polymer solutions do not differ much from those in neat water. This indicates C343, by virtue of its hydrophilic nature, locates in the water-rich region and away from the interfacial locations populated by C153.

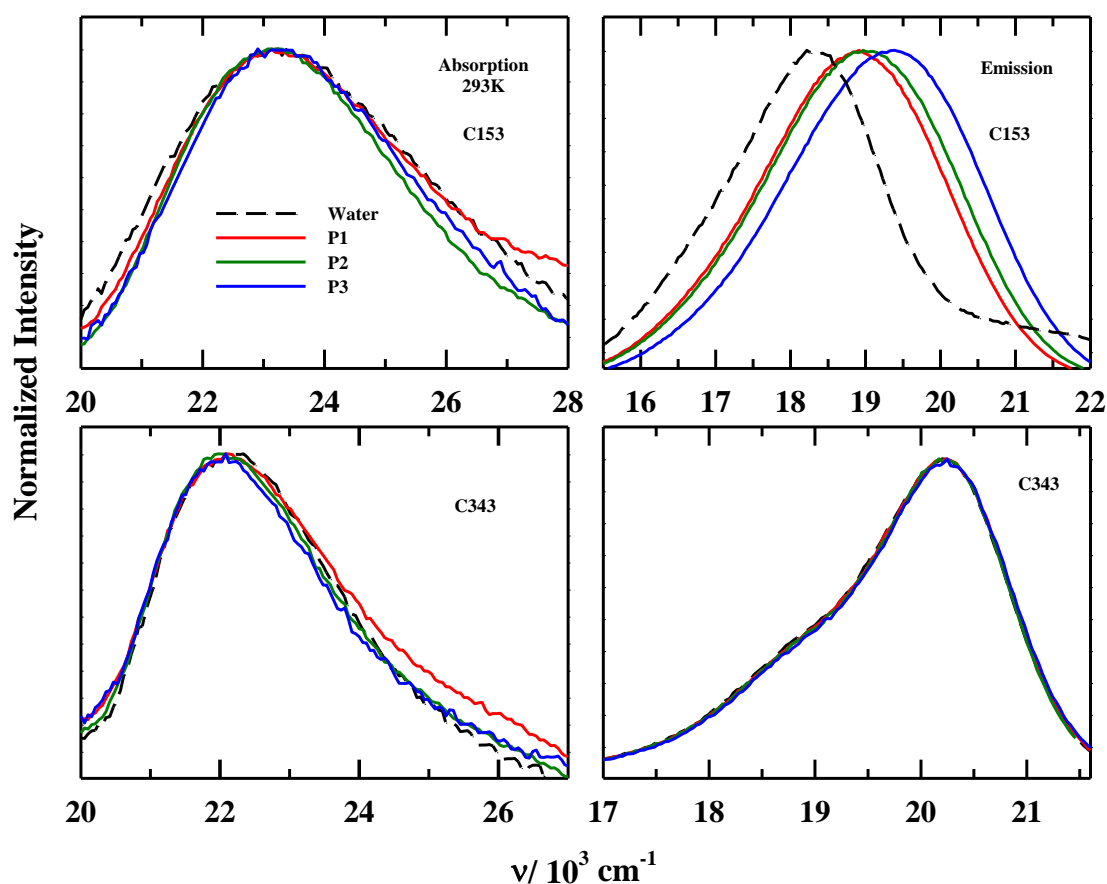


Figure 7.5: Representative steady state UV-Vis absorption (left panels) and fluorescence emission (right panels) spectra of C153 (upper panels) and C343 (lower panels) in the aqueous solution of three random copolymers (P1-P3) at 293 K. Black dashed lines in each spectra depict the respective spectra of probes in neat water. Representations are colour coded.

Because the formation of self-assembled structures in aqueous medium leads to inhomogeneous solution structure, the presence of microheterogeneity in these polymer solutions (P1-P3) have been investigated via monitoring the excitation wavelength (λ_{exc})

dependence of fluorescence emission spectrum of C153.⁶⁰⁻⁶² Note C153 has been chosen for this study because of its preferential location at the interfacial regions in aqueous solutions of these polymers. Representative λ_{exc} dependent fluorescence emission frequencies (left panels) and spectral widths (right panels) are shown in Figure 7.6. Figure A.e.4 (Appendix) is an alternate approach of Figure 7.6 where λ_{exc} dependent shift of fluorescence emission wavelength (left panels) and spectral widths (right panels) are provided. A moderate λ_{exc} induced shift of emission frequency with concomitant spectral narrowing is detected. Note that λ_{exc} dependent total emission shift, $\Delta\nu_{\text{em}}(\lambda_{\text{exc}}) = \nu_{\text{em}}(\lambda_{\text{exc}}^{\text{b}}, 380\text{nm}) - \nu_{\text{em}}(\lambda_{\text{exc}}^{\text{r}}, 480\text{nm})$, do not show any abrupt change as the solution temperature approaches to the T_{cp} . The extent of emission shift ($\Delta\nu_{\text{em}}(\lambda_{\text{exc}})$) decreases gradually with the rise of temperature which suggests temperature-induced faster inter-conversions among differing solute environments.^{63,64}

Note that the extent of emission spectral shift with λ_{exc} increases as the hydrophobic/hydrophilic ratio in copolymer increases, producing the following order (of decreasing heterogeneity): P3>P2>P1. This indicates increase of micro-heterogeneity in local solvation structure due to an increase in hydrophobicity of the polymer units in these aqueous solutions. Figure A.e.5 (Appendix) shows the representative λ_{exc} dependent emission results for C343 in these solutions, which reveals relatively more homogeneous environments surrounding this hydrophilic probe. This further confirms different locations for C153 and C343 in these solutions. These steady state spectral features therefore strongly suggest that solute-environment interactions lead the variations of solute spectra in these solutions where T_{cp} plays either a secondary or no role. Note critical density fluctuations have also been found earlier to play a minor or no role in augmentation of local solvent density surrounding external solutes in supercritical fluids.^{45,46} Solute (C153/C343) centric relaxation dynamics is next investigated by applying time-resolved fluorescence measurements to explore whether relaxation dynamics is influenced by the T_{cp} in these copolymer solutions.

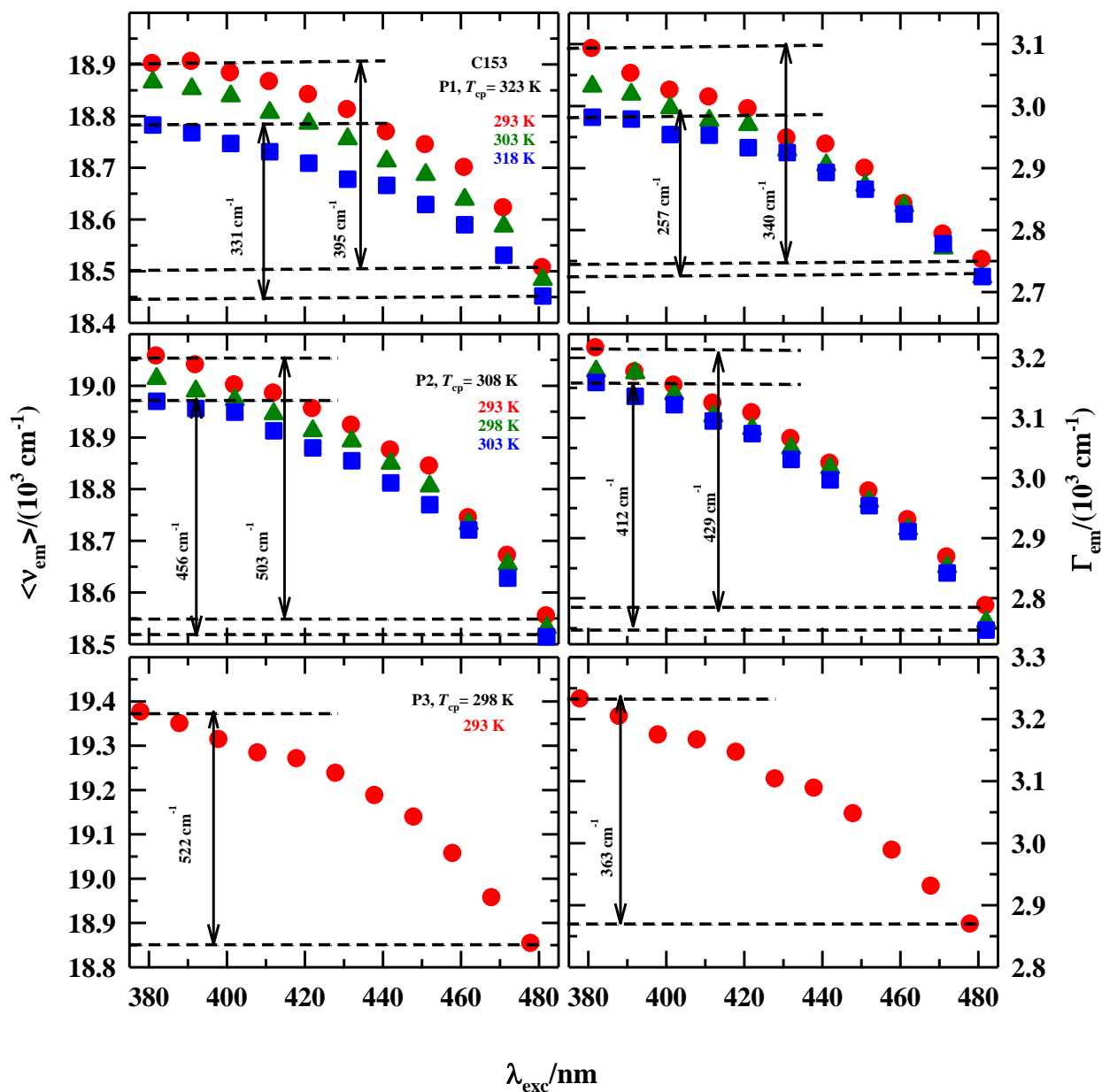


Figure 7.6: Excitation wavelength dependence (λ_{exc}) of steady state average emission frequencies ($\langle v_{em} \rangle$) (left panels) and spectral widths (FWHM, Γ_{em}) (right panels) of C153 in aqueous P1, P2 and P3 solutions at different temperatures. All representations are colour coded.

7.3.5 Time-Resolved Fluorescence Spectroscopy Measurements

7.3.5.1 Fluorescence Lifetime Measurements

Average excited state lifetimes ($\langle \tau_{life} \rangle$) of C153 and C343 in these aqueous polymer solutions are summarized in Table 7.1. Note $\langle \tau_{life} \rangle$ of C153 in these copolymer solutions is ~ 2 times longer than that in neat water, while $\langle \tau_{life} \rangle$ for C343 in these solutions are quite close to that in neat water. This differential sensitivity of $\langle \tau_{life} \rangle$ again reflects the difference in the nature of environments surrounding these solutes in these aqueous polymeric solutions. In addition, $\langle \tau_{life} \rangle$ of C153 in P3 solution is longer than in P1 solution. This suggests that C153 probes more extensively the hydrophobic interfacial regions than the other solute which is hydrophilic in nature. The limited temperature dependent $\langle \tau_{life} \rangle$ data provided here also reveal that the temperature dependence of lifetime is more pronounced for C153 than C343.

Table 7.1: Temperature dependent excited state average lifetime $\langle \tau_{life} \rangle$ of C153 and C343 in aqueous solutions (2 mg/mL) of three copolymers P1-P3.^a

C153								
Polymer	T/K	a ₁	τ_1 /ns	a ₂	τ_2 /ns	a ₃	τ_3 /ns	$\langle \tau_{life} \rangle$ /ns
P1	293	0.20	0.32	0.38	1.79	0.42	5.07	2.87
	298	0.20	0.32	0.38	1.75	0.42	4.85	2.76
	303	0.19	0.26	0.37	1.59	0.44	4.62	2.67
	308	0.22	0.34	0.38	1.81	0.40	4.64	2.62
	313	0.21	0.28	0.38	1.62	0.41	4.40	2.47
	318	0.22	0.29	0.40	1.58	0.38	4.19	2.29
P2	293	0.22	0.24	0.38	1.69	0.40	5.32	2.82
	298	0.24	0.24	0.37	1.64	0.39	5.09	2.65
	303	0.24	0.20	0.37	1.55	0.39	4.91	2.54
P3	293	0.17	0.20	0.20	1.74	0.63	6.00	4.16
Water	293	0.04	0.800	0.96	1.731	-	-	1.70
C343								
P1	293	-	-	0.02	1.50	0.98	4.24	4.19
	298	-	-	0.04	1.80	0.96	4.25	4.16
	303	-	-	0.04	1.50	0.96	4.25	4.14
	308	-	-	0.04	1.80	0.96	4.22	4.12
	313	-	-	0.06	1.90	0.94	4.26	4.12
	318	-	-	0.08	1.90	0.92	4.27	4.08
P2	283	-	-	0.04	1.50	0.96	4.18	4.08
	288	-	-	0.06	1.50	0.94	4.19	4.04
	293	-	-	0.04	1.50	0.96	4.18	4.08
	298	-	-	0.06	1.50	0.94	4.17	4.02
	303	-	-	0.06	1.50	0.94	4.16	4.00
P3	293	-	-	0.06	1.50	0.94	4.23	4.08
Water	293	-	-	-	-	1.00	4.29	4.29

^aIndividual amplitudes and time constants can be reproduced within $\pm 5\%$ of the reported values.

Using the present picosecond set-up we could not measure solvation response via the dynamic Stokes shift experiments because the major contribution in solvent relaxation in these aqueous polymer solutions arises from the ultrafast reorganization of water molecules. However, we could carry out time-resolved rotational anisotropy measurements for both C153 and C343 in these media because rotational relaxation of these solutes is much slower than water reorientation dynamics. We have followed the temperature dependence of solute rotational

dynamics in order to investigate whether any slowing down in dynamics is induced as solution temperature is approaching the T_{cp} and whether such slowing down is transduced on rotational relaxation of the dissolved solute. In addition, impact of hydrophilic/ hydrophobic component ratio in copolymer on rotational dynamics of C153 and C343 in these solutions has been explored.

7.3.5.2 Time-Resolved Fluorescence Anisotropy Decay Measurements

Figure 7.7 represents rotational anisotropy decays ($r(t)$) of C153 and C343 in aqueous solution of P1 at 293 K. Respective bi-exponential fit parameters are provided in the inset. Note that the $r(t)$ decay for C343 is much faster (~6 times) than that for C153 although both the decays are characterized by a similar fast decay time constant in the sub-nanosecond regime. This fast sub-nanosecond decay component is dominant for C343 and significant for C153. Interestingly, this strong non-exponentiality in the decay, which is completely absent in their rotational relaxation in neat water, persists at all other temperatures studied here (see Table 7.2). This clearly indicates that both the solutes are, although preferentially located in different regions of these aqueous polymer solutions because of their hydrophobic and hydrophilic nature, probing environments qualitatively different from bulk-like water. Representative temperature dependent rotational anisotropy decays of C153 in aqueous copolymer solutions of P1 and P2 are shown in Figure 7.8. A comparison of rotational anisotropy decay of two aqueous copolymers (P1, P3) solutions at 293 K is shown in Figure A.e.6. Table 7.2 summarizes the bi-exponential fit parameters required for all the collected temperature dependent anisotropy decays involving these two solutes.

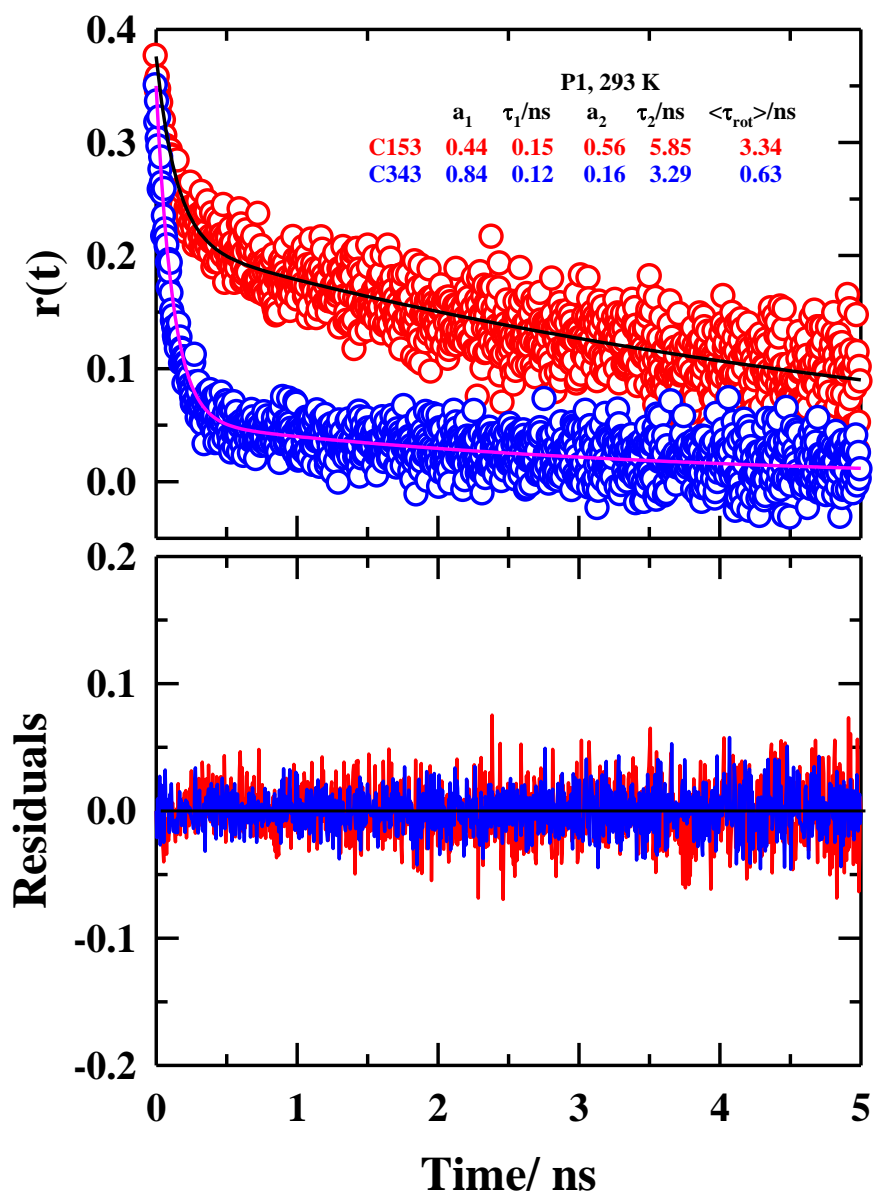


Figure 7.7: Representative rotational anisotropy, $r(t)$, decays of C153 and C343 in aqueous P1 solution (upper panel) at 293 K and the corresponding residuals (lower panel). Experimental data are shown by circles. Solid lines going through data represent bi-exponential fits. Fit parameters are shown in the inset. All representations are colour-coded.

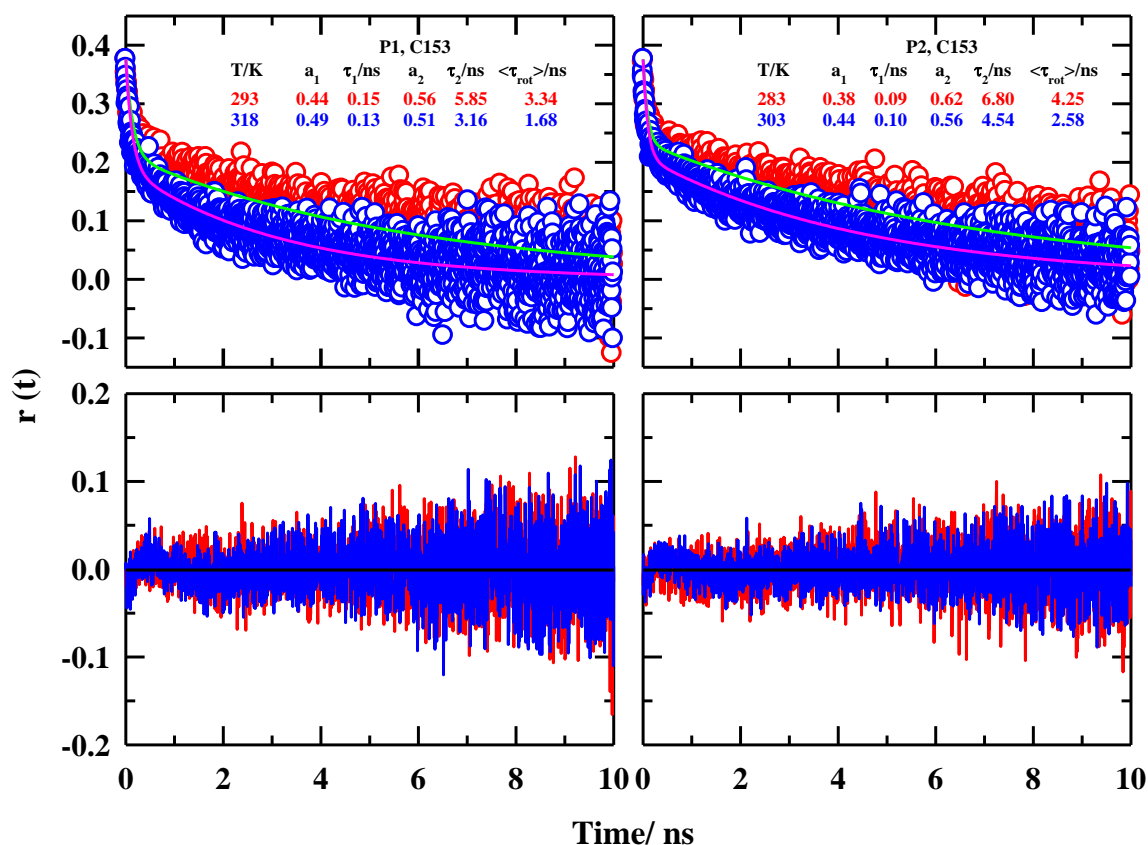


Figure 7.8: Representative temperature dependent rotational anisotropy, $r(t)$, decays of C153 in aqueous P1 and P2 solutions (upper panels) and the corresponding residuals (lower panels). Experimental data are shown by circles; solid lines going through data represent bi-exponential fits. Fit parameters are shown in the inset. All representations are colour-coded.

A general feature that can be immediately detected from the data in Table 7.2 is that anisotropy decays for these solutes depict a strongly biphasic non-Markovian frictional response with relaxation time constants separated by at least an order of magnitude. This is striking if one considers that these solutions are characterized with bulk-water like viscosity. The local environments then impart this non-exponential character in the relaxation which may either originate from a modification of the motional feature of these solutes due to solute-environment interactions or from a strong non-exponential frictional kernel generated by the reorientational relaxation of the local particles. In either of the cases, the general character of the microscopic friction that these solutes track is qualitatively different in these polymer solutions than that in neat water. This is a manifest of solute-environment interaction at the dynamic level which separates the view of solution structure provided by the solute-centred dynamics from that

reflected by the bulk solution properties. The slow time constant of a few nanosecond with dominating or significant amplitude indicates hindered (more restricted than governed by bulk solution viscosity) rotational relaxation of the dissolved solute.^{43,65} This hindered rotation suggests that the hydrophobic polar probe C153 resides in the vicinity of the interface of the self-assembly formed by these amphiphilic polymers in aqueous medium. We would like to mention here that bimodal anisotropy decay with well separated time constants are a general observation for various solute probes in aqueous micellar solutions.^{66,67} The lengthening of $\langle \tau_{\text{rot}} \rangle$ in more hydrophobic unit containing copolymer supports the view that C153 resides in a close proximity to hydrophobic domain of the interface. This becomes even more obvious when we note that the average rotation times for both these solutes in neat water is comparable but differ by a factor of ~ 5 in polymer solutions.

We next investigate whether cloud point has an impact on solute rotation similar to the dynamical slowing down caused by critical temperature by approaching T_{cp} from below for these polymer solutions and simultaneously measuring the dynamic fluorescence anisotropies. Average rotation times in Table 7.2 already suggest rotation becoming faster with the rise in solution temperature. This observation itself hints that the solute rotation is not sensing any ‘critical temperature like medium slow-down’ even if such a slow-down is induced by the T_{cp} in these solutions. In fact, the solution viscosity, like in usual scenarios, controls the solute rotation in these solutions as well, although the temperature-induced modification in rotation times may not be directly proportional to the concomitant decrease in viscosity.

Table 7.2: Temperature dependent $r(t)$ decay fit parameters of C153 and C343 in aqueous solutions (2 mg/mL) of three copolymers P1-P3.^a

A: C153							
Polymer	T/ K	a_1^b	τ_1/ ns^c	a_2	τ_2/ ns	$\langle \tau_{rot} \rangle / ns$	η / cP
P1	293	0.44	0.15	0.56	5.85	3.34	1.056
	298	0.44	0.18	0.56	5.32	3.04	0.941
	303	0.47	0.16	0.53	4.84	2.64	0.847
	308	0.45	0.18	0.55	4.21	2.40	0.768
	313	0.47	0.16	0.53	3.62	1.99	0.702
	318	0.49	0.13	0.51	3.16	1.68	0.647
P2	283	0.38	0.09	0.62	6.80	4.25	1.348
	288	0.38	0.10	0.62	6.07	3.80	1.164
	293	0.40	0.11	0.60	5.57	3.38	1.046
	298	0.41	0.11	0.59	5.12	3.06	0.933
	303	0.44	0.10	0.56	4.54	2.58	0.839
P3	293	0.39	0.07	0.61	6.46	3.97	1.051
Water	293	-	-	1.00	0.10	0.10	1.002
B: C343							
P1	293	0.84	0.12	0.16	3.29	0.63	1.056
	298	0.84	0.12	0.16	2.68	0.53	0.941
	303	0.86	0.10	0.14	2.69	0.46	0.847
	308	0.84	0.10	0.16	1.61	0.34	0.768
	313	0.87	0.09	0.13	1.34	0.25	0.702
	318	0.90	0.07	0.10	1.08	0.18	0.647
P2	283	0.77	0.17	0.23	4.99	1.28	1.348
	288	0.79	0.14	0.21	3.87	0.92	1.164
	293	0.78	0.13	0.22	3.46	0.87	1.046
	298	0.80	0.11	0.20	3.01	0.69	0.933
	303	0.82	0.09	0.18	2.23	0.48	0.839
P3	293	0.79	0.12	0.21	4.03	0.94	1.051
Water	293	-	-	1.00	0.13	0.13	1.002

^aFit parameters were obtained after fixing the r_0 value at 0.376 for C153 and 0.35 for C343.

^{b,c}Individual amplitudes and time constants can be reproduced within $\pm 5\%$ of the reported values.

Investigations with near critical fluids have revealed that the mutual diffusion coefficient, D , changes by following an asymptotic critical power law: $D = D_0 \left(\frac{T - T_C}{T_C} \right)^\gamma$ where T is the experimental temperature, T_C the critical temperature, and γ the universal critical exponent

having values of 0.67.² We have investigated the temperature dependence of average rotational relaxation rate, $\langle \tau_{\text{rot}} \rangle^{-1}$, for C153 and C343 in two aqueous copolymer (P1 and P2) solutions by showing them as a function of reduced temperature, $(|T - T_{\text{cp}}|/T_{\text{cp}})$. Figure 7.9 displays such a dependence in a double-logarithmic fashion. Interestingly, a linear dependence of $\langle \tau_{\text{rot}} \rangle^{-1}$ with reduced temperature is observed with negative exponent values, $\gamma \approx -0.4$ for C153 and $\gamma \approx -0.7$ for C343. This difference in γ values is a reflection of solute locations for these hydrophobic and hydrophilic solutes in these media, and hence dominated by the temperature dependence of the local solute-environment interactions. Similar values of γ for a solute during both solution temperature approaching the $T_{\text{cp}} - 5$ K (that is, $T \rightarrow T_{\text{cp}} - 5$ K) and moving away from it ($T \leftarrow T_{\text{cp}} - 5$ K) provide further support to this view of local solute-solvent interactions dominating the friction. In earlier investigation on binary solvent mixture, 2-butoxy ethanol (BE)+water, possessing a closed loop miscibility gap with LCST $T_{\text{c}}(\text{K}) = 322.5$ and concentration x_{c}^{BE} (mole fraction) = 0.06, a nonlinear dependence of $\langle \tau_{\text{rot}} \rangle^{-1}$ with $(|T - T_{\text{c}}|/T_{\text{c}})$ for C153 was observed when examined in a similar fashion.⁶⁸ All these probably indicate that cloud point impact is strictly confined within a narrow range around the cloud point temperature, and the later and its impact on solution dynamics may be qualitatively different from the conventional critical temperature and its effects.

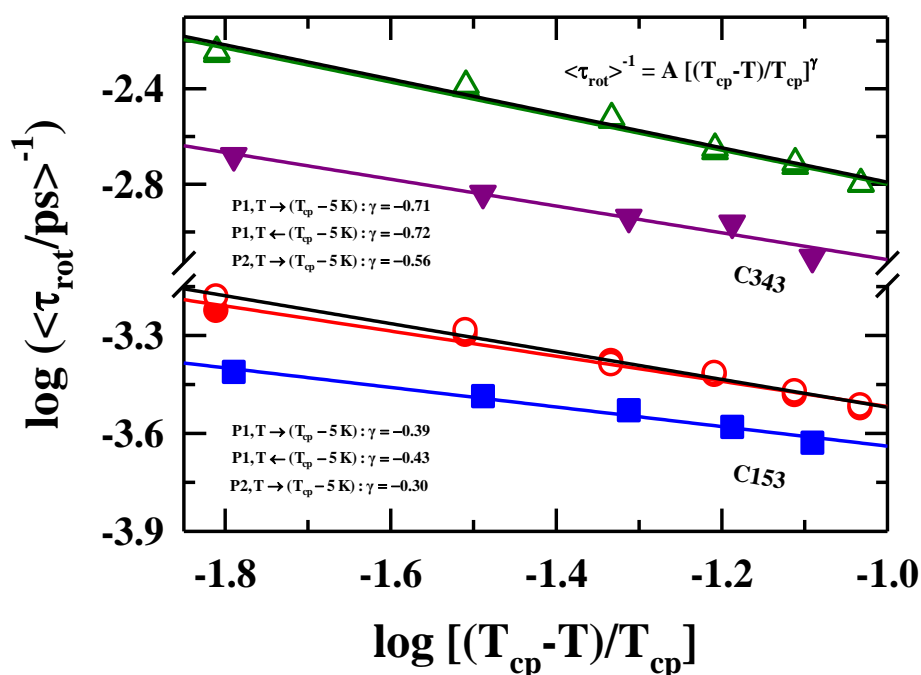


Figure 7.9: Double logarithmic plot of the rotational relaxation rate $\langle \tau_{\text{rot}} \rangle^{-1}$ of C153 and C343 in two aqueous copolymer solutions (P1 and P2) versus reduced temperature $\left((T - T_{\text{cp}}) / T_{\text{cp}} \right)$. Solid lines going through the data depict the linear fits with negative exponents. All representations are colour-coded.

Next the coupling between the viscosity and average rotation times for these solutes in these solutions has been explored. Note that deviation from the hydrodynamic viscosity dependence is expected here because the measured solute rotation times in these solutions have already been found to be controlled by the local interactions and not governed by the bulk solution viscosity. A plot of $\langle \tau_{\text{rot}} \rangle$ as a function of η/T and simultaneous comparisons with the hydrodynamic predictions will therefore provide a concise description of this disagreement between the measurements and hydrodynamic predictions. Representative results are provided in Figure 7.10 where measured rotation times ($\langle \tau_{\text{rot}} \rangle$) for C153 and C343 in aqueous P1 are shown as a function of temperature-reduced bulk solution viscosity, η/T . Similar comparison for these solutes in aqueous solution of P2 is shown in Figure A.e.7 (see Appendix). For both the solutes the measured rotation times not only follow a viscosity coupling much different from that predicted by the hydrodynamics but reflect also a dependence on the chemical nature

of the rotating solute: hydrophobic or hydrophilic. In addition, measured rotation times are much longer than the corresponding stick hydrodynamic predictions, the difference being larger for the hydrophobic solute (C153⁵⁰) than the hydrophilic one (C343⁶⁹). Such a solute dependence confirms again the overwhelming domination of the solute-medium interaction at the local level, leaving a secondary or no role for the T_{cp} to dictate the solution frictional response.

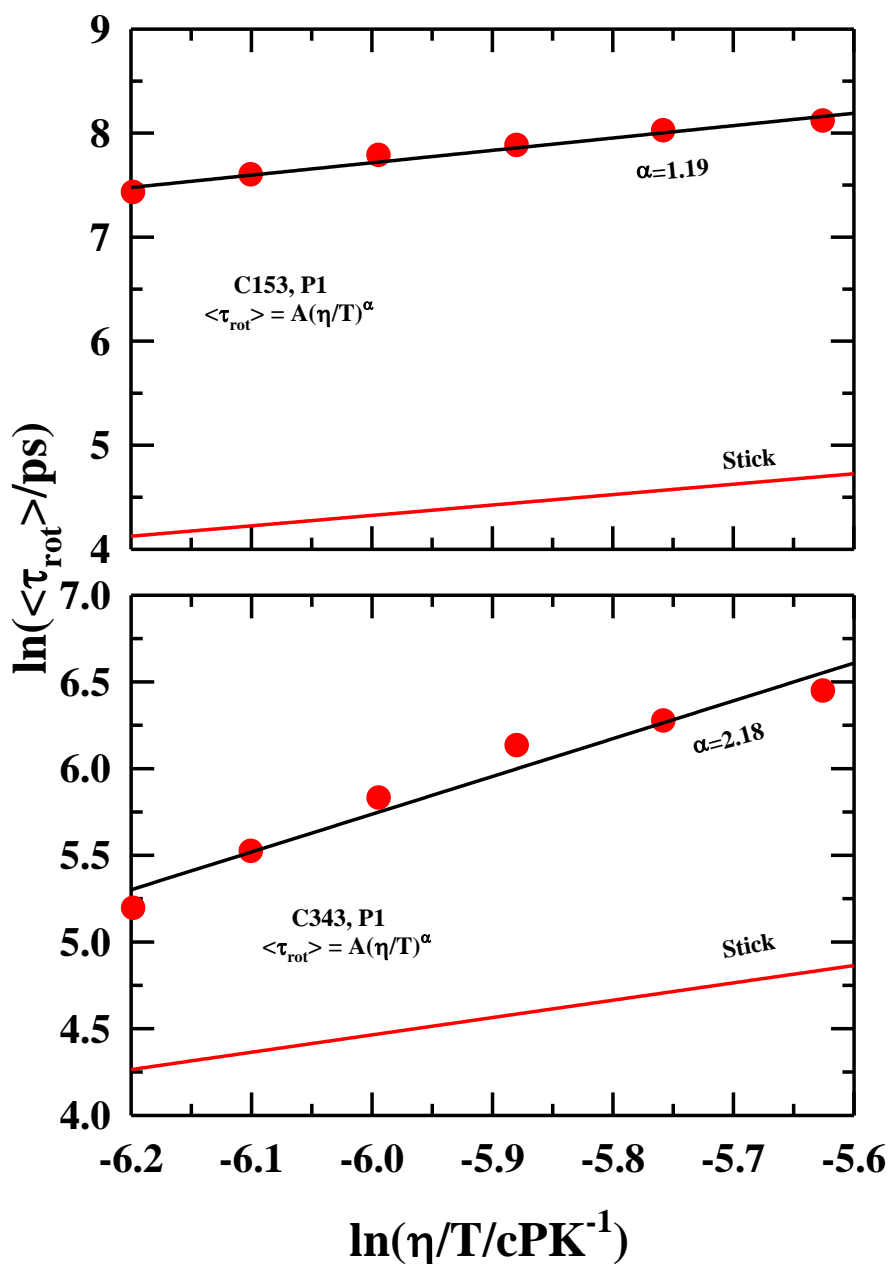


Figure 7.10: A comparison of solution viscosity coupling between the measured rotation times, and that from hydrodynamic prediction for both C153 and C343 in aqueous solution of one of the polymers considered in the present study. While filled circles represent experimental data, lines going through them depict a fit to the following expression: $\langle \tau_{\text{rot}} \rangle \propto (\eta/T)^\alpha$. Hydrodynamic predictions employing slip boundary condition are not shown because the measured rotation times are much longer than even predictions using stick boundary condition.

7.4 Conclusion

In summary, the rationally designed and characterised thermoresponsive random copolymers with tuneable T_{cp} s did not show any clear signature of criticality-induced interaction and dynamics when explored employing fluorescent solutes in their aqueous solutions via steady state and time resolved measurements. Temperature dependent measurements indicated overwhelming domination of the interactions at the local level in guiding the individual locations of the solutes in these polymer solutions, and the solution frictional resistance associated with their orientational relaxations. Solution heterogeneity was found to be dictated by a balance between the hydrophobic/hydrophilic segments in these polymer molecules, and detection of such heterogeneity depended on solute location. This allowed the chemical nature of solutes (hydrophilic or hydrophobic) becoming a factor while responding to the inherent complexities of these aqueous solutions. Interestingly, both hydrophobic and hydrophilic solutes showed biphasic anisotropic decays (in contrast to single-exponential decays in solutions of neat water) with much slower average rotation times than those determined in neat water. This resulted a significant deviation from the hydrodynamic behaviour yet the subsequent temperature dependent solute dynamics remained slave to the local interactions and the resultant friction. Further studies are warranted to better understand the roles of cloud points in dictating interaction and dynamics in aqueous solutions of rationally designed polymers with application potentials.

References

1. E. D. Siebert and C. M. Knobler, *Phys. Rev. Lett.* **52**, 1133 (1984).
2. C. Ikier, H. Klein and D. Woermann, *J. Chem. Phys.* **96**, 859 (1992).
3. J. S. Huang, W. I. Goldberg and M. R. Moldover, *Phys. Rev. Lett.* **34**, 639 (1975).
4. A. J. Schwartz, S. Krishnamurthy and W. I. Goldberg, *Phys. Rev. A* **21**, 1331 (1980).
5. J. S. Huang, S. Vernon and N. C. Wong, *Phys. Rev. Lett.* **33**, 140 (1974).
6. S. Krishnamurthy and R. Bansil, *Phys. Rev. Lett.* **50**, 2010 (1983).
7. P. C. Hohenberg and B. I. Halperin, *Rev. Mod. Phys.* **49**, 435 (1977).
8. F. Liu and M. W. Urban, *Prog. Polym. Sci.* **35**, 3 (2010).
9. G. Pasparakis and M. Vamvakaki, *Polym. Chem.* **2**, 1234 (2011).
10. G. Kocak, C. Tuncer and V. Bütün, *Polym. Chem.* **8**, 144 (2017).
11. K. Bauri, S. G. Roy, S. Pant and P. De, *Langmuir* **29**, 2764 (2013).
12. A. Bordat, T. Boissenot, J. Nicolas and N. Tsapis, *Adv. Drug Deliv. Rev.* **138**, 167 (2019).
13. D. Roy, W. L. A. Brooks and B. S. Sumerlin, *Chem. Soc. Rev.* **42**, 7214 (2013).
14. Q. Yan, D. Han and Y. Zhao, *Polym. Chem.* **4**, 5026 (2013).
15. D. Roy and B. S. Sumerlin, *Macromol. Rapid. Commun.* **35**, 174 (2014).
16. X. Zhang, L. Han, M. Liu, K. Wang, L. Tao, Q. Wan and Y. Wei, *Mater. Chem. Front.* **1**, 807 (2017).
17. B. Saha, U. Haldar and P. De, *Macromol. Rapid. Commun.* **37**, 1015 (2016).
18. J. Ge, E. Neofytou, T. J. Cahill, R. E. Beygui and R. N. Zare, *ACS Nano* **6**, 227 (2012).
19. T. Manouras and M. Vamvakaki, *Polym. Chem.* **8**, 74 (2017).
20. Q. Zhang, C. Weber, U. S. Schubert and R. Hoogenboom, *Mater. Horizons* **4**, 109 (2017).
21. M. A. Ward and T. K. Georgiou, *Polymers* **3**, 1215 (2011).
22. I. Chakraborty, K. Mukherjee, P. De and R. Bhattacharyya, *J. Phys. Chem. B* **122**, 6094 (2018).
23. B. Saha, K. Bauri, A. Bag, P. K. Ghorai and P. De, *Polym. Chem.* **7**, 6895 (2016).
24. I. C. Barker, J. M. G. Cowie, T. N. Huckerby, D. A. Shaw, I. Soutar and L. Swanson, *Macromolecules* **36**, 7765 (2003).
25. M. M. Ali and H. D. H. Stöver, *Macromolecules* **37**, 5219 (2004).
26. N. A. Cortez-Lemus and A. Licea-Claverie, *Prog. Polym. Sci.* **53**, 1 (2016).
27. X. Han, X. Zhang, H. Zhu, Q. Yin, H. Liu and Y. Hu, *Langmuir* **29**, 1024 (2013).

28. Z. Hu, T. Cai and C. Chi, *Soft Matter* **6**, 2115 (2010).
29. J.-F. Lutz, *J. Polym. Sci. Part. A: Polym. Chem.* **46**, 3459 (2008).
30. M. Luzon, C. Boyer, C. Peinado, T. Corrales, M. Whittaker, L. Tao and T. P. Davis, *J. Polym. Sci. Part. A: Polym. Chem.* **48**, 2783 (2010).
31. K. Bauri, S. Pant, S. G. Roy and P. De, *Polym. Chem.* **4**, 4052 (2013).
32. J.-F. Lutz and A. Hoth, *Macromolecules* **39**, 893 (2006).
33. H. Otsuka, Y. Nagasaki and K. Kataoka, *Adv. Drug Deliv. Rev.* **55**, 403 (2003).
34. T. Terashima, T. Sugita, K. Fukae and M. Sawamoto, *Macromolecules* **47**, 589 (2014).
35. G. Hattori, Y. Hirai, M. Sawamoto and T. Terashima, *Polym. Chem.* **8**, 7248 (2017).
36. Y. Hirai, T. Terashima, M. Takenaka and M. Sawamoto, *Macromolecules* **49**, 5084 (2016).
37. Y. Kimura, T. Terashima and M. Sawamoto, *Macromol. Chem. Phys.* **218**, 1700230 (2017).
38. S. Imai, Y. Hirai, C. Nagao, M. Sawamoto and T. Terashima, *Macromolecules* **51**, 398 (2018).
39. K. Matsumoto, T. Terashima, T. Sugita, M. Takenaka and M. Sawamoto, *Macromolecules* **49**, 7917 (2016).
40. K. Kumbhakar, B. Saha, P. De and R. Biswas, *J. Phys. Chem. B* **123**, 11042 (2019).
41. E. Tarif, K. Mukherjee, A. Barman and R. Biswas, *J. Chem. Sci.* **131**, 43 (2019).
42. K. Kumbhakar, E. Tarif, K. Mukherjee and R. Biswas, *J. Mol. Liq.* **290**, 111225 (2019).
43. K. Mukherjee, A. Barman and R. Biswas, *J. Mol. Liq.* **222**, 495 (2016).
44. E. Tarif, B. Saha, K. Mukherjee, P. De and R. Biswas, *J. Phys. Chem. B* **123**, 5892 (2019).
45. R. Biswas, J. E. Lewis and M. Maroncelli, *Chem. Phys. Lett.* **310**, 485 (1999).
46. J. E. Lewis, R. Biswas, A. G. Robinson and M. Maroncelli, *J. Phys. Chem. B* **105**, 3306 (2001).
47. T. Pradhan and R. Biswas, *J. Phys. Chem. A* **111**, 11524 (2007).
48. T. Pradhan, P. Ghoshal and R. Biswas, *J. Phys. Chem. A* **112**, 915 (2008).
49. T. Pradhan, P. Ghoshal and R. Biswas, *J. Chem. Sci.* **120**, 275 (2008).
50. M. L. Horng, J. A. Gardecki and M. Maroncelli, *J. Phys. Chem. A* **101**, 1030 (1997).
51. S. Koley, H. Kaur and S. Ghosh, *Phys. Chem. Chem. Phys.* **16**, 22352 (2014).
52. B. Maiti, S. Maiti and P. De, *RSC advances* **6**, 19322 (2016).
53. M. Shibata, M. Matsumoto, Y. Hirai, M. Takenaka, M. Sawamoto and T. Terashima, *Macromolecules* **51**, 3738 (2018).
54. S. Pal, S. Ghosh Roy and P. De, *Polym. Chem.* **5**, 1275 (2014).
55. J.-F. Lutz, K. Weichenhan, Ö. Akdemir and A. Hoth, *Macromolecules* **40**, 2503 (2007).
56. L. Hou and P. Wu, *Soft Matter* **10**, 3578 (2014).

57. M. Maroncelli and G. R. Fleming, *J. Chem. Phys.* **86**, 6221 (1987).
58. P. Sen, D. Roy, S. K. Mondal, K. Sahu, S. Ghosh and K. Bhattacharyya, *J. Phys. Chem. A* **109**, 9716 (2005).
59. H. Shirota, Y. Tamoto and H. Segawa, *J. Phys. Chem. A* **108**, 3244 (2004).
60. Z. Hu and C. J. Margulis, *Proc. Natl. Acad. Sci. U. S. A.* **103**, 831 (2006).
61. A. Samanta, *J. Phys. Chem. B* **110**, 13704 (2006).
62. S. Indra, B. Guchhait and R. Biswas, *J. Chem. Phys.* **144**, 124506 (2016).
63. S. Indra and R. Biswas, *J. Phys. Chem. B* **120**, 11214 (2016).
64. A. Das and R. Biswas, *J. Phys. Chem. B* **119**, 10102 (2015).
65. B. Guchhait, R. Biswas and P. K. Ghorai, *J. Phys. Chem. B* **117**, 3345 (2013).
66. M. Kumbhakar, T. Goel, T. Mukherjee and H. Pal, *J. Phys. Chem. B* **109**, 18528 (2005).
67. M. Kumbhakar, T. Goel, T. Mukherjee and H. Pal, *J. Phys. Chem. B* **108**, 19246 (2004).
68. S. Indra and R. Biswas, *J. Chem. Phys.* **142**, 204501 (2015).
69. G. B. Dutt and T. K. Ghanty, *J. Phys. Chem. B* **107**, 3257 (2003).

Chapter 8

Interactions and Dynamics in Aqueous Solutions of pH-Responsive Polymers: A Combined Fluorescence and Dielectric Relaxation Studies

8.1 Introduction

Biodegradable synthetic polymers have drawn special attention everywhere because of several exquisite features such as biocompatibility, biodegradability and tunable physico-chemical characteristics.¹ These polymers are often preferred in biomedical and environmental remediation applications over the natural bio-polymers such as proteins, polysaccharides, nucleic acids. This is because (i) despite being biocompatible, the natural bio-polymers often induce immune-response, and (ii) it is difficult to chemically modify them to suit requirements compared to the corresponding synthetic polymers.¹ Spontaneous stimuli-responsive behaviour of proteins and nucleic acids triggers scientists to design smart synthetic biodegradable and biocompatible polymers.² Stimuli responsive polymers, also termed as smart polymers, exhibit a sharp reversible change in properties with various environmental conditions such as pH,^{3,4} temperature,^{5,6} ionic strength,^{7,8} chemical agents,⁹ light,^{10,11} redox potential,^{12,13} electric¹⁴ and magnetic field¹⁵ and others.^{16,17} Smart polymer-based drug delivery agents possessing stimuli-controlled drug release capability are the most desirable candidates because of their accessibility through easy modification driven by on-demand physical and chemical features.^{18,19} These polymers are cheaper and safer non-viral therapeutic gene carrier.^{18,20} Tissue engineering,²¹ chemo/bio-sensors,^{16,22,23} and environmental remediation^{24,25} are other application-based areas that are driving wide applications of smart polymers.

Among various smart polymers, pH-responsive polymers have applications in drug delivery, gene delivery, sensor development, surface creation and modification, membrane modification, and in chromatography-based techniques.²⁶⁻²⁸ These polymers possess acidic or basic functional groups which undergo ionization depending on solution pH. Depending upon solution pH, these polymers exhibit reversible change of solubility, conformation, volume etc.²⁸ Solution pH adjustment alters different interactions: ionic, hydrogen bonding, hydrophobic interactions leading to reversible self-organization or microphase separation.²⁸ At low pH, homo or copolymers of poly(N,N,-diethylaminoethyl methacrylate) (PDEA)

possessing amine group as side chain moiety have been reported to be water soluble due to protonation of amine groups but become water insoluble at neutral or basic pH.²⁸ In the last few decades, significant numbers of different pH responsive polymers have been synthesized and characterized by several groups where synthesis of targeted application-based pH-responsive polymers, followed by study of solution phase properties like morphology, aggregation behaviour have dominated the activity.^{4,7,28-35}

The application-oriented usage of these smart polymers in biotechnology and nanotechnology demands a thorough understanding of microscopic interactions, dynamics, and the underlying frictional profile that governs the relaxation in aqueous solutions. This is because the efficacy of stimuli-responsive polymers cannot be parameterized only by pH-responsiveness and engineering of morphology by manipulating medium pH but also by the extent of tunable polymer-medium interactions and the inherent dynamics. Surprisingly, very few investigations have so far been carried out to reveal the interaction-dynamics relationship in stimuli-responsive polymers.^{17,36} These unexplored aspects have motivated us to perform systematic studies of interaction and relaxation dynamics of aqueous solutions of a closely-related series of pH-responsive copolymers. We have chosen a series of pH-responsive random copolymers containing amino acid side chain. Steady state and time-resolved fluorescence (TRF) spectroscopic study of these aqueous polymer solutions employing external fluorophores and dielectric relaxation spectroscopic (DRS) investigations have been performed. We ask the following questions: Is there any significant change in solution phase interaction and relaxation dynamics as the solution pH approaches close to their respective phase transition pH? What kind of interactions is involved between polymer and water, and how medium pH affects the polymer-water interaction? Relaxation dynamics in aqueous polymer solutions and the impact of pH on it have also been explored in the present study.

We have taken a series of pH-responsive random copolymers $P(\text{NH}_3^+\text{-L-Leu-HEMA-co-MMA})$ comprising of 2-((leucinyloxy)ethyl methacrylate (L-Leu-HEMA) and methyl methacrylate (MMA). These series of pH-responsive copolymers have been designed, synthesized and characterized by a research group in IISER Kolkata, India.³⁷ Here we have used the amino acid segment as the pH-responsive unit. Relative ratio between L-Leu-HEMA and MMA units in the series of present copolymers (also termed as ‘polymer’ in the rest of the chapter) provide us the opportunity to play with polymers having a range of phase transition pH from 5 to 7. The extensively used gold standard fluorescent probe coumarin 153 (C153), which is a polar hydrophobic solute, is employed as local reporter in the current fluorescence

measurements. It is well known that fluorescence characteristics of C153 are sensitive to solvent³⁸ and is widely utilized to explore interactions, dynamics in numerous systems including various solvents,³⁸ multi-component mixtures,³⁹⁻⁴³ micelles,⁴⁴⁻⁴⁷ polymers^{17,48} etc. Steady state and time-resolved fluorescence measurements track the modifications due to change in solution pH. DRS measurements have been performed to explore the intrinsic relaxation dynamics in these aqueous polymer solutions.

8.2 Experimental Details

8.2.1 Materials and Sample Preparation for Measurements

Coumarin 153 (C153) was purchased from Sigma-Aldrich and used as received. Experimental stock solutions were prepared by mixing required amount of copolymers in Milli-Q water. A series of four copolymers (P(NH₃⁺-L-Leu-HEMA-*co*-MMA)) (DPL, DP20, DP40 and DP60) with different chain length of L-Leu-HEMA (m) and MMA (n) (DPL (m=75, n=0), DP20 (m=52, n=30), DP40 (m=31, n=49)) and DP60 (m=17, n=59)) were used in the current work.³⁷ Aqueous copolymer mixture was then kept at room temperature till complete dissolution of copolymer. The concentrations of stock copolymer solutions were fixed at 1 mg/mL. For each of the copolymers, initial pH of the stock aqueous solution of copolymers was recorded and afterward the pH of the freshly prepared stock solution was incrementally increased using 0.1 M NaOH solutions. Due to addition 0.1 M NaOH, concentration of aqueous copolymer solution (1mg/ml) at different pH, prepared from the same stock solutions, may differ slightly. In this work we have not considered the impact of such minute copolymer concentration variation in the interpretation of experimental results. Optical measurements of these solutions were performed as follows: 2-3 μ L of freshly prepared solutions of coumarin 153 (C153) in hexane was taken in a quartz cuvette of 1 cm optical path length. The nonpolar solvent was then evaporated off by uniformly blowing hot air around the outer surface of the cuvette. Approximately 2.5-3 mL of sample solution was then poured into the cuvette containing C153 gains. Concentration of C153 in each of these samples was maintained at $\leq 10^{-5}$ M. Spectroscopic measurements were carried out in a humidity-controlled environment. The chemical structures of the copolymers and C153 are shown in Scheme 8.1. All measurements were carried out at 298 \pm 1 K.

8.2.2 pH- Measurements

pH measurements of the aqueous copolymer solutions were carried out by a Bench-top multiparameter electrochemical meter (SESHIN BIOTECH, Model: ECM-610). Data presented here were recorded at 298 ± 1 K. Accuracy associated with pH measurements is ± 0.3 .

8.2.3 Dynamic Light Scattering (DLS) Measurements

Dynamic light scattering (DLS) measurements were conducted by using a Malvern Nano Zetasizer (Malvern Instrument Ltd., Malvern, UK) equipped with a He–Ne laser beam operating at $\lambda = 633$ nm at a scattering angle of 173° . All aqueous copolymer solutions were filtered through a $0.45 \mu\text{m}$ syringe filter prior to measurements. pH dependent DLS measurements were carried out for each copolymer at a fixed concentration of 1 mg/mL in water.

8.2.4 Density and Viscosity Coefficient Measurements

Densities (ρ) and viscosity coefficients (η) of the solutions were measured by using an automated temperature-controlled density-cum-sound analyzer (Anton Paar, model DSA 5000) and automated micro viscometer (AMVn, Anton Paar), respectively.¹⁷

8.2.5 Refractive Index Measurements

An automated temperature-controlled refractometer (RUDOLPH, J357) was used to record refractive indices of the aqueous copolymer solutions.⁴⁹

8.2.6 Data Collection and Analysis for Steady State UV-Vis Absorption and Fluorescence Emission Studies

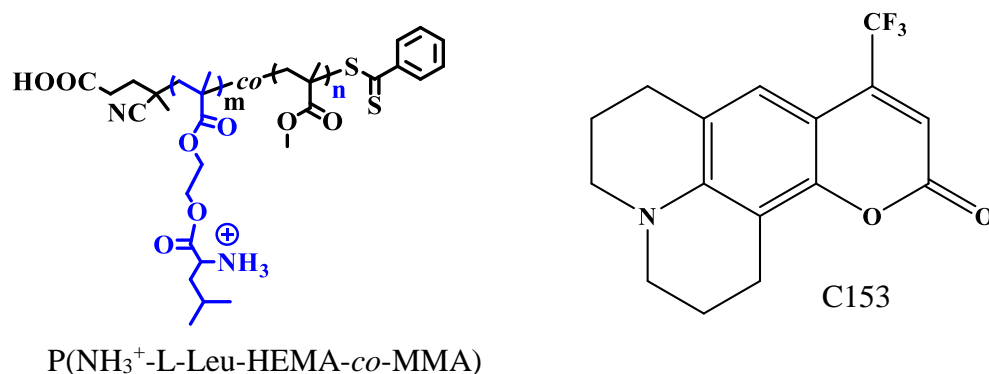
UV-Visible spectrophotometer (UV-2600, Shimadzu), and a fluorimeter (Fluorolog, Jobin-Yvon, Horiba) were used for recording steady state absorption and fluorescence emission spectra, respectively.⁴⁰ Temperature was controlled by using Peltier temperature controller (accuracy ± 1 K). Steady-state absorption spectra were taken at 2 nm slit width and fluorescence spectra were recorded using 2 nm slits at both the excitation and emission ends. The standard spectral analysis procedure was followed to determine spectral frequencies.^{50,51} The typical error bar for the determined spectral frequencies and spectral widths (full width at half maxima, FWHM) were $\pm 200 \text{ cm}^{-1}$. Detailed descriptions of these techniques are same as discussed in chapter 2.

8.2.7 Data Collection and Analysis for Time-Resolved Fluorescence Emission Studies

Time-resolved fluorescence measurements were performed with a time-correlated single-photon counting (TCSPC) system (LifeSpec-ps) from Edinburgh Instruments (Livingston, U.K.). Laser emission centred at 409 nm was used as excitation light for C153 dissolved in aqueous copolymer solution using an excitation slit of 2 nm. Magic angle (54.7°) intensity decay at 409 nm of a scattering medium (water) produced an instrument response function (IRF) ~ 85 ps. Temperature was controlled via a Julabo temperature controller (accuracy ± 1 K). Lifetime emission decays (magic angle intensity decays) were recorded at the wavelength corresponding to peak of steady state emission spectra ($\lambda_{\text{max}}^{\text{em}}$) of dissolved C153. Data collection and analysis for fluorescence anisotropy were the same as described in chapter 2 and references.^{38,41,52-55}

8.2.8 Data Collection and Analysis for Dielectric Relaxation Spectroscopy Studies

Dielectric measurements of samples in the frequency range of $0.2 \leq \nu / \text{GHz} \leq 50$ were performed with PNA-L network analyzer (N5235B) combined with an open-ended coaxial probe kit (N1501A). Details of the experimental technique and data analyses are the same as discussed in chapter 2 and references.^{45,49,56-59}



Scheme 8.1: Chemical structures of copolymers (P(NH₃⁺-L-Leu-HEMA-co-MMA)) and C153.

8.3 Results and Discussion

8.3.1 Determination of Phase Transition pH

Owing to the ability of protonation/ deprotonation of side chain primary amine group, these polymers are anticipated to show pH responsiveness in aqueous solution. Hence, the turbidity measurements of these polymers (DPL, DP20, DP40, DP60) have been performed by monitoring the percentage of transmittance (%*T*) with gradually increasing solution pH using UV-Vis spectroscopy at 500 nm.³⁵ The phase transition pH (pH^{tr}) is considered as the pH where %*T* is reduced to 50%.²⁷ Figure 8.1 represents the percentage of transmittance (%*T*) variation with pH in the four polymer (DPL-DP60) solutions. Phase transition pH values so obtained are provided in Table 8.1. As anticipated, the transition pH decreases with the decrease of L-Leu-HEMA and increase in MMA content in the polymer, and therefore reduces the number of ionizable units that can be protonated/deprotonated with environmental change due to alteration of solution pH. These copolymers form transparent colourless solutions in aqueous medium below their respective transition pH and turn opaque (milky white) as pH of the solutions reach their respective transition pH.

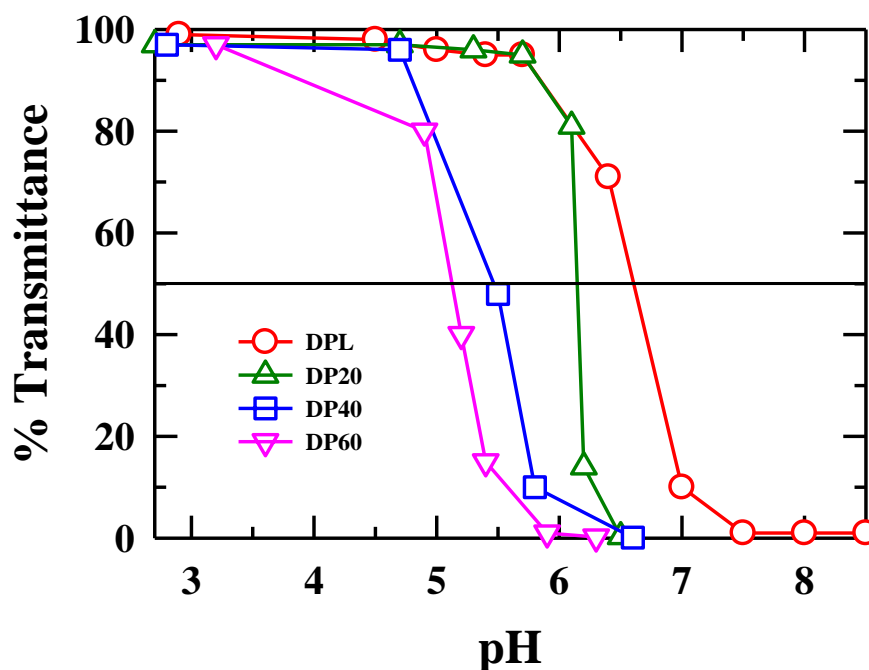


Figure 8.1: pH dependent transmittance (%*T*) measurements in aqueous polymer solutions (1 mg/mL) at ~298 K. All presentations are colour-coded.

Table 8.1: Phase transition pH and pH dependent variation of hydrodynamic diameter (D_h) of the polymers in aqueous solutions (1 mg/mL) at T~298 K.

Polymers	Phase Transition pH	Hydrodynamic diameters (D_h)/ nm	
		pH = 4	pH = 7
DPL	6.6	5	190
DP20	6.1	4	160
DP40	5.5	8	140
DP60	5.1	2	340

Dynamic light scattering is a well-known experimental technique for probing the hydrodynamic size of various macroscopic and mesoscopic species. Therefore, the phase transition pH (pH^{tr}) driven size change of polymer species in the aqueous DPL-DP60 solutions are monitored by pH-dependent DLS measurements below and above their respective transition pH. The DLS diagrams of the copolymer solutions (1 mg/mL) at variable pH are presented in Figure 8.2. The D_h values at pH = 4 (below the transition pH) were found to be ~6–8 nm and increased up to 170–1000 nm at pH = 7 (above the transition pH), summarized in Table 8.1. Below phase transition pH (pH^{tr}) the obtained D_h s (< 10 nm) are attributed to the single copolymer chain conformation.⁶⁰ On the other hand, the large aggregated structures (> 100 nm) formed beyond the transition pH which signifies the transformation of the co-polymer conformation from a single polymer chain to large globular microparticles. This is ascribed to the pH driven phase separation of these copolymers in aqueous medium. Similar DLS size distribution with phase transition phenomena was reported in thermo-responsive aqueous copolymer solutions.¹⁷ Lowering of solubility due to deprotonation of positively charged primary amino group of pH-responsive polymers above their transition pH (pH^{tr}) are considered to be the reason for generating large size particles.

Note that we have restricted the solution pH ~ 0.5 below the individual phase transition pH (that is, $\text{pH}^{\text{expt}} \sim \text{pH}^{\text{tr}} - 0.5$) during the steady state and time-resolved spectroscopic measurements in order to avoid complications arising from the formation of larger particles.

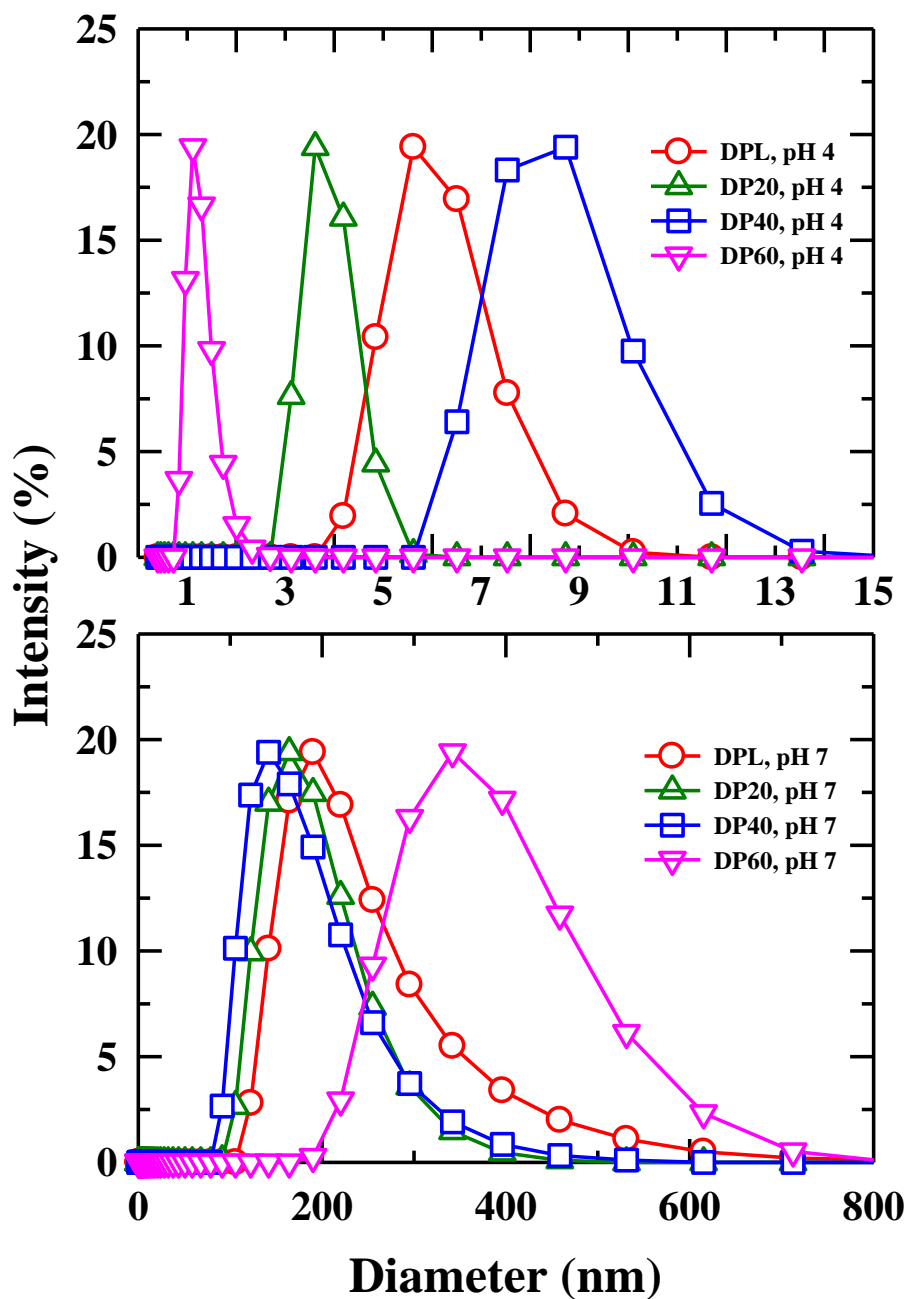


Figure 8.2: Hydrodynamic size distributions of aqueous polymer solutions (1 mg/ml) of pH ~4 (upper panel) and pH ~7 (lower panel) at ~298 K. Representations are colour-coded.

8.3.2 Density, Viscosity Coefficients and Refractive Indices: pH Dependence

The measured pH-dependent densities (ρ), viscosity coefficients (η) and refractive indices (n) of three aqueous copolymer solutions are summarized in Table 8.2. Note that densities, viscosity coefficients and refractive indices of these solutions are quite close to that of neat water. Also, the pH dependence is negligible.

Table 8.2: pH dependent densities (ρ), viscosity coefficients (η) and refractive indices (n) of aqueous solutions of polymers (1mg/ml) at 298 K.

pH	ρ /gcm ⁻³	η /cP	Refractive Index (n)
DPL			
3.5	0.9973	0.934	1.332
4.5	0.9974	0.930	1.333
6.3	0.9974	0.928	1.332
DP20			
3.5	0.9973	0.924	1.332
4.5	0.9973	0.922	1.332
6.2	0.9974	0.924	1.333
DP40			
3.5	0.9973	0.922	1.333
4.5	0.9973	0.918	1.333
5.8	0.9973	0.922	1.333
DP60			
3.5	0.9973	0.920	1.333
4.5	0.9973	0.925	1.333
5.5	0.9973	0.921	1.333
Water	0.997	0.89	1.332

8.3.3 Steady State UV-Vis Absorption and Fluorescence Emission Studies

Figure 8.3 and 8.4 respectively represent the pH dependent absorption and emission spectra of C153 in aqueous solution of pH-responsive polymers (DPL, DP20, DP40 and DP60). Note that for any given polymer solution, absorption and emission spectral characteristics of C153 at pH away from phase transition pH are quite similar to those at a pH nearest to the transition pH. The emission spectrum was recorded after exciting the sample at the wavelength of absorption maximum. In any of the present polymer solutions, the spectral features of C153 do not exhibit any abrupt changes with pH, suggesting a negligible role for transition pH in governing the pH-dependent solute-medium interactions. Interestingly, cloud point driven absorption and fluorescence emission with the same solute dissolved in a series of aqueous thermoresponsive copolymer solutions did not register any sudden change at temperature away from the phase transition temperature (cloud point, T_{cp}) to those at a temperature nearest to the T_{cp} .¹⁷

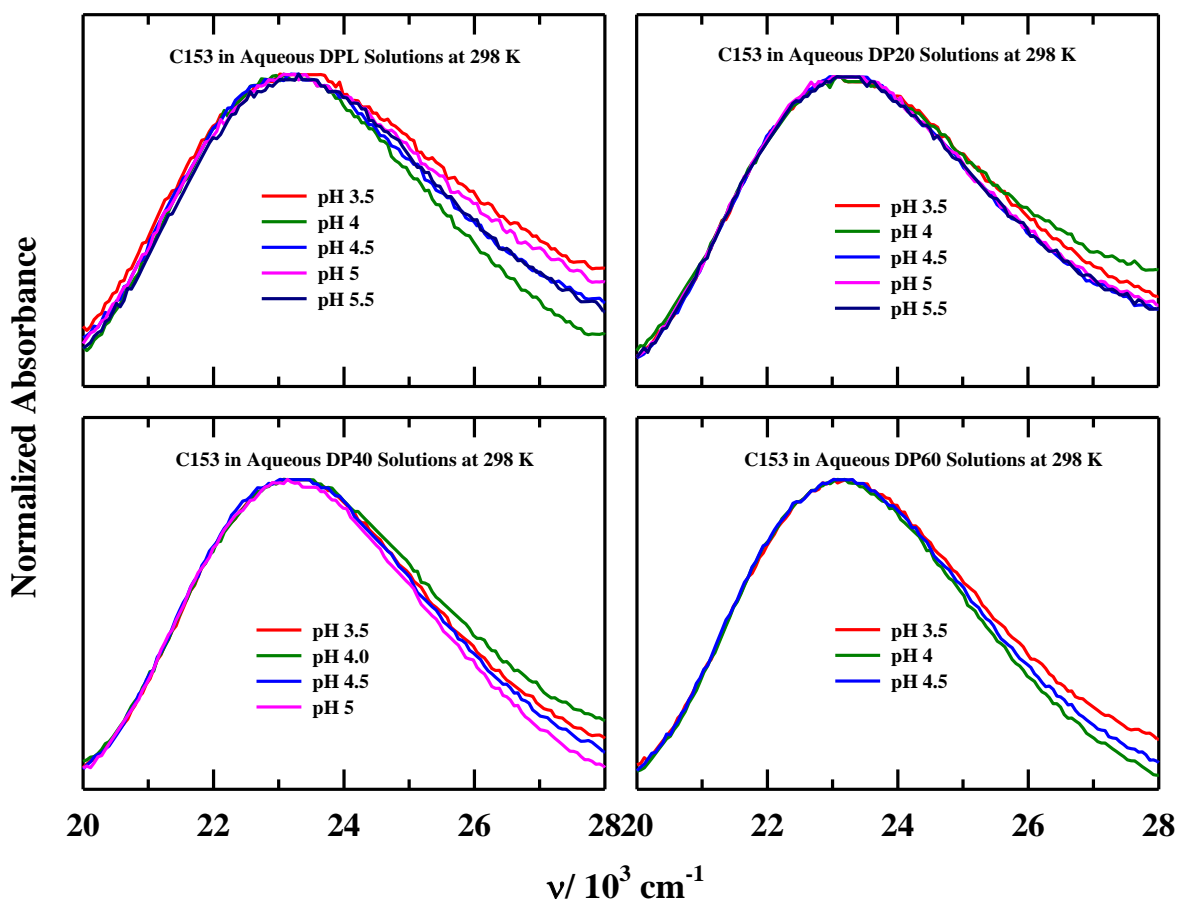


Figure 8.3: pH dependent steady state UV-Vis absorption spectra of C153 in aqueous polymer solutions (1mg/ml) at ~298 K. All presentations are colour-coded.

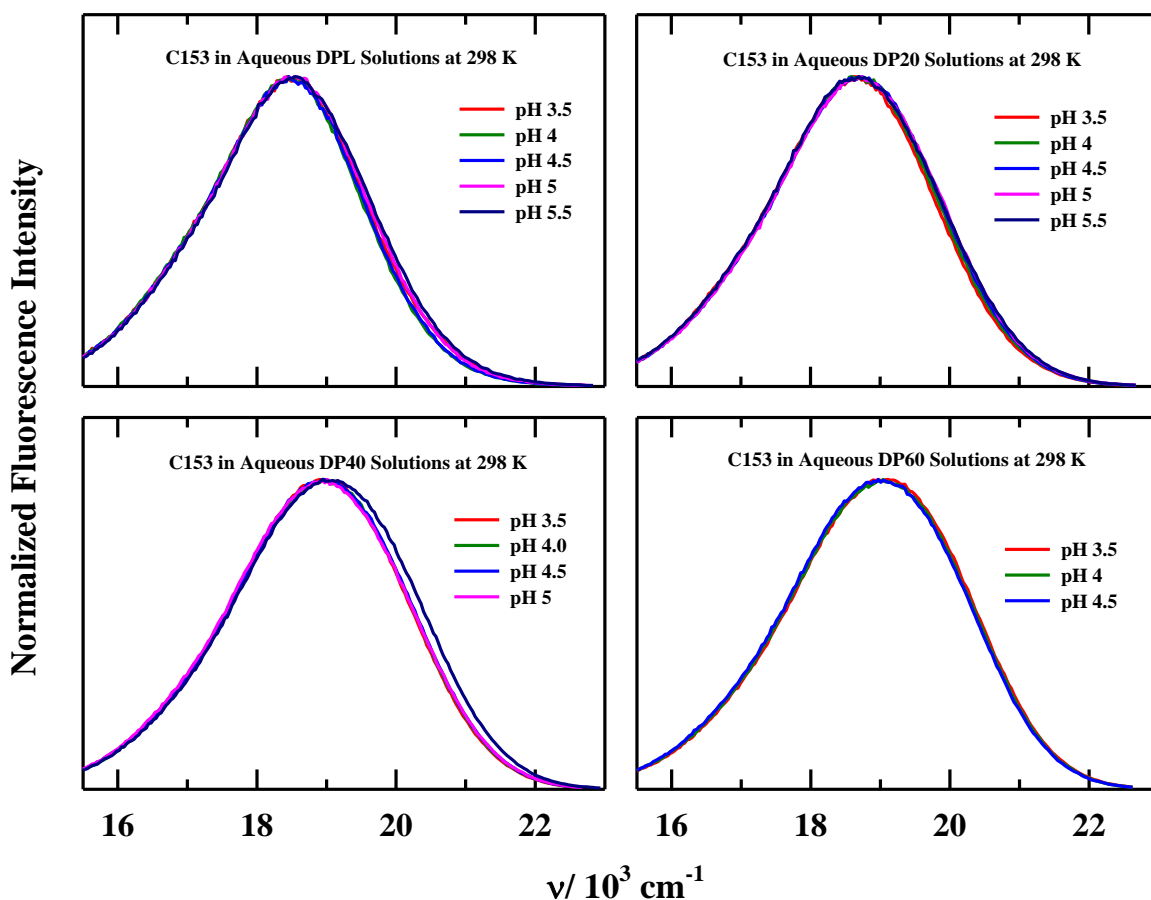


Figure 8.4: pH dependent steady state fluorescence emission spectra of C153 in aqueous polymer solutions (1mg/ml) at 298 K. Representations are colour-coded.

Next, we have investigated the impact of L-Leu-HEMA/MMA unit ratio on steady state UV-Vis absorption and fluorescence emission spectra of C153 in these three aqueous copolymer (DPL-DP60) solutions. Representative absorption and emission spectra of C153 in aqueous solutions of these polymers are shown in Figure 8.5. Note the pH values mentioned in this figure correspond to the inherent solution pH; that is, no external chemical (here 0.1 M NaOH) has been added to tune the solution pH. Corresponding absorption and emission spectra in neat water are represented in this figure for comparison. The emission frequencies for C153 in these aqueous polymer solutions are blue shifted by $\sim 500\text{-}1000\text{ cm}^{-1}$ compared to that in neat water and the extent of blue shift increases successively from DPL to DP60. This suggests that local environments surrounding C153 in these solutions are less polar than that in neat water.^{17,48,61} With the decrease of L-Leu-HEMA/MMA unit ratio (from DPL to DP60), the polymers

become more and more hydrophobic. Static dielectric constants (ϵ_s) of these polymer solutions are very close to that of neat water (Table 8.5). Thus polymer induced ~ 500 - 1000 cm^{-1} blue shift observed here suggests that C153 resides at the interfacial region of polymer and water, and this region is less polar than bulk water. Similar absorption and fluorescence emission spectral features were reported in aqueous solution of amphiphilic copolymers where blue shift of fluorescence spectra was attributed to arise from preferential location of hydrophobic C153 at the interfacial region of self-assembled structures.^{17,48,62,63}

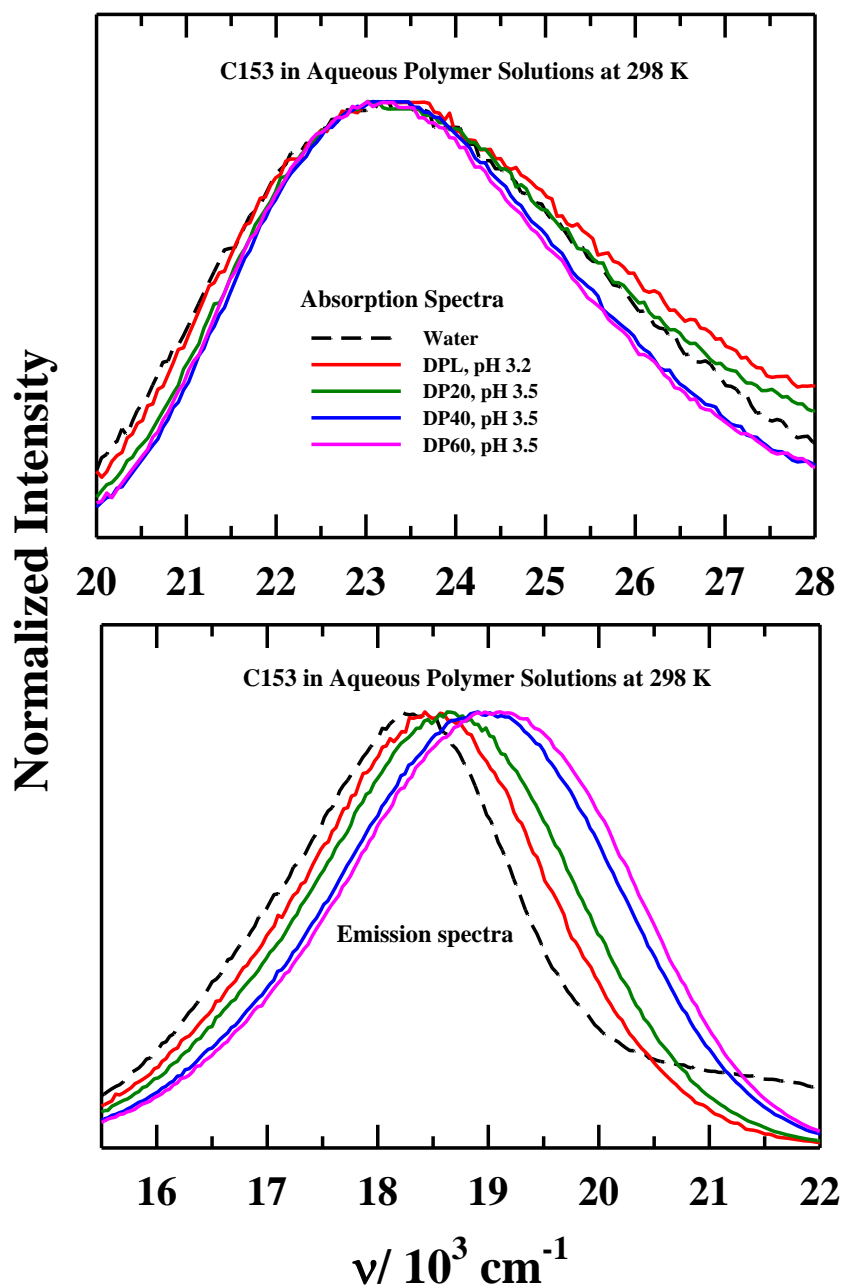


Figure 8.5: Steady state UV-Vis absorption (upper panel) and fluorescence emission (lower panel) spectra of C153 in aqueous polymer solutions (1mg/ml) at 298 K. pH value mentioned in the figure is the intrinsic pH of the polymer solutions (that is, in the absence of NaOH which has been used to vary pH of the solutions). Different colours are used to specify individual polymer solutions.

The presence of microheterogeneity in these polymer solutions (DPL to DP60) has been investigated via monitoring the excitation wavelength (λ_{exc}) dependence of fluorescence emission spectrum of C153. If microenvironments around probe molecules in solution do not

interconvert among themselves at a rate much faster than the average rate of fluorescence emission of the probe (here C153), the fluorescence emission shall show excitation wavelength dependence. Here, 10-12 equally spaced λ_{exc} across the absorption spectrum, shown in Figure A.f.1 (Appendix), are considered for the λ_{exc} dependence of fluorescence emission measurements. Figure 8.6 presents λ_{exc} dependent fluorescence emission frequencies of C153 in the polymer solutions with different pH. Corresponding λ_{exc} dependent shift of spectral widths (FWHM) are shown in Figure A.f.2 (see Appendix). A moderate λ_{exc} induced shift of emission frequencies ($\sim 300\text{-}500\text{ cm}^{-1}$) with concomitant spectral narrowing has been registered. Note that λ_{exc} dependent total emission shift, $\Delta\nu_{em}(\lambda_{exc}) = \nu_{em}(\lambda_{exc}^{blue\text{end}}, 380\text{nm}) - \nu_{em}(\lambda_{exc}^{red\text{end}}, 480\text{nm})$, shows a non-monotonous pH dependence, shown in Figure 8.7. Furthermore, for a particular pH, the extent of total emission spectral shift with λ_{exc} has been studied to explore the impact of tuning L-Leu-HEMA/MMA ratio in polymers. A non-monotonic change, shown in Figure 8.7 has been observed. Solute (C153) centric relaxation dynamics is next investigated by applying time-resolved fluorescence measurements to explore whether relaxation dynamics is influenced by the variation of solution pH in these copolymer solutions and also the impact of phase transition pH on dynamical behaviour of solutions.

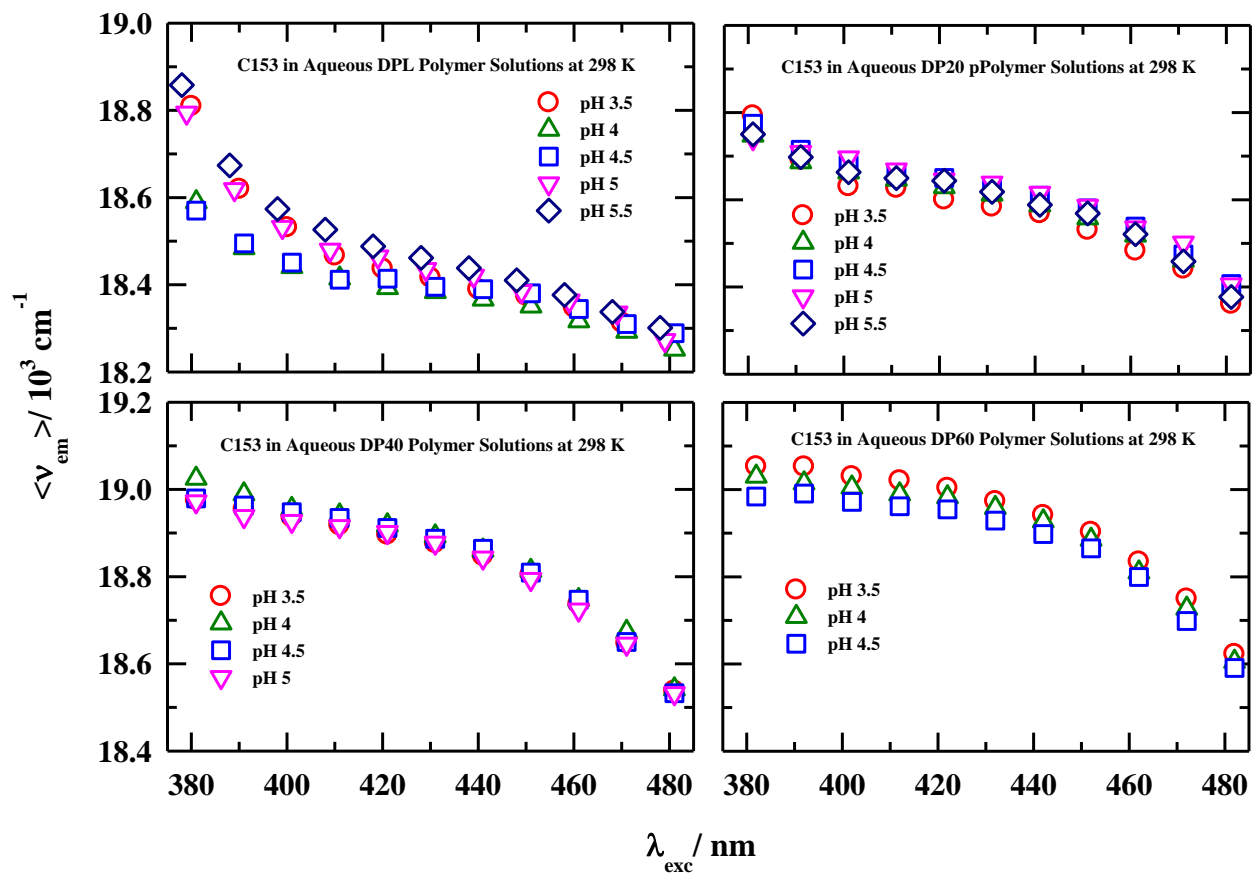


Figure 8.6: Excitation wavelength (λ_{exc}) dependent average peak emission frequencies ($\langle \nu_{em} \rangle$) of C153 in aqueous polymer solutions (1mg/ml) for various pH at 298 K. Colour-code is used to identify different pH values.

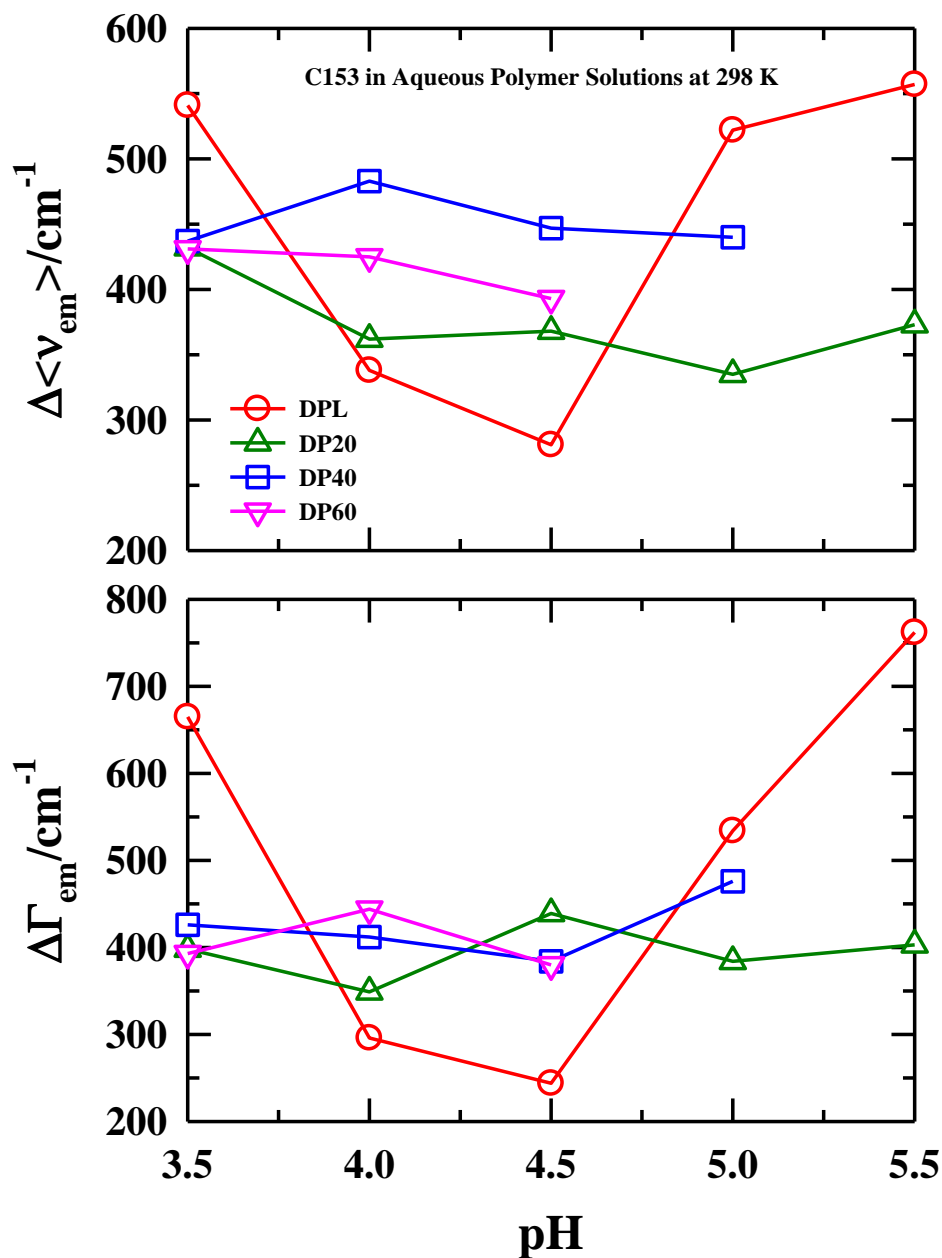


Figure 8.7: pH dependent total shift of excitation wavelength (λ_{exc}) dependent fluorescence emission frequencies ($\Delta \nu_{em}$) and spectral widths ($\Delta \Gamma_{em}$) of C153 in aqueous polymer solutions (1mg/ml) at ~298 K. Note that $\Delta x = x(\lambda_{exc}^{blue\ end}) - x(\lambda_{exc}^{red\ end})$ where x is ν or Γ . All presentations are colour-coded.

8.3.4 Time-Resolved Fluorescence Spectroscopy Measurements

8.3.4.1 Fluorescence Lifetime Measurements

Average excited state lifetimes ($\langle \tau_{life} \rangle$) of C153 in these aqueous polymer solutions as well as in neat water are summarized in Table 8.3. Note $\langle \tau_{life} \rangle$ of C153 in these copolymer solutions is ~ 1.5 times longer than that in neat water. This again suggests that C153 resides in a region different from bulk water. A small increase of $\langle \tau_{life} \rangle$ is observed with decreasing L-Leu-HEMA/MMA ratio. No significant impact of solution pH variation on excited state fluorescence lifetime has been detected in any of the present copolymer solutions.

Table 8.3: pH dependent average fluorescence lifetimes ($\langle \tau_{life} \rangle$) of C153 in aqueous solutions of polymers (1mg/ml) at 298 K.^a

pH	$\langle \tau_{life} \rangle$ /ns				Water
	DPL	DP20	DP40	DP60	
3.5	2.22	1.99	2.53	2.49	1.76
4	2.16	2.21	2.59	2.62	
4.5	1.96	2.24	2.66	2.22	
5	2.24	2.36	2.61	-	
5.5	2.14	2.03	-	-	

^aThe reported life-times can be reproduced within $\pm 10\%$ of the reported values.

Because of a broad temporal resolution employed in the present measurements (IRF ~ 85 ps), signature of dynamic Stokes shift has not been detected in the aqueous polymer solutions (DPL to DP60) where the major contribution in solvent relaxation arises from the ultrafast reorganization of water molecules. Time-resolved fluorescence anisotropy measurement of C153 has been performed in order to investigate the impact of solutions pH variation on the friction imparted on a rotating solute (here C153). Furthermore, impact of L-Leu-HEMA/MMA ratio in copolymer on rotational dynamics of C153 in these solutions has been explored.

8.3.4.2 Time-Resolved Fluorescence Anisotropy Decay Measurements

Figure 8.8 represents rotational anisotropy decays ($r(t)$) of C153 and corresponding bi-exponential fits in aqueous solution of DPL to DP60 at two representative pH. pH dependent bi-exponential fit parameters are provided in the Table 8.4. Note that the $r(t)$ decays are strongly non-exponential, characterized by a fast component (time constant ~ 100 -200 ps) and

a slow nanosecond (3-5 ns) component although in neat water (nearly as viscous as these aqueous polymer solutions), $r(t)$ of C153 shows an exponential decay with $\tau_{rot} \sim 100$ ps.^{17,41} This strong non-exponential character of $r(t)$ decay persists at all other pH considered here indicates that the local environment of C153 is qualitatively different from bulk-like water. Representative pH dependent rotational anisotropy decays of C153 in aqueous copolymer solutions (DPL to DP60) are shown in Figure 8.8. For each of these solutions, no significant impact of solution pH variation are registered in the collected $r(t)$ decays. This indicates that the medium friction exerted on a rotating solute in solutions of pH away from pH^{tr} is no different than that in solutions of pH close to pH^{tr} . This suggests that pH-induced polymer-water phase separation is a sharp phenomenon and therefore, it is not reflected in solute-medium interaction as well as solute-medium friction with successive change of solution pH approaching pH^{tr} but limits at $\text{pH}^{\text{expt}} = \text{pH}^{\text{tr}} - 0.5$.

Rotational anisotropy decay has been further employed to explore the impact of L-Leu-HEMA/MMA unit ratio on solute-medium friction. A comparison of rotational anisotropy decay in aqueous polymer (DPL to DP60) solutions with their intrinsic pH is shown in Figure 8.9 and the corresponding fit parameters are provided in Table 8.4. Note, these $r(t)$ decays are characterized by a sum of two exponentials (bi-exponential function of time) with widely different time constants. Surprisingly, viscosities of these solutions are nearly identical to each other and very close to that of neat water. The substantially slowed-down rotational dynamics therefore suggests that the hydrophobic polar probe C153 resides in the vicinity of the polymer-water interface in these aqueous solutions. We would like to mention here that the bimodal anisotropy decay with well separated time constants are a general observation for various solute probes in aqueous micellar solutions.^{64,65} Interestingly, $\langle \tau_{rot} \rangle$ increases with the decrease of L-Leu-HEMA/MMA component ratio in the polymer from DPL to DP60. The lengthening of $\langle \tau_{rot} \rangle$ in more hydrophobic unit containing copolymer supports the view that C153 resides in a close proximity to hydrophobic domain of the interface.

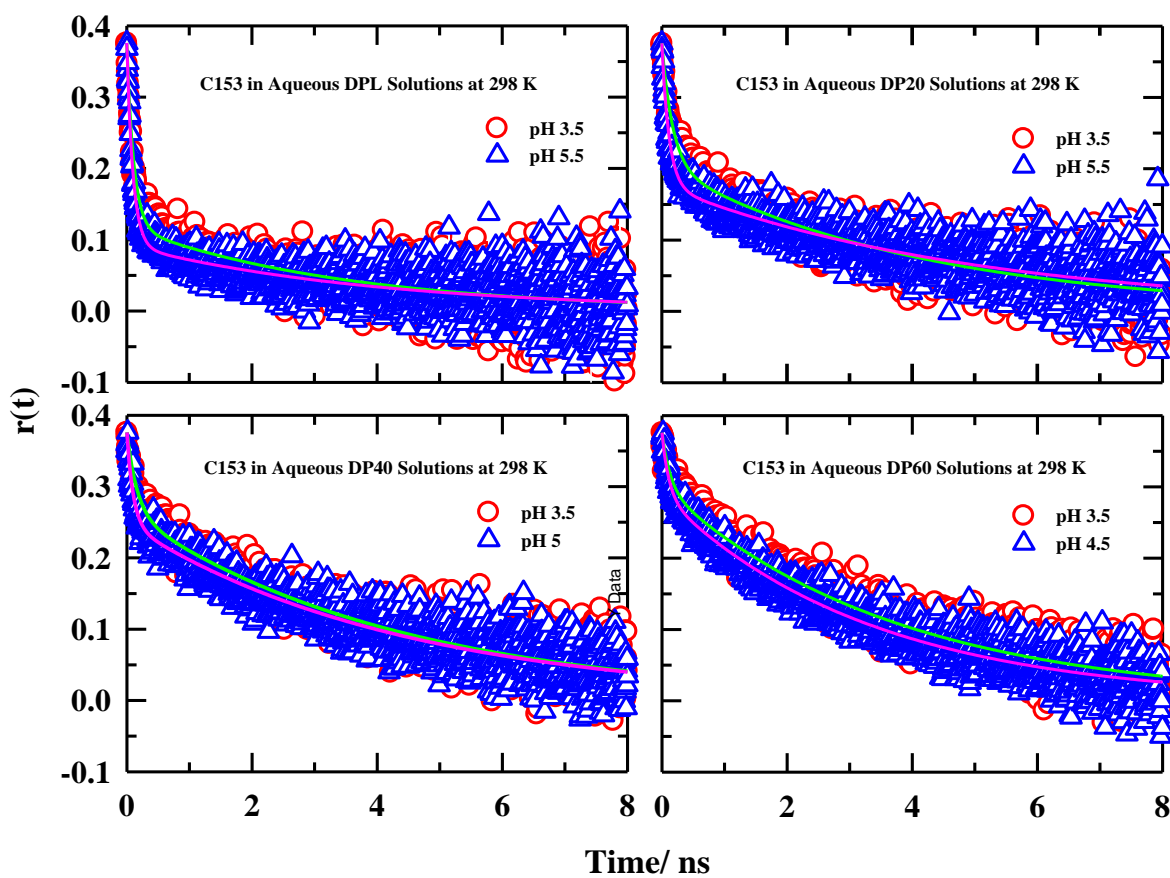


Figure 8.8: pH dependent rotational anisotropy decays ($r(t)$) of C153 in aqueous polymer solutions (1mg/ml) at ~298 K. Experimental $r(t)$ data points are shown by symbols and lines through them depict multi-exponential fits. Separate colours have been used to indicate different pH of the solutions.

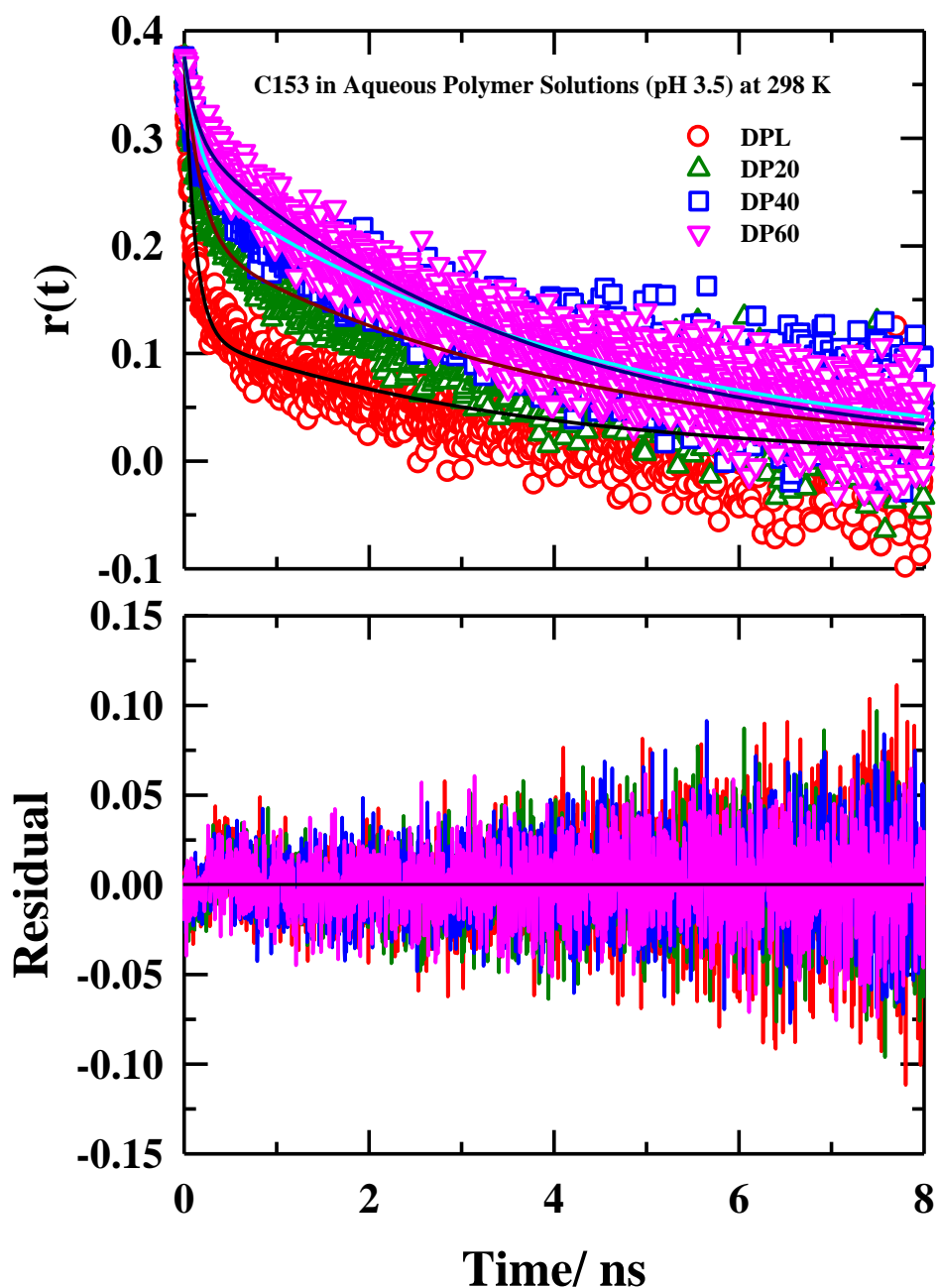


Figure 8.9: Rotational anisotropy decays, $r(t)$, (upper panel) and corresponding residuals (lower panel) of C153 in aqueous polymer solutions (1mg/ml) at their intrinsic pH (i.e. in the absence of NaOH which has been used to vary pH of the solutions) at ~ 298 K. In the upper panel, experimental data points are shown as symbols and lines through them depict multi-exponential fits. Specific identities of polymers are shown in the inset.

Table 8.4: pH dependent $r(t)$ decay fit parameters of C153 in aqueous solutions of polymers (1 mg/ml) at 298 K.^a

DPL					
pH	a_1	τ_1 /ps	a_2	τ_2 /ps	$\langle \tau_{rot} \rangle$ /ps
3.5	0.68	113	0.32	3506	1181
4	0.70	107	0.30	3325	1088
4.5	0.68	119	0.32	3433	1172
5	0.72	108	0.28	3897	1169
5.5	0.76	99	0.24	4006	1037
DP20					
3.5	0.45	175	0.55	4081	2310
4	0.47	184	0.53	4562	2504
4.5	0.46	160	0.54	4590	2533
5	0.46	130	0.54	4338	2414
5.5	0.53	116	0.47	5005	2414
DP40					
3.5	0.30	164	0.70	4303	3077
4	0.30	157	0.70	4286	3066
4.5	0.28	122	0.72	4255	3097
5	0.34	102	0.66	4384	2922
DP60					
3.5	0.20	133	0.80	3692	2977
4	0.21	157	0.79	3629	2896
4.5	0.23	111	0.77	3329	2584

^aIndividual amplitudes and time constants can be reproduced within $\pm 10\%$ of the reported values.

8.3.5 Dielectric Relaxation Spectroscopic Study

Figure 8.10 represents pH dependent real (ϵ') and imaginary (ϵ'') components of the complex dielectric spectra of aqueous pH responsive polymer solutions along with the Debye fits. For comparison dielectric spectra of neat water are also shown in the same figure. Single Debye (1 D) model is sufficient to describe all these dielectric spectra. Corresponding quality of single Debye fits are represented by residuals, shown in Figure A.f.3 (see Appendix). Fit parameters are summarized in Table 8.5. Close similarity of τ_{DR} (~ 8 ps) and static dielectric constant (ϵ_s) between aqueous pH responsive polymer solution and neat water suggests that the dielectric response in these polymer solutions is arising mainly from the cooperative relaxation of bulk water.^{45,66-69} Note, DR of water molecules in these polymer-water interfacial regions also behave like bulk water. This is quite interesting because slow interfacial water dynamics is observed in various self-assembled aqueous systems.^{45,48} Next, the impact of decreasing Leu-HEMA/MMA unit ratio on DR of aqueous polymer solutions is explored at a representative

pH (pH \sim 3.5, the intrinsic pH of the aqueous polymer solutions). The real and imaginary components of complex dielectric spectra along with single Debye fits are shown in Figure 8.11. Respective residuals are presented in Figure A.f.4 (see Appendix). Dielectric spectra and residuals in neat water are also presented in the Figures 8.11 and Figure A.f.4 (Appendix), respectively. In this case also, no significant difference in DR features between aqueous polymer solutions and neat water is observed.

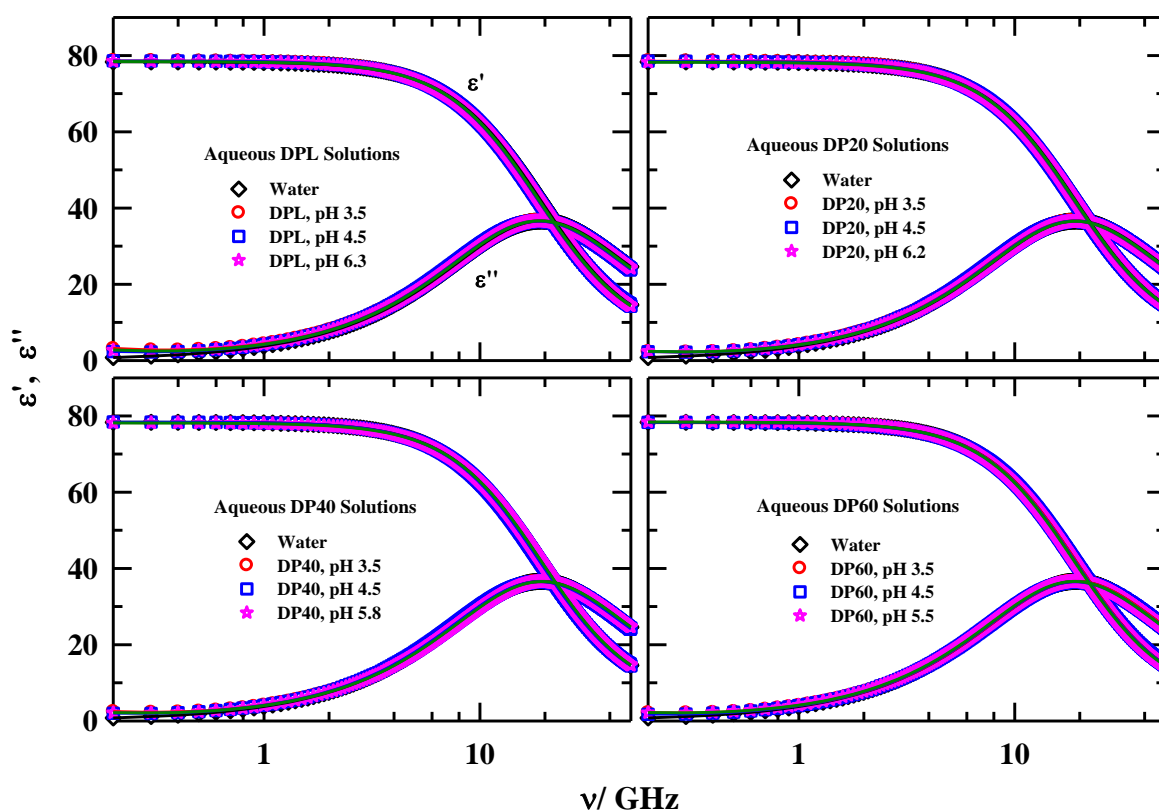


Figure 8.10: Representative real (ϵ') and imaginary (ϵ'') components of complex dielectric constant at various pH for each aqueous polymer solutions at temperature \sim 298 K. Symbols denote the experimental data and lines passing through them denote single Debye (1D) fits. For comparison, the same for neat water also presented in each panel of the figure. All presentations are colour-coded. Note here that the relaxation due to inter-molecular vibrations and librations of water at the high frequency wing is missing because of the limited frequency window.

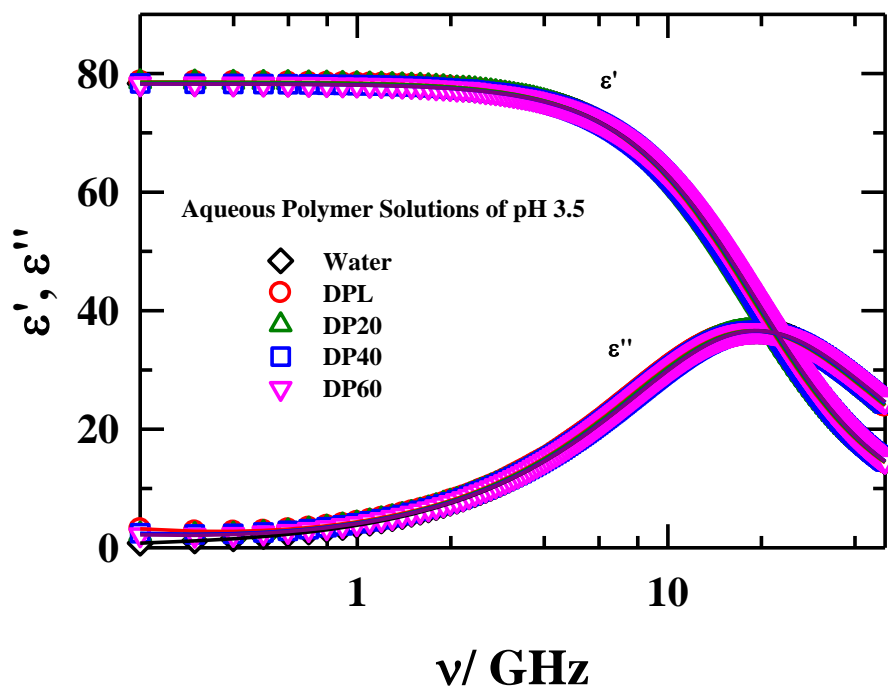


Figure 8.11: Representative real (ϵ') and imaginary (ϵ'') components of complex dielectric constant of aqueous polymer solutions at temperature ~ 300 K. Symbols are the experimental data points while lines passing through the data depict single Debye fits. For comparison, the DR for neat water is also presented in the same figure. pH mentioned in the figure is the intrinsic pH of the polymer solutions. Colour-code have been used to specify the individual polymers.

Table 8.5: pH dependent dielectric relaxation fit parameters of aqueous solutions of polymers (1 mg/ml) at 298±1 K.^a

pH	ϵ_s	$\Delta\epsilon$	τ / ps	ϵ_∞	n^2	κ_{fit} /Sm ⁻¹
DPL						
3.5	78.59	73.18	8.54	5.41	1.774	0.027
4.5	78.59	73.12	8.53	5.47	1.777	0.018
6.3	78.43	73.23	8.42	5.20	1.774	0.018
DP20						
3.5	78.54	73.16	8.46	5.38	1.775	0.018
4.5	78.44	73.13	8.41	5.31	1.775	0.018
6.2	78.25	73.03	8.33	5.22	1.776	0.018
DP40						
3.5	78.26	73.01	8.30	5.25	1.776	0.019
4.5	78.38	73.01	8.41	5.37	1.776	0.014
5.8	78.16	73.08	8.21	5.08	1.776	0.015
DP60						
3.5	78.25	73.15	8.24	5.10	1.776	0.016
4.5	78.30	72.96	8.36	5.34	1.776	0.011
5.5	78.40	73.15	8.42	5.25	1.777	0.016
Water	78.36	73.23	8.27	5.13	1.774	0

^aIndividual amplitudes and time constants can be reproduced within ±5% of the reported values.

8.4 Conclusion

In summary, steady state and time-resolved fluorescence studies in the current aqueous copolymer solutions indicate solute (C153) - medium interaction is qualitatively different from C153-neat water interaction. Preferential interaction of hydrophobic solute C153 with the hydrophobic part of these pH-responsive polymers in aqueous medium (i.e. the polymer-water interfacial region) is the main regulatory factor for the observed spectral signatures and the strongly non-exponential fluorescence anisotropy decays. Bulk water like dielectric features are reflected from the MHz-GHz DR measurements in aqueous solutions of these pH-responsive polymers. No signature of pH^{tr} driven abrupt change in static and dynamic properties of aqueous polymer solutions have been registered from pH dependent fluorescence and DR measurements. This is probably because this phase transition is quite a sharp phenomenon and therefore an abrupt change in static and dynamic properties in that case is likely to occur at a close vicinity of pH^{tr}. Blue shift in fluorescence emission (~500-1000 cm⁻¹) of C153 dissolved in these polymer solutions (DPL-DP60) suggests preferential location of C153 in the polymer-water interfacial region. Despite possessing water like viscosity, strong

non-exponential solute rotational anisotropy decay and slowing down of the average rotational relaxation time with successive decrease of L-Leu-HEMA/MMA segment ratio in polymers arises from the restricted solute rotation at the polymer-water interfacial region. This again supports the preferential location of the hydrophilic solute at the interfacial region.

References

1. H. Tian, Z. Tang, X. Zhuang, X. Chen and X. Jing, *Prog. Polym. Sci.* **37**, 237 (2012).
2. E. Cabane, X. Zhang, K. Langowska, C. G. Palivan and W. Meier, *Biointerphases* **7**, 9 (2012).
3. K. Bauri, S. G. Roy, S. Pant and P. De, *Langmuir* **29**, 2764 (2013).
4. G. Kocak, C. Tuncer and V. Bütün, *Polym. Chem.* **8**, 144 (2017).
5. A. Bordat, T. Boissenot, J. Nicolas and N. Tsapis, *Adv. Drug Deliv. Rev.* **138**, 167 (2019).
6. D. Roy, W. L. Brooks and B. S. Sumerlin, *Chem. Soc. Rev.* **42**, 7214 (2013).
7. G. Ma, W. Lin, Z. Yuan, J. Wu, H. Qian, L. Xu and S. Chen, *J. Mater. Chem. B* **5**, 935 (2017).
8. M. C. García, in *Stimuli Responsive Polymeric Nanocarriers for Drug Delivery Applications* (Elsevier, 2019).
9. J. Zhuang, M. R. Gordon, J. Ventura, L. Li and S. Thayumanavan, *Chem. Soc. Rev.* **42**, 7421 (2013).
10. Q. Yan, D. Han and Y. Zhao, *Polym. Chem.* **4**, 5026 (2013).
11. D. Roy and B. S. Sumerlin, *Macromol. Rapid. Commun.* **35**, 174 (2014).
12. X. Zhang, L. Han, M. Liu, K. Wang, L. Tao, Q. Wan and Y. Wei, *Mater. Chem. Front.* **1**, 807 (2017).
13. B. Saha, U. Haldar and P. De, *Macromol. Rapid. Commun.* **37**, 1015 (2016).
14. J. Ge, E. Neofytou, T. J. Cahill III, R. E. Beygui and R. N. Zare, *ACS Nano* **6**, 227 (2012).
15. T. Manouras and M. Vamvakaki, *Polym. Chem.* **8**, 74 (2017).
16. M. Wei, Y. Gao, X. Li and M. J. Serpe, *Polym. Chem.* **8**, 127 (2017).
17. K. Kumbhakar, B. Saha, P. De and R. Biswas, *J. Phys. Chem. B* **123**, 11042 (2019).
18. M. A. Ward and T. K. Georgiou, *Polymers* **3**, 1215 (2011).
19. P. C. Bessa, R. Machado, S. Nürnberger, D. Dopler, A. Banerjee, A. M. Cunha, J. C. Rodríguez-Cabello, H. Redl, M. van Griensven and R. L. Reis, *J. Control. Release* **142**, 312 (2010).
20. S.-o. Han, R. I. Mahato, Y. K. Sung and S. W. Kim, *Mol. Ther.* **2**, 302 (2000).
21. S. E. Stabenfeldt, A. J. García and M. C. LaPlaca, *J. Biomed. Mater. Res. A* **77**, 718 (2006).
22. M. A. C. Stuart, W. T. S. Huck, J. Genzer, M. Müller, C. Ober, M. Stamm, G. B. Sukhorukov, I. Szleifer, V. V. Tsukruk and M. Urban, *Nat. Mater.* **9**, 101 (2010).

23. J. Hu and S. Liu, *Macromolecules* **43**, 8315 (2010).
24. J. Kostal, A. Mulchandani, K. E. Gropp and W. Chen, *Environ. Sci. Technol.* **37**, 4457 (2003).
25. D. Parasuraman and M. J. Serpe, *ACS Appl. Mater. Interfaces* **3**, 2732 (2011).
26. J. Hu, G. Zhang, Z. Ge and S. Liu, *Prog. Polym. Sci.* **39**, 1096 (2014).
27. A. S. Hoffman, *Adv. Drug Deliv. Rev.* **64**, 18 (2012).
28. S. Dai, P. Ravi and K. C. Tam, *Soft Matter* **4**, 435 (2008).
29. F. Bignotti, M. Penco, L. Sartore, I. Peroni, R. Mendichi, M. Casolaro and A. D'Amore, *Polymer* **41**, 8247 (2000).
30. B. Zhao and J. S. Moore, *Langmuir* **17**, 4758 (2001).
31. D. Schmaljohann, *Adv. Drug Deliv. Rev.* **58**, 1655 (2006).
32. C. Fodor, B. Gajewska, O. Rifaie-Graham, E. A. Apebende, J. Pollard and N. Bruns, *Polym. Chem.* **7**, 6617 (2016).
33. I. Chakraborty, I. Mukherjee, U. Haldar, P. De and R. Bhattacharyya, *Phys. Chem. Chem. Phys.* **19**, 17360 (2017).
34. S. G. Roy and P. De, *J. Appl. Polym. Sci.* **131**, 41084 (2014).
35. S. Pal, S. G. Roy and P. De, *Polym. Chem.* **5**, 1275 (2014).
36. N. Kedia, S. G. Roy, P. De and S. Bagchi, *J. Phys. Chem. B* **118**, 4683 (2014).
37. K. Kumbhakar, A. Dey, A. Mondal, P. De and R. Biswas, *Interactions and Dynamics in Aqueous Solutions of pH-Responsive Polymers: A Combined Fluorescence and Dielectric Relaxation Studies* (Ready for Submission).
38. M. L. Horng, J. A. Gardecki, A. Papazyan and M. Maroncelli, *J. Phys. Chem.* **99**, 17311 (1995).
39. E. Tarif, J. Mondal and R. Biswas, *J. Mol. Liq.* **303**, 112451 (2020).
40. K. Kumbhakar, E. Tarif, K. Mukherjee and R. Biswas, *J. Mol. Liq.* **290**, 111225 (2019).
41. T. Pradhan, P. Ghoshal and R. Biswas, *J. Chem. Sci.* **120**, 275 (2008).
42. B. Guchhait, H. Al Rasid Gazi, H. K. Kashyap and R. Biswas, *J. Phys. Chem. B* **114**, 5066 (2010).
43. S. Indra and R. Biswas, *J. Chem. Phys.* **142**, 204501 (2015).
44. E. Tarif, K. Mukherjee, K. Kumbhakar, A. Barman and R. Biswas, *J. Chem. Phys.* **151**, 154902 (2019).
45. K. Mukherjee, A. Barman and R. Biswas, *J. Mol. Liq.* **222**, 495 (2016).
46. B. Guchhait, R. Biswas and P. K. Ghorai, *J. Phys. Chem. B* **117**, 3345 (2013).
47. S. Sen, P. Dutta, S. Mukherjee and K. Bhattacharyya, *J. Phys. Chem. B* **106**, 7745 (2002).

48. E. Tarif, B. Saha, K. Mukherjee, P. De and R. Biswas, *J. Phys. Chem. B* **123**, 5892 (2019).
49. K. Mukherjee, A. Das, S. Choudhury, A. Barman and R. Biswas, *J. Phys. Chem. B* **119**, 8063 (2015).
50. J. Lewis, R. Biswas, A. Robinson and M. Maroncelli, *J. Phys. Chem. B* **105**, 3306 (2001).
51. R. Biswas, J. Lewis and M. Maroncelli, *Chem. Phys. Lett.* **310**, 485 (1999).
52. M. L. Horng, J. A. Gardecki and M. Maroncelli, *J. Phys. Chem. A* **101**, 1030 (1997).
53. T. Pradhan and R. Biswas, *J. Phys. Chem. A* **111**, 11524 (2007).
54. S. Koley, H. Kaur and S. Ghosh, *Phys. Chem. Chem. Phys.* **16**, 22352 (2014).
55. N. Sarma, J. M. Borah, S. Mahiuddin, H. A. R. Gazi, B. Guchhait and R. Biswas, *J. Phys. Chem. B* **115**, 9040 (2011).
56. C. J. F. Böttcher and P. Bordewijk, *Theory of Electric Polarization* (Elsevier: Amsterdam, The Netherlands, 1978).
57. F. Kremer and A. Schönhal, *Broadband Dielectric Spectroscopy* (Springer Science & Business Media, 2002).
58. P. R. Bevington and D. K. Robinson, *Data Reduction and Error Analysis* (McGraw-Hill, New York, 2003).
59. K. Mukherjee, E. Tarif, A. Barman and R. Biswas, *Fluid. Phase. Equilib.* **448**, 22 (2017).
60. J. F. Lutz, K. Weichenhan, Ö. Akdemir and A. Hoth, *Macromolecules* **40**, 2503 (2007).
61. M. Maroncelli and G. R. Fleming, *J. Chem. Phys.* **86**, 6221 (1987).
62. H. Shirota, Y. Tamoto and H. Segawa, *J. Phys. Chem. A* **108**, 3244 (2004).
63. P. Sen, D. Roy, S. K. Mondal, K. Sahu, S. Ghosh and K. Bhattacharyya, *J. Phys. Chem. A* **109**, 9716 (2005).
64. M. Kumbhakar, T. Goel, T. Mukherjee and H. Pal, *J. Phys. Chem. B* **108**, 19246 (2004).
65. M. Kumbhakar, T. Goel, T. Mukherjee and H. Pal, *J. Phys. Chem. B* **109**, 18528 (2005).
66. R. Buchner, J. Barthel and J. Stauber, *Chem. Phys. Lett.* **306**, 57 (1999).
67. K. Nörtemann, J. Hilland and U. Kaatz, *J. Phys. Chem. A* **101**, 6864 (1997).
68. W. Qi, J. Chen, J. Yang, X. Lei, B. Song and H. Fang, *J. Phys. Chem. B* **117**, 7967 (2013).
69. M. Neumann, *J. Chem. Phys.* **85**, 1567 (1986).

Chapter 9

Concluding Remarks and Future Problems

9.1 Concluding Remarks

To summarize, we have investigated interactions and dynamics of several complex systems in this Thesis using steady state, time-resolved fluorescence (TRF) and dielectric relaxation spectroscopy. Multi-component cryoprotectant mixtures, lithium-ion battery electrolyte materials, aqueous solutions of stimuli-responsive polymers etc. are the studied complex systems in this Thesis. Spatio-temporal heterogeneity has been extensively explored in these complex systems. DR and solute-centric (coumarin 153 and coumarin 343) time-resolved fluorescence in glucose/glycerol (Glu/Gly) cryoprotectant solutions report strong spatio-temporal heterogeneity. In the high viscosity regime solute rotation in these Glu/Gly solutions has been found to deviate from the hydrodynamic limit, giving rise to sub-slip behaviour. Spatial heterogeneity with domain persistent time in the sub-ns regime has been observed in lithium-ion battery electrolyte materials that contain ethylene carbonate (EC), propylene carbonate (PC) and lithium perchlorate (LiClO_4). A mild solute translation-rotation decoupling has been found in polypropylene glycol based polymer gel electrolyte systems. Phase transition point driven interaction and relaxation dynamics have been explored in aqueous solution of thermoresponsive and pH –responsive synthetic random copolymers.

Since each chapter contains conclusions separately, we refrain from dedicating a full chapter for drawing conclusions of the research study reported in this Thesis. Rather, a number of interesting and relevant problems are briefly discussed below which may be considered for future explorations.

9.2 Future Problems

9.2.1 Heterogeneity in Biocompatible Cryoprotectant Mixtures: Temperature and Composition Dependent Time-Resolved Fluorescence (TRF) and Dielectric Relaxation Spectroscopic (DRS) Studies

Due to tremendous demand of cryopreservation technology, cryoprotectants have now become indispensable for low-temperature preservation of live cells, tissues, organs, proteins etc.¹ Several sugars such as glucose, trehalose, sucrose, maltose, sugar alcohols like glycerol, xylitol, sorbitol etc. act as intracellular/ extracellular cryoprotectant agent (CPA).² It has been proved that instead of employing single component alone, use of multi-component cryoprotectants mixtures such as trehalose/proline, glucose/glycerol, trehalose/glycerol increase the cryopreservation efficiency.³⁻⁷ Recent investigations on trehalose/glycerol cryoprotectant mixtures⁸ and the TRF and DRS studies in glucose/glycerol mixtures discussed in chapter 3 and chapter 4 of the current Thesis have revealed presence of strong heterogeneity. Therefore, more studies employing various combinations of cryoprotectants are warranted to investigate spatio-temporal heterogeneity and its possible connection to cryopreservation efficiency. Glucose/ethylene glycol, sucrose/glycerol, xylitol/glycerol, trehalose/proline etc. are few examples of multi-component cryoprotectant mixtures that may be studied via steady state fluorescence emission, TRF and DRS.

9.2.2 Exploring Medium Static and Dynamic Properties in Highly Potential Polymeric Cryoprotectant Mixtures

To survive in ice-rich environments, extremophile organisms adopted many strategies,⁹ for example, arctic fishes produce various antifreeze proteins (AFPs). These AFPs are potential ice recrystallization inhibitors.¹⁰⁻¹² These AFPs cannot be easily synthesized in large scale. Moreover, their immunological/toxicological studies are not sufficient.¹³ These issues limit the application of AFPs in cryopreservation. To overcome these limitations, AFP mimicking synthetic polymers, which are biocompatible and nontoxic, are emerging as potential cryoprotectant candidates in cryopreservation.¹⁴⁻¹⁷ Polyvinyl alcohol (PVA), poly(ampholyte)s based synthetic polymers are well known to exhibit ice recrystallization inhibition.¹³ It has been reported that mixtures of polyvinyl alcohol (PVA)/polyethylene glycol (PEG) could be successfully applied to cryopreservation of microorganisms.¹³ Interaction and dynamics of AFP-mimicking materials (biocompatible and nontoxic) thus have importance in the

development of cryopreservation technology. Steady state fluorescence emission, TRF and DRS in PVA/PEG, PVA/polypropylene glycol cryoprotectant systems would be interesting in this regard.

9.2.3 Impact of Water on Interactions and Dynamics of Cryoprotectants Mixtures

During low temperature preservation of biologically important substances such as proteins, live cells, tissues etc., formation of ice crystal has deadly impact on the preserved substances. Use of cryoprotectants prevent ice-crystallization during low temperature preservation (cryopreservation) of such biologically important molecules.¹ The cryoprotectants take part in extensive H-bond formation with water present in the preserved material and minimise ice formation. It has been reported that instead of employing single component alone, use of multi-component cryoprotectants mixtures such as trehalose/proline, glucose/glycerol, trehalose/glycerol increase the cryopreservation efficiency.³⁻⁷ Systematic investigation of interaction and associated dynamics of multi-component cryoprotectant formulations in presence of water as minor component will be an interesting research topic in this regards. Both simulations and experiments would be needed to fully understand these systems.

9.2.4 Dielectric Relaxation of Lithium-Ion Battery Electrolytes

Electrolyte materials are one of the most important components for technologically relevant lithium-ion battery.¹⁸ In an electrochemical cell, charge carriers (ions in electrolyte medium) undergo translational motion through electrolyte medium between pair of electrodes.¹⁹ Medium impact through frictional resistance on ion transport largely governs their suitability in storage and supply-on-demand applications. In chapter 5 and 6, we have discussed the frictional decoupling of rotation, translation and solvation of C153 in liquid (consist of lithium perchlorate (LiClO_4), ethylene carbonate (EC) and propylene carbonate (PC)) and polymer gel electrolytes (made of LiClO_4 , PC and polypropylene glycol (PPG425)). Composition and temperature dependent MHz-GHz DRS measurements can be carried out to explore the inherent relaxation dynamics and the frictional decoupling of motional attributes.

9.2.5 Polymer Chain Length Induced Interaction and Dynamics of Polymer Gel Electrolytes: TRF and DRS Measurements

Generally, polyethylene oxide (PEO), polypropylene oxide (PPO), polymethyl methacrylate (PMMA) are used as polymeric substance in polymer gel electrolytes. Time-resolved fluorescence measurements in PPG (lower homolog of PPO) based polymer gel electrolyte

Chapter 9

systems are discussed in chapter 6. Significant impact of the polymer on medium interaction and relaxation dynamics has been observed. It will be very interesting to see the effects of polymer chain length on the dynamics of these polymer gel electrolyte systems keeping the other two components unchanged.

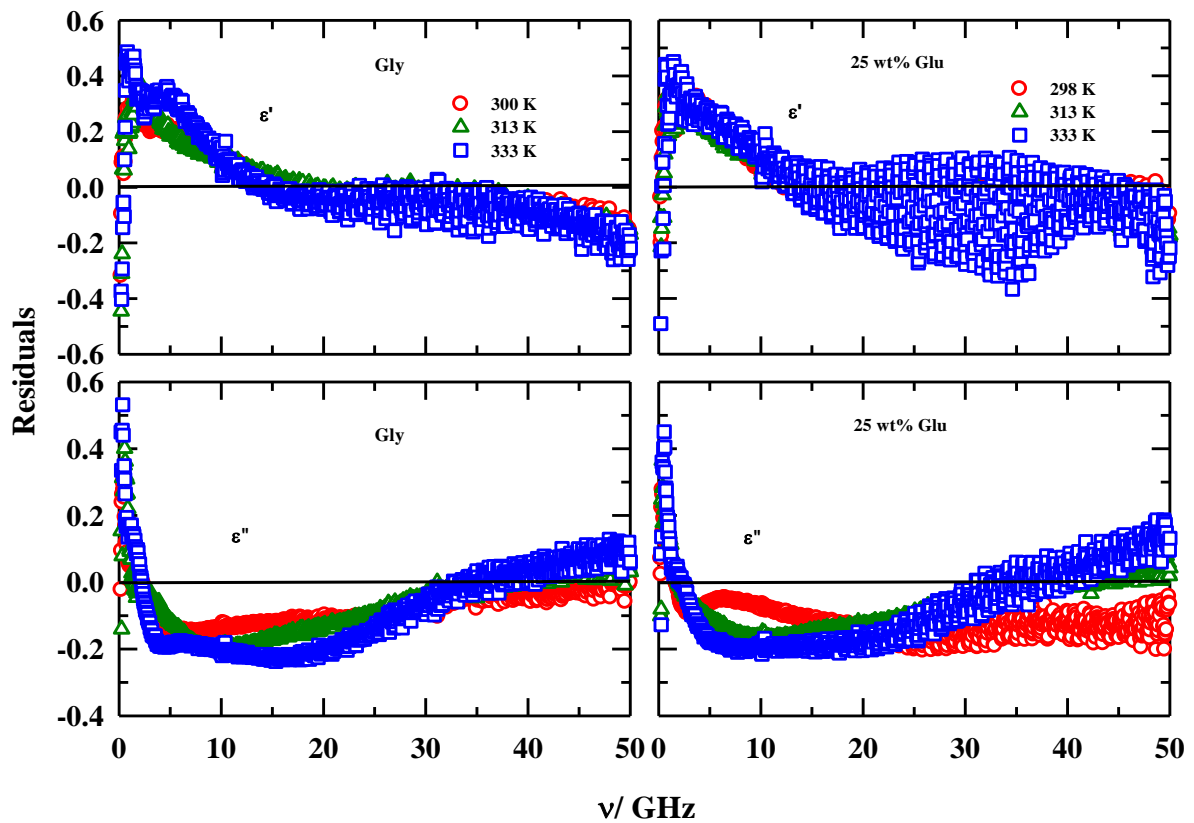
References

1. B. J. Fuller, *CryoLetters* **25**, 375 (2004).
2. G. D. Elliot, S. Wang and B. J. Fuller, *Cryobiology* **76**, 74 (2017).
3. M. T. Cicerone and C. L. Soles, *Biophys. J.* **86**, 3836 (2004).
4. A. S. Rudolph and J. H. Crowe, *Cryobiology* **22**, 367 (1985).
5. M. De los Reyes, L. Saenz, L. Lapierre, J. Crosby and C. Barros, *Vet. Rec.* **151**, 477 (2002).
6. F. Guo and J. M. Friedman, *J. Phys. Chem. B* **113**, 16632 (2009).
7. L. M. Sasnoor, V. P. Kale and L. S. Limaye, *Transplantation* **80**, 1251 (2005).
8. S. Indra and R. Biswas, *J. Phys. Chem. B* **120**, 11214 (2016).
9. E. V. Pikuta, R. B. Hoover and J. Tang, *Crit. Rev. Microbiol.* **33**, 183 (2007).
10. P. L. Davies, *Trends Biochem. Sci.* **39**, 548 (2014).
11. C. Sidebottom, S. Buckley, P. Pudney, S. Twigg, C. Jarman, C. Holt, J. Telford, A. McArthur, D. Worrall and R. Hubbard, *Nature* **406**, 256 (2000).
12. C. I. Biggs, T. L. Bailey, B. Graham, C. Stubbs, A. Fayter and M. I. Gibson, *Nat. Commun.* **8**, 1 (2017).
13. M. Hasan, A. E. R. Fayter and M. I. Gibson, *Biomacromolecules* **19**, 3371 (2018).
14. M. I. Gibson, *Polym. Chem.* **1**, 1141 (2010).
15. B. Graham, A. E. R. Fayter, J. E. Houston, R. C. Evans and M. I. Gibson, *J. Am. Chem. Soc.* **140**, 5682 (2018).
16. D. E. Mitchell, N. R. Cameron and M. I. Gibson, *ChemComm.* **51**, 12977 (2015).
17. K. Matsumura, J. Y. Bae, H. H. Kim and S. H. Hyon, *Cryobiology* **63**, 76 (2011).
18. J. M. Taracson and M. Armand, *Nature* **414**, 359 (2001).
19. K. Xu, *Chem. Rev.* **104**, 4303 (2004).

Appendix A.a

Table A.a.1: Temperature dependent densities (ρ / gcm^{-3}) of Glu/Gly solutions at various Glu concentrations.

T/K	Densities (ρ / gcm^{-3}) of Glu/Gly solutions			
	0 wt%	5 wt% Glu	15 wt% Glu	25 wt% Glu
293	1.26	1.27	1.30	1.32
303	1.25	1.26	1.29	1.31
313	1.25	1.26	1.28	1.31
318	1.24	1.26	1.28	1.30
323	1.24	1.25	1.28	1.30
328	1.24	1.25	1.27	1.30
333	1.23	1.25	1.27	1.29
338	1.23	1.24	1.27	1.29
343	1.23	1.24	1.26	1.29

**Figure A.a.2:** Residuals from multi-Debye fits to temperature dependent real (ϵ') (upper panels) and imaginary (ϵ'') (lower panels) components of the complex dielectric spectra at different Glu concentrations in Glu/Gly solution. All representations are colour-coded.

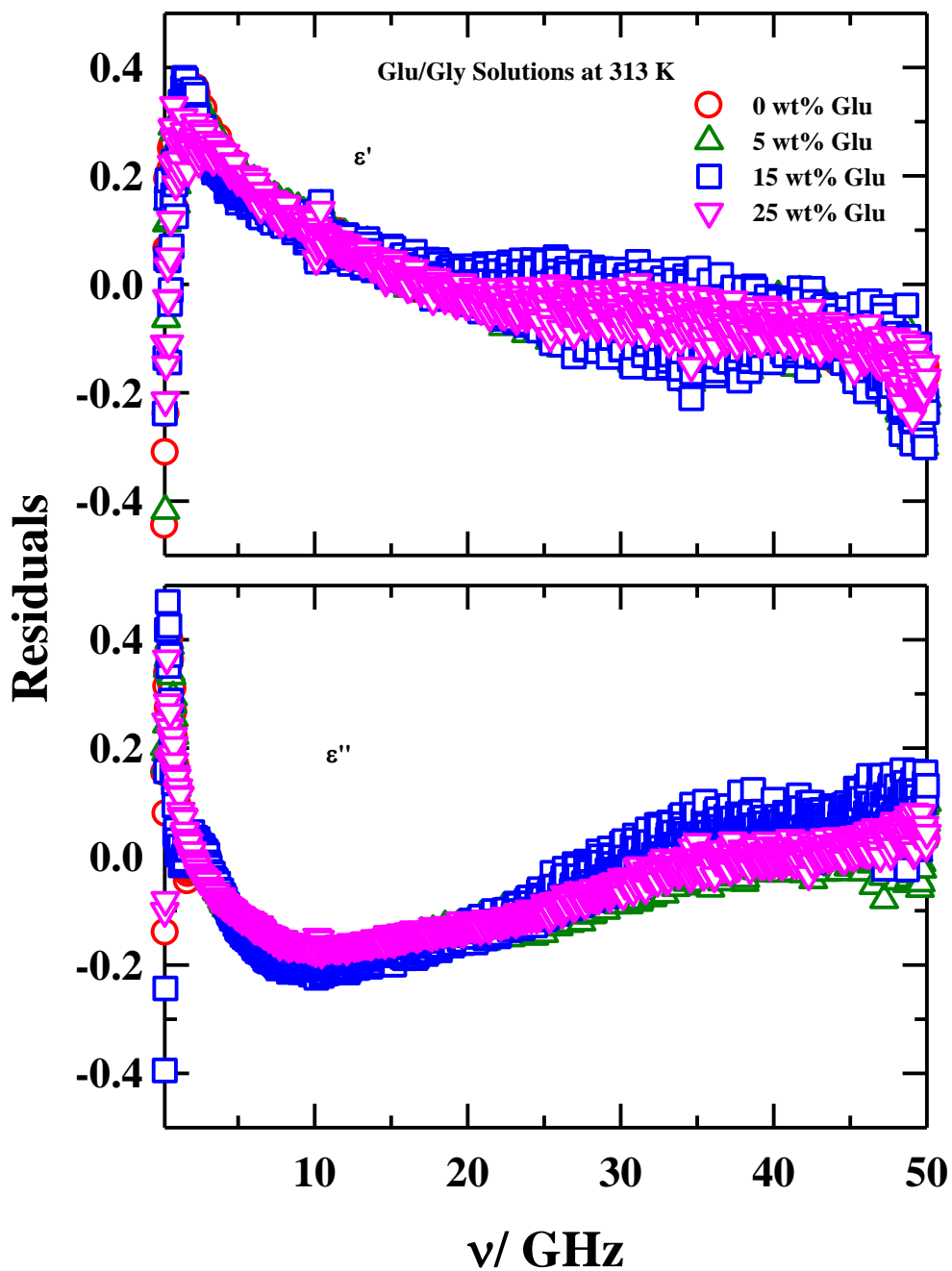


Figure A.a.3: Residuals for real (ϵ') (upper panel) and imaginary (ϵ'') (lower panel) components of complex dielectric spectra for various Glu concentrations in Glu/Gly solutions at a representative temperature (313 K). All representations are colour-coded.

Appendix A.a

Table A.a.4: Individual viscosity coefficient (η) and dielectric relaxation time ($\langle \tau_{DR} \rangle$) ratios between two temperature (313 and 333 K) for four Glu wt% in Glu/Gly solutions.

Ratio	0 wt%	5 wt%	15 wt%	25 wt%
$\frac{\eta^{333K}}{\eta^{313K}}$	3.42	3.59	3.98	4.56
$\frac{\langle \tau_{DR} \rangle^{333K}}{\langle \tau_{DR} \rangle^{313K}}$	2.66	2.11	2.02	3.50

Appendix A.b

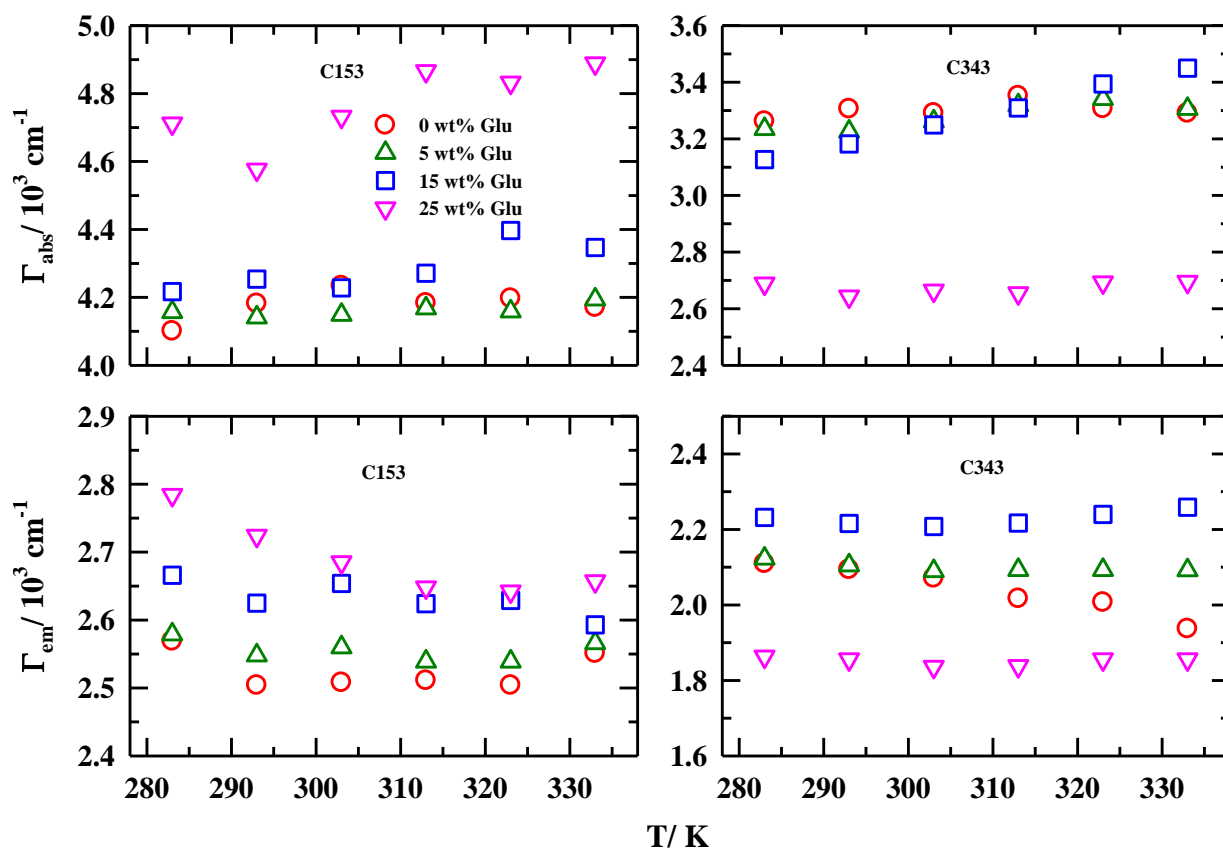


Figure A.b.1: Temperature dependent steady state absorption (upper panels) (Γ_{abs}) and fluorescence emission spectral widths (lower panels) (Γ_{em}) of C153 (left panels) and C343 (right panels) dissolved in Glu/ Gly solutions. All representations are colour-coded.

Table A.b.2: Excited state fluorescence lifetimes of C153 and C343 in Glu/Gly solutions.

T/K	$\langle \tau_{life} \rangle / \text{ns}$					
	C343			C153		
	0 wt%	5 wt%	25 wt%	0 wt%	5 wt%	25 wt%
283	2.98	3.02	3.14	2.72	2.86	4.15
293	3.38	3.08	2.92	2.38	2.41	3.92
303	3.34	3.24	2.83	-	-	3.57
313	3.29	3.25	2.73	-	-	3.41
323	3.40	3.36	3.10	-	-	3.32
333	-	3.34	3.18	-	-	2.67

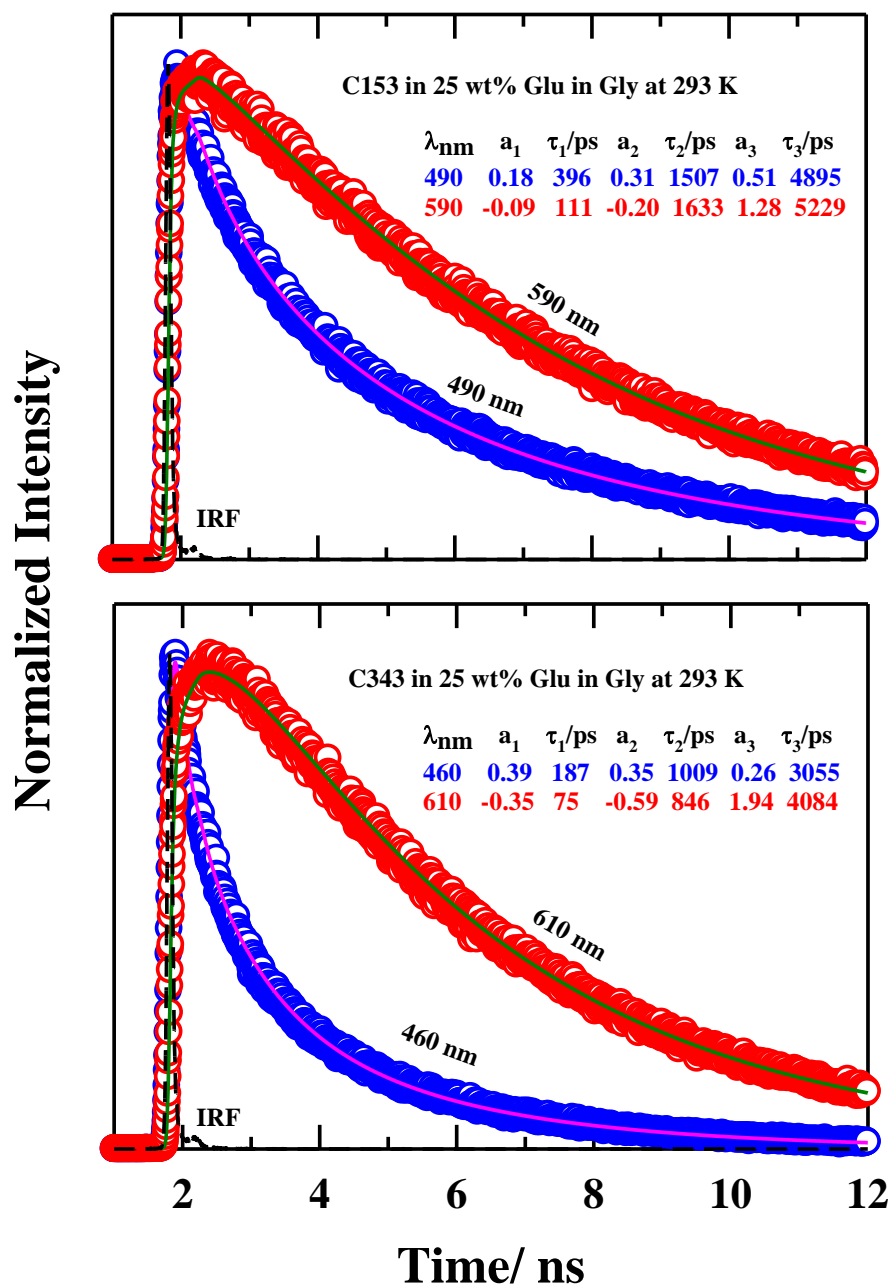


Figure A.b.3: Fluorescence intensity decays of C153 (upper panel) and C343 (lower panel) at blue and red end wavelengths of the respective steady state emission spectrum in 25 wt% Glu containing solution at 293 K. Experimental data points are represented by circles while solid lines denote the corresponding tri-exponential fits. Fit parameters are shown in the insets. Black dashed lines are the instrumental response function. All presentations are colour-coded.

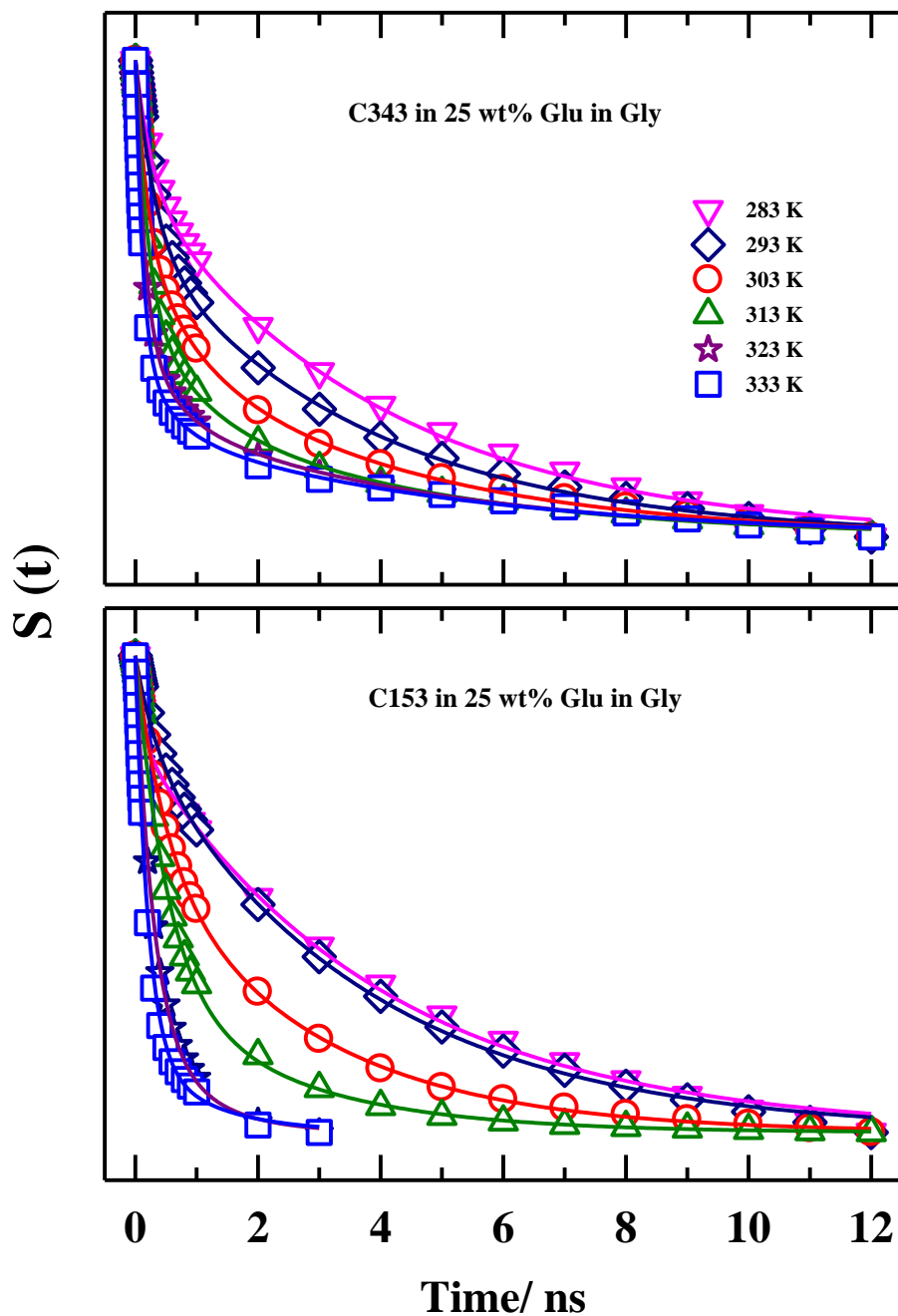


Figure A.b.4: Temperature dependent decays of the measured solvation response function ($S(t)$) of C343 (upper panel) and C153 (lower panel) at 25 wt% of Glu in Gly. Experimental data points for $S(t)$ are shown by symbols; solid lines passing through the data represent fits. All presentations are colour-coded.

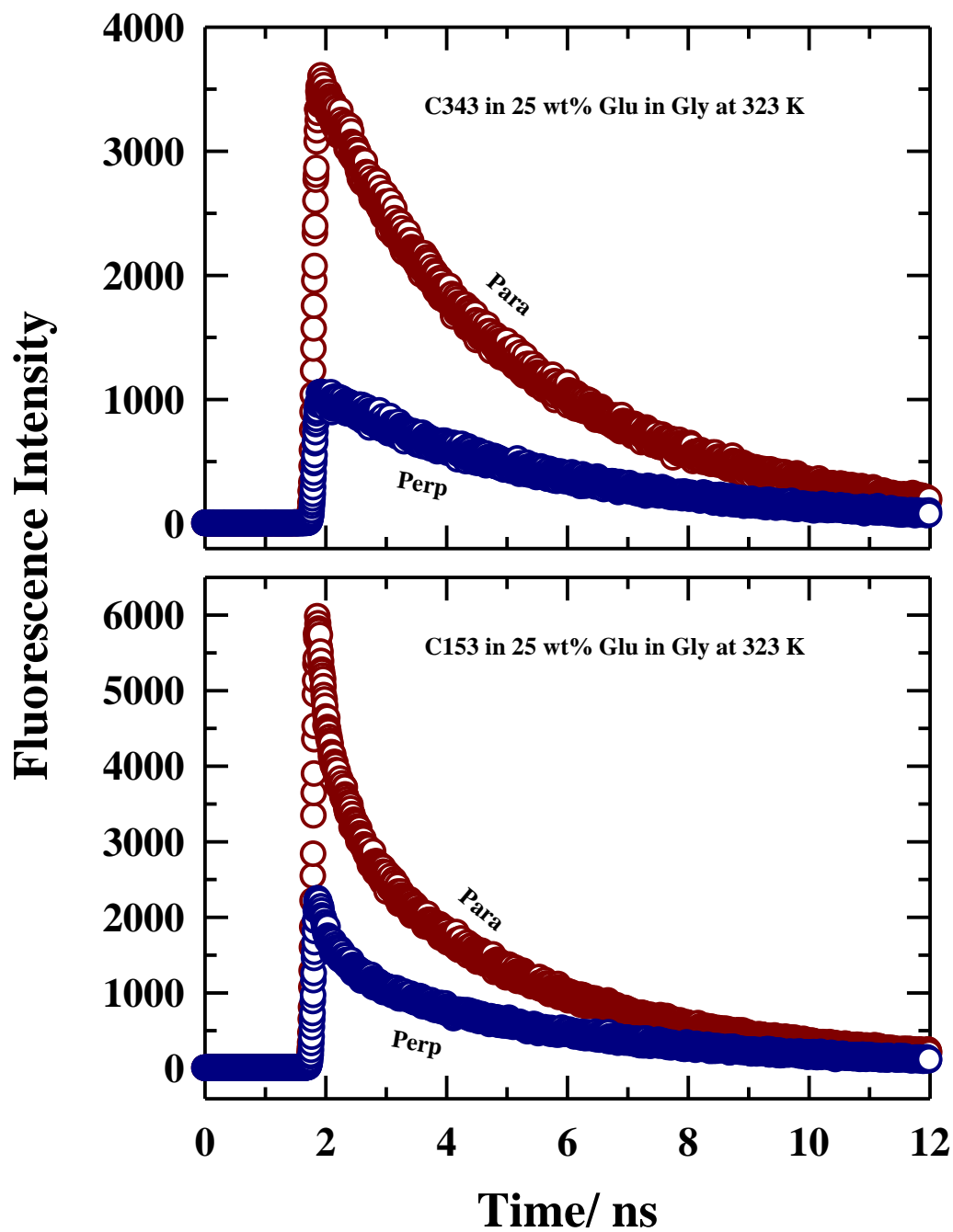


Figure A.b.5: Fluorescence intensity decays of C343 (upper panel) and C153 (lower panel) at parallel and perpendicular polarizations (with respect to vertically polarized excitation) in 25 wt% Glu containing solution at 323 K. Experimental data points are represented by circles. All presentations are colour-coded.

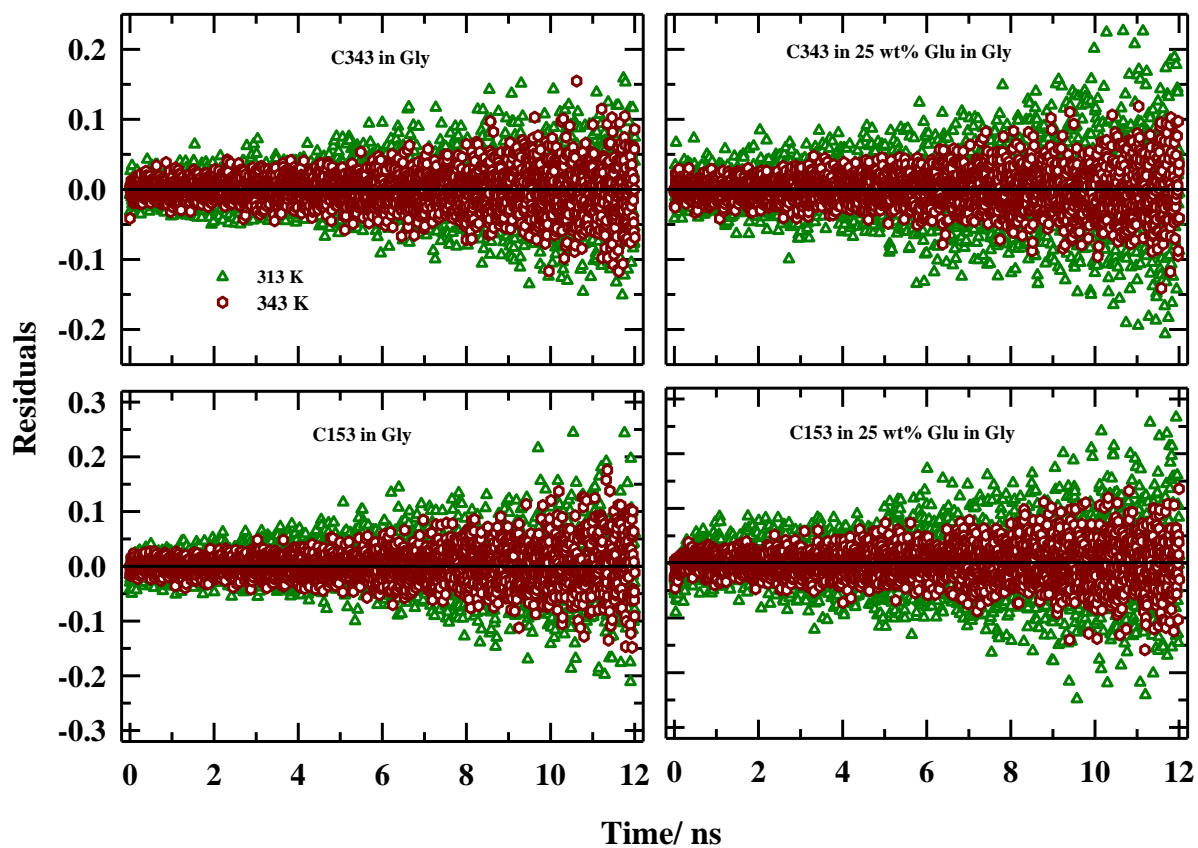


Figure A.b.6: Residuals of $r(t)$ decays of C343 (upper panels) and C153 (lower panels) of Gly (left panels) and in 25 wt% Glu containing solution (right panels) at 313 and 343 K. All representations are colour-coded.

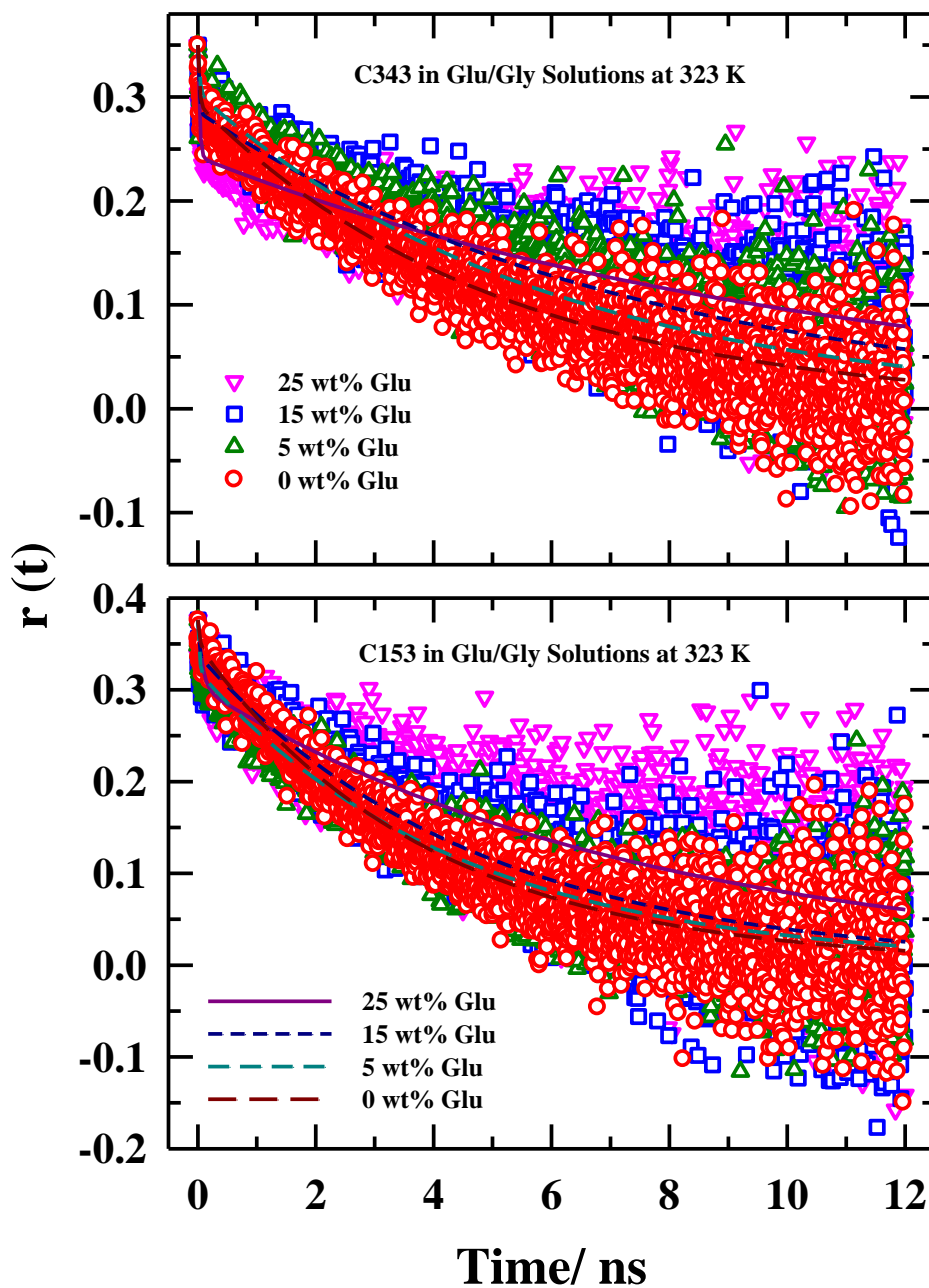


Figure A.b.7: Rotational anisotropy ($r(t)$) decays of C343 (upper panel) and C153 (lower panel) in various Glu wt% in Glu/ Gly solutions at 323 K. Symbols represent experimental data while lines passing through data points are multi-exponential fits. All representations are colour-coded.

Appendix A.b

Table A.b.8: Average rotational times, $\langle \tau_{rot} \rangle$ for C153 and C343 in Glu/Gly solutions obtained from dynamic anisotropy measurements and predictions from the SED relation using the stick and the slip boundary conditions at different Glu concentrations and temperatures.

Glu wt%	T/K	η /cP	C153 rotation			C343 rotation		
			Measured $\langle \tau_{rot} \rangle$ /ns	Predicted $\langle \tau_{rot} \rangle$ /ns from SED relation		Measured $\langle \tau_{rot} \rangle$ /ns	Predicted $\langle \tau_{rot} \rangle$ /ns from SED relation	
				Stick	Slip		Stick	Slip
0	313	298	4.82	29.02	6.97	6.32	33.36	6.01
	318	211	4.32	20.23	4.85	4.70	23.25	4.19
	323	153	3.59	14.44	3.47	4.27	16.60	2.99
	328	114	2.63	10.59	2.54	3.81	12.18	2.19
	333	87	2.22	7.96	1.91	3.59	9.15	1.65
	338	67	1.80	6.04	1.45	2.65	6.95	1.25
	343	53	1.32	4.71	1.13	2.13	5.41	0.97
5	313	399	5.00	38.86	9.33	6.41	44.67	8.04
	318	280	3.96	26.84	6.44	5.88	30.85	5.55
	323	201	3.70	18.97	4.55	5.18	21.81	3.93
	328	148	2.90	13.75	3.30	4.30	15.81	2.85
	333	111	2.63	10.16	2.44	3.78	11.68	2.10
	338	84	1.87	7.58	1.82	2.68	8.71	1.57
	343	66	1.51	5.87	1.41	2.58	6.74	1.21
15	313	685	6.83	66.71	16.01	7.33	76.69	13.80
	318	467	5.43	44.77	10.74	7.01	51.46	9.26
	323	327	4.16	30.86	7.41	6.11	35.48	6.39
	328	236	3.74	21.93	5.26	5.56	25.21	4.54
	333	172	3.54	15.74	3.78	4.74	18.10	3.26
	338	129	3.10	11.63	2.79	4.26	13.37	2.41
	343	98	2.27	8.71	2.09	3.80	10.01	1.80
25	313	1446	8.42	140.82	33.80	8.65	161.88	29.14
	318	954	6.68	91.45	21.95	8.20	105.12	18.92
	323	647	6.04	61.06	14.65	7.52	70.19	12.63
	328	448	5.60	41.63	9.99	6.67	47.86	8.62
	333	317	5.52	29.02	6.96	5.58	33.36	6.00
	338	230	4.59	20.74	4.98	5.35	23.84	4.29
	343	170	4.05	15.11	3.63	3.72	17.37	3.13

Appendix A.c

Table A.c.1: Temperature dependent densities (ρ) of the solvent mixture [9.795{xEC+(1-x)PC}] and electrolyte solutions [9.795{xEC+(1-x)PC}+0.869LiClO₄].

T/ K	Density (ρ /gcm ⁻³) of [9.795{xEC+(1-x)PC}]					
	x _{EC} = 0	x _{EC} = 0.204	x _{EC} = 0.409	x _{EC} = 0.613	x _{EC} = 0.817	x _{EC} = 1
293	1.21	1.23	1.25	1.28	1.31	-
298	1.20	-	-	-	-	-
303	1.20	-	-	-	-	-
308	1.19	-	-	-	-	-
313	1.18	-	-	-	-	1.32
318	1.18	-	-	-	-	1.32
T/ K	Density (ρ /gcm ⁻³) of [9.795{xEC+(1-x)PC}+0.869LiClO ₄]					
	x _{EC} = 0	x _{EC} = 0.204	x _{EC} = 0.409	x _{EC} = 0.613	x _{EC} = 0.817	x _{EC} = 1
293	1.26	1.29	1.31	1.34	1.38	1.42
298	1.26	1.28	1.31	1.34	1.37	1.40
303	1.25	1.28	1.30	1.33	1.36	1.40
308	1.25	1.27	1.30	1.33	1.36	1.39
313	1.24	1.27	1.29	1.32	1.35	1.38
318	1.24	1.26	1.29	1.32	1.35	1.38

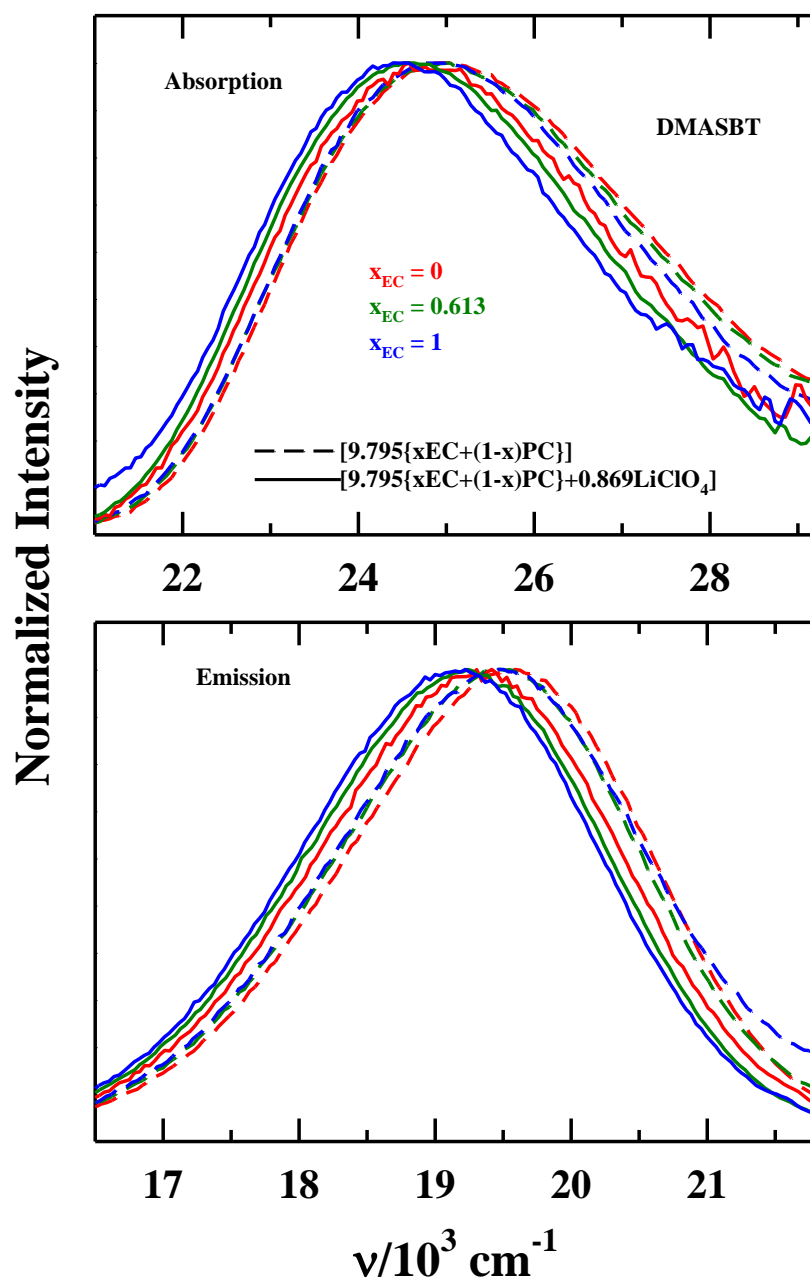


Figure A.c.2: Steady-state absorption (upper panel) and emission spectra (lower panel) of DMASBT for three mole fraction of EC (x_{EC}) in the binary solvent mixtures, $[9.795\{x_{EC}+(1-x)PC\}]$ and electrolyte solutions, $[9.795\{x_{EC}+(1-x)PC\}+0.869LiClO_4]$ at 293 K, and corresponding spectrum in neat EC at 313 K. All presentations are colour-coded.

Table A.c.3: Absorption and emission frequencies and spectral widths of C153 in [9.795{xEC+(1-x)PC}] and [9.795{xEC+(1-x)PC}+0.869LiClO₄] at 293 K.

[9.795{xEC+(1-x)PC}]				
	Absorption		Emission	
x _{EC}	Spectral Width(FWHM)/ 10 ³ cm ⁻¹	Average Frequency/ 10 ³ cm ⁻¹	Spectral Width(FWHM)/ 10 ³ cm ⁻¹	Average Frequency/ 10 ³ cm ⁻¹
0	3.962	23.871	2.882	18.897
0.204	3.935	23.827	2.914	18.865
0.409	4.113	23.892	2.897	18.833
0.613	4.114	23.871	2.908	18.834
0.817	4.056	23.842	2.877	18.768
1 (313K)	4.193	23.833	2.908	18.775
[9.795{xEC+(1-x)PC}+0.869LiClO ₄]				
	Absorption		Emission	
x _{EC}	Spectral Width(FWHM)/ 10 ³ cm ⁻¹	Average Frequency/ 10 ³ cm ⁻¹	Spectral Width(FWHM)/ 10 ³ cm ⁻¹	Average Frequency/ 10 ³ cm ⁻¹
0	4.304	23.413	2.753	18.502
0.204	4.289	23.391	2.783	18.470
0.409	4.245	23.364	2.750	18.453
0.613	4.324	23.397	2.693	18.440
0.817	4.312	23.359	2.704	18.407
1	4.273	23.306	2.686	18.373

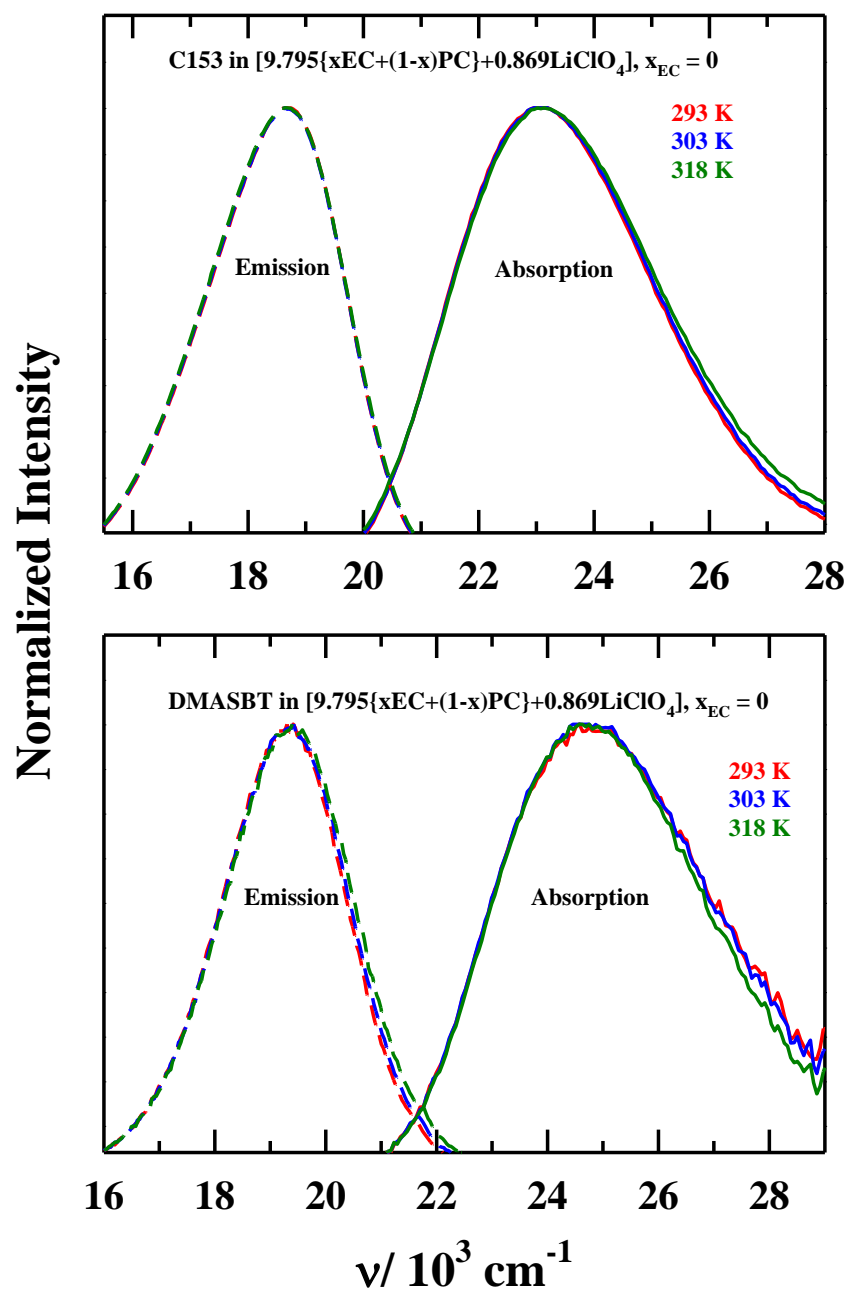


Figure A.c.4: Representative temperature dependent steady state absorption and emission spectra of C153 (upper panel) and DMASBT (lower panel) in $[9.795\{x_{\text{EC}}+(1-x)\text{PC}\}+0.869\text{LiClO}_4]$ at $x_{\text{EC}}=0$. All presentations are colour-coded.

Appendix A.c

Table A.c.5: Temperature dependent average life-time ($\langle \tau_{\text{life}} \rangle$) of C153 and DMASBT in [9.795{xEC+(1-x)PC}+0.869LiClO₄] at 293K.^a

A: DMASBT							B: C153
x _{EC}	T/ K	a ₁	τ ₁ / ps	a ₂	τ ₂ / ps	$\langle \tau_{\text{life}} \rangle$ / ps	$\langle \tau_{\text{life}} \rangle$ / ps
0	293	0.99	182	0.01	997	193	5306
	298	0.99	163	0.01	974	173	5210
	303	0.99	144	0.01	901	153	5173
	308	0.99	127	0.01	960	137	5136
	313	0.99	115	0.01	988	124	5077
	318	0.99	102	0.01	948	110	4973
0.613	293	0.97	189	0.03	603	201	-
	298	0.99	169	0.01	640	176	-
	303	0.99	150	0.01	743	158	-
	308	1	135	0	-	135	-
	313	1	121	0	-	121	-
	318	1	110	0	-	110	-
1	293	0.92	198	0.08	390	213	-
	298	0.95	178	0.05	373	188	-
	303	0.96	159	0.04	355	166	-
	308	0.99	147	0.01	521	151	-
	313	1	132	0	-	132	-
	318	1	121	0	-	120	-

^aIndividual time constants are better than $\pm 5\%$ of the reported values for C153 and $\pm 10\%$ for DMASBT.

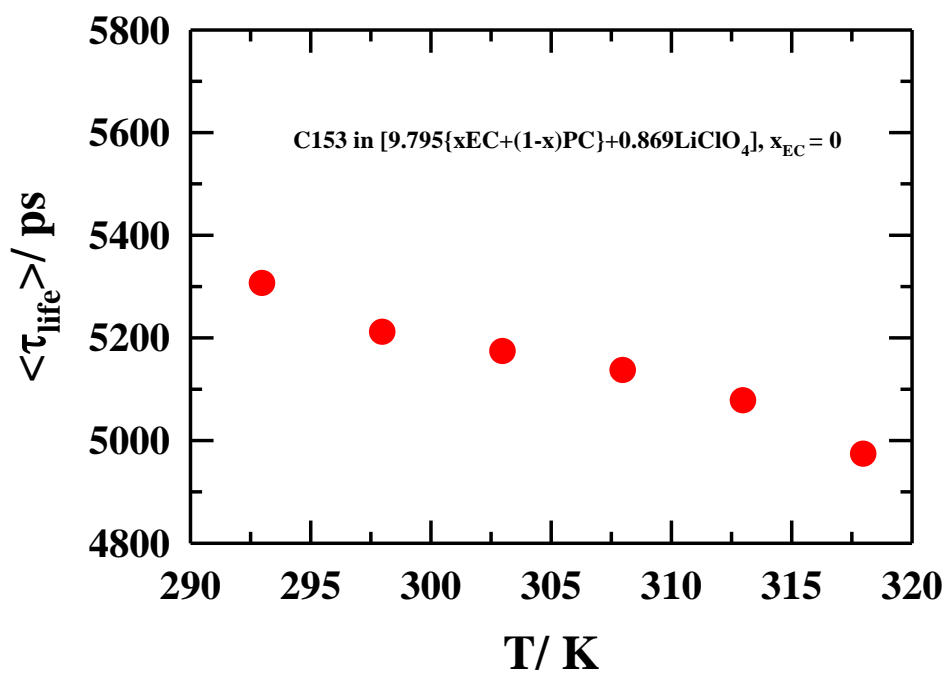


Figure A.c.6: Representative temperature dependent average lifetime ($\langle \tau_{\text{life}} \rangle$) of C153 in [9.795{xEC+(1-x)PC}+0.869LiClO₄] at x_{EC} = 0.

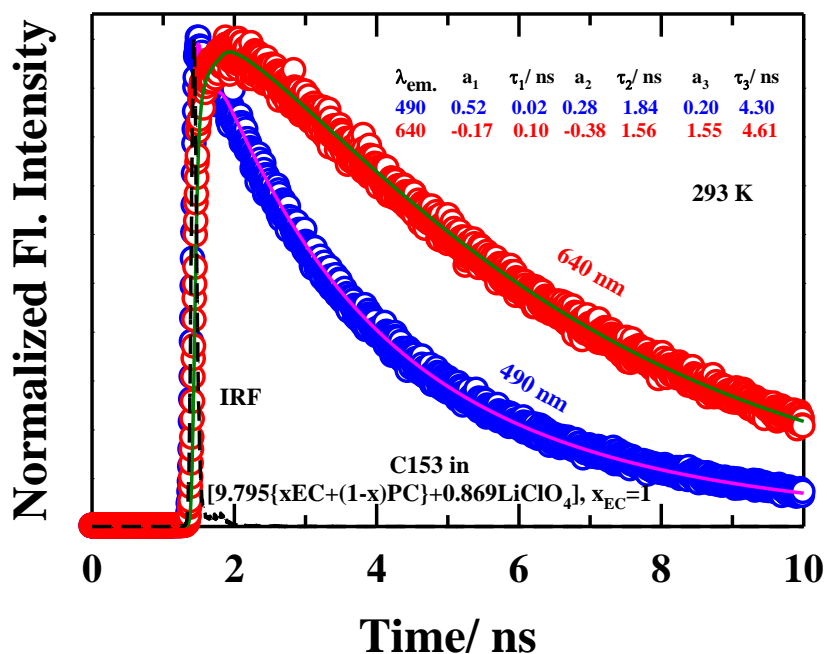


Figure A.c.7: Representative fluorescence intensity decay of C153 in [9.795{xEC+(1-x)PC}+0.869LiClO₄] with $x_{EC} = 1$ collected at blue (490 nm) and red (640 nm) wavelengths with respect to the peak wavelength of the corresponding steady state emission spectrum at 293 K. Experimental data are represented by circles, and solid lines passing through the data are fits. Black dashed lines denote the instrument response function. Multi-exponential decay fit parameters are shown in the inset. All representations are colour-coded.

Table A.c.8: Estimated translational (Stokes-Einstein) and rotational (Stokes-Einstein-Debye) diffusion time¹ of different species in [9.795{xEC+(1-x)PC}+0.869LiClO₄] at x_{EC} =0 at 293K, $\eta = 9.37$ mPas. Radii of Li⁺, PC, ClO₄⁻ are taken from Ref. 2.

Species	Radius/Å	τ_{trans} /ns (stick boundary condition)	τ_{trans} /ns (slip boundary condition)	τ_{rot} /ns (stick boundary condition)
Li ⁺	0.76	0.077	0.051	-
PC	2.76	3.672	2.448	0.612
ClO ₄ ⁻	2.36	2.296	1.530	0.383
Li ⁺ – PC	3.52	7.617	5.078	1.269
ClO ₄ ⁻ – PC	5.12	23.439	15.626	3.906
Li ⁺ – ClO ₄ ⁻	3.12	5.304	3.536	0.884

A. Translational (Stokes-Einstein) diffusion time: Stokes-Einstein equation for translation diffusion constant of a spherical particle with diameter σ in a medium with viscosity η at

temperature T , $D_{\text{trans}} = \frac{k_B T}{C\pi\eta\sigma}$, k_B = Boltzmann constant. The value of $C = 2$ and 3 for slip and

stick limit respectively. Corresponding translational diffusion time τ_{trans} is related to D_{trans} via

$$\tau_{\text{trans}} = \frac{\sigma^2}{D_{\text{trans}}}.^1$$

B. Rotational (Stokes-Einstein-Debye) diffusion time: Stokes-Einstein-Debye equation for rotational diffusion time of a spherical particle with molecular volume V in medium with

viscosity η at temperature T , $\tau_{\text{rot}} = \frac{3V\eta}{k_B T}.^1$

Table A.c.9: Temperature and composition dependent $r(t)$ fit parameters of C153 and DMASBT in $[9.795\{x\text{EC}+(1-x)\text{PC}\}+0.869\text{LiClO}_4]$ solutions.^a

A: C153 in $[9.795\{x\text{EC}+(1-x)\text{PC}\}+0.869\text{LiClO}_4]$						
x_{EC} (mole fraction)	T/ K	a_1	τ_1/ ps	a_2	τ_2/ ps	$\langle \tau_{\text{rot}} \rangle / \text{ps}$
0	293	0.47	255	0.53	762	524
	298	0.41	138	0.59	677	456
	303	0.22	69	0.78	454	369
	308	0.38	124	0.62	476	342
	313	0.46	82	0.54	474	294
	318	0.55	104	0.45	406	240
0.204	293	0.49	191	0.51	849	527
	298	0.51	199	0.49	755	471
	303	0.44	187	0.56	581	408
	308	0.51	149	0.49	575	358
	313	0.40	86	0.60	445	301
	318	0.33	59	0.67	340	247
0.409	293	0.61	268	0.39	1003	555
	298	0.55	213	0.45	856	502
	303	0.48	150	0.52	658	414
	308	0.52	178	0.48	593	377
	313	0.55	147	0.45	534	321
	318	0.45	94	0.55	427	277
0.613	293	0.52	183	0.48	865	510
	298	0.50	205	0.50	771	488
	303	0.38	125	0.62	560	395
	308	0.40	113	0.60	477	331
	313	0.54	144	0.46	489	303
	318	0.67	155	0.33	478	262
0.817	293	0.60	316	0.40	1018	597
	298	0.60	220	0.40	928	503
	303	0.43	153	0.57	618	418
	308	0.51	120	0.49	600	355
	313	0.65	194	0.35	573	327
	318	0.49	113	0.51	401	260
1	293	0.67	298	0.33	1090	559
	298	0.37	147	0.63	609	438
	303	0.57	207	0.43	675	408
	308	0.67	183	0.33	732	364
	313	0.62	165	0.38	546	310
	318	0.40	91	0.60	373	260

Appendix A.c

B: DMASBT in [9.795{xEC+(1-x)PC}+0.869LiClO ₄]						
x _{EC} (mole fraction)	T/ K	a ₁	τ ₁ / ps	a ₂	τ ₂ / ps	⟨τ _{rot} ⟩/ ps
0	293	-	-	1	812	812
	298	0.03	50	0.97	739	718
	303	-	-	1	657	657
	308	-	-	1	605	605
	313	0.10	33	0.90	599	542
0.613	293	0.13	22	0.87	484	424
	298	0.16	39	0.84	477	407
	303	0.08	33	0.92	397	368
	308	0.08	33	0.92	378	350
	313	0.14	42	0.84	374	320
1	293	0.11	33	0.89	411	369
	298	0.12	33	0.88	347	309
	303	0.06	33	0.94	305	289
	308	0.15	32	0.85	311	269
	313	0.18	36	0.82	302	248

“Fit parameters have been obtained after fixing the r_0 value at 0.376 for C153 and 0.38 for DMASBT. Individual time constants are better than $\pm 5\%$ of the reported values for C153 and $\pm 10\%$ for DMASBT.

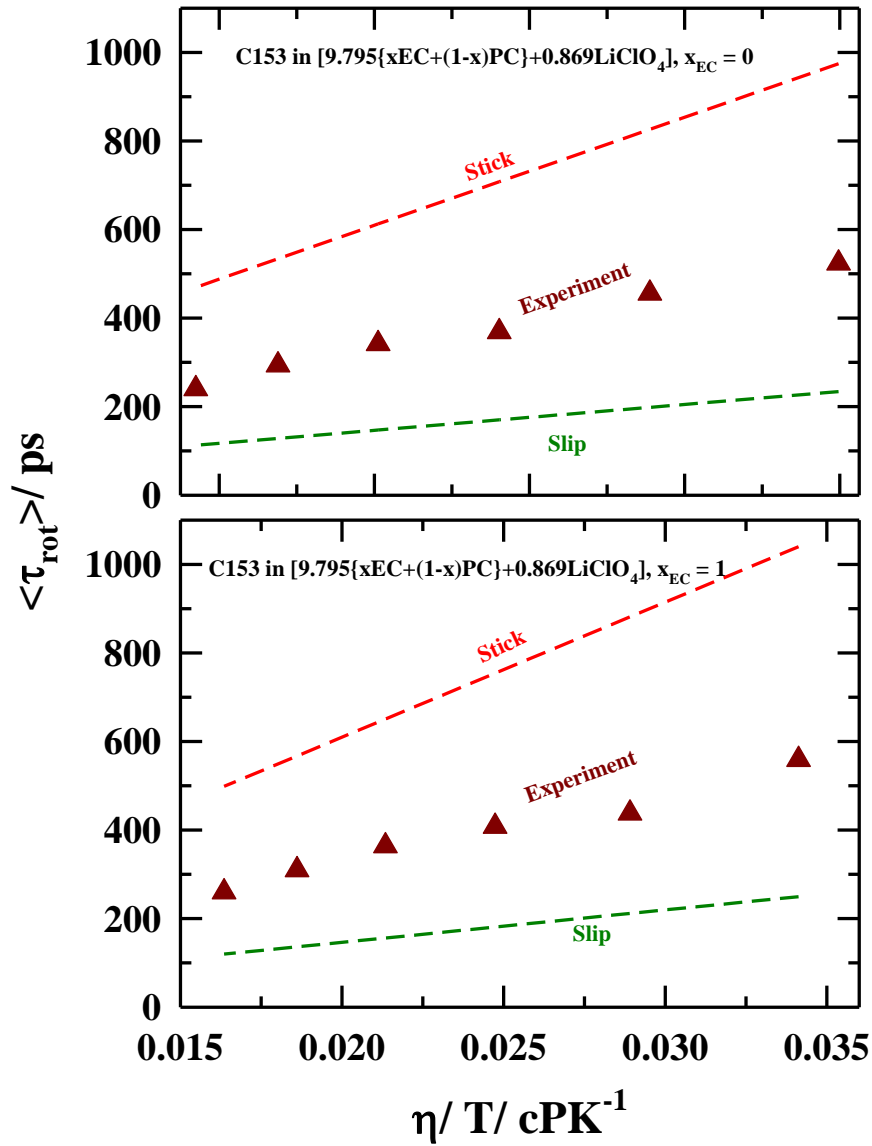


Figure A.c.10: Representative plot of average rotation time ($\langle \tau_{\text{rot}} \rangle$) versus temperature-reduced viscosity (η/T) of C153 in electrolyte solution, [9.795{xEC+(1-x)PC}+0.869LiClO₄], at $x_{\text{EC}} = 0$ (upper panel) and 1 (lower panel). Red and green dashed lines represent the stick and the slip hydrodynamic limits, respectively. Triangles represent measured rotation times.

References

1. B. Bagchi, *Molecular relaxation in liquids* (Oxford University Press, New York, 2012).
2. M. Ue, J. Electrochem. Soc. **141** 3336 (1994).

Appendix A.d

Table A.d.1: Temperature and PPG wt% dependent viscosity coefficients (η) and densities (ρ) of polymer gel electrolyte, [(PC+LiClO₄)+ wt%PPG].

wt% of PPG in [(PC+LiClO ₄)+wt%PPG]	η /cP					
	293 K	298 K	303 K	308 K	313 K	318 K
0	9.37	8.08	7.04	6.19	5.48	4.90
10	8.54	7.35	6.40	5.63	5.02	4.50
20	9.12	7.77	6.73	5.88	5.19	4.62
30	11.91	9.95	8.47	7.29	6.33	5.56
40	16.77	13.76	11.46	9.70	8.28	7.18
50	24.80	19.83	16.17	13.38	11.22	9.59
60	33.84	26.56	21.21	17.28	14.25	11.93
100	98.31	70.79	52.72	40.10	31.22	24.81
	ρ / gcm ⁻³					
0	1.263	1.258	1.253	1.248	1.243	1.238
10	1.232	1.227	1.222	1.217	1.212	1.207
20	1.204	1.199	1.194	1.190	1.185	1.180
30	1.177	1.173	1.168	1.163	1.158	1.154
40	1.150	1.146	1.141	1.137	1.132	1.128
50	1.125	1.121	1.116	1.112	1.107	1.103
60	1.101	1.096	1.092	1.088	1.083	1.079
100	1.008	1.004	1.000	0.996	0.992	0.988

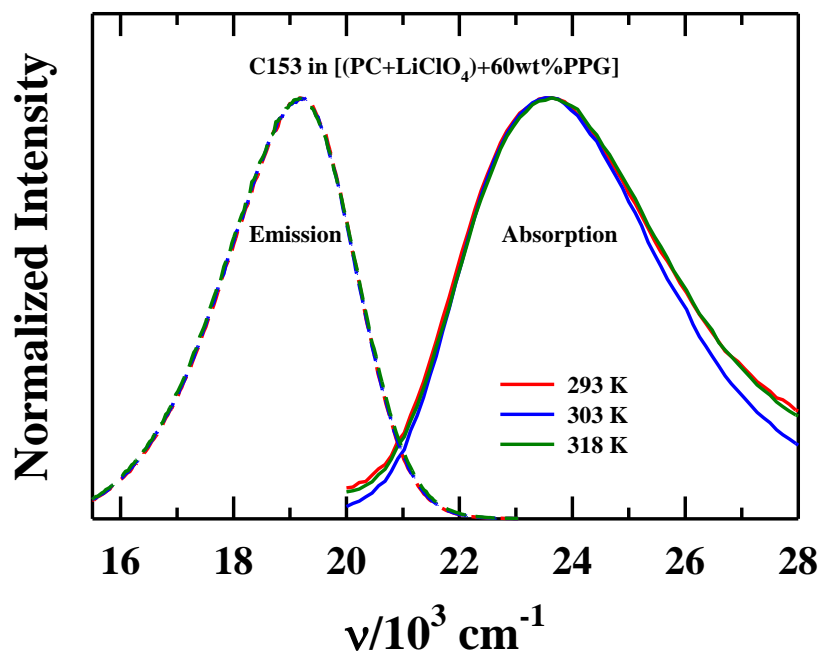


Figure A.d.2: Temperature dependent absorption and emission spectra of C153 in [(PC+LiClO₄)+60wt%PPG]. All representations are colour-coded.

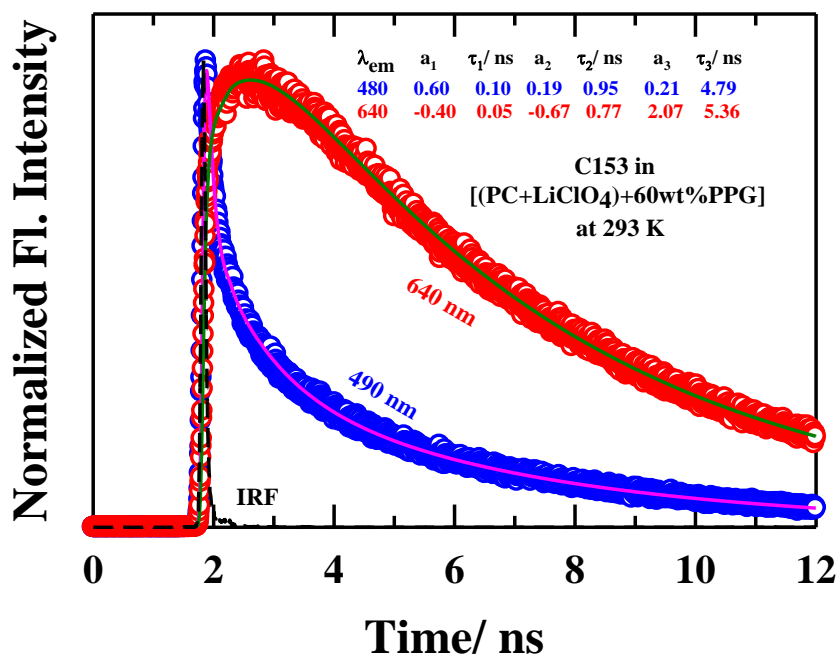


Figure A.d.3: Representative fluorescence intensity decays of C153 with 60wt% in [(PC+LiClO₄)+wt%PPG], collected at blue (490 nm) and red end (640 nm) wavelength with respect to the peak wavelength of the corresponding steady state emission spectrum at 293 K. Experimental data are presented by circles; solid lines passing through the data are fits. Black dashed lines are the instrument response function. Multi-exponential decay fit parameters are shown in the inset. All representations are colour-coded.

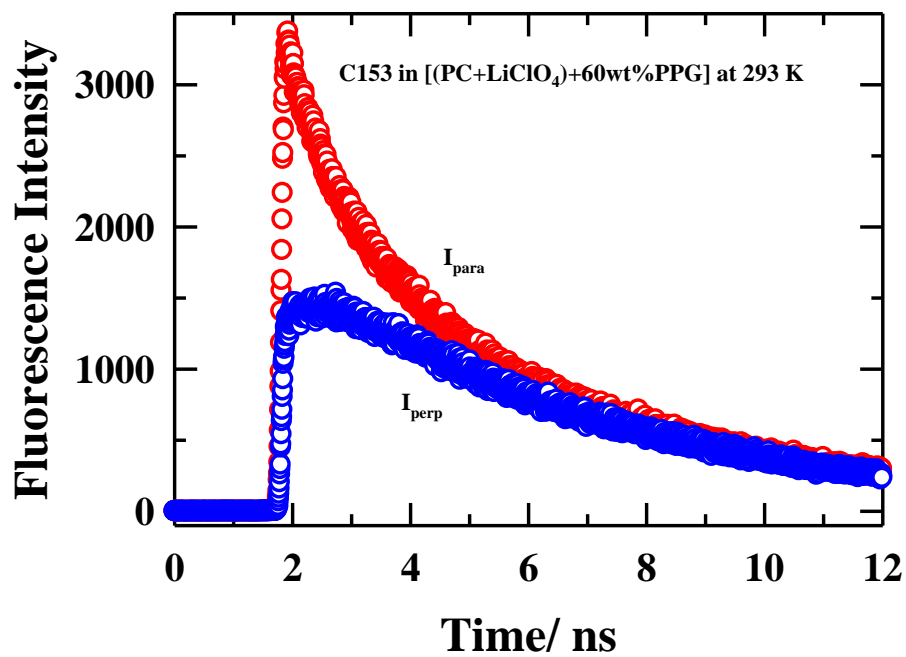


Figure A.d.4: Fluorescence intensity decay at parallel and perpendicular polarization of C153 in [(PC+LiClO₄)+60wt%PPG] at 293 K. All presentations are colour-coded.

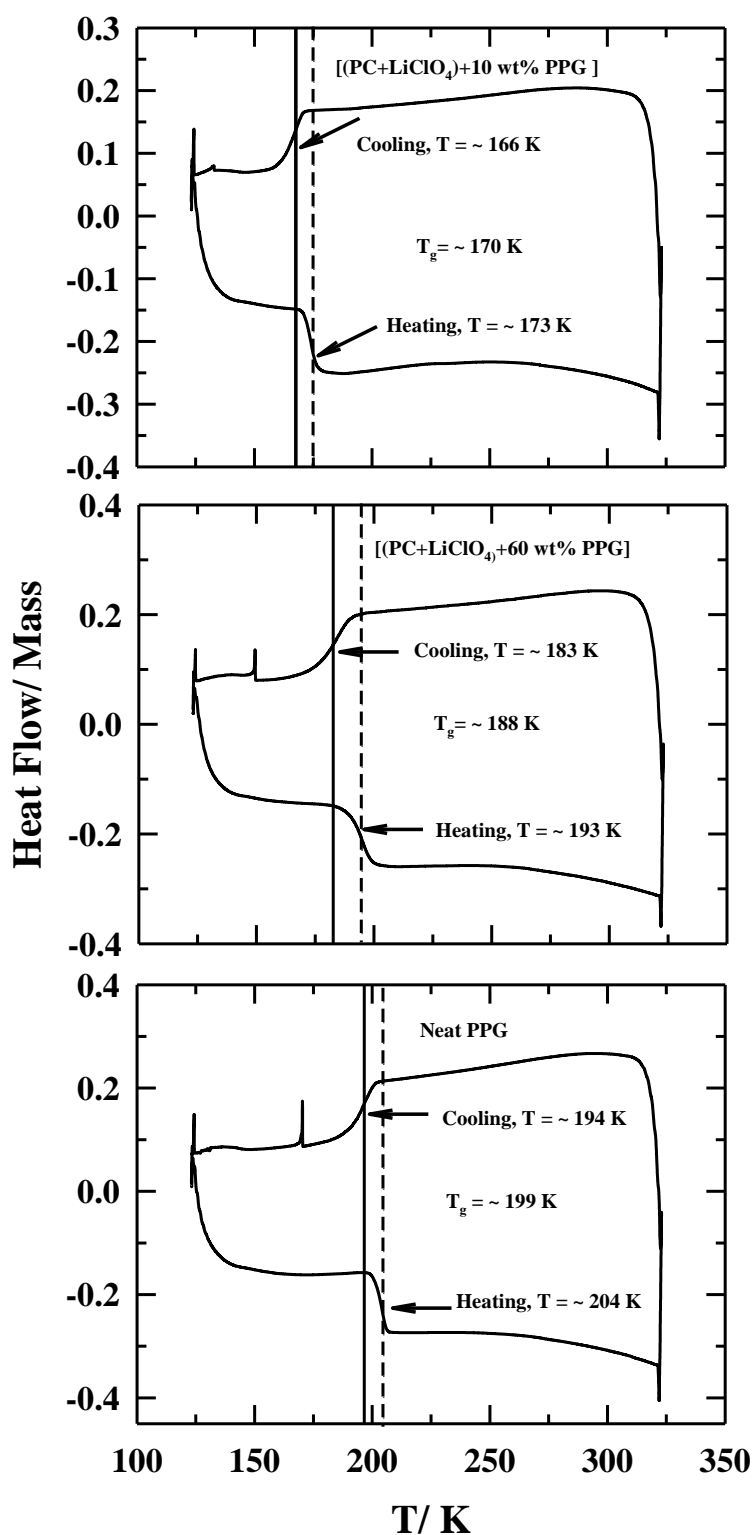


Figure A.d.5: Representative differential scanning calorimetric (DSC) traces for $[(PC+LiClO_4)+\text{wt\% PPG}]$ polymer gel electrolytes. Respective glass transition temperatures are indicated in each panel of the figure.

Appendix A.e

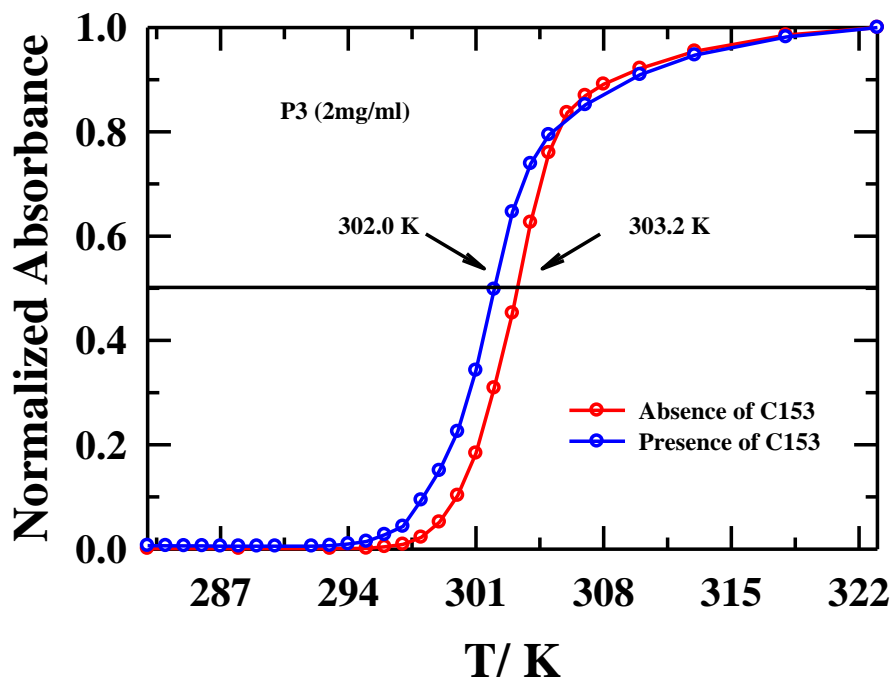


Figure A.e.1: Impact of third component (C153) in T_{cp} determination: temperature dependent absorbance of the aqueous solution (2 mg/mL) of the random copolymer, P3 in presence and absence of C153. Respective T_{cp} for each case are indicated with arrows.

Table A.e.2: Temperature dependent densities (ρ), viscosity coefficients (η) of aqueous solutions (2 mg/mL) of three copolymers P1-P3.

T/K	P1		P2		P3		Water	
	ρ / gcm^{-3}	η / cP						
293	0.997	1.06	0.998	1.05	0.998	1.05	0.998	1.00
298	0.997	0.94	0.997	0.93	0.997	0.94	0.997	0.89
303	0.996	0.85	0.996	0.84	0.995	0.86	0.996	0.80
308	0.994	0.77	0.994	0.76	-	-	0.994	0.72
313	0.993	0.70	0.992	0.70	-	-	0.992	0.65
318	0.991	0.65	-	-	-	-	0.990	0.60
323	0.988	0.61	-	-	-	-	0.988	0.55

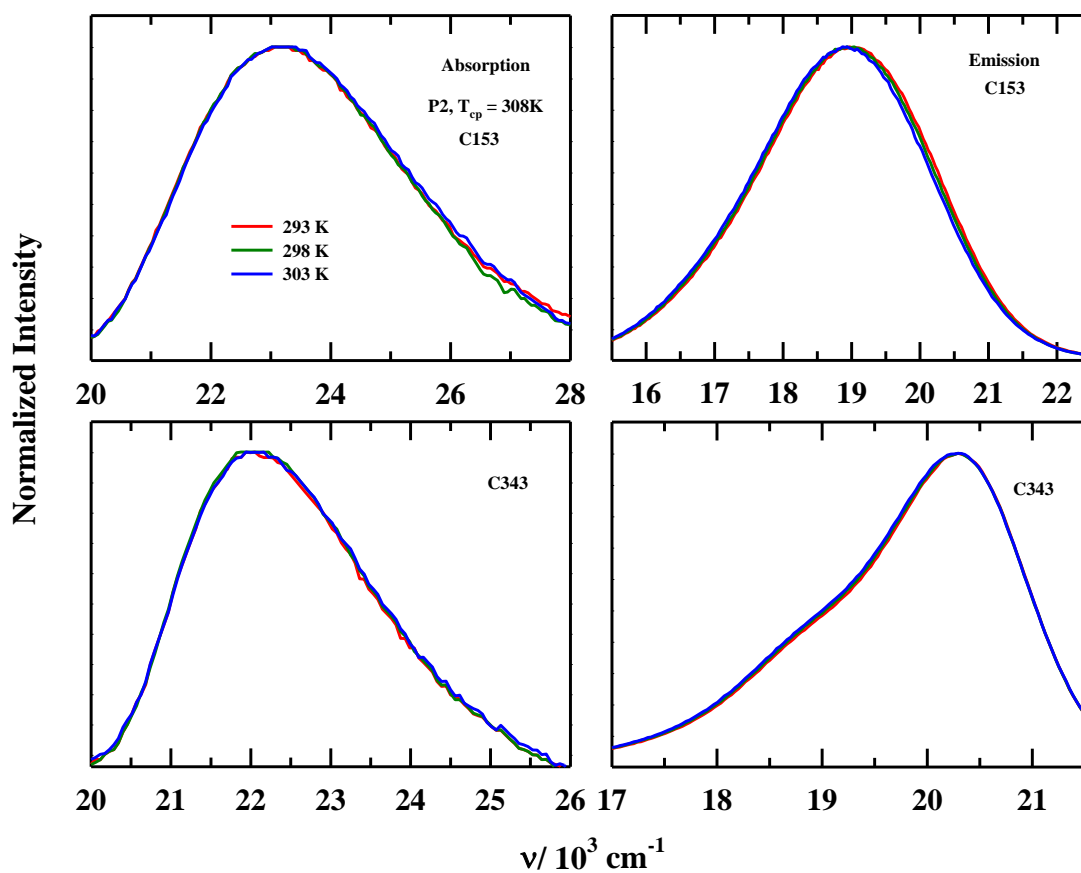


Figure A.e.3: Representative temperature dependent UV-Vis absorption (left panels), and steady state fluorescence emission spectra (right panels) of C153 (upper panels), and C343 (lower panels) in aqueous solutions of P2. All presentations are colour-coded.

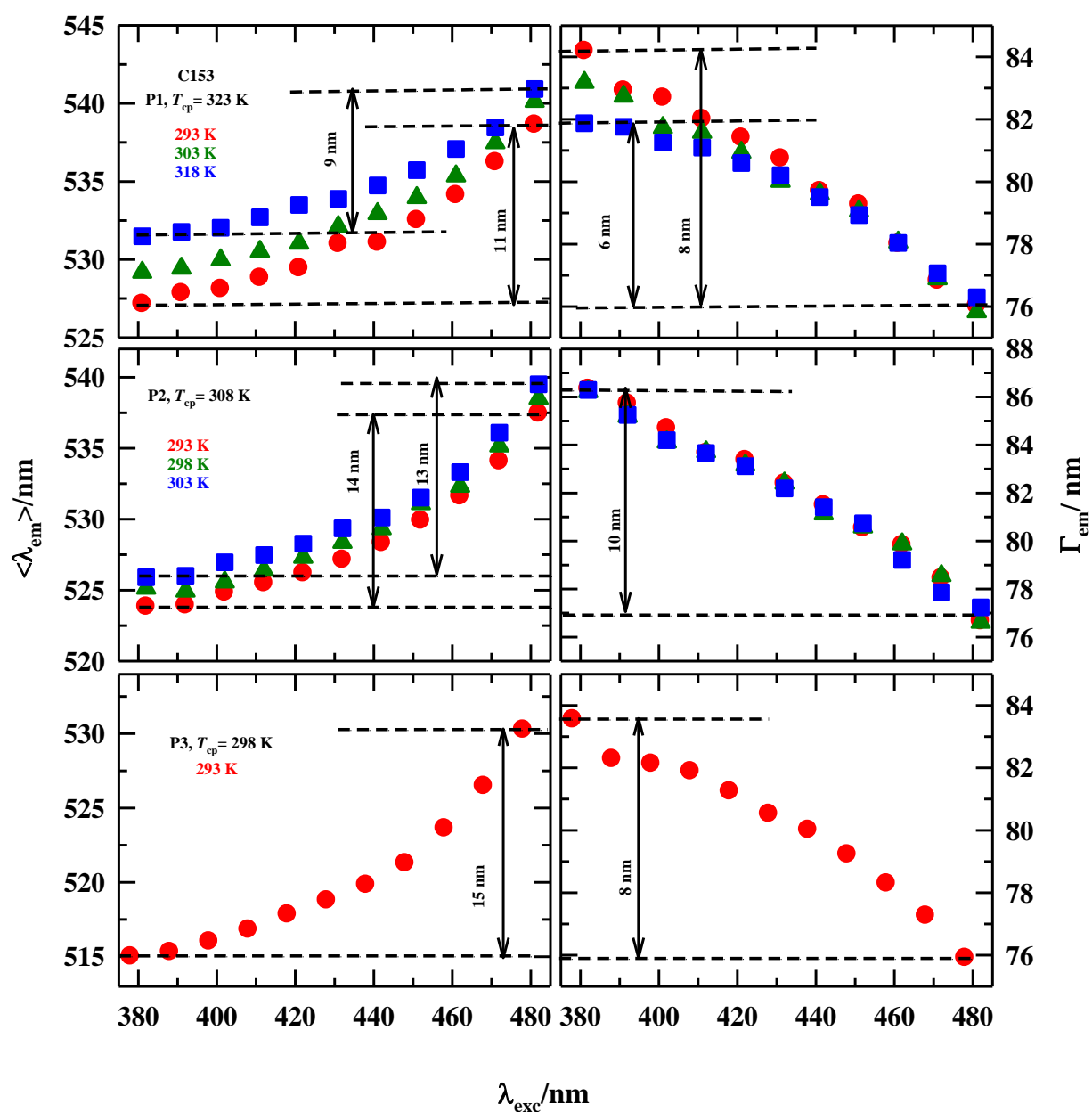


Figure A.e.4: Excitation wavelength dependence (λ_{exc}) of steady state average emission wavelength ($\langle \lambda_{em} \rangle$) (left panels) and spectral widths (FWHM, Γ_{em}) (right panels) of C153 in aqueous P1, P2 and P3 solutions at different temperatures. All representations are colour coded.

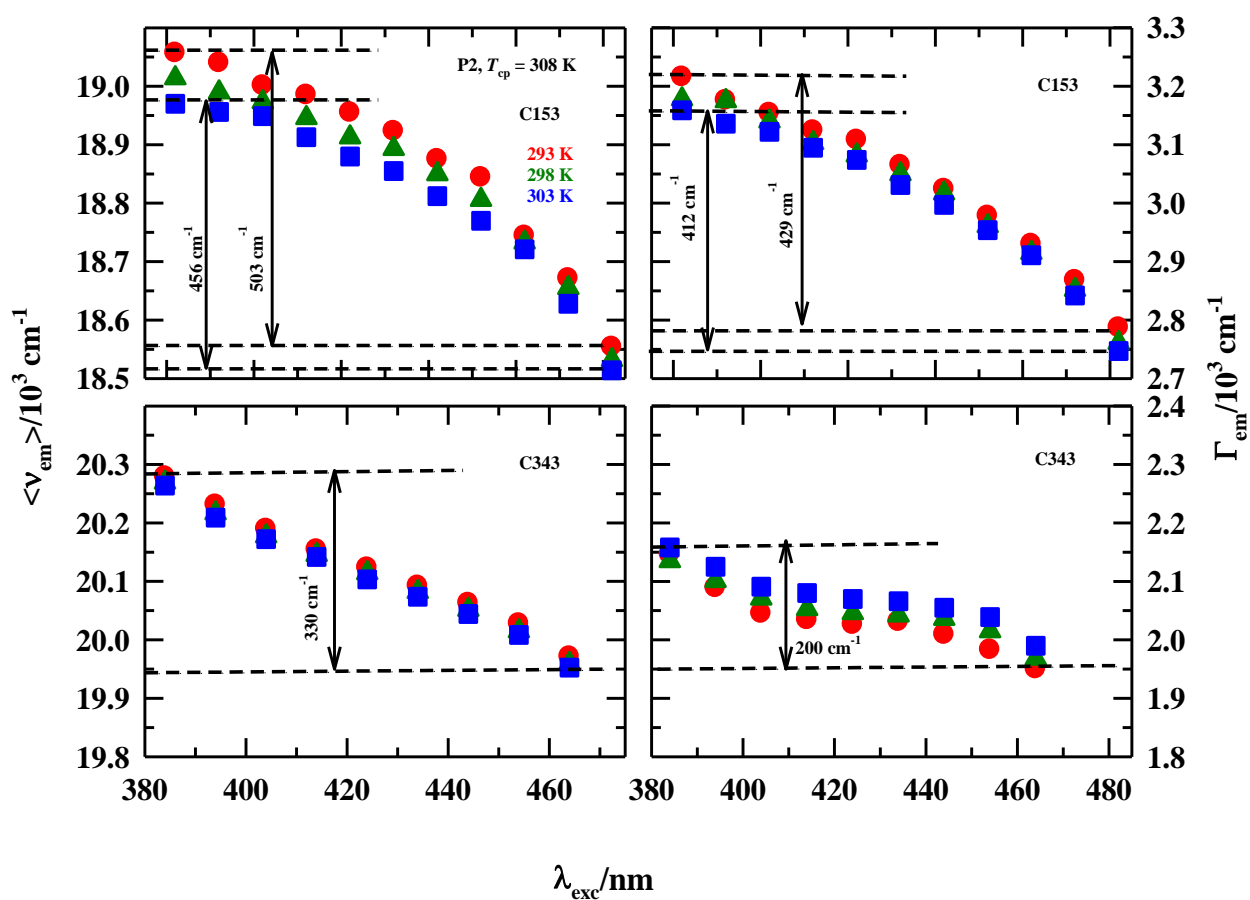


Figure A.e.5: Excitation wavelength dependence (λ_{exc}) of steady state average emission frequencies ($\langle \nu_{\text{em}} \rangle$) (left panels) and spectral widths (FWHM, Γ_{em}) (right panels) of C153 (upper panels) and C343 (lower panels) in aqueous P2 solutions at different temperatures. All representations are colour-coded.

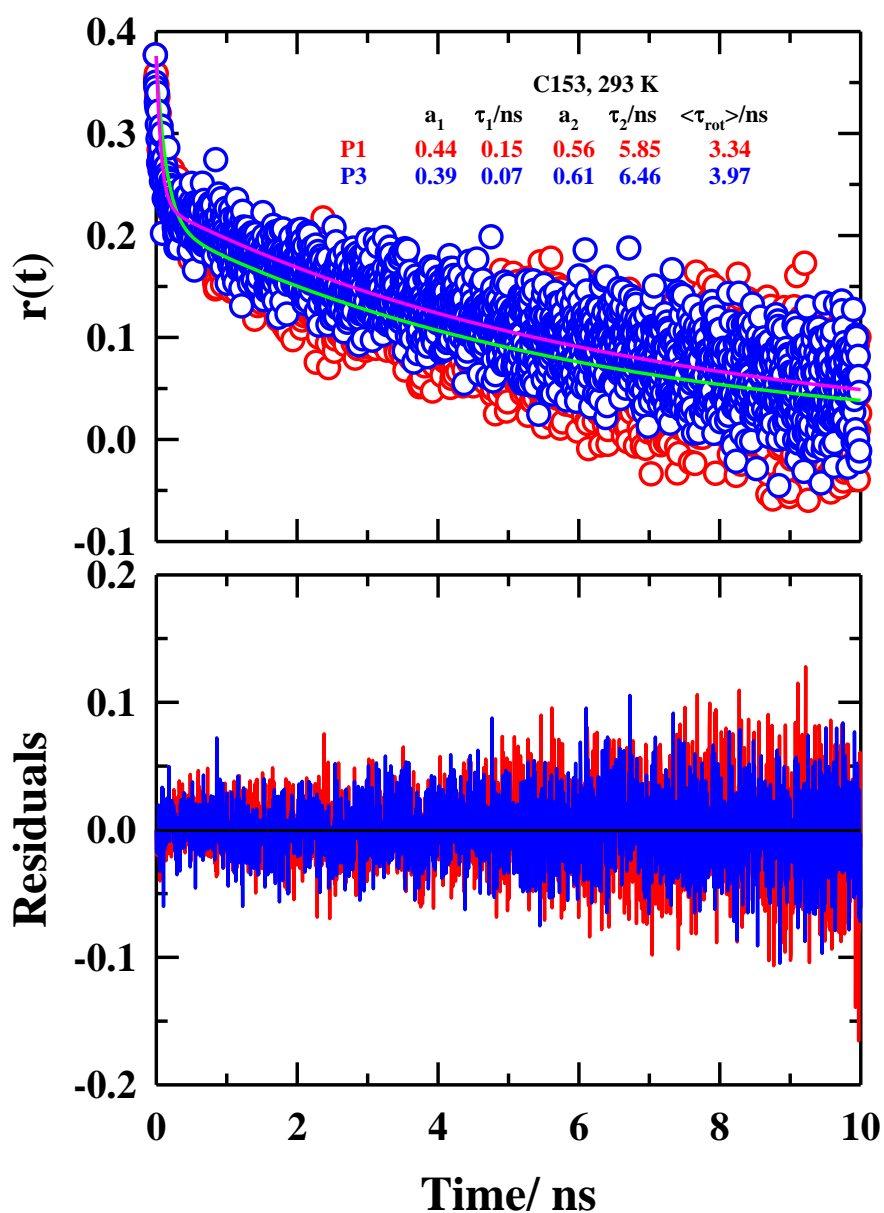


Figure A.e.6: Representative rotational anisotropy, $r(t)$, decays of C153 in aqueous P1 and P3 solutions (upper panel) and corresponding residuals (lower panel) at 293 K. Experimental data are shown by circles; solid lines going through data represent bi-exponential fits. Fit parameters are shown in the inset. All representations are colour-coded.

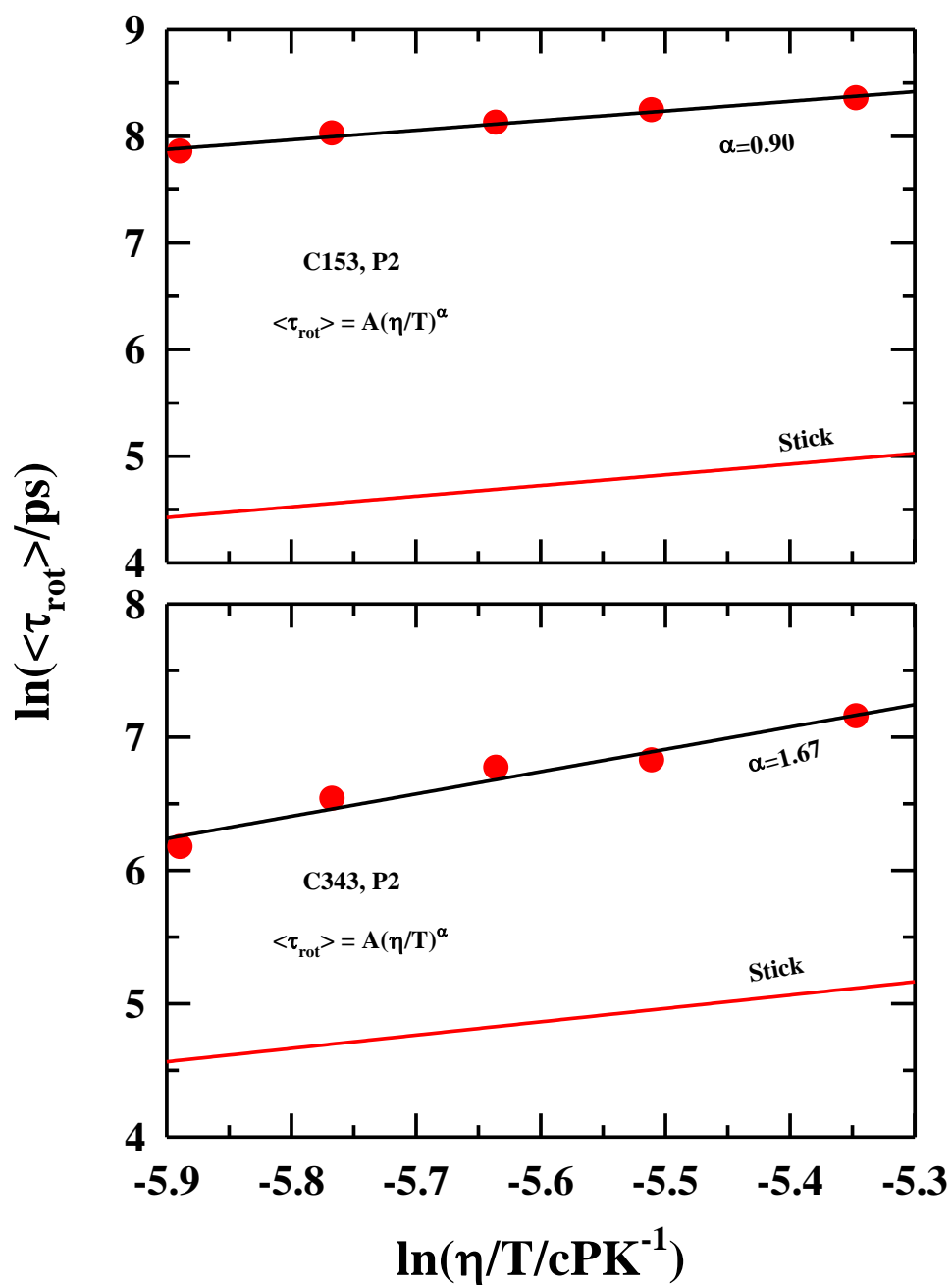


Figure A.e.7: Viscosity coupling of solute rotation in aqueous solution of P2 as observed from temperature dependent measurements, and a comparison with the hydrodynamic prediction.

Appendix A.f

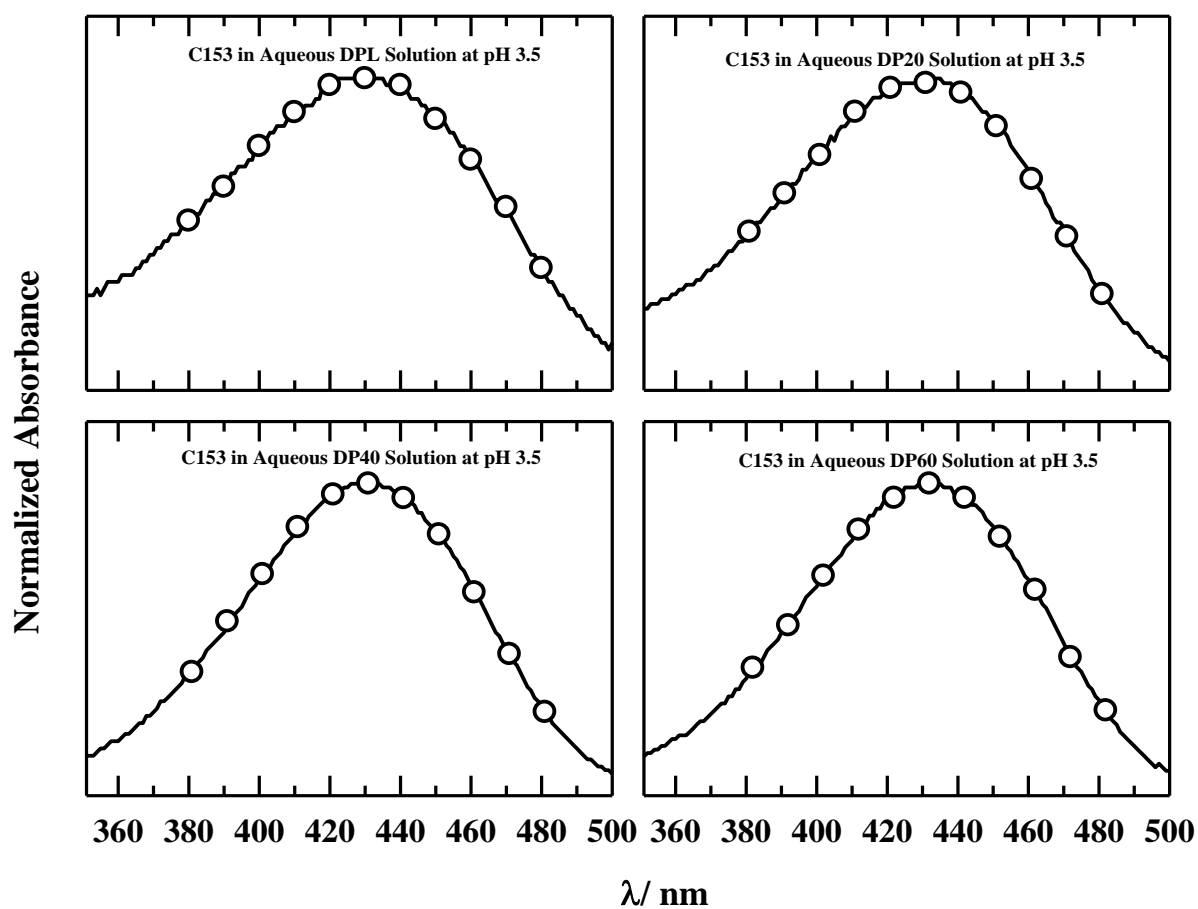


Figure A.f.1: Steady state UV-Vis absorption spectra of C153 in aqueous polymer solutions (1mg/ml) at 298 K. Circles denote λ_{exc} positions considered for λ_{exc} dependent fluorescence emission measurements.

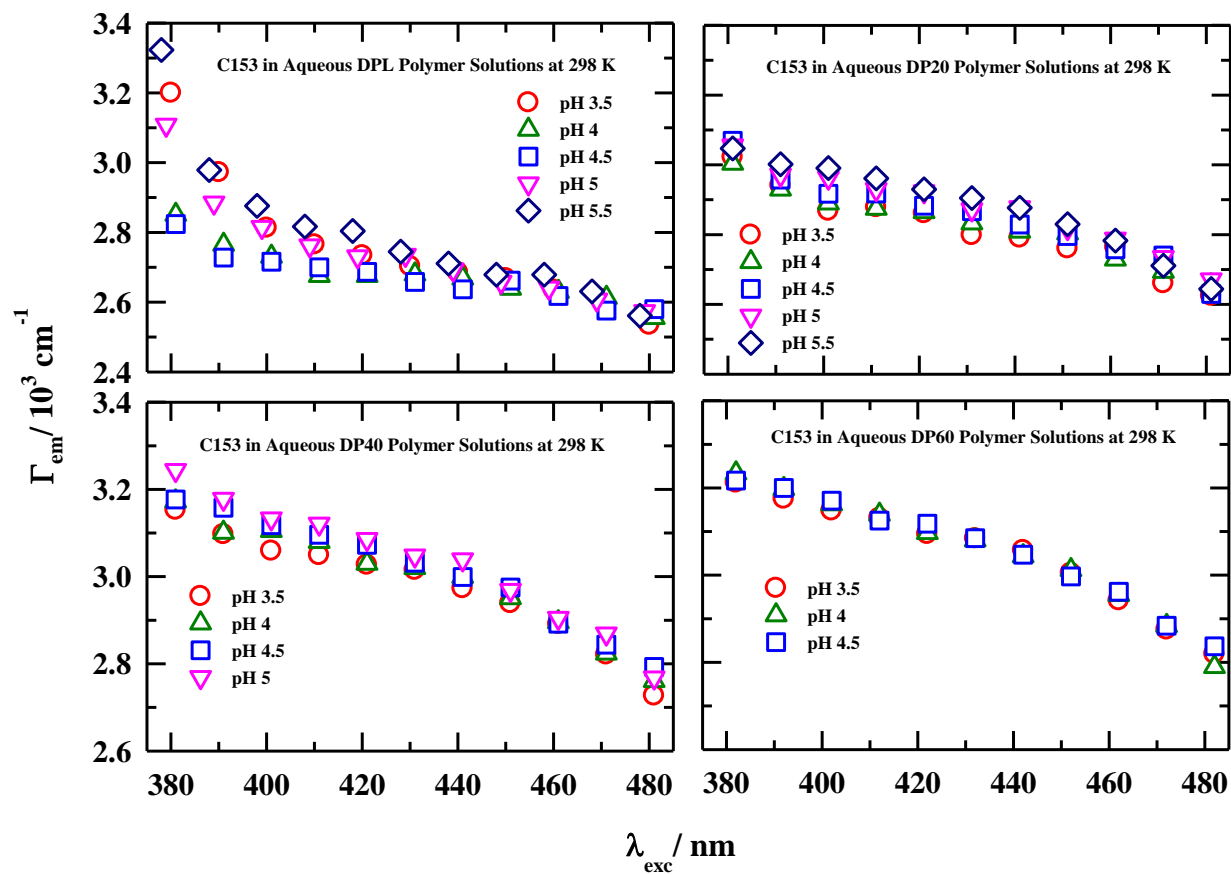


Figure A.f.2: Excitation wavelength (λ_{exc}) dependent emission spectral widths (FWHM, Γ_{em}) of C153 in aqueous polymer solutions (1mg/ml) for various pH at ~298 K. Representations are colour-coded.

Appendix A.f

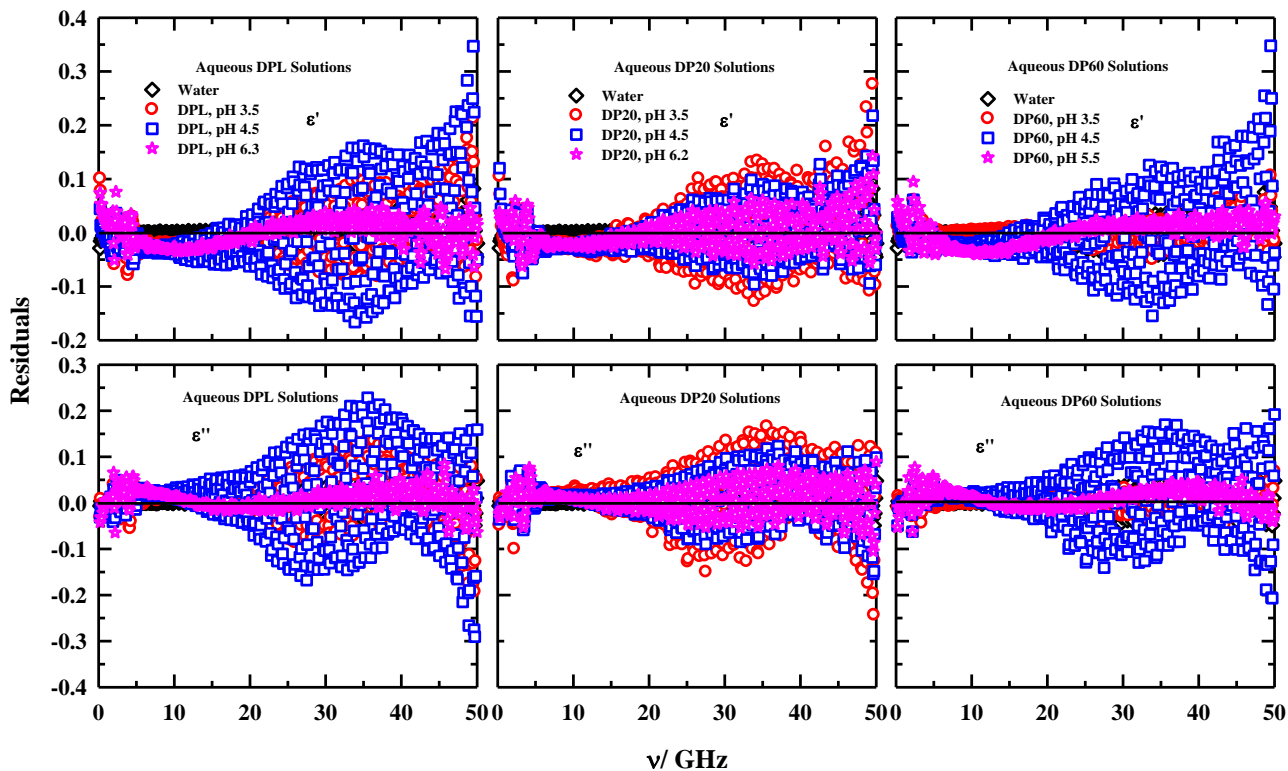


Figure A.f.3: Representative residuals from single Debye (1 D) simultaneous fits of the real (ϵ') and imaginary (ϵ'') parts of the measured complex DR spectra in aqueous copolymer solutions with different pH at ~ 298 K. All presentations are colour-coded.

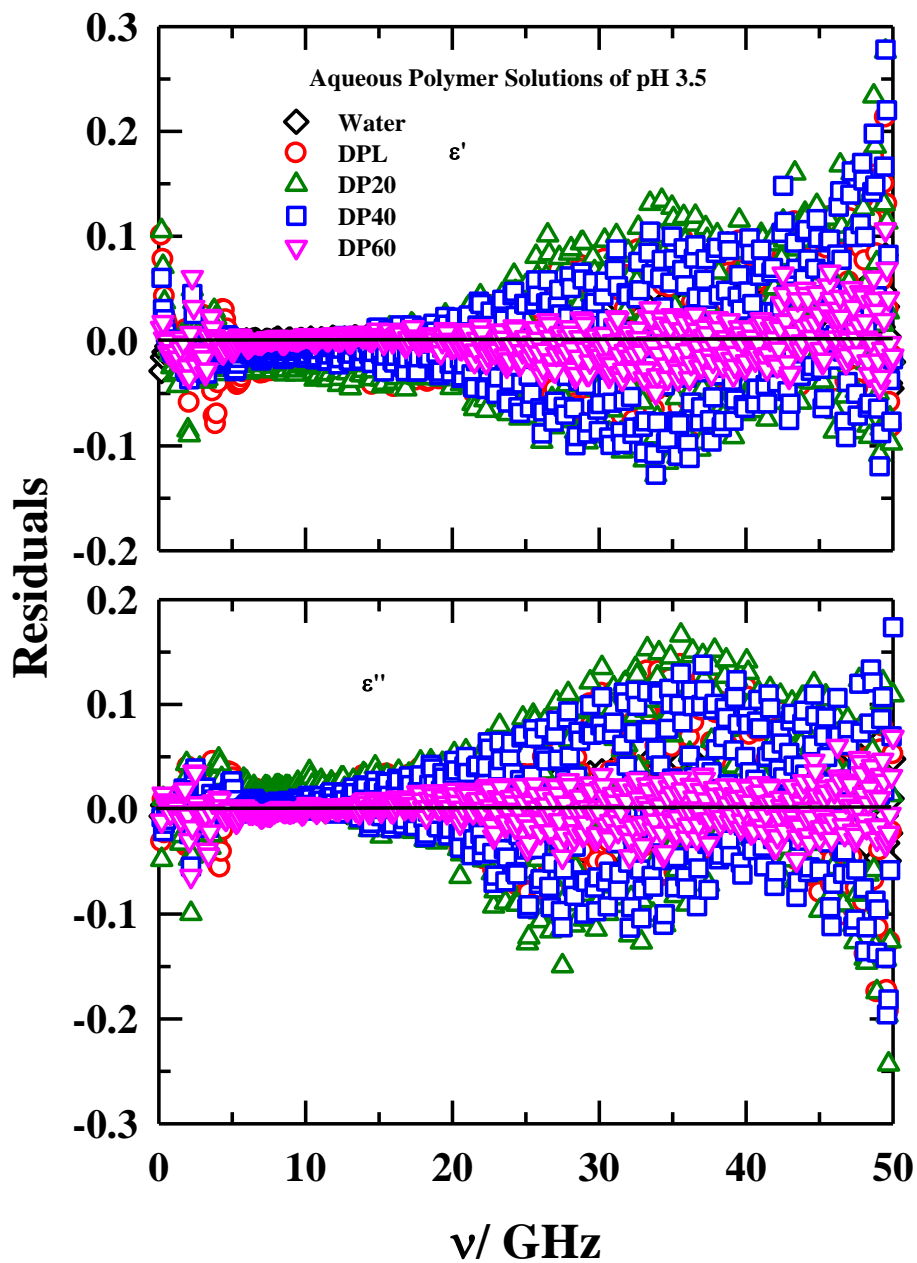


Figure A.f.4: Residuals from single Debye simultaneous fits to the real (ϵ') and imaginary (ϵ'') components of the measured complex DR spectra in aqueous copolymer solutions at ~ 298 K. pH of these polymer solutions are ~ 3.5 . All presentations are colour-coded.